INFORMATION TO USERS

This manuscript has been reproduced from the microfilm master. UMI films the text directly from the original or copy submitted. Thus, some thesis and dissertation copies are in typewriter face, while others may be from any type of computer printer.

The quality of this reproduction is dependent upon the quality of the copy submitted. Broken or indistinct print, colored or poor quality illustrations and photographs, print bleedthrough, substandard margins, and improper alignment can adversely affect reproduction.

In the unlikely event that the author did not send UMI a complete manuscript and there are missing pages, these will be noted. Also, if unauthorized copyright material had to be removed, a note will indicate the deletion.

Oversize materials (e.g., maps, drawings, charts) are reproduced by sectioning the original, beginning at the upper left-hand corner and continuing from left to right in equal sections with small overlaps.

Photographs included in the original manuscript have been reproduced xerographically in this copy. Higher quality 6" x 9" black and white photographic prints are available for any photographs or illustrations appearing in this copy for an additional charge. Contact UMI directly to order.

Bell & Howell Information and Learning
300 North Zeeb Road, Ann Arbor, MI 48106-1346 USA
800-521-0600



Downloaded from SHAREOK. Persistent Handle URL: https://hdl.handle.net/11244/478

UNIVERSITY OF OKLAHOMA

GRADUATE COLLEGE

TIGHTER PEAK-TO-PEAK PERFORMANCE BOUNDS FOR PIECEWISE LINEAR SYSTEMS WITH APPLICATION TO A CLASS OF SEMI-ACTIVE CONTROL PROBLEMS

A Dissertation

SUBMITTED TO THE GRADUATE FACULTY

in partial fulfillment of the requirements for the

degree of

DOCTOR OF PHILOSOPHY

By

DAVID S. EPP

Norman, Oklahoma

2002

UMI Number: 3053174



UMI Microform 3053174

Copyright 2002 by ProQuest Information and Learning Company.
All rights reserved. This microform edition is protected against unauthorized copying under Title 17, United States Code.

ProQuest Information and Learning Company
300 North Zeeb Road
P.O. Box 1346
Ann Arbor, MI 48106-1346

© Copyright by DAVID S. EPP 2002
All Rights Reserved

TIGHTER PEAK-TO-PEAK PERFORMANCE BOUNDS FOR PIECEWISE LINEAR SYSTEMS WITH APPLICATION TO A CLASS OF SEMI-ACTIVE CONTROL PROBLEMS

A Dissertation APPROVED FOR THE SCHOOL OF AEROPSACE AND MECHANICAL ENGINEERING

BY



Dr. Harold Stalford (Committee Chair)

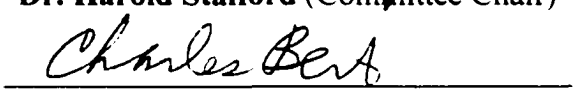

Dr Charles Bert

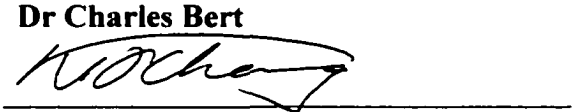

Dr Kuang-Hua Chang



Dr William Sutton

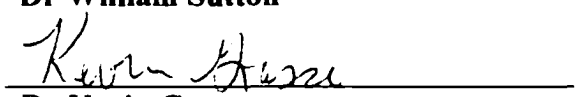

Dr Kevin Grasse

ACKNOWLEDGEMENTS

I would like to thank my advisor, Harold Stalford, for his support and encouragement throughout my dissertation research. I owe a debt of gratitude to William Patten for introducing me to control theory and starting me on the road to a Ph.D., and I would like to thank Jeffrey Kuehn for mentoring me through the first three years of the endeavor. I have really enjoyed working with all of the other students at the Center for Structural Control and my good friends in the AME shop, Billy Mays and Greg Williams. I could not have done this without the love and support of my family and wife.

TABLE OF CONTENTS

Acknowledgements iv

List of Figures x

List of Tables xviii

Abstract xxii

Chapter 1: Introduction 1

Chapter 2: Semi-Active Control: Modeling and Stability 8

2.1 Background 9

2.2 Structural System with Semi-Active Control Device 15

2.3 Nonlinear Modeling of Variable Orifice Hydraulic Semi-Active Actuator 16

2.4 Affine Model of Semi-Active Actuator Dynamics 19

2.5 Linear Model of Semi-Active Actuator Dynamics 22

2.6 Structural System with Nonlinear Actuator Dynamics 24

2.7 Structural System with Affine Actuator Dynamics 25

2.8 Structural System with Linear Actuator Dynamics 26

2.9 Stability of Semi-Active Control System with Nonlinear Actuator Dynamics 27

2.10 Piecewise Affine Model 32

2.11 Piecewise Linear Model 34

2.12 Summary 37

Chapter 3: Description of Performance Problem 38

3.1 Definition of Signal Norms 38

3.2 Definition of System Norms 40

3.3 Definition of the Reachable Set 44

3.4 Stable LTI SISO Systems 46

3.5 Description of the Performance Problem 48

3.6 Background 49

3.7 Performance Problem for this Dissertation 59

Chapter 4: Examples to Illustrate Performance Problem 62

4.1 Disturbance Logic 63

4.2 2D Example #1 65

4.3 2D Example #2 73

4.4 3D Example 82

4.5 7D Example 93

4.6 Summary 101

Chapter 5: Classical Lyapunov Bounds and a New Extension 103

5.1 Results for Example Systems 105

5.2 Summary 111

Chapter 6: Linear Matrix Inequalities (LMI) Method and Examples 112

6.1 Background 113

6.2 Single P LMI Method 117

6.3 Piecewise LMI Method 122

6.4 Results for Example Systems 135

6.5 Summary 153

Chapter 7: Tight Bounds and Reachable Set Solutions for 3D Semi-Active Control Problems 155

7.1 Method for Constructing Reachable Set for 3D Semi-Active Control Problems 157

7.1.1 Summary of Semi-Active Control System Dynamics 157

7.1.2 System Radial Symmetry 159

7.1.3 Open and Closed Valve Dynamics 160

7.1.4 Equilibrium Points for the Semi-Active System 164

7.1.5 Reachability of the Semi-Active Equilibrium Points 166

7.1.6 Constructing Individual Parts of the Candidate Reachable Set, R 169

7.1.7 Check that the Candidate Reachable Set is Closed and Continuous 174

7.1.8 Check that All Trajectories Follow the Surface or Point Inwards 177

7.1.9 Show that the Semi-Active System Converges to R from Outside 181

7.1.10 Getting to the Candidate Reachable Set Boundary from Inside 186

7.1.11 Claim that the Candidate Reachable Set is the Actual Reachable Set 187

7.2 Control Versions 5 and 4 188

7.3 Control Versions 3 and 1 192

7.4 Control Version 6 199

7.5 Control Version 2 203

7.6 New Simulation Results 210

7.7 Summary 212

Chapter 8: LMI Method Revisited 215

8.1 Quadratic Modeling 215

8.2 Modeling the Reachable Set of Control Version 5 of the 3D Example 216

8.3 Extension of LMI Method Formulated in Chapter 6 225

8.4 Can the LMI Method Provide a Tight Fit to the Reachable Set for Control Version 5? 231

8.5 Solution of the Expanded LMI Problem 234

8.6 Conclusions 236

Chapter 9: Application of Micro-Electro-Mechanical Sensors to Semi-Active Systems 238

9.1 General Sensing Requirements for Semi-Active Control Systems 238

9.2 Currently Available MEMS Sensors 241

9.3 Efforts Toward Useful Pressure Sensors and Accelerometers at Sandia National Laboratories 245

9.4 Summary 247

Chapter 10: Conclusions 248

References 254

Appendix I: Control Matrices for Example Problems 264

AI.1 2D Example #1 264

AI.2 2D Example #2 264

AI.3 3D Example 265

AI.4 7D Example 266

Appendix II: Derivation of Bounding Methods Based on a Classical Lyapunov Method and a New Extension 270

AII.1 Bound on Reachable Set Using a Continuous Lyapunov Function 271

AII.2 Intersection of Positive Definite Functions 273

AII.3 A Class of Lyapunov Functions 277

AII.4 Application to Semi-Active Control Systems 281

AII.5 Computing Performance Bounds for the Class of Semi-Active Control Systems 282

LIST OF FIGURES

Figure 2.1:	Summary of Semi-Active Modeling in the Literature	14
Figure 2.2a:	Schematic diagram of a nonlinear hydraulic semi-active actuator	16
Figure 2.2b:	Experimental Valve Discharge Coefficient vs. Choke Number (Kuehn, 2000)	18
Figure 2.3:	Example Nonlinear Behavior	21
Figure 2.4:	Example Nonlinear Behavior with Affine Approximation in Red	21
Figure 2.5:	Example Nonlinear Behavior with Linear Approximation in Red	23
Figure 3.1:	Comparison of Signals with Equal Energy and Disparate Peaks	40
Figure 3.2:	Input/Output System Model	40
Figure 3.3:	Categorization of Previous Peak-to-Peak Related References	58
Figure 4.1:	System 1-Norm Results for System (4.3) (Open Valve)	67
Figure 4.2:	Bound on Output Peak for Unit-Energy Input for System (4.3) (Open Valve)	68
Figure 4.3:	Reachable Set for System (4.3) with Unit-Peak Input (Open Valve)	69

Figure 4.4a:	Comparison of the System 1-Norm and Actual Reachable Set with Unit Peak Input for System (4.3) (Open Valve)	70
Figure 4.4b:	Comparison of the Reachable Set with Unit Energy Input and the Reachable Set with Unit Peak Input for System (4.3) (Open Valve)	71
Figure 4.5:	Simulation Results for System (4.3) with Disturbance (4.1) and (4.7) (Open Valve)	71
Figure 4.6:	Comparison of Reachable Sets for Open Valve Case and Control Case for System (4.2)	72
Figure 4.7:	System 1-Norm Results for System (4.11) (Open Valve)	75
Figure 4.8:	Bound on Output Peak for Unit-Energy Input for System (4.11) (Open Valve)	75
Figure 4.9a:	Reachable Set for the System (4.11) with Unit Peak Input (Open Valve)	77
Figure 4.9b:	Comparison of the System 1-Norm and Actual Reachable Set with Unit Peak Input for System (4.11) (Open Valve)	77
Figure 4.9c:	Comparison of the Reachable Set with Unit Energy Input and the Reachable Set with Unit Peak Input for System (4.11) (Open Valve)	78
Figure 4.10:	Simulation Results for System (4.11) with Disturbance (4.1) (Open Valve)	78
Figure 4.11:	Reachable Sets for Controlled Cases for 2D Example #2	80

Figure 4.12:	Peak-to-Peak Gain Relative to Angle Between Switching Planes for 2D Example #2	81
Figure 4.13:	Example problem – Linear system with switched Semi-active element	82
Figure 4.14:	Simulated 3D system response with an initial condition of (1,1,2) and no Disturbance	84
Figure 4.15:	System 1-Norm Result for System (4.15) (Open Valve)	86
Figure 4.16a:	Bound on Output Peak for Unit-Energy Input for System (4.17) (Open Valve)	86
Figure 4.16b:	Tight Covering of the Reachable Set for System (4.17) (Open Valve)	88
Figure 4.17a:	Simulated Response of System (4.17) with a Disturbance (4.1a) (Open Valve)	88
Figure 4.17b:	Results Summary for the 3D example	91
Figure 4.18:	Views of the Simulated Response of (4.21) with Control Version 6 and Disturbance (4.1)	92
Figure 4.19:	Picture of a Three-Story Scale Building whose Model is Used Here for an Example	94
Figure 4.20:	Schematic Drawing of a Three-Story Scale Building whose Model is Used Here for an Example	95
Figure 4.21:	Semi-active Actuator Installation Position	95
Figure 5.1:	Results Summary for the 3D Example	108

Figure 6.1:	Regions and vertex directions for the 2D example #2. Grey area are where $A=A_{u=0}$ and white areas are where $A=A_{u=1}$.	125
Figure 6.2:	Ellipsoid bound on the Reachable set found with the LMI method for the 2D example #1 compared to earlier results	136
Figure 6.3a:	Ellipsoid bound on the Reachable set found with the LMI method for the Open Valve 2D example #2 along with Simulation Results	139
Figure 6.3b:	Ellipsoid bound on the Reachable set found with the LMI method for the controlled 2D example #2 along with Simulation Results for Control Version 1	140
Figure 6.4	LMI Results for Control Version 1	142
Figure 6.5	LMI Results for Control Version 2	142
Figure 6.6	LMI Results for Control Version 3	143
Figure 6.7	LMI Results for Control Version 4	143
Figure 6.8	LMI Results for Control Version 5	144
Figure 6.9	LMI Results for Control Version 6	144
Figure 6.10	Time to Solution for Quadrahedral Discretization of Control Version 6 for 3D Example	145
Figure 6.11	Results Summary for the 3D Example	147
Figure 6.12:	LMI result for 3D example in Open Valve Case.	147
Figure 6.13:	LMI result for 3D example with control version 1 with 4 partitions showing the value of $\dot{V}$ in the surface color.	148
Figure 6.14:	Best LMI result for 3D example with control version 1.	149

Figure 6.15:	Best LMI result for 3D example with control version 6.	150
Figure 6.16:	LMI result for 3D example with control version 1 with 4 partitions showing the simulation results for comparison.	151
Figure 7.1:	Side View of the First Open Valve Mode in State Space Coordinates	162
Figure 7.2:	Intersection of Switching Planes (7.2-7.3) with the x_1x_3-Plane for Control Versions 1,3,4,5,6	165
Figure 7.3:	Intersection of Switching Planes (7.2-7.3) with the x_1x_3-Plane for Control Version 2	165
Figure 7.4:	Three Views of the Dynamics to get Semi-Active Control Version 5 from the Origin to the Extreme Equilibrium Point (0.0445, 0, 0)	169
Figure 7.5:	Surface Generated from System Trajectories in the Closed Valve Region X_0^* for Control Version 5	171
Figure 7.6:	Surface Generated from System Trajectories in the Open Valve Region X_1^* for Control Version 5	172
Figure 7.7:	Final Values for B and B' on the x_3=0 Plane after 3 Iterations for Control Version 5	173
Figure 7.8:	Exploded View of Component Parts for Candidate Reachable Set of Control Version 5	174
Figure 7.9:	Close Up View of Tip of Candidate Reachable Set	176
Figure 7.10:	Assembled View of the Candidate Reachable Set for the Semi-Active Control Problem with Control Version 5	176

Figure 7.11	Cross-Section of the Candidate Reachable Set for Control Version 5 at the Plane $x_1=0$	178
Figure 7.12	Typical Trajectory with Initial Condition Outside Candidate Reachable Set and Between Planes Formed by Parts BP and BP' at the Equilibrium Points for Control Version 5	184
Figure 7.13	Typical Trajectory for the System when $x_3-x_1<-0.0445$.	185
Figure 7.14	Trajectory from an Equilibrium Point Along the Surface of the Candidate Reachable Set	187
Figure 7.15	Assembled View of the Candidate Reachable Set for the Semi-Active Control Problem with Control Version 4	189
Figure 7.16:	Cross-Section of the Candidate Reachable Set for Control Version 4 at the Plane $x_1=0$	189
Figure 7.17:	Assembled View of the Candidate Reachable Set for the Semi-Active Control Problem with Control Version 3	194
Figure 7.18:	Cross-Section of the Candidate Reachable Set for Control Version 3 at the Plane $x_1=0$ (Sliding Mode Between A and B)	194
Figure 7.19:	Assembled View of the Candidate Reachable Set for the Semi-Active Control Problem with Control Version 1	195
Figure 7.20:	Cross-Section of the Candidate Reachable Set for Control Version 1 at the Plane $x_1=0$ (Sliding Mode Between A and B)	195

Figure 7.21:	**Assembled View of the Candidate Reachable Set for the Semi-Active Control Problem with Control Version 6**	**200**
Figure 7.22:	**Cross-Section of the Candidate Reachable Set for Control Version 6 at the Plane $x_1=0$**	**201**
Figure 7.23:	**Assembled View of the Candidate Reachable Set for the Semi-Active Control Problem with Control Version 2**	**205**
Figure 7.24	**Cross-Section of the Candidate Reachable Set for Control Version 2 at the Plane $x_1=0$ (Sliding Mode Between A and B)**	**206**
Figure 7.25	**Simulated Trajectory for Control Version 5**	**211**
Figure 7.26	**Results Summary for the 3D Example**	**213**
Figure 8.1	**Coarse Discretization of Reachable Set for Quadratic Estimation**	**219**
Figure 8.2	**Residual Values for Least Squares Quadratic Estimate with Coarse Discretization**	**219**
Figure 8.3	**Finer Discretization of Reachable Set for Quadratic Estimation**	**221**
Figure 8.4	**Residual Values for Least Squares Quadratic Estimate with Refined Discretization**	**222**
Figure 8.5	**Lyapunov Derivative for Least Squares Quadratic Estimate with Refined Discretization (min –1.3601e2 max 7.7762e1)**	**223**
Figure 8.6	**Discretization of Reachable Set for Quadratic Estimation with Gradient Error Included**	**223**

Figure 8.7	Residual Values for Least Squares Quadratic Estimate with Gradient Error Included	224
Figure 8.8	Lyapunov Derivative for Least Squares Quadratic Estimate with Gradient Error Included (min –1.3601e2 max 7.7762e1)	225
Figure 8.9	Four Views of the Comparison Between the Reachable Set from Chapter 7 (Red) and LMI Solution from Chapter 6 (Black Mesh) for the 3D Example with Control Version 1	230
Figure 8.10	Finest Discretization of the OP Region	233
Figure 9.1	ICSensor Pressure Sensor Model 87N in Two Package Configurations	242
Figure 9.2	Crossbow LP Series Accelerometer in Nylon Package	244

LIST OF TABLES

Table 4.1:	Results for 2D Example #1	73
Table 4.2:	Values used for Positive Definite Symmetric P Matrix in Candidate Controllers for 2D example #2	79
Table 4.3:	Results for 2D example #1	81
Table 4.4:	Values used for Positive Definite Symmetric P Matrix in Candidate Controllers for 3-D Example	89
Table 4.5:	System 1-Norm Results for 3D example (Open Valve)	91
Table 4.6:	Maximum Simulated Radius Results for 3D example with Candidate Controllers	93
Table 4.7:	System 1-Norm Results for the 7D example (Open Valve)	98
Table 4.8:	Values used for *PB* Vector in Candidate Controllers for 7-D Example	100
Table 4.9	Simulation Results for 7D Example with Candidate Controllers	100
Table 5.1:	Summary of previous results for the 2D example #1	105
Table 5.2:	Results for the 2D Example #2	106
Table 5.3:	Intersecting P Method Results for the 2D example #2	107
Table 5.4:	Results for the 3D Example	107
Table 5.5:	Intersecting P Method Results for the 3D Example	109
Table 5.6:	Results for 7D example	110
Table 6.1:	Results for 2D example #1	136

Table 6.2:	Summary of previous results for the 2D example #2	137
Table 6.3:	LMI results for 2D example #2	138
Table 6.4:	Summary of Previous Results for the 3D example	140
Table 6.5:	LMI Results for 3D Example	146
Table 6.6:	Summary of previous results and LMI results for 7D example	152
Table 7.1:	Values for the Angle α in the Figures 7.2-7.3 for Control Versions 1-6 in Degrees	166
Table 7.2:	Extreme values for the Candidate Reachable Set for Control Version 5 shown in Figure 7.10	177
Table 7.3:	Angle of System Trajectory with Candidate Reachable Set Surface for Control Version 5 with Disturbance that Generated Surface R.	180
Table 7.4:	Angle of System Trajectory with Candidate Reachable Set Surface for Control Version 5 with Opposite Disturbance	180
Table 7.5:	Angle of System Trajectory with Candidate Reachable Set Surface for Control Version 4 with Disturbance that Generated Surface R.	190
Table 7.6:	Angle of System Trajectory with Candidate Reachable Set Surface for Control Version 4 with Opposite Disturbance	191
Table 7.6b:	Summary of Extreme values for the Reachable Sets of Control Versions 5 and 4	191

Table 7.7:	Angle of System Trajectory with Candidate Reachable Set Surface for Control Version 3 with Disturbance that Generated Surface R.	196
Table 7.8:	Angle of System Trajectory with Candidate Reachable Set Surface for Control Version 3 with Opposite Disturbance	197
Table 7.9:	Angle of System Trajectory with Candidate Reachable Set Surface for Control Version 1 with Disturbance that Generated Surface R.	197
Table 7.10:	Angle of System Trajectory with Candidate Reachable Set Surface for Control Version 1 with Opposite Disturbance	198
Table 7.11:	Summary of Extreme values for the Reachable Sets of Control Versions 3 and 1	199
Table 7.11b:	Angle of System Trajectory with Candidate Reachable Set Surface for Control Version 6 with Disturbance that Generated Surface R.	202
Table 7.12:	Angle of System Trajectory with Candidate Reachable Set Surface for Control Version 6 with Opposite Disturbance	202
Table 7.13:	Summary of Extreme values for the Reachable Sets of Control Version 6	203
Table 7.14:	Angle of System Trajectory with Candidate Reachable Set Surface for Control Version 2 with Disturbance that Generated Surface R.	208

Table 7.15:	**Angle of System Trajectory with Candidate Reachable Set Surface for Control Version 2 with Opposite Disturbance**	**209**
Table 7.16:	**Summary of Extreme values for the Reachable Sets of Control Version 2**	**209**
Table 7.17:	**New Simulation Values for the 3D Example**	**211**
Table 7.18:	**Results Summary for the 3D Example**	**214**
Table 8.1	**Results for Feasibility of $\bar{P}_j - \bar{E}_j \bar{W}_j \bar{E}_j > 0$ for Coarse Model**	**232**
Table 8.2	**Results for Feasibility of $\bar{P}_j - \bar{E}_j \bar{W}_j \bar{E}_j > 0$ for Finer Model**	**232**
Table 8.3	**Results for Feasibility of $\bar{P}_j - \bar{E}_j \bar{W}_j \bar{E}_j > 0$ for Model with Gradient Error**	**232**
Table 8.4	**Results for Feasibility of $\bar{P}_j - \bar{E}_j \bar{W}_j \bar{E}_j > 0$ for Finest Discretization of OP Region**	**233**
Table 8.5	**Extended LMI Results for 3D Example**	**235**

ABSTRACT

One of the open problems in the literature is determining tight bounds for L_1 performance (peak-to-peak gain) of piecewise linear systems. A certain class of piecewise linear systems results from stabilizing linear semi-active control systems. These systems use piecewise constant Lyapunov controllers based on two switching hyperplanes. In computing peak-to-peak performance gains for this class of piecewise linear systems, previous works in the literature have used a classical Lyapunov-based method to compute upper bounds and have used extensive simulations to compute lower bounds. These upper and lower bounds are usually separated by a gap of several orders of magnitude. In this dissertation, the open problem of finding tighter bounds for peak-to-peak performance gains of such piecewise linear systems is investigated.

For the purpose of evaluating the tightness of peak-to-peak performance gain methods, four semi-active control system examples are defined. Two 2D examples, a 3D example and a 7D example are presented based on previous work in hydraulic semi-active control. Several stabilizing piecewise constant Lyapunov type (bang-bang) controllers are derived for each of these four systems. The peak-to-peak performance gain of the stable, linear, "open valve" system (i.e., the hydraulic valve is left open at all times) is used as a benchmark to gauge the relative size of the performance bounds. Actual peak-to-peak performance gains for the control cases are expected to be less than (i.e., better than) the "open valve" benchmark value. For the 3-D semi-active control problem example, this "open valve" benchmark value is 2.59. When applied to the six control cases for this example, the classical method yields upper bound values that range

from 140 to 1.6 million. These values are 2-6 orders of magnitude larger than the benchmark value. Extensive simulation of the six control cases yields lower bound values that range from 0.22 to 0.36. These values are about one order of magnitude less than the benchmark value.

The first major contribution of this dissertation is the development of a Linear Matrix Inequality (LMI) method applicable to our class of piecewise linear systems, which provides a tighter upper bound on the peak-to-peak gain performance. In its application to the six control cases of the 3D example for determining the peak-to-peak performance gain, the new LMI method yields the lowest upper bound values of 0.55, 1.19, 1.63, 3.50, 3.57, and 0.65 for the various mesh sizes used. Some of these are up to 4.5 times better than the benchmark value of the open valve case. This new LMI method provides upper bounds that are significantly tighter than those of the classical method. Even tighter values are possible with finer meshing of the regions and with exponentially increasing convergence times. Some improvement is also possible with non-uniform meshing of the regions. The gap between the LMI upper and lower bounds of simulation is reduced significantly below one order of magnitude for the 3-D system. This method is able to predict that the semi-actively controlled system will outperform the open valve case in most instances. Some of this work was presented at the American Control Conference, May 8-10, 2002 and published in its proceedings.

The second major contribution is the development of a special method for determining the reachable sets for unit peak inputs associated with the six control cases of the 3-D semi-active control system. The maximum radii of the reachable sets yield tight peak-to-peak performance gains for the six control cases. The tight bounds are found to

have values that range from 0.38 to 0.41. Also of significance, these reachable sets have closed, continuous, and piecewise C^1 surfaces, which present some interesting new surface topography.

Finally, the piecewise C^1 parts of the surface of the reachable sets are subdivided into several smaller regions and tightly fit with quadratic models. The quadratic models have non-zero constant and first order terms as well as non-zero second order terms. This form of the quadratic model is significantly different from that used in the earlier LMI formulation, which only had non-zero second order terms. A new LMI formulation is considered in which all three terms of the quadratic models are variables. We have to add a small ε to ensure that the models from the earlier LMI formulation are a subset of this new formulation. It is determined that this new formulation will not tightly fit the reachable sets for the 3D example. It does, however, find upper bounds that are close to the LMI solutions found using only the non-zero second order term.

CHAPTER 1

INTRODUCTION

Semi-active control elements have become popular for reducing vibration in various dynamic systems, particularly in situations where the limited power available precludes the use of active control elements. Semi-active elements are used in systems ranging from automotive suspensions to seismic protection for buildings and have been shown to produce results that, in many cases, approach the performance of active control at a fraction of the power cost. Semi-active devices were first introduced to improve the ride and handling of automobiles almost 30 years ago (Karnopp, et al., 1974). Since then, their application has spread to many areas of vibration control, and many authors have treated semi-active devices and systems. Two examples are Hrovat, et al. (1983), who first applied semi-active systems to civil structures, and Leitmann (1994), who was one of the earliest authors to treat semi-active system stability. More background on semi-active systems, particularly in regards to application in civil structures, is presented in Chapter 2.

For more than a decade, researchers at the University of Oklahoma have been successfully applying semi-active systems to real problems. Much of the early work at OU centered on semi-active control of automotive suspension systems (Patten, et al., 1991) (Wu, 1994) (Mo, 1996). Proprietary work, done at OU but supported by General Motors, was done on semi-active suspension for the Corvette. Some early work also centered on semi-active control of floor systems (Ebrahimpour, et al., 1993). With the formation of The Center for Structural Control, the focus of semi-active research began to

shift to vibration control of civil structures (Li, 1998) (Patten and Kuehn, 1996). The work with civil structures peaked with two full-scale tests of semi-active systems for bridges on Walnut Creek Bridge on Interstate 35. These tests were documented by two reports presented to the Oklahoma Department of Transportation (Patten, et al., 1997) (Stalford and Kuehn, 1999). Recent work on semi-active systems at OU has focused on more analytical research. This work originally focused on design optimization and control design (Patten, et al., 1998) (Lee, 1998). The most recent work has focused on analytical stability of nonlinear semi-active systems.

Even though the dynamics (e.g., structural aspects) of many systems are stable and linear, semi-active control elements usually add nonlinear dynamics (Patten, et al., 1998) (Kuehn and Stalford, 2000) (Kuehn, 2000) and/or discontinuous behavior (Kuehn and Stalford, 2000) (Kuehn, 2000) (Reithmeier and Leitmann, 2001) to the overall system dynamics. Some popular semi-active controllers are constructed by using two hyperplanes to define the regions of state space where the valve of a variable orifice hydraulic semi-active actuator is either open or closed. Consequently, in its simplest form and using only one actuator, one large class of semi-active control systems, with a linearized hydraulic semi-active actuator and a valve that is either open or closed, can be represented as a piecewise linear single input single output (SISO) system:

$$\dot{x} = A_i x + Dd, \quad x \in X_i, \quad |d| \le 1, \quad i = 0,1 \tag{1.1}$$

$$w = Cx, \quad . \tag{1.2}$$

In this system A_1 is a stable matrix representing the system with an open valve, and A_0 is a marginally stable matrix with one pole at the origin representing the system with a

closed valve. The semi-active controller has the valve open in $\mathcal{X}_1$ and closed in the rest of the space, $\mathcal{X}_0$. The input disturbance signal d and the output signal w are scalars, and the transfer function $g_1 = C(sI - A_1)^{-1}D$ from d to w is non-zero. We assume that (1.1) and (1.2) form a minimal realization.

The most general and useful method for studying nonlinear system stability is Lyapunov Stability Theory (Lyapunov, 1892). Although this theory received little attention at first, this method was brought to the attention of the larger controls community in the early 1960s and has been used extensively since (Lasalle and Lefschetz, 1961) (Yoshizawa, 1966). There are several methods based on this stability theory available for designing stabilizing controllers for (1.1) and (1.2) (Kuehn and Stalford, 2000) (Kuehn, 2000) (Reithmeier and Leitmann, 2001). Recently, Kuehn and Stalford (2000) proved that this type of semi-active control system is stable to some "ball of ultimate boundedness" for a bounded disturbance. This stability result also gave very conservative performance results for these systems.

The method of linear matrix inequalities (LMI) has been seen in the literature throughout the last two decades (Boyd, et al., 1994). This method is most often applied to robust control problems and problems that are written in terms of Lyapunov functions and their derivatives. Of particular interest here, the method has been used to find performance bounds for nonlinear systems modeled as uncertain or piecewise linear systems. Johansson and Rantzer (1998) used a piecewise Lyapunov function to find stability for piecewise linear and affine systems. They also treated the problem of finding a bound on L_2 system performance (Rantzer and Johansson, 2000). Boyd, et al. (1994) developed a method to find an upper bound on the peak-to-peak gain for uncertain linear

systems. In a paper by Hassibi and Boyd (1998) that also treated L_2 system performance for piecewise linear systems, the authors mentioned that the LMI method could also be used to treat L_1 system performance for piecewise linear systems. They did not, however, develop the method.

In many semi-active applications, the peak system response to persistent bounded disturbances is an important design criterion. For example, in seismic protection of buildings, knowing that the maximum building deflection in an earthquake will not exceed a certain limit is of utmost importance. The focus in this dissertation is on the performance problem, which is to determine the peak-to-peak gain in the output signal w for persistent bounded disturbances d. We are not focusing here on finding a controller, but rather on finding a method to quantify the peak-to-peak gain performance of previously determined controllers. Currently, a method for determining a non-conservative (i.e., tight) performance bound on the peak-to-peak gain for system (1.1) and (1.2) does not exist.

We begin by reviewing semi-active system modeling and a method for designing stable semi-active control laws in Chapter 2. A nonlinear model is first developed for the structure and semi-active actuator. A stable controller is then designed based on the work of Kuehn (2000). We then reduce the controlled nonlinear semi-active system to a piecewise linear system of the form (1.1) and (1.2), based on the controller design.

Next, Chapter 3 concisely defines the performance problem of interest. A definition for a system's reachable set with unit peak input is given, and the peak-to-peak gain is then defined based on this set. The goal of this dissertation is as follows.

Find a tight (or tighter) upper bound for the peak-to-peak gain of the piecewise linear semi-active control system of the form (1.1), with the regions defined by the control law (2.29) as

$$\begin{aligned} x \in X_0 \quad & iff \quad x^T v_1 v_2^T x < 0 \\ x \in X_1 \quad & iff \quad x^T v_1 v_2^T x \geq 0 \end{aligned}, \tag{1.3}$$

where v_1 and v_2 are non-zero column vectors.

In Chapter 4, we present a group of example piecewise linear semi-active problems that will be used to illustrate the techniques and results in this dissertation. Two 2D examples and two higher dimensional examples are presented. The first of these higher dimensional problems is a 3D problem based on an air-suspended heavy truck model. The second is a 7D problem based on a 3-story building from earlier work (Kuehn, 2000). The currently unsolved problem that we are treating in this dissertation is the problem of finding a tight bound on the peak-to-peak gain for these higher dimensional piecewise linear problems.

We next present a classical Lyapunov method for finding an elliptical bound on the peak-to-peak gain for nonlinear semi-active systems in Chapter 5. This method is from the work of Kuehn and Stalford (2000), where a matrix, $Q > 0$, is used to solve the Lyapunov equation $-Q = A^T P + PA$ and to get the Lyapunov function in the form

$$V(x) = x^T Px, x \in \Re^n. \tag{1.4}$$

This method is known to produce bounds that are very conservative (up to 6 orders of magnitude above bounds from simulation studies), but it is applicable to both nonlinear semi-active systems and piecewise linear semi-active systems. A method for using intersecting Lyapunov functions of the form (1.4) is also discussed, and results are

presented (i.e. Lyapunov function of the form $V(x) = \max_i \{x^T P_i x\}$ where $-Q_i = A^T P_i + P_i A$ and $Q_i > 0$). The results from this method are no better than those obtained from the method with a single Lyapunov function.

In Chapter 6, we present a new method for bounding the system response with a continuous, piecewise C^1 quadratic Lyapunov function, which is based on the method of linear matrix inequalities (LMI). This method is original work that has not appeared in the literature prior to the author's paper (Epp and Stalford, 2002). The Lyapunov function used is of the form

$$V(x) = x^T P_i x, \; x \in X_i, \; \bigcup_i X_i = E^n . \tag{1.5}$$

This is an optimization method that allows us to minimize the peak-to-peak gain based on the Lyapunov function while bounding the system response. This method is only applicable to piecewise linear systems.

A special method is used in Chapter 7 to find the actual reachable sets for the 3D example problems. This method is specific to the 3D case and is based on a graphical understanding of the system dynamics. These reachable sets and the peak-to-peak gains for each version of the 3D semi-active control problem are presented, and the results are compared to the previous simulations and estimates.

Chapter 8 presents models for the reachable sets in Chapter 7, based on functions with nonzero quadratic, linear, and constant terms. These models are shown to fit the reachable sets for the 3D example problems and can be used to generate approximations of the reachable sets without transferring large sets of surface data. An extension of the LMI method in Chapter 6 that allows for this expanded surface model is presented.

Application of sensors based on micro-scale technology to semi-active actuators is discussed in Chapter 9. These micro-electro-mechanical system (MEMS) sensors can be used to integrate some of the necessary sensing into the actuator itself. Several possible areas of development for future sensors applicable to semi-active systems are also discussed.

Finally, conclusions are presented in Chapter 10 on our findings for tighter peak-to-peak gains for semi-active control systems.

CHAPTER 2

SEMI-ACTIVE CONTROL: MODELING AND STABILITY

Semi-active control devices are used extensively for such things as automotive suspension control, control of traffic-induced vibration in bridges, seismic protection of structures, and many other applications where the goal is to stabilize vibration. Semi-active devices are similar to passive devices in that they are only able to react to the motion of the system to which they are connected. The difference is that the response characteristics of the semi-active device can be varied in real time. This real time variability allows the effectiveness of semi-active devices to approach that of active devices while expending significantly less actuation energy.

The work in this dissertation is based on a specific class of semi-active systems, consisting of a reasonably general model of a linear structural system coupled with a nonlinear semi-active actuator. This coupled model is general enough to represent most of the typical applications for semi-active control, including seismic protection for buildings and suspension systems in automobiles, and covers a variety of semi-active actuators. The coupling between the structural system and the actuator has rarely been investigated in the literature. Most of the semi-active control literature disregards the interaction between the structural system and the semi-active actuator, even though this relationship is important.

This chapter will begin with an overview of semi-active control systems in the literature with specific interest in modeling. Next, the linear structural system model and the nonlinear actuator model will be developed separately and then their coupled

dynamics will be discussed. Linear and Affine approximations for the nonlinear actuator dynamics will also be discussed. Then, the Lyapunov based steepest descent control law will be shown to provide a stable controller for the semi-active system. Finally, the piecewise linear system model for the controlled semi-active system will be presented. This piecewise linear model will be used throughout the dissertation.

2.1 Background

Since their introduction, semi-active devices have been applied to a large variety of dynamic systems and have been constructed and modeled in various ways. The background that follows is a brief overview covering several applications, modeling methods, and control algorithms. The section is organized according to the complexity of the various semi-active device models used for control design in the literature. A brief discussion of the performance measures used is included. Special attention is paid to whether the performance measures are solely based on simulation and experimentation, or if mathematical measures are developed based on the system equations and control logic. A graphic chart at the end of the section will summarize this.

The earliest work with semi-active devices neglected actuator dynamics and simply replaced it with an equivalent force generator. Some modern authors also make this same assumption. Semi-active devices were first introduced to improve the ride and handling of automobiles by Karnopp, et al. (1974). That work used semi-active force generators with no dynamics and claimed that they could provide significantly improved performance over passive suspensions. The performance for the system was quantified with transfer functions based on simulated response of the semi-active system.

The earliest work in applying semi-active devices to structures was done by Hrovat, et al. (1983). A clipped linear quadratic controller was implemented to reduce wind-induced vibrations in a single-degree-of-freedom building model using a semi-active tuned mass damper. The semi-active device used was assumed to have some maximum possible force and to be dissipative. Integral performance index numbers based on simulation results were used to compare the performance of the semi-active system to passive and active systems. It showed that, for a certain performance index, the semi-active system performed almost as well as the active system.

Besinger et al. (1995) used a hardware-in-the-loop simulation to verify the performance of a semi-active device for automotive suspensions. They used a force feedback around the actuator to track a desired force generated by a PID control that did not use the actuator dynamics. The performance of the controller was only reported in terms of reductions in RMS values in simulation and experiment. Kitching et al. (2000) used a similar control that was applied to heavy trucks while developing a new semi-active damper and also reported performance only in terms of simulation and experimental response.

Dyke et al. (1996) experimentally verified the seismic response characteristics of a planar three-story structure with a magnetorheological damper. A bi-state law on the voltage to the MR damper was used to track a desired force found with an H_2/LQG control design method that did not include the semi-active actuator dynamics. The performance of this control was quantified with simulation results for a particular earthquake event. Kasturi and Dupont (1998) formulated a constrained optimal control to maximize energy dissipation for a semi-active damper with no dynamics. Although a

controller was formulated with an integral cost function, the performance of this system was reported only in terms of simulation results.

Most work in the literature models semi-active devices as adjustable linear or bilinear systems. Such models come in three varieties: adjustable stiffness, adjustable damping, or some combination of the two. In most cases the systems are considered to be instantaneously adjustable.

The first of the adjustable linear models is variable stiffness. Symans and Constantinou (1997) used variable linear damping devices to reduce the vibration of a three-story building from seismic loading. They used clipped LQR and sliding mode control designs for the semi-active device, but their tests showed that a passive high damping configuration provided better performance than both of the semi-active controllers. This performance judgment was made using peak simulation and experimental values for floor deflection. Sadek and Mohraz (1998) presented control strategies for structures with variable linear damping devices. They concluded that, of the strategies tried, the generalized clipped LQR algorithm provided the best response characteristics. The authors used the maximum floor displacement and acceleration from simulations to come to their performance conclusions.

There are also many examples of models where the semi-active actuator was modeled as a variable damping. This seems to be the most popular linear model for semi-active actuators in the literature. Hrovat et al. (1988) used an optimization routine to try to approach an optimal control algorithm for a variable damper semi-active actuator in an automotive application. Their results, which were based on simulation studies, showed that it was possible to solve for such a controller, but the performance was not

better than older LQ control formulations. Yi and Hedrick (1993) also used a variable damping model, but they were interested in reducing the tire force dynamics in automobiles. A clipped optimal control based on an LQ performance index was designed to reduce the dynamic tire deflections from an unknown road disturbance, and transfer function data from simulations and experiments were used to verify the control performance.

Kobori, et al. (1993) developed an open loop control law for a full-scale model building equipped with variable stiffness actuators in which the bi-state stiffness was adjusted based on the seismic disturbance. The performance of the system was presented in spectral plots of the system states. Tseng and Hedrick (1994) also used a variable damping model to derive an optimal control law and compared it to the popular clipped optimal design for semi-active systems. Their work showed that a truly optimal solution for a semi-active problem should be time varying as opposed to the time invariant solution from the clipped optimal control. They used simulation results to show performance index values and transfer functions for a quarter car model. Nell and Steyn (1998) used a variable damping model and a bi-state control design to improve the discrete obstacle performance and ride quality of an off-road vehicle. Their control strategy was such that it maximized the body mass deceleration. The performance of their system was shown with simulation and experimental values for the body and axle RMS accelerations. Nagarajaiah and Mate (1998) utilized a maximum dissipativeness control switching logic for a continuously variable linear semi-active stiffness device and showed simulation results.

The final type of linear model used for semi-active systems is the one that combines variable stiffness and variable damping. Leitmann (1994) treated all three types of linear models discussed here. He compared two control strategies for all these models. The first control strategy was aimed at minimizing the rate of change of system energy, while the second was developed using Lyapunov stability theory. A "ball of ultimate boundedness" was derived for these control laws that would bound the system response, but no numerical values were presented. Loh and Ma (1994) compared three control strategies for seismically excited buildings with semi-active devices with adjustable damping and stiffness coefficients. Based on simulation results, the optimal control strategy provided significantly better reduction in peak floor displacements than the alternate controllers. Reithmeier and Leitmann (2001) used a general bilinear system model and applied semi-active control based on Lyapunov stability. They also derived a region of attraction for the controlled system that contained the motion of the system once it is inside or if it began inside.

Only a few researchers included nonlinear dynamics in their control design as it adds significant complexity, and the control design tools for nonlinear systems are limited. Patten et al. (1994) and Patten (1998) used a nonlinear actuator model with a control law aimed at minimizing the first derivative of a quadratic Lyapunov function to mitigate structural vibrations and bridge vibrations respectively. The Lyapunov function in both cases included the structural states and semi-active actuator states. No mathematical performance bounds were derived, but simulation results were used to quantify performance. The model used by Patten was further developed by Mo et al. (1996) with the same control law and was shown to match empirical data well for the

hydraulic semi-active actuators used. Gavin and Doke (1999) used a nonlinear model of a hydraulic semi-active device to explore the relative merits of using the nonlinear device to approximate a variable stiffness device or a variable damping device. They concluded that if the valve orifice area was constrained to certain ranges the device could be used in these two ways and that the variable stiffness range gave much better results when applied to a seismic isolation problem. The damped natural frequencies of the system were used to illustrate performance with and without the semi-active control.

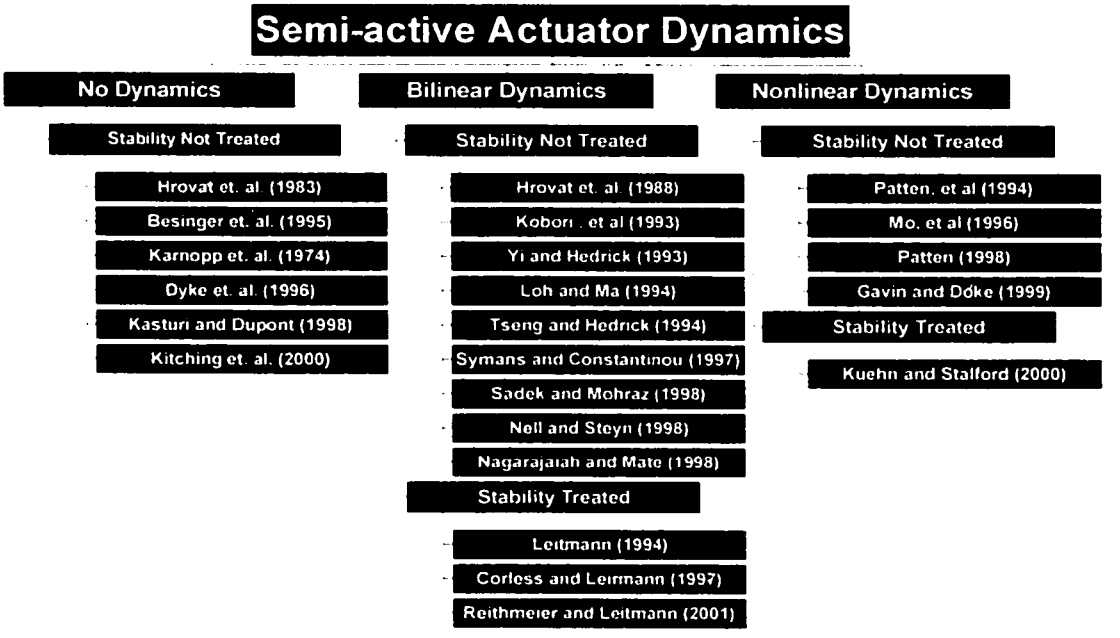

Figure 2.1: Summary of Semi-Active Modeling in the Literature

Although semi-active systems have been researched extensively in the last three decades, very little work has been devoted to the stability of semi-active systems. Several researchers (Dyke, et al., 1998) (Spencer, et al., 1998) have asserted that semi-active systems are inherently stable in the bounded input – bounded output sense without proof. It has been shown elsewhere (Corless and Leitmann, 1997), however, that a variable stiffness semi-active device could destabilize a system if the control logic was

chosen improperly. Leitmann (1994) treated the stability of semi-active systems that had adjustable stiffness and damping. For a control law based on Lyapunov stability theory, the system was shown to be stable to a ball around the origin for a bounded input. Very recently, Kuehn and Stalford (2000) proved stability for a semi-active system with nonlinear dynamics using a Lyapunov control design. They also showed that the system was stable to a ball centered at the origin for the bounded disturbance case.

The semi-active structural control design research in the literature is categorized in Figure 2.1. The works are divided by modeling method and treatment of stability.

2.2 Structural System with Semi-Active Control Device

The structural system in this work is modeled as a linear time-invariant (LTI) system. This allows a very broad application of the work, because LTI systems are used to describe a very broad range of systems. Many automotive suspension models and most finite element structural models can be rewritten in this form.

A minimal realization of the structural system is modeled using the state space form,

$$\dot{x} = A_S x + B_S y + D_S d \tag{2.1}$$

where x is the state vector of the structural system, y is the scalar state of the semi-active element, d is the scalar input disturbance to the system, and A_S, B_S, and D_S are LTI system matrices. A_S is stable (Hurwitz) in most applications.

2.3 Nonlinear Modeling of Variable Orifice Hydraulic Semi-Active Actuator

A nonlinear hydraulic semi-active actuator is the basis for the semi-active element used here. A general model for this device (Patten, et al., 1998) (Kuehn and Stalford, 2000) (Kuehn, 2000) is

$$\dot{y} = A_{sa}x - B_{sa}(y)yu\,. \tag{2.2}$$

A_{sa} is a system matrix, $B_{sa}(y)$ is a function of the semi-active state that depends on whether the flow is turbulent or laminar, and u is the input control variable to the system, which varies from a value of 0 (i.e., control valve is closed) to a value of 1 (i.e., the control valve is open). This is shown schematically in Figure 2.2a.

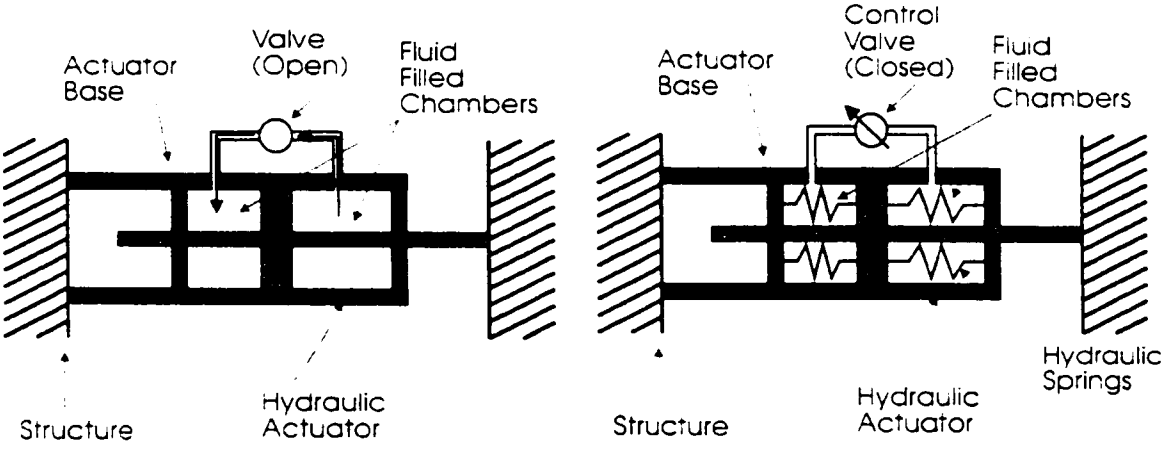

Figure 2.2a: Schematic diagram of a nonlinear hydraulic semi-active actuator

We will discuss the characteristics of $B_{sa}(y)y$ for hydraulic semi-active devices later in this section. In the context of the actual hydraulic actuator, the state y is the differential pressure between chambers, and u is the normalized valve area connecting the chambers. Qualitatively, when the valve is open ($u=1$) the actuator state is a linear function of the structural system states and a nonlinear function of the actuator state

itself, depending on the flow regime. When the valve is closed ($u=0$) the actuator state is a linear function of the structural system states only. The semi-active actuator affects the vibration of the system to which it is attached by modulating between these two control valve positions.

There are many types of semi-active actuators other than hydraulic ones. Adjustable friction devices and semi-active magnetorheological devices are two examples. The model in (2.2) can easily be extended to encompass many of these other types of devices. The work in this dissertation, however, focuses on the model for bi-state hydraulic semi-active actuators.

To apply the model (2.2) to specific semi-active systems we must design a model for $B_{sa}(y)$ that represents the dynamics of the specific system. In this dissertation we will focus on variable orifice hydraulic semi-active actuators. These actuators use a valve connecting the two chambers of the hydraulic actuator to regulate the flow between them. Such actuators have received extensive attention as discussed in Section 2.1.

Modeling of such actuators has been treated recently in Kuehn (2000), and Kuehn and Stalford (2000). In that work the authors assumed that the variation of the volume in each chamber was small, and the bulk modulus of the hydraulic oil was constant. In that case, using differential pressure as the semi-active state y in (2.2), the model for $B_{sa}(y)y$ is

$$B_{sa}(y)y = \alpha_0 C_d(y)\sqrt{\frac{2}{\rho|y|}}y, \tag{2.3}$$

where α_0 is a constant that depends on the actuator geometry and the hydraulic fluid properties, $C_d(y)$ is the valve discharge coefficient that is a function of the differential

pressure, y, and ρ is the hydraulic oil density. The behavior of the discharge coefficient is reasonably well known for simple orifice configurations (Merritt, 1967). Typically, the discharge coefficient exhibits varying characteristics depending on whether the flow regime is laminar, transitional, or turbulent. A characterization of the coefficient of discharge from experimental studies conducted on a semi-active hydraulic device is shown in Figure 2.2b. The coefficient of discharge in the figure is plotted against the nondimensional choke number. The choke number is a function of the Reynolds number Re, the hydraulic diameter of the orifice D_h and the length of the orifice L.

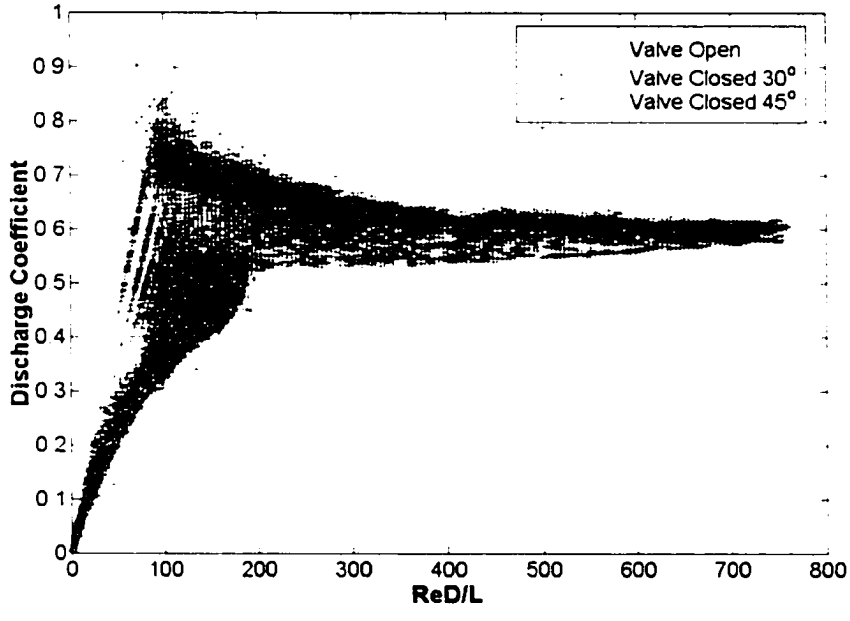

Figure 2.2b: Experimental Valve Discharge Coefficient vs. Choke Number (Kuehn, 2000)

One approximate model for the behavior of the discharge coefficient was proposed by Kuehn and Stalford (2000). For laminar flow

$$C_d(y) = k|y|^{1/2}, \quad 0 \le |y| \le y_1. \tag{2.4}$$

In the transition from laminar to turbulent flow

$$C_d(y_1) \le C_d(y) \le C_{d_{max}}, \quad y_1 \le |y| \le y_2. \tag{2.5}$$

In the turbulent region

$$C_d(y) = C_{d2}, \quad y_2 \le |y|. \tag{2.6}$$

This assumes that $C_d(y_1) \le C_{d2}$. Combining this approximation for the discharge coefficient with the model in (2.2) and (2.3) gives a nonlinear model. For laminar flow

$$\dot{y} = A_{ad}x - \alpha_0 k\sqrt{\frac{2}{\rho}}yu. \tag{2.7}$$

For transition flow we cannot write the actual model without better understanding the discharge coefficient in that flow regime. This typically comes from experimental data similar to Figure 2.2. For turbulent flow

$$\dot{y} = A_{ad}x - \alpha_0 C_{d2}\sqrt{\frac{2}{\rho|y|}}yu. \tag{2.8}$$

Typically, the nonlinear model is simplified to treat only the turbulent flow regime. Work by Mo, et al. (1996) indicated that a model assuming only turbulent flow in the form (2.8) accurately predicts differential pressure in experiments with semi-active hydraulic control systems. Equation (2.8) is a final nonlinear model for the hydraulic semi-active actuator. This model of the nonlinear semi-active actuator can also be simplified into linear and affine models for a simplification of later analysis.

2.4 Affine Model of Semi-Active Actuator Dynamics

An affine approximation of the nonlinear actuator dynamics can be constructed. This is a simplification of the nonlinear dynamics that allows some analysis techniques to be used on the system that are not applicable to nonlinear dynamics. Specifically,

methods in Chapter 6 will be discussed that are applicable to this type of approximate system.

We will not, in fact, be constructing an affine approximation of (2.2) but rather an affine approximation of part of the term on the right hand side, $B_u(y)y$. This will allow the development of an affine approximation for (2.2) if u is held fixed. Since we are interested here in bang-bang semi-active systems, u will be held constant most of the time.

The affine model of $B_u(y)y$ has the form

$$B_u(y)y \approx by + a, \tag{2.9}$$

where b and a are constants. This is probably best shown with an example. For this example, we will assume that the transition region is small enough to be negligible, since we do not have a reasonable model for that region. Thus, we will only have a turbulent region and a laminar region. This can be seen in Figure 2.3, where the laminar region is $|y| \le 20$ and the turbulent region is $|y| > 20$. We will then try to approximate the nonlinear behavior shown with affine approximations.

The nonlinear behavior in Figure 2.3 is as follows.

$$\begin{aligned} B_u(y)y &= 0.223y, \ |y| \le 20 \\ B_u(y)y &= \sqrt{\frac{1}{|y|}}y, \ |y| > 20 \end{aligned} \tag{2.10}$$

These are simple versions of the model in (2.3) with the approximations (2.4) and (2.6).

Now, to approximate this with an affine approximation like (2.9), we actually have to split this up into regions and use an approximation on each of these regions. Figure 2.4 shows an affine approximation constructed to approximate (2.10).

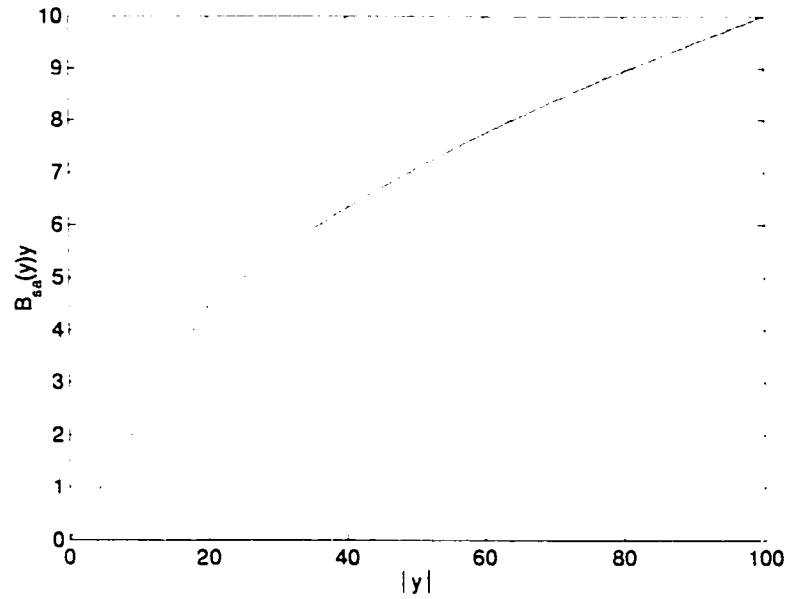

Figure 2.3: Example Nonlinear Behavior

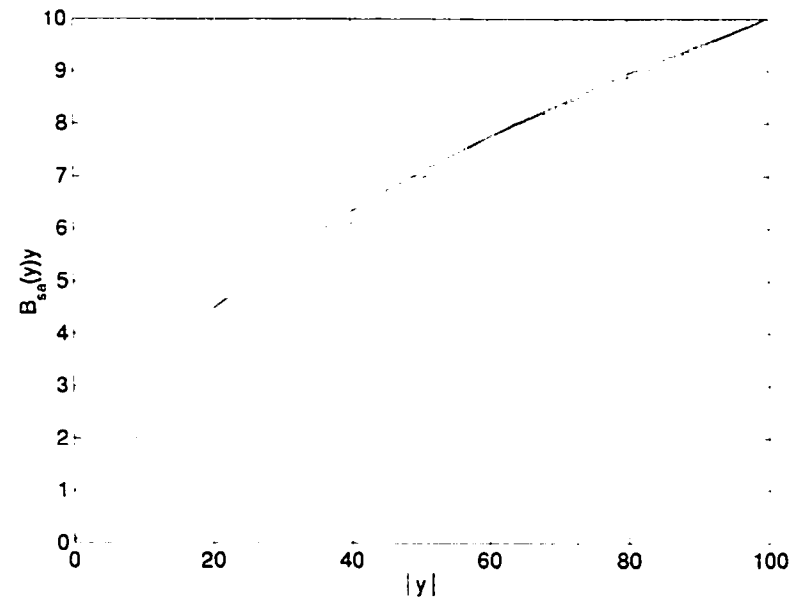

Figure 2.4: Example Nonlinear Behavior with Affine Approximation in Red

This affine approximation can be written as

$$\begin{aligned} B_{va}(y)\,y &= 0.223y, \ |y| < 20 \\ B_{va}(y)\,y &= 0.082y + 2.84, \ 20 \le |y| < 60 . \\ B_{va}(y)\,y &= 0.056y + 4.36, \ |y| \ge 60 \end{aligned} \tag{2.11}$$

Note that for the region where the flow is laminar the affine approximation is linear, since the offset constant a in the affine definition (2.9) is zero. Using this affine approximation, the model for the semi-active hydraulic actuator can be rewritten as

$$\dot{y} = A_{va}x - (by + a)u, \quad y_1 \le |y| < y_2 . \tag{2.12}$$

In this way, affine models are developed for nonlinear hydraulic semi-active actuators. Such affine approximations can be used to simplify the nonlinear model without significant loss of information about the dynamics. We can also go one step further and use a linear approximation for these dynamics.

2.5 Linear Model of Semi-Active Actuator Dynamics

In its simplest form, the actuator dynamics in (2.2) can be represented as a single linear approximation on the whole length of $|y|$. This model will be used extensively in the following chapters, as this simplest form allows the application of much more theory based on linear systems.

As in the section on affine approximations above, we are not linearizing the actuator dynamics directly but rather linearizing the term $B_{va}(y)y$. This will give us linear actuator dynamics when u is held fixed.

The linear model of $B_{va}(y)y$ has the form

$$B_{va}(y)y \approx by , \tag{2.13}$$

where b is a constant. This is probably best shown with an example. Here we will use the same example as we used for the affine approximations above. Figure 2.5 shows a linear approximation for the function shown in Figure 2.3 and described in (2.10). If we compare Figure 2.5 to Figure 2.4, it is obvious that the affine approximation does a much better job of capturing the actual trends in the function.

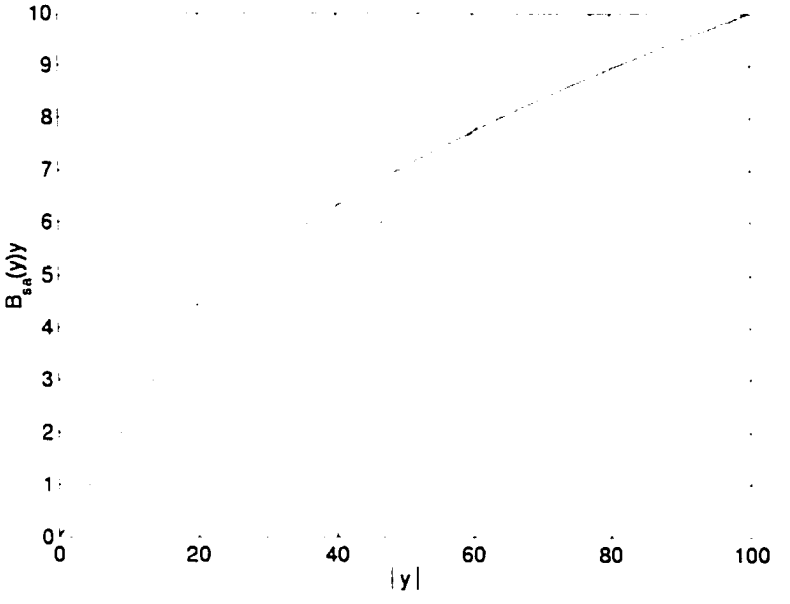

Figure 2.5: Example Nonlinear Behavior with Linear Approximation in Red

This linear model can be written as

$$B_{sa}(y)y = 0.13y. \tag{2.14}$$

Essentially, this means that the value of $B_{sa}(y)$ is a constant, and the new linear approximation for the semi-active hydraulic actuator can be written as

$$\dot{y} = A_{sa}x - byu. \tag{2.15}$$

This linear approximation for the actuator dynamics will be used in later chapters. For stability, we took the worst case slope. The worst case performance can be bounded when we use this worst case slope.

2.6 Structural System with Nonlinear Actuator Dynamics

The models for the structure and the semi-active actuator are combined in this section. A complete model is developed that can be used to observe the dynamics associated with a semi-active actuator installed in a structure.

We start by defining a new state vector that is a combination of the structural states and the semi-active actuator states.

$$z = \begin{bmatrix} x & y \end{bmatrix}^T . \tag{2.16}$$

We use this new state vector to combine the linear model of the structure (2.1) with the nonlinear model of the semi-active actuator (2.2). The combined system can be written as

$$\dot{z} = Az + B\left(\delta y u_{\max} - B_{va}(y) y u\right) + Dd , \tag{2.17}$$

where

$$\begin{aligned} A &= \begin{bmatrix} A_s & B_s \\ A_{va} & -\delta u_{\max} \end{bmatrix} \\ B &= \begin{bmatrix} 0 \\ 1 \end{bmatrix} \\ D &= \begin{bmatrix} D_s \\ 0 \end{bmatrix} \end{aligned} , \tag{2.18}$$

and δ is the largest lower bound of $B_{va}(y)$ (Kuehn and Stalford, 2000). The model in (2.17) and (2.18) is a general nonlinear model for a semi-active actuator installed in a

structure. In this dissertation, we assume that A_s, B_s, and A_{sa} are such that the matrix A is stable for all positive values of δu_{max}.

Since we are interested in bang-bang controllers, we assume that the valve area can take on only values of 1 or 0. If we set $u=0$, which corresponds to the closed valve case, and do some rearranging, we get a simplified system description

$$\dot{z} = \begin{bmatrix} A_s & B_s \\ A_{sa} & 0 \end{bmatrix} z + \begin{bmatrix} D_s \\ 0 \end{bmatrix} d. \tag{2.19}$$

In this dissertation we consider systems that have a pole at the origin whenever the valve is closed. For real systems with a closed valve, the A matrix in (2.19) usually has a pole at the origin. For such a case, the system is marginally stable since A_s is stable. There is no simplification of (2.17) and (2.18) in the open valve case where $u=1$.

2.7 Structural System with Affine Actuator Dynamics

Starting with the same combined state vector (2.16) as we used for the fully nonlinear model above and combining (2.1) and (2.12), we can write the system dynamics in some range of $|y|$ as

$$\dot{z} = Az + B(\delta y u_{max} - (by + a)u) + Dd, \quad y_1 \le |y| < y_2, \tag{2.20}$$

where the system matrices are given by (2.18), and b and a are scalar constants based on the affine approximation of the term $B_{sa}(y)y$ from equation (2.2), as shown in Section 2.4.

Again, allowing u to take on only two values, the system dynamics in (2.20) can be simplified for these two values. When $u=0$ we again get the system dynamics shown

in (2.19), which in the worst case has a pole at the origin, making the system marginally stable. When $u=1$ we can rewrite (2.20) as

$$\dot{z} = \begin{bmatrix} A_{11} & B_1 \\ A_{21} & -b \end{bmatrix} z - \begin{bmatrix} 0 \\ a \end{bmatrix} + \begin{bmatrix} D_1 \\ 0 \end{bmatrix} d, \quad y_1 \le |y| < y_2 . \tag{2.21}$$

For $b>0$ the A matrix in (2.21) is stable by previous assumption. Even for zero disturbance, its equilibrium point is offset from the origin due to the affine nature of the approximation for the semi-active actuator dynamics.

Making use of the example affine approximation in (2.11) and assuming that we have a structure described by (2.1), we can write the overall system dynamics for our example with $u=0$ as (2.19) and the overall system dynamics with $u=1$ as

$$\begin{aligned} \dot{z} &= \begin{bmatrix} A_{11} & B_1 \\ A_{21} & -0.0223 \end{bmatrix} z + \begin{bmatrix} D_1 \\ 0 \end{bmatrix} d, \quad |y| \le 20 \\ \dot{z} &= \begin{bmatrix} A_{11} & B_1 \\ A_{21} & -0.0082 \end{bmatrix} z - \begin{bmatrix} 0 \\ 2.84 \end{bmatrix} + \begin{bmatrix} D_1 \\ 0 \end{bmatrix} d, \quad 60 \ge |y| < 20 . \\ \dot{z} &= \begin{bmatrix} A_{11} & B_1 \\ A_{21} & -0.0056 \end{bmatrix} z - \begin{bmatrix} 0 \\ 4.36 \end{bmatrix} + \begin{bmatrix} D_1 \\ 0 \end{bmatrix} d, \quad |y| > 60 \end{aligned} \tag{2.22}$$

Thus, the system dynamics are affine when we set $u=1$. In fact, in the region closest to the origin, the dynamics are linear and stable to the origin. Even though the dynamics are affine, the systems motion is attracted to the origin asymptotically (Kuehn, 2000).

2.8 Structural System with Linear Actuator Dynamics

Finally, we combine the structural system (2.1) and the linear approximation for the semi-active actuator dynamics (2.15). Using the new state vector (2.16) we write the combined system dynamics with linear actuator dynamics as

$$\dot{z} = Az + B(\delta y u_{\max} - byu) + Dd , \tag{2.23}$$

where the system matrices are given by (2.18) and b is a scalar constant based on the linear approximation of the term $B_{wa}(y)y$ from equation (2.2) as shown in Section 2.5.

We rewrite the system (2.23) for the two cases corresponding to the two values that u can assume. For $u=0$ we again have the dynamics in (2.19), and, assuming that we have a pole at the origin, the system is marginally stable. If $u=1$ we can reduce the system to

$$\dot{z} = \begin{bmatrix} A_{11} & B_{11} \\ A_{wa} & -b \end{bmatrix} z + \begin{bmatrix} D_{11} \\ 0 \end{bmatrix} d, \tag{2.24}$$

which is stable by previous assumption.

Following our example from Section 2.5, where the actuator dynamics are modeled as (2.14), we get

$$\dot{z} = \begin{bmatrix} A_{11} & B_{11} \\ A_{wa} & -0.13 \end{bmatrix} z + \begin{bmatrix} D_{11} \\ 0 \end{bmatrix} d. \tag{2.25}$$

Throughout most of the rest of this dissertation, the linear model (2.23) will be used for the system analysis.

2.9 Stability of Semi-Active Control System with Nonlinear Actuator Dynamics

In this section, we derive a control law based on Lyapunov arguments that stabilizes systems of the form (2.17). This control law is typically called a quickest descent control law in the literature. Since the system dynamics with the affine approximation (2.20) and the system dynamics with the linear approximation (2.23) have the form (2.17), it follows from Kuehn and Stalford (2000) that the derived control law will stabilize the system in question regardless of which approximation we use.

The quickest descent control law is essentially a bang-bang controller that tries to maximize the energy loss from the system through the semi-active nonlinear actuators (Vincent and Grantham, 1997). To derive this control law, one begins with a quadratic Lyapunov function, which represents some measure of the energy in the system

$$V = z^T P z, \tag{2.26}$$

where z is the coupled state vector (2.16) for the linear structural system and the nonlinear actuators, and P is a symmetric positive definite weighting matrix that is yet to be determined. The time rate of change of this function can be seen as some measure of the rate of change of energy in the system.

$$\dot{V} = z^T P \dot{z} + \dot{z}^T P z . \tag{2.27}$$

Then, substituting the nonlinear coupled system equation (2.20) gives

$$\dot{V} = z^T \left(PA + A^T P\right) z + 2 z^T P B \delta y u_{\max} - 2 z^T P B B_{ia}(y) y u + 2 z^T P D d . \tag{2.28}$$

To dissipate the maximum amount of energy from the system at all times, the right hand side of this equation must be minimized at all times. Since the control logic can adjust only the third term on the left side, and noting that $B_{ia}(y)$ is always positive, it is easy to see that the control logic

$$u = \begin{cases} 0 & \text{if } z^T P B y < 0 \\ u_{\max} & \text{if } z^T P B y \geq 0 \end{cases} \tag{2.29a}$$

will make the equation as negative as possible. Interestingly, this actually means that there are two switching surfaces defined by the control law. Their normals are PB and $\left[0_{(n-1)} \quad 1\right]^T$. This second vector is most often just B from equation (2.17). This is not true in one case in Chapter 4, but we can transform the system so that it is. The value of the control u depends on where in space a trajectory is located relative to these switching

surfaces. This will become important later when we will need to partition the space to reduce the problem to linearized systems in certain regions. We will have to at least partition the space at these switching surfaces so that, in each region, we will no longer be dealing with a discontinuous system.

For the methodologies in Chapter 6, it will be more useful to describe the regions in the control law as quadratic regions with symmetric descriptions in some cases. Since $B^T z = y$ we can rewrite (2.29a) as

$$u = \begin{cases} 0 & \text{if } z^T \left(PBB^T\right) z < 0 \\ u_{\max} & \text{if } z^T \left(PBB^T\right) z \geq 0 \end{cases}. \tag{2.29b}$$

We see that the control law (2.29b) can be written in the form

$$u = \begin{cases} 0 & \text{if } z^T Rz < 0 \\ u_{\max} & \text{if } z^T Rz \geq 0 \end{cases}, \tag{2.29c}$$

where $R = \left(PBB^T + BB^T P\right)$ is symmetric.

If the P matrix is formed in a particular way, this control law will guarantee a stable system (Kuehn and Stalford, 2000). First, the time rate of change of the Lyapunov function (2.28) is rewritten in the form

$$\dot{V} = -z^T Qz + 2z^T PB\delta y u_{\max} - 2z^T PBB_{sd}(y) yu + 2z^T PDd, \tag{2.30}$$

where Q is defined as

$$Q = -(PA + A^T P). \tag{2.31}$$

It can be shown that for a positive definite Q and a stable system matrix A, this equation can be solved for a unique positive definite P. This value of P can then be used in equations (2.26) to (2.29) to determine the control logic. Since the nonlinear model of the system that is described in equation (2.17) and (2.18) guarantees that A is stable, a

solution can be found and used for the control logic. The resulting control law will be stable to a ball around the origin for bounded disturbances.

We can show that the control law in (2.29) stabilizes the system described in (2.17) and (2.18) in the following way. The Lyapunov derivative function that is written for the quickest descent control law is shown in (2.28), and the resulting control logic is shown in (2.29). We will start by looking at the term in the Lyapunov derivative equation that is effected by the control law.

Proposition 2.1

Considering the Lyapunov function derivative in (2.28), and recalling (2.29), an upper bound on the Lyapunov function is

$$\dot{V} \le -z^T Qz + 2z^T PDd\,, \tag{2.32}$$

for all z that satisfy the system in (2.17) and (2.18).

Proof

It suffices to show that the following is always true

$$2z^T PB\left(\delta y u_{\max} - \overline{B}(y) yu\right) \le 0\,. \tag{2.33}$$

From the definition of the system (2.17) and (2.18) we know that

$$\delta \le B_{\omega}(y). \tag{2.34}$$

From the control law in (2.29) we have three cases:

Case 1: $z^T PBy < 0$

In this case the control law sets $u=0$. Therefore,

$$2z^T PB\left(\delta y u_{\max} - \overline{B}(y) yu\right) = 2z^T PB\delta y u_{\max}\,, \tag{2.35}$$

and, since δ is nonnegative, we have (2.33).

Case 2: $z^T PBy > 0$

In this case the control law sets $u = u_{\max}$. Therefore,

$$2z^T PB(\delta y u_{\max} - \overline{B}(y) y u) = 2z^T PB(\delta y - \overline{B}(y) y) u_{\max}. \tag{2.36}$$

and, since δ is a lower bound for $\overline{B}(y)$, we have (2.33).

Case 3: $z^T PBy = 0$

In this case, regardless of what the control law does, (2.33) is satisfied as

$$2z^T PB(\delta y u_{\max} - \overline{B}(y) y u) = 2z^T PBy(\delta u_{\max} - \overline{B}(y) u) = 0. \tag{2.37}$$

Now we must define several elliptical regions and some related values. A slight change in the Lyapunov function bound in Proposition 2.1 is accomplished with the following change of variables.

$$z_d = 2Q^{-1} PDd. \tag{2.38}$$

This leads to the new bound on the Lyapunov function derivative

$$\dot{V} \le -z^T Qz + z^T Q z_d. \tag{2.39}$$

Definition 2.1

For the value

$$V_{d_{\max}} = \max\{z_d{}^T Q z_d : |d| < d_{\max}\}, \tag{2.40}$$

define the ellipse

$$E_{V_{d_{\max}}} = \{z \in \Re^{n+1} : z^T Qz \le V_{d_{\max}}\}. \tag{2.41}$$

Definition 2.2

Let V_{min} be the minimum value of σ such that if $z^T Qz \le V_{d_{\max}}$ then $z^T Pz \le \sigma$ and define the ellipsoid

$$E_{\min} = \left\{ z \in \Re^{n+1} : z^T P z \le V_{\min} \right\}. \tag{2.42}$$

Finally we can construct the following proposition.

Proposition 2.2

For some bounded disturbance, $|d| \le d_{\max}$, the control law in (2.29) provides quadratic convergence to the ellipsoid E_{min}. In particular, if $z \notin E_{1,d_{\max}}$ then

$$\dot{V}(z) < (\lambda - 1)^2 V_{d_{\max}}, \tag{2.43}$$

where

$$\lambda = \sqrt{\frac{z^T Q z}{V_{d_{\max}}}} > 1. \tag{2.44}$$

Proof

Refer to Kuehn, 2000 and Kuehn and Stalford, 2000.

Thus the system (2.17) and (2.18) with the control law (2.29) is guaranteed to be stable to the ellipsoid E_{min} if it is outside that ellipsoid. The control law will stabilize any system that can be written as (2.17) and (2.18) where the A matrix is stable. This includes both systems with an affine approximation (2.20) and systems with a linear approximation (2.23). Thus, if we design a control logic in this way for one of these systems, that control law will stabilize any of them.

2.10 Piecewise Affine Model

For the work that follows in this dissertation, we present a general way to describe the semi-active system dynamics with the affine approximation in the case where a control logic has been designed. We define regions in the state space where the system description is constant and just switch between these constant systems at the region

boundaries. Since the control logic in (2.29) actually defines regions in the system space where u is constant, it seems logical to use these regions to define a unified system description. In the affine case, we also need to use the regions of the space that are defined by the affine approximation (e.g. (2.22)). So, a general system description that is constant in regions of space can be written as

$$\dot{z} = A_i z + a_i + Dd, \quad z \in X_i, \tag{2.45}$$

where X_i is a region of the state space that can be defined so that the system matrices are constant in this region. The regions X_i can be unbounded but must satisfy

$$\bigcup_i X_i = X. \tag{2.46}$$

where X is the whole state space $\Re^n$.

If we return to our affine approximation example from (2.21) and (2.22) and assume that some control of the form (2.29) has been designed for it, we can show how this system would be split into regions X_i. First note that two planes, whose normals are PB and B, define the control logic. Also, the affine approximation in (2.22) defines some further planes across which the dynamics change, $|y| = 20$ and $|y| = 60$. So, the region where the valve is closed with $u=0$ would be defined as

$$X_0 = \left\{ z \middle| z^T \left(PBB^T \right) z < 0 \right\}. \tag{2.47}$$

Since $u=0$ everywhere in this region we can set

$$\begin{aligned} A_0 &= \begin{bmatrix} A_s & B_s \\ A_{sa} & 0 \end{bmatrix} \\ a_0 &= \begin{bmatrix} 0 \\ 0 \end{bmatrix} \\ D &= \begin{bmatrix} D_s \\ 0 \end{bmatrix} \end{aligned} \quad . \tag{2.48}$$

In the region of space where $u=1$ we will need to further subdivide into the regions defined in (2.22). This leads to

$$\begin{aligned} X_1 &= \left\{z \middle| z^T\left(PBB^T\right)z \geq 0 \text{ and } |y| \leq 20\right\} \\ X_2 &= \left\{z \middle| z^T\left(PBB^T\right)z \geq 0 \text{ and } 20 < |y| \leq 60\right\}, \\ X_3 &= \left\{z \middle| z^T\left(PBB^T\right)z \geq 0 \text{ and } |y| > 60\right\} \end{aligned} \tag{2.49}$$

and, from the equations in (2.22), we have

$$\begin{aligned} A_1 &= \begin{bmatrix} A_s & B_s \\ A_{su} & -0.0223 \end{bmatrix}, \quad a_1 = \begin{bmatrix} 0 \\ 0 \end{bmatrix} \\ A_2 &= \begin{bmatrix} A_s & B_s \\ A_{su} & -0.0082 \end{bmatrix}, \quad a_2 = \begin{bmatrix} 0 \\ 2.84 \end{bmatrix}, \\ A_3 &= \begin{bmatrix} A_s & B_s \\ A_{su} & -0.0056 \end{bmatrix}, \quad a_2 = \begin{bmatrix} 0 \\ 4.36 \end{bmatrix} \end{aligned} \tag{2.50}$$

and D is the same as the $u=0$ case. This is, of course, the simplest way to subdivide the system space. We can also subdivide each of these subdivisions to get more regions. This is essentially similar to a finite element mesh where the domain of the problem is divided into small elements and some approximation function is used in each element. The method for describing the semi-active system with an affine approximation in regions, as shown in (2.45), can be used to approximate a nonlinear system to an arbitrary accuracy if enough regions are used.

2.11 Piecewise Linear Model

We can also write a general system description in terms of piecewise linear systems to approximate the controlled semi-active dynamic system. Here, we will use regions similar to those in the last section, but the system dynamics in each region will be linear rather than affine. This can be written as

$$\dot{z} = A_i z + Dd, \quad z \in X_i. \tag{2.51}$$

where X_i is a region of the state space that can be defined so that the system matrices are constant in this region. The regions X_i can be unbounded but must satisfy

$$\bigcup_i X_i = X. \tag{2.52}$$

where X is the whole state space $\Re^n$.

If we return to our linear example in (2.24) and (2.25) and assume that we have designed a control logic according to (2.29), we can rewrite the system in terms of (2.51). In the linear case, we only have regions defined by the planes of the control law, PB and B. We can write the region where $u=0$ as

$$X_0 = \left\{ z \middle| z^T \left(PBB^T \right) z < 0 \right\}, \tag{2.53}$$

where

$$\begin{aligned} A_0 &= \begin{bmatrix} A_s & B_s \\ A_{sa} & 0 \end{bmatrix}, \\ D &= \begin{bmatrix} D_s \\ 0 \end{bmatrix} \end{aligned} \tag{2.54}$$

and the region where $u=1$ as

$$X_1 = \left\{ z \middle| z^T \left(PBB^T \right) z \geq 0 \right\}, \tag{2.55}$$

where

$$\begin{aligned} A_1 &= \begin{bmatrix} A_s & B_s \\ A_{sa} & -0.13 \end{bmatrix}, \\ D &= \begin{bmatrix} D_s \\ 0 \end{bmatrix} \end{aligned} \tag{2.56}$$

This piecewise linear system can be subdivided further as in the case of the piecewise affine system, but the accuracy of the approximation does not improve as it would in the

affine case. This further subdivision will become necessary in Chapter 6 for the application of linear matrix inequalities (LMI) to semi-active control problems.

These systems also exhibit a type of symmetry that will be used in later chapters. Both the regions defined by the control law and the system dynamics exhibit this behavior. The symmetry is defined as follows.

Definition 2.3 (Radial Symmetry)

A set of points, S, is radially symmetric provided $x \in S$ iff $-x \in S$.

It is obvious that this applies to the regions defined by the control laws as shown in the following Proposition.

Proposition 2.3 (Radial Symmetry of the Open and Closed Valve Regions)

$$\begin{aligned} X_0 &= \{x | xPBx_3 < 0\} \\ X_1 &= \{x | xPBx_3 \geq 0\} \end{aligned} \tag{2.57}$$

are each radially symmetric. The proof of this is trivial.

This will be very useful in the developments of Chapter 7.

To summarize, the piecewise linear class of semi-active control problems treated in this dissertation has the following properties.

1. $A_0 = A_1 + BB^T T\sigma$, where $\sigma = -A_1(n,n)$ and B is a unit vector in the ξ_n direction. T is a state transformation matrix that is usually the identity matrix. In some cases, it will be set to something else. It will be used in Section 4.3.
2. A_1 is a stable matrix.
3. A_0 has one pole at the origin and all other eigenvalues are stable.
4. The region where the valve is closed ($u=0$) is denoted as $X_0 = \{z | z^T Rz < 0\}$, where $R = (PBB^T T + T^T BB^T P)$ and $P>0$.

5. The region where the valve is open ($u=1$) is denoted as $X_0 = \{z | z^T Rz \geq 0\}$ where $R = \left(PBB^T T + T^T BB^T P\right)$ and $P>0$.

6. The regions in 4 and 5 are both radially symmetric.

2.12 Summary

In this chapter, we developed the piecewise linear (2.51) and piecewise affine (2.45) system approximations that will be used in subsequent chapters to find some bound on the desired system performance. We developed these piecewise models based on regions defined by a quickest descent control law that guarantees system stability for the nonlinear system as well as for the approximations derived. The control logic for this type of controller is designed by choosing a Q matrix and solving Lyapunov's equation (2.31) for a P matrix, which in turn defines a control logic in (2.29). Currently, there is no method for choosing an effective Q matrix other than guessing and checking. The work in this dissertation is focused on finding a specific performance index that will allow one to compare the relative value of Q matrices with respect to system performance. This problem is defined in detail in Chapter 3.

CHAPTER 3

DESCRIPTION OF PERFORMANCE PROBLEM

In this chapter, we will describe in detail the performance problem that we are addressing in this dissertation. This will include a discussion of various performance measures and how to calculate them. We will also discuss various system descriptions that are commonly used in relation to such performance measures. This will provide a framework for describing what has and has not been done in the past. Finally, at the end of the chapter, we will specifically define the performance problem in which we are interested.

Our real interest is to find some means of calculating the peak system output for some bounded peak input for the class of semi-active control systems described in Chapter 2. To accomplish this, our major focus will be on the problem of bounding this value for piecewise linear systems. The problem of bounding this value for piecewise affine systems that approximate the nonlinear semi-active system will also receive some attention.

The literature background for this subject will be presented in Section 3.7, after sufficient introductory material has been covered.

3.1 Definition of Signal Norms

System performance can be characterized in many ways. For the work here, we are interested in a particular measure of the output signal when the system has some bounded disturbance acting on it. Two common ways of presenting this information for

the input or output signals are signal energy and signal peak. The signal energy is defined using the signal 2-norm as follows.

Definition 3.1 (Signal 2-Norm for Finite Energy)

For some signal in time, $y(t)$, the signal 2-norm, if it exists, is defined as

$$\|y\|_2 = \left[\int_0^\infty (y(t))^2 dt\right]^{\frac{1}{2}}. \tag{3.1}$$

The peak value of the signal is defined next by the signal ∞-norm.

Definition 3.2 (Signal ∞-Norm for Bounded Signals)

For some signal in time, $y(t)$, the signal ∞-norm, if it exists, is defined as

$$\|y\|_\infty = \sup_t |y(t)|. \tag{3.2}$$

These two indicators of performance can actually give very disparate pictures of a signal. Take, for example, the two graphs in Figure 3.1. These two plots show two signals where the energy in the signals are equal, as indicated by the 2-norm, but the peak response varies widely, as indicated by the ∞-norm. The first graph has a very large initial peak and quickly dies away, while the second dies away so slowly that one can hardly tell that it is decaying.

In using one of the signal norms above as a measure of performance for the output of a system, it is important to keep in mind the critical engineering issues involved. Choosing the energy based performance measure, such as that shown in (3.1), when the critical issue is the peak signal value, can be disastrous. This can be particularly true when approaching yield strength of materials in a building excited by an earthquake, for example. The work here focuses on just such a problem. We are considering a structural system with a semi-active actuator installed, as modeled in Chapter 2.

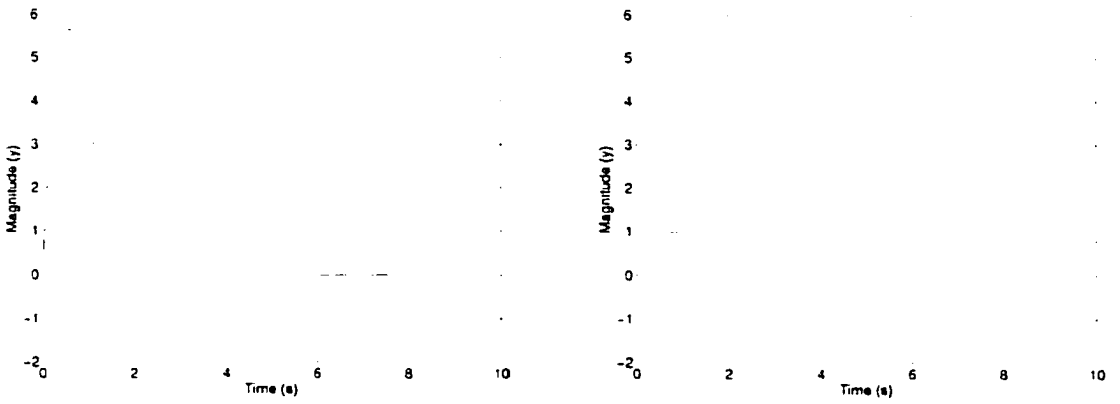

$\|y\|_2 = 15.81$
$\|y\|_\infty = 5.66$

$\|y\|_2 = 15.81$
$\|y\|_\infty = 0.54$

Figure 3.1: Comparison of Signals with Equal Energy and Disparate Peaks

3.2 Definition of System Norms

In this section, we will look at several definitions for system norms that can be applied to linear systems. For the system norms defined below, the stable system *G(s)* in question is in the form shown in Figure 3.2 below.



Figure 3.2: Input/Output System Model

Using this system, the system H_∞-norm can be defined as

Definition 3.3 (System H_∞-Norm for Stable LTI Systems)

For the stable LTI system where

$$y(s) = G(s)d(s), \tag{3.3}$$

the system H_∞-norm is defined as

$$\|G\|_\infty = \sup_\omega |G(j\omega)|. \tag{3.4}$$

This norm then can be used to calculate a tight bound for the ratio of the output signal 2-norm to the input signal 2-norm. This is shown in the following proposition.

Proposition 3.1

For system (3.3) the system H_∞-norm shown in Definition 3.3 is a tight bound on

$$\sup_{\|d\|_2 \le 1} \|y\|_2 \equiv \|G\|_\infty. \tag{3.5}$$

Proof

Refer to Zhou and Doyle (1998)

This norm is defined and used for a large variety of systems and is used extensively in dynamics and control theory. It can predict the maximum energy gain across a system for a huge variety of linear problems. It cannot, however, predict the peak system value in which we are interested. So, we will move on to discuss the system 1-norm.

Definition 3.4 (System 1-Norm)

For a stable LTI single-input-single-output (SISO) system where

$$y(s) = g(s)d(s). \tag{3.6}$$

which has an impulse response $g(t)$, the system 1-norm for unit peak inputs is defined as

$$\|g\|_1 = \int_{-\infty}^{\infty} |g(\tau)| d\tau. \tag{3.7}$$

Then, this can be used to find a tight bound on the ratio of the input peak to the output peak for the system (3.6).

Proposition 3.2

For the system (3.6), the system 1-norm shown in Definition 3.4 is a tight bound on the ratio

$$\sup_{\|d\|_\infty \le 1} \|y\|_\infty \equiv \|g\|_1 . \tag{3.8}$$

Proof

Let there be some SISO LTI system with the following minimal state space representation

$$\begin{aligned} \dot{x} &= Ax + Dd \\ y &= Cx \end{aligned} . \tag{3.9}$$

This can be represented as a transfer function by

$$g(s) = C(sI - A)^{-1} D . \tag{3.10}$$

Let the impulse response of this system be *g(t)*. Then, the response of the system to an arbitrary disturbance can be written as the convolution integral

$$y(t) = \int_{-\infty}^{\infty} g(\tau) d(t - \tau) d\tau . \tag{3.11}$$

Then, taking the absolute value of this convolution gives

$$|y(t)| \le \int_{-\infty}^{\infty} |g(\tau) d(t - \tau)| d\tau \le \int_{-\infty}^{\infty} |g(\tau)| d\tau \cdot \|d\|_\infty = \|g\|_1 \|d\|_\infty . \tag{3.12}$$

which yields

$$\|y\|_\infty \le \|g\|_1 \|d\|_\infty . \tag{3.13}$$

This means that the system 1-norm is an upper bound for the ratio in (3.8). Next, we must show that this is a tight upper bound. To do this, we fix t and look at

$y(t)$. We pick the particular disturbance $d(t-\tau)=\text{sgn}(|g(\tau)|)$, which is obviously bounded by unity. From (3.11) this leads to

$$y(t)=\int_{-\infty}^{\infty}|g(\tau)|d\tau=\|g\|_1. \tag{3.14}$$

This then implies that

$$\|y(t)\|_\infty \geq y(t)=\|g\|_1. \tag{3.15}$$

Since the disturbance here is bounded by unity, we can see that the system 1-norm is a least upper bound for the ratio in (3.8).

Note again that this is applicable only to stable SISO LTI systems. Because of this fact, we cannot apply this technique to the class of piecewise linear semi-active control systems discussed in Chapter 2. The goal in this dissertation is to find a tight bound on the peak output in Proposition 3.2 for the piecewise linear semi-active controlled structural system described in Chapter 2. This more general problem is defined as follows:

Definition 3.5 (Peak-to-Peak Gain)

Given some general system having an output that is bounded for a bounded input (BIBO)

$$y(t)=f(x(t),d(t)), \tag{3.16}$$

where x is a vector of states and d is some disturbance vector, the peak-to-peak gain for this system is defined as

$$gain_{p2p}=\sup_{\|d\|_\infty\leq 1}\|y\|_\infty. \tag{3.17}$$

This is very similar to the ratio in (3.8), but, because we are defining (3.17) for a very general BIBO system, we cannot use the system 1-norm of Definition 3.4 unless the

system (3.16) is LTI. Currently, there is no general way to find the exact peak-to-peak gain for systems like (3.16). The work in this dissertation is concentrated on finding some way to determine a tight bound on the peak-to-peak gain for the class of piecewise linear semi-active control system defined in Section 2.11.

3.3 Definition of the Reachable Set

We define two types of reachable sets here. The first is the reachable set with a unit peak input, and the second is the reachable set with a unit energy input. Reachable set solutions of the first kind for piecewise linear systems of order higher than 2 are not available in the literature. Such reachable sets contain the peak response information that we seek in this dissertation. We will also define a related set called an attractor set. This has some similarity to the reachable set. Using a Lyapunov function and conditions we seek a bound that contains both of these sets.

We are interested in the reachable set with unit peak input specifically, because it quantifies the maximal system response to a bounded disturbance and contains the peak-to-peak gain information. The reachable sets can be defined as

Definition 3.6 (Reachable Set with Unit Peak Input)

For the system

$$\dot{x} = f(x(t), d(t)), \quad |d| \le 1, \tag{3.18}$$

the reachable set with unit peak input is the set of all $x(t)$ that satisfy (3.18) when $x(0) = 0$ and $t > 0$.

Definition 3.7 (Reachable Set with Unit Energy Input)

For the system

$$\dot{x} = f(x(t), d(t)), \quad \|d\|_2 \le 1. \tag{3.19}$$

the reachable set with unit energy input is the set of all $x(t)$ that satisfy (3.19) when $x(0) = 0$ and $t > 0$.

In the rest of this dissertation, when we refer to the reachable set with no qualifier on the input, we mean the reachable set with unit peak input. This is a very general description for the set that includes every possible trajectory of the system for a disturbance with a particular bound when the system starts at the origin. For a stable system, this set will be finite as $t \to \infty$. This idea has been around for many years and has been called by many names. With some slight changes in the definition, a bounded reachable set for the system in (3.18) is the same result as BIBO stability (Khalil, 1992), Lagrange stability (La Salle and Lefschetz, 1961), the stable attractor or ultimate boundedness result (Kuehn and Stalford, 2000), and total stability (Slotine and Li, 1991). All of these methods find some guaranteed output bound based on some bounded input.

The attractor set is another set that is slightly different from the reachable set. This is essentially the set to which the system will converge if it starts outside the set. The definition is as follows:

Definition 3.8 (Attractor Set)

Let S_A be a closed, bounded subset of $\Re^n$ that contains the origin $x = 0$, and let $x(t), 0 \le t < \infty$ be a trajectory of (3.18) for some initial condition $x(0) = x_0$. The set S_A is called an attractor set for the dynamical system (3.18) if the following conditions hold:

i. For the portion of the trajectory $x(t)$ belonging to $\Re^n \sim S_A$, it converges asymptotically to S_A.

ii. If the trajectory $x(t)$ belongs to S_A at any time t_1, then $x(t) \in S_A$ for all $t \geq t_1$.

The attractor set and the reachable set for the system (3.18) are very closely related but do not necessarily have to be the same set. For most of this dissertation, Lyapunov functions and conditions will be sought to find a bound on one or the other of these sets.

3.4 Stable LTI SISO Systems

Stable LTI systems have received considerable attention when it comes to developing methods for bounding the performance of the system. Two interesting results are the system 1-norm described in Section 3.2 and a method for finding reachable sets with unit energy inputs (Section 3.3) described in Boyd et al. (1994). Both of these methods are applicable only to stable LTI systems, so we cannot apply them to the piecewise linear semi-active controlled structural system from Chapter 2 in any of the forms discussed there. We can, however, apply these methods to the system where $u=1$ is held fixed (open valve case).

To apply the system 1-norm we must bound the peak input. Since we are looking for the peak-to-peak gain in general, we restrict the disturbance to be bounded by unity. The open valve system has the form

$$\begin{aligned} \dot{x} &= A_1 x + Dd, \quad |d| \leq 1, \quad A_1 \text{ stable} \\ y &= Cx \end{aligned} \tag{3.20}$$

where A_1 and D come from the linearized semi-active system described in Section 2.11, and d and y are scalar functions of time. The quantity C can be arbitrarily chosen so that application of the system 1-norm will give a peak-to-peak gain for any scalar linear combination of the system states. Since this is true, we can also use the system 1-norm repeatedly while we vary C to get bounds on the peak-to-peak gain for every scalar linear combination of the states. Using this technique, we will in fact be able to find a closed surface that bounds the response of the system (3.20). This will be shown in Chapter 4 when the example problems are introduced.

The method for bounding the output peak with a unit-energy input given by Boyd et al. (1994) requires a slight change in the system description from (3.20). Instead of using a peak bound on the input we will rewrite it as

$$\begin{aligned} \dot{x} &= A_1 x + Dd, \quad \|d\|_2 \le 1, \quad A_1 \text{ stable} \\ y &= Cx \end{aligned} \tag{3.21}$$

so that the system is in the form from Definition 3.7. With this system, the reachable set is the ellipsoid $\left\{x \middle| x^T W_c^{-1} x \le 1\right\}$ where W_c is the controllability Gramian defined by

$$W_c \equiv \int_0^\infty \left(e^{At} DD^T e^{A^T t}\right) dt. \tag{3.22a}$$

This can easily be solved for by solving the Lyapunov equation of the form

$$AW_c + W_c A = -DD^T. \tag{3.22b}$$

We will use this as an interesting comparison with the system 1-norm result for the open valve case when we describe our example systems in Chapter 4.

3.5 Description of the Performance Problem

For each stabilizing semi-active control law that is designed according to Section 2.8, we can get a piecewise linear approximation of the controlled semi-active system (Section 2.11). We want to find a tight bound on the peak-to-peak gain for this system with a unity bounded peak disturbance acting on it. Since we are interested only in the peak-to-peak gain for the semi-active structural system from Chapter 2, the reachable set defined above contains more information than is necessary. However, the maximum radius of this set corresponds to the peak-to-peak gain of the system in Definition 3.5. This means that any method to find the reachable set or a bound on the set will also give us the peak-to-peak gain information for which we are searching.

So far, the only tools available to us for constructing tighter bounds are ones that treat LTI systems. This means that, for the case where the valve is held open, we can get some results. Namely, we can use the system 1-norm to find an accurate value for the peak-to-peak gain of the open valve system. Then we can say that, since it should be possible to design semi-active controllers that outperform the open valve case, the performance bound for a good semi-active controller should have a value less than this benchmark norm. For our purposes here, this system 1-norm can be considered to be an upper bound for good semi-active controllers of the linearized system given in Chapter 2.

One tool that is available to us for finding bounds on the reachable set with unit peak input is the Lyapunov method of stability analysis. This method can be applied to linear and nonlinear systems alike and can be used to find a guaranteed bound on the system's reachable set. Unfortunately, there is no systematic way to apply this method nor is there any guarantee that the resulting bound will be tight. The method is as follows

Definition 3.8 (Lyapunov Stability Bound for the Reachable Set with Unit Peak Input)

Given a Lyapunov function V for the system (3.18), the reachable set with unit peak input is upper bounded by the surface $V=1$ if we have $dV/dt \leq 0$ for all x and d satisfying $V>1$ and (3.18).

Since we are in fact interested in the reachable set for the piecewise linear semi-active system from Section 2.11, we can in fact look at a continuous, piecewise C^1 Lyapunov function for that system. Referring back to the system descriptions in (2.51) and (2.53) to (2.56), the conditions in Definition 3.8 can be rewritten. Given a continuous, piecewise C^1 Lyapunov function defined by V_i on the regions $\mathcal{X}_i$, the reachable set with unit peak input for the system (2.51) and (2.53) to (2.56) is upper bounded in each region by the surface $V_i=1$ if we have $dV_i/dt \leq 0$ for all $x \in \mathcal{X}_i$ and d satisfying $V_i>1$ and (2.50). This is a problem of checking that one inequality holds when another also holds. This problem is in fact infinite dimensional. For the case where the Lyapunov functions are quadratic functions in the variable x, merely verifying that the conditions hold for a fixed Lyapunov function is as hard as solving a general indefinite quadratic program, which is NP-complete (Boyd et al., 1994). We will show a way to simplify this problem in Chapter 6 when we apply the method of linear matrix inequalities. Unfortunately, this simplification also introduces some conservatism in the problem.

3.6 Background

Before we present the various references for system performance, a list of system descriptions will be given for reference. This is done in an effort to help make clear what

has and has not been done for various systems. It also allows us to refer back to it when discussing various systems used in later chapters, so we do not have to redefine the system description each time.

The system descriptions that are relevant here or later in the dissertation are as follows. Throughout the descriptions below, u is the control input, d is the disturbance input, and x is the state vector. LTI systems with no control or disturbance are written as

$$\dot{x} = Ax, \quad A \text{ stable}. \tag{3.23a}$$

If there is some uncertainty in the A matrix this becomes

$$\dot{x} = A(t)x, \quad A(t) \text{ stable}. \tag{3.23b}$$

If the system is piecewise linear with no disturbances it becomes

$$\dot{x} = A_i x, \quad x \in X_i, \quad \bigcup_i X_i = X, \tag{3.23c}$$

where X is the whole space $\Re^n$. Next an LTI system with a disturbance is

$$\dot{x} = Ax + Dd, \tag{3.23d}$$

with A stable and $|d| \le 1$. LTI systems with the addition of a disturbance and/or control are written as

$$\dot{x} = Ax + Bu + Dd, \tag{3.24a}$$

with (A,B) controllable and (A,D) observable. With the addition of uncertainty in the system matrices this becomes

$$\dot{x} = A(t)x + B(t)u + D(t)d, \tag{3.24b}$$

with $(A(t),B(t))$ controllable and $(A(t),D(t))$ observable. A simpler version of this is also treated in the literature.

$$\dot{x} = A(t)x + D(t)d\,. \tag{3.24c}$$

where $(A(t), B(t))$ provide BIBO stability. There is also the general continuous and differentiable nonlinear dynamical system without disturbances or control

$$\dot{x} = f(x,t), \quad t \geq 0 \tag{3.25}$$

and the general continuous and differentiable nonlinear dynamical system with control and/or disturbance

$$\dot{x} = f(x,u,d,t), \quad t \geq 0\,. \tag{3.26}$$

Next we have several models that are much more specifically structured. The nonlinear model for the semi-actively controlled structural system in (2.17) can be generalized to the following nonlinear system dynamics.

$$\dot{x} = Ax + B(x,d)u + E(x,d,t), \quad A \text{ stable} \tag{3.27}$$

Also from the discussion in Chapter 2, we have piecewise linear systems with disturbances which are approximations of piecewise nonlinear systems

$$\dot{x} = A_i x + D_i d, \quad x \in X_i, \quad \bigcup_i X_i = X\,. \tag{3.28a}$$

where X is the whole space $\Re^n$, and piecewise affine systems with disturbances

$$\dot{x} = A_i x + a_i + D_i d, \quad x \in X_i, \quad \bigcup_i X_i = X\,. \tag{3.28b}$$

where X is the whole space $\Re^n$. Finally we have the special class of piecewise linear semi-active systems that we described in Section 2.11. These systems have the form

$$\begin{aligned} &\dot{x} = A_i x + Dd, \quad x \in X_i \\ &\bigcup_{i=0}^{1} X_i = X, \quad i = 0,1 \end{aligned} \tag{3.29}$$

and also satisfy all the specific properties listed in Section 2.11 for these systems. These system descriptions will be referred to throughout the rest of this dissertation.

There has been much work in the area of finding performance measures for systems that are based on using the signal 2-norm or signal ∞-norm as measures for the input or output of the system dynamics. The most prevalent methods are optimal control techniques and Lyapunov stability arguments. Some of these are discussed below.

In their book Boyd et al. (1994) provided a unified presentation of the application of linear matrix inequalities (LMIs) to the analysis of linear dynamic systems and control. The work in that book treated both signal 2-norm and ∞-norm bounds for problems of the forms (3.23a-b) and (3.24a-b). Since most of those results were based on ellipsoidal approximations for the boundaries, the results are only approximate. The LMI method will be treated in more detail and extended to treat the reachable set with unit peak input for the system (3.29) in Chapter 6. Hu and Eberhard (1999) presented response bounds for systems of the form (3.23a) and (3.24a). In all cases, the authors were interested in signal 2-norm and signal ∞-norm bounds for the output of finite element formulations of the systems, so the bounds are all functions of the mass, stiffness and damping matrices that are more common in finite element analysis formulations. For the system (3.23a) bounds were shown that were functions of the system matrices. These bounds were tight in the case where the system was classically damped. In the case of systems of the form (3.24a) bounds were also shown to depend on the system matrices, but no results were given for the tightness of the bounds. Recall, also, that the system 1-norm gives a tight bound on the peak-to-peak gain of the system (3.23d).

In the textbook by Pontryagin, et al. (1962) the authors used optimal control arguments to find the set of reachable points for the system (3.23d). They provided a method to find the boundary of the set of reachable points for the retro dynamics of (3.23d) by finding optimal inputs that drive the system from the origin to boundary proximity points in finite time. Gayek (1986) proposed a method for system (3.24a) where the system was decomposed into decoupled one and two-dimensional subsystems and each of these subsystems was treated independently. An approximation for the reachable set of each of these subsystems was generated using optimal control trajectories to move the subsystem dynamics to their boundaries. These boundaries on the subsystems were used to generate an n-dimensional box containing the reachable set of the original system. This generated an over estimate of the reachable set for the overall system.

A good survey of available techniques for finding the reachable set of various systems prior to 1991 can be found in a paper by Gayek (1991). In that paper the author discussed techniques for systems of the form (3.24a) for both continuous time and discrete time. He also reviewed techniques for a special case of the system (3.26). Sabin and Summers (1990) used a Lyapunov method to find a bound on the reachable set for the system (3.24a). The technique used provides an over-estimate of the reachable set. Their technique required the solution of a nonlinear optimization problem. Balikrishnan and Boyd (1992) presented results for improving the accuracy of calculations for the peak-to-peak gain of discrete time systems of the form (3.24a). This method allowed the calculation of such bounds to any accuracy for discrete time systems. They also extended

these results to provide bounds on the peak-to-peak gain for systems (3.24b) with diagonal uncertainty.

Shishido and Tomlin (2000) provided optimal control arguments to characterize the reachable set of systems (3.24a) as an ellipsoid. Since the direct solution of these optimal conditions is not practical, they provided methods for under and over approximating this ellipsoid, using time varying ellipsoid approximations. They specifically stated in their paper that bounds found in this manner are not tight to the actual reachable set of such systems but do bound them. Fisher et al. (1995) described a method for under-estimating the reachable set for continuous and discrete time systems (3.24a). This method was based on choosing a feedback control law that makes all the eigenvalues of the closed loop system unstable. These results and Lyapunov stability theory were then used to formulate the derivation of the control law as a nonlinear optimization problem. The solution of the nonlinear optimization problem provided ellipsoidal under-estimates for the system. Fashoro et al. (1992) also treated systems of the form (3.24a). In their paper, they used simulation solutions to find the reachable sets for simple systems and pointed out many properties of such reachable sets.

Rokityanskii (1997) showed the formulation of an ellipsoidal boundary for the reachable set of the system (3.24b). His proposed method used a finite difference approximation for the system evolution in time and derived time varying equations for the evolution of the ellipsoid approximation for the reachable set in time. Pancake et al. (2000) derived a method based on linear matrix inequalities for finding some minimal upper bound on the reachable set of systems (3.24b). This technique was an iterative version of work by Boyd et al. (1994).

Asarin et al. (2000) derived a numerical technique for tracking the reachable set of systems (3.25) in time. The method used piecewise polyhedrons to over and under approximate the reachable set as it evolved in time. The method was extended to specific special cases, (3.23c) and (3.24a). La Salle and Lefschetz (1961) showed that Lyapunov arguments can be used to find a bound on the system dynamics for systems of the form (3.25). They defined that such a system is ultimately bounded if its trajectories enter the region defined with the Lyapunov arguments in finite time and stay there as time approaches ∞. No arguments were made to indicate that this bound is tight to the actual reachable set for the system. Halkin (1963) introduced what he called the "Principle of Optimal Evolution" in which he derived optimal conditions for trajectories of the system (3.25) to be on the boundary of the reachable set.

Grantham (1981) used Lyapunov arguments to find a bound on the reachable set for a system (3.26). The solution was found by solving the derived optimization problem multiple times. The final bound on the reachable set was the intersection of the multiple solutions to the optimization problem. Fialho and Georgiou (1999) worked out a framework for evaluating the maximal value of the output under bounded disturbances for problems like (3.26). The authors used optimal control arguments to formulate conditions for finding the reachable set of the system (3.26) and applied finite difference methods to solve these conditions.

Kuehn and Stalford (2000) and Reithmeier and Leitmann (2001) both presented signal ∞-norm bounds for the output of system (3.27) with signal ∞-norm bounds on the input. Both of these papers dealt with semi-actively controlled structures similar to the

systems described in Chapter 2 of this dissertation. The bounds found were based on Lyapunov arguments and were very conservative.

Rantzer and Johansson (2000) treated the signal 2-norm bounds for the output of the system (3.28b) using linear matrix inequalities to generate ellipsoidal bounds on the output. In their method, they actually estimated both upper and lower bounds and then partitioned the space into regions and solved the problem in each region with the constraint that the solution is continuous across regions. They required 32 regions for their bounds to converge to within 10% of each other for a 2D problem. None of the literature that is currently available provides tight bound results on the peak-to-peak gain for the system (3.29). There has been work on signal 2-norm bounds for these systems, but none of these authors treated the signal ∞-norm case. The problem of finding the reachable set for a disturbance bounded by unity for these systems was only touched upon by Hassibi and Boyd (1998). In this paper the authors found signal 2-norm bounds for the system (3.28b) and mentioned that it is possible to find the reachable set that we are interested in here but did not go any further:

> "Using standard Lyapunov arguments, many other performance measures can be explored for the [piecewise linear] system [3.28b]. These include, L_2 gain, decay rate, output energy, output peak, reachable sets, etc."
>
> Hassibi and Boyd (1998).

The chart in Figure 3.3 shows a summary of the literature on the subject of calculating peak-to-peak gain bounds on the output of system dynamics based on some bounded peak input. Some of the discussion above focused on other bounds for these systems, but these are not included in the chart since we are solely interested in peak-to-

peak gain. Note that we have combined systems (3.27) and (3.28a,b). This is because the bounds that are discussed in the papers related to (3.27) are applicable to (3.28a,b) but are very conservative. This is noted in the figure. As can clearly be seen, non-conservative bounds on the peak-to-peak gain for systems (3.28a-b) are not available and remain an open problem in the literature.

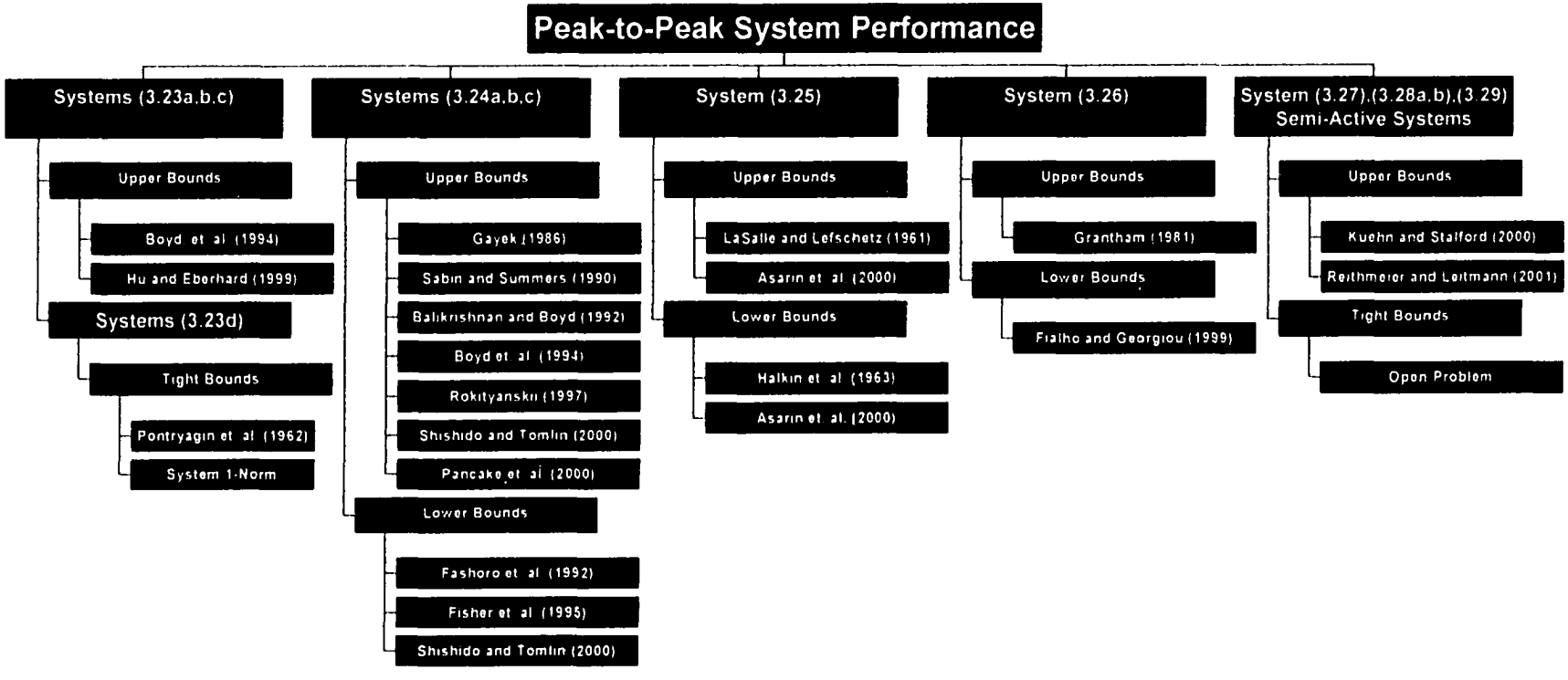

Figure 3.3: Categorization of Previous Peak-to-Peak Related References

3.7 Performance Problem for this Dissertation

For the purposes of this dissertation, we will now concisely define the performance problem in which we are interested. This will be the focus of the rest of the work here.

Find a tight (or tighter) upper bound for the peak-to-peak gain of the piecewise linear semi-active control system of the form (3.29) defined by the control law (2.29).

Here we will be trying to find some description of the reachable set and extract from that set a bound on the peak-to-peak gain for the system. The standard way to prove that a set bounds the reachable set and the attractor set is to use Lyapunov functions and conditions. Qualitatively, we can say that if there exists a Lyapunov function whose derivative is negative everywhere outside that function, then the Lyapunov function bounds both sets. For the piecewise linear system described in Chapter 2, we could define a continuous, piecewise C^1 Lyapunov function, V, where

$$V(x) = V_i(x), \quad x \in X_i, \quad i = 1,2, \tag{3.30}$$

with $P_i > 0$, and

$$V_i(x) = x^T P_i x, \quad x \in X_i, \quad i = 1,2, \tag{3.31}$$

where the X_i are the regions in space where the valve is open or closed as determined by the control logic (2.29). Then the reachable set is bounded by the set defined by $V(x) = 1$, if we can satisfy the following conditions in each of the regions X_i.

$$\frac{dV_i(x)}{dt} \le 0 \text{ when } V_i(x) > 1, \quad x \in X_i, \quad i = 1,2. \tag{3.32}$$

Expanding both (3.31) and (3.32) using the piecewise linear system in Section 2.11 gives us the following inequalities with $P_i > 0$.

$$\dot{V}_i(x) = x^T \left(P_i A_i + A_i^T P_i\right) x + 2x^T P_i D d \le 0, \quad x \in X_i, \quad i = 1,2, \tag{3.33a}$$

when

$$V_i(x) = x^T P_i x > 1, \quad x \in X_i, \quad i = 1,2. \tag{3.33b}$$

This gives us a condition that must be satisfied in each region for the Lyapunov function to be used as an upper boundary for the reachable set. For each i, the inequality constraints in (3.33) represent an infinite number of linear inequalities on P_i. The problem of determining whether there exists P_i such that (3.33) hold is one of high complexity. In fact, verifying that (3.33) hold is as hard as solving a general indefinite quadratic program, which is NP-complete (Boyd, 1994). Here NP stands for nondeterministic polynomial time. NP-complete is a term from computational complexity theory, which essentially means that solving this problem is computationally intractable in this form (i.e. there is no tractable algorithm that can find a P_i such that (3.33) are satisfied).

The fact that this condition (3.33) needs to be satisfied only in a region X_i can be used to modify the problem so that it becomes tractable with polynomial time computational algorithms. This will become important in later chapters when new methods can be applied only to conditions on the whole space. Some techniques (e.g. LMI of Chapter 6) require adding additional terms to (3.33) so that the inequalities are valid on the whole space. Such additions usually add

significant conservatism to the obtained bounds but reduce the problem to one that is tractable with fast algorithms (interior point methods in that case of LMIs). This will be particularly evident in Chapter 6.

CHAPTER 4

EXAMPLES TO ILLUSTRATE PERFORMANCE PROBLEM

Several examples will be used throughout the rest of this work to illustrate the methodologies discussed. They will be used to test the effectiveness of the methodologies explored in the pursuit of some tight (or tighter) bound on system peak output for a bounded peak input. Each of the models will be developed, and several control laws will be chosen as examples to be used in later chapters. The dynamics of each system will be discussed and shown graphically when possible.

Before models are discussed, the disturbance logic that we will use to estimate a worst case disturbance will be shown. In the example problems, simulation studies conducted with this disturbance logic will be used to provide a lower bound for the system's peak output with a bounded peak input.

The first two examples are 2D systems that satisfy all of the properties for piecewise linear semi-active systems described in section 2.11. The second of these 2D examples requires a change of variables to do this. These systems do not, however, exhibit all of the dynamic characteristics of the higher dimensional systems, because they do not have distinct actuator dynamics. This has been characterized by the system eigenvalue behavior when a switching logic is applied to the system. The obvious benefit of using a 2D example is that a simple phase plane analysis can be applied to analyze the problem. Also, exact solutions for the reachable sets of 2D problems can be found in

several ways, including limit cycle analysis. This also makes it very simple to visualize the system dynamics and present the results graphically in later chapters. One of the issues with the 2D example is that many analysis techniques that work well in 2D do not work in higher dimensions.

The 3D problem described below is the smallest dimension system that has distinct actuator dynamics and fits within the semi-active control framework described in Chapter 2. Fortunately, since it is only 3D, we are still able to view many results graphically. However, the graphics are significantly more complicated than those for the 2D system. The 3D system will be used to illustrate the effectiveness of methods for higher dimensions in later chapters.

The final system to be used as an example is a 7D system used previously by Kuehn (2000). Simulation and experimental results for this system, as well as a stability analysis, are reported in his dissertation. This system will be used as the final test for the methods in later chapters, and results will be compared to both simulation and experimental results from his work.

4.1 Disturbance Logic

Since we are interested in the worst case output magnitude from the system, with some worst case input that is bounded, we must come up with a way to approximate this worst case input so that simulation studies can have some bearing on the problem. The disturbance logic that follows has been used to get results for several problems. For example, Stalford (1995a), (1995b), (1995c) used it to construct stabilizing controllers for uncertain systems like (3.23b). Kuehn (2000), used it to estimate a lower bound on the

worst case system response. No mathematical claims were made as to its suitability for this role, but extensive simulation studies have shown that, of the disturbance schemes tried, this disturbance consistently produced the worst system response. In 2D problems, this disturbance can in fact be used to find a tight bound for the reachable set.

The following disturbance law has been used in certain underdamped systems to approximate peak-to-peak performance.

Definition 4.1a: (Empirical approximation for worst case disturbance)

Define an empirical approximation of the worst case disturbance for underdamped systems as one that satisfies

$$\sup_{d \le 1} \frac{x^T \dot{x}}{\|x\|_2 \|\dot{x}\|_2} \tag{4.1a}$$

evaluated at each point in time.

For general systems, this definition needs to be modified as follows.

Definition 4.1b: (General Empirical approximation for worst case disturbance)

Define an empirical approximation of the worst case disturbance for general systems as one that satisfies

$$\sup_{d \le 1} \frac{k_n(x)^T \dot{x}}{\|k_n(x)\|_2 \|\dot{x}\|_2} \tag{4.1b}$$

evaluated at each point in time. We choose $k_n(x)$ so that all possible $\dot{x}(|d| \le 1)$ lie on one side of the tangent plane dividing $k_n(x)$ from $\dot{x}(|d| \le 1)$.

This essentially allows us to direct the system velocities in the direction desired.

In the 2D case with dynamics that circle the origin and do not have any equilibrium points except the origin, Definition 4.1a allows us to find a limit cycle around

the origin that bounds the system response. If there are other equilibrium points, we must modify the disturbance in regions where the reachable set boundary is moving from a maximum to a minimum radius. In this region, the vector k_n is set to some vector that is within 90° of both the surface tangent and the radius vector. Examples of the solutions for these systems will be shown in the next two sections.

The ease with which 2D reachable sets are found does not translate into higher dimensions. In higher dimensions we will use Proposition 4.1b mentioned above, but it will no longer generate a boundary for the reachable set. Instead it will generate some empirical worst-case simulation results that we can use to under-approximate the peak-to-peak gain. Since the reachable set in higher dimensions is an n-dimensional surface, we cannot generate it using simulation results, which are only an n-dimensional line in the space.

4.2 2D Example #1

This 2D example was designed to exhibit similar characteristics to the physical systems that fit within the framework in Chapter 2. Its eigenvalues show some similar characteristics to the higher dimensional models, which will be discussed later in this chapter. When the system is in the open valve state, the system exhibits stable overdamped dynamics that converge to the origin. On the other hand, when the system is in the closed valve state, one of the eigenvalues is zero and the other is a stable decay.

The system is the following

$$\dot{x} = \begin{bmatrix} -1 & -1 \\ 0 & -2 \end{bmatrix} x + \begin{bmatrix} 0 \\ 2 \end{bmatrix} (u_{\max} - u) x_2 + \begin{bmatrix} 0 \\ 1 \end{bmatrix} d, \quad |d| \le 1. \tag{4.2}$$

This is in the form of the semi-active system with a linear approximation in (2.23). For this system, we are taking the valve closed case to be $u=0$ and the valve open case to be $u=u_{max}=1$. When $u=0$, the eigenvalues are -1 and 0, and when $u=1$, the eigenvalues are -1 and -2.

We will begin by discussing this system for the case where the valve is held open. This will give us a baseline for comparison when we design and implement a control logic such as (2.29). When the valve is held open, we set $u=u_{max}=1$ for all time. This leads to a simplified system as follows.

$$\dot{x} = \begin{bmatrix} -1 & -1 \\ 0 & -2 \end{bmatrix} x + \begin{bmatrix} 0 \\ 1 \end{bmatrix} d, \quad |d| \le 1. \tag{4.3}$$

or equivalently,

$$\dot{x} = A_1 x + Dd, \quad |d| \le 1. \tag{4.4}$$

Recall from Section 3.2 that there are several techniques that can be applied to LTI systems that allow us to garner some knowledge about the system. The first of these techniques is the system 1-norm, which requires systems to have the form (3.9). This means that we must add an output matrix to the system in (4.4) to apply this method. To this end, we will rewrite (4.4) as

$$\begin{aligned} \dot{x} &= A_1 x + Dd, \quad |d| \le 1 \\ y &= Cx \end{aligned}, \tag{4.5}$$

where

$$C = \begin{bmatrix} \cos(\phi) & \sin(\phi) \end{bmatrix}, \quad 0 \le \phi < 2\pi. \tag{4.6}$$

This will generate the system 1-norm result in every direction. This will also give us an over-estimate of the reachable set, except in the directions of the maximum and minimum

radii for the set, where it will be exact. Figure 4.1 shows the system 1-norm results for system (4.3). The maximum radius is 0.7071 at the point (-0.5,0.5), and the minimum radius is 0.3536 at the point (0.2544,0.2456). This plot is symmetric, so it also takes on these radii at points 180° from these points.

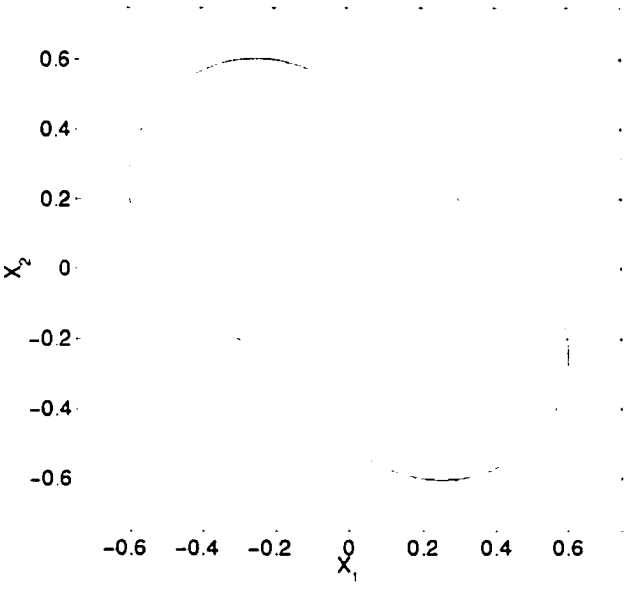

Figure 4.1: System 1-Norm Results for System (4.3) (Open Valve)

As we mentioned in Section 3.3, it is also reasonably simple to calculate the peak system response to input whose energy is bounded by unity. To do this, we must solve the Lyapunov equation shown in (3.22b). The resulting ellipsoidal bound is shown in Figure 4.2. This figure takes on a maximum radius of 4.5261 at the point (4.1815,1.7321) and a minimum radius of 1.8748 at the point (-0.7174,1.7321). Again the figure is symmetric, so it also takes on these radii at points 180° from these points as well. Obviously, the results here are significantly larger than the results in Figure 4.1. This illustrates the significant differences that occur when an energy norm is used instead of a peak norm to measure the significance of a signal.

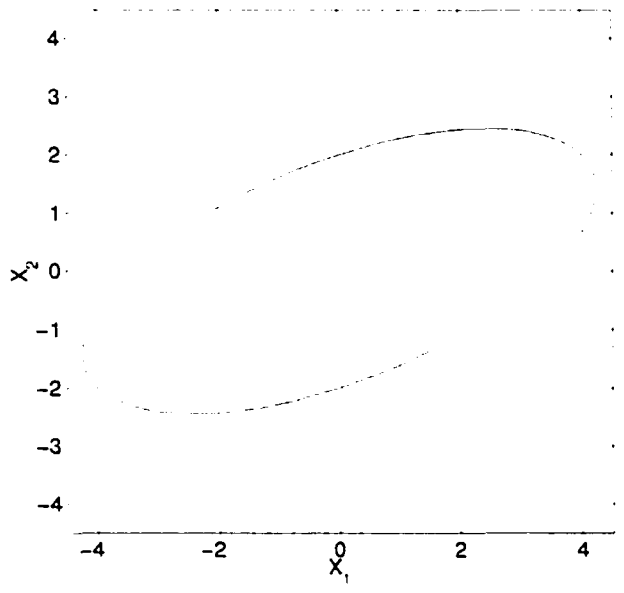

Figure 4.2: Bound on Output Peak for Unit-Energy Input for System (4.3) (Open Valve)

Finally, as we mentioned in the last section, we can use (4.1b) to find the reachable set boundary for this problem. However, a judicious choice for k_n is necessary. We will use the following values for k_n.

$$k_n = \begin{cases} [-1 \quad -1]^T, & \text{if } (x_2 - x_1 > 0) \& (x_2 + x_1 < 0) \\ [1 \quad 1]^T, & \text{if } (x_2 - x_1 < 0) \& (x_2 + x_1 > 0). \\ x, & \text{otherwise} \end{cases} \tag{4.7}$$

Using this value in the disturbance law (4.1b) and simulating the system (4.3) we get the reachable set shown in Figure 4.3. Note that this system has equilibrium points at the corners of the reachable set and at these points we have to stop the simulation and restart just on the other side of these points. The colors indicate regions where the varying values of k_n are used. The direction of the system flow is also indicated on the graph. We can see that this system has two peak radii, and since the disturbance was bounded by

unity, these radii translate into the system's peak-to-peak gain. For this system the peak-to-peak gain is 0.7071 and it occurs twice on the plot at $\theta = \frac{3\pi}{4}, -\frac{\pi}{4}$.

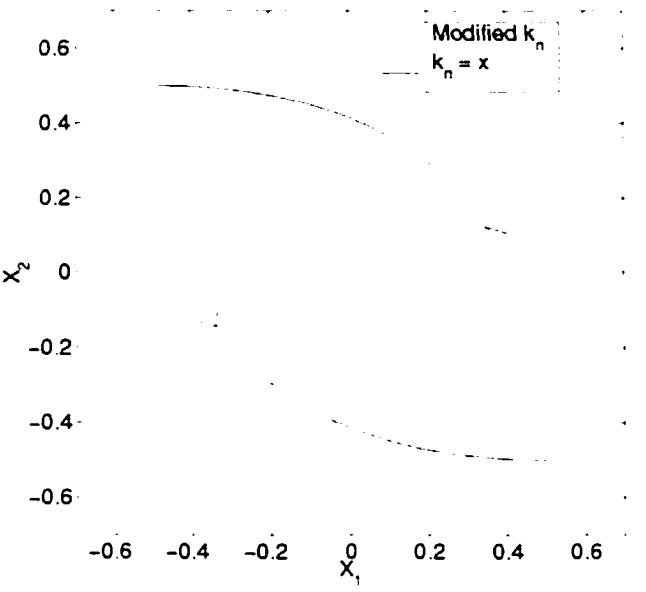

Figure 4.3: Reachable Set for System (4.3) with Unit-Peak Input (Open Valve)

Figures 4.4a and 4.4b compare the reachable set with unit peak input to the previous results. We can see in the case of Figure 4.4a that the system 1-norm gives tight results for the local extrema. For reference, Figure 4.5 shows the system trajectories for a simulation with *x(0)=0* and a disturbance (4.1b) with (4.7). This essentially drives the system from the origin to the equilibrium points. Which equilibrium point the system moves to depends on the initial value for the disturbance when the system is at the origin. Both cases are plotted in Figure 4.5.

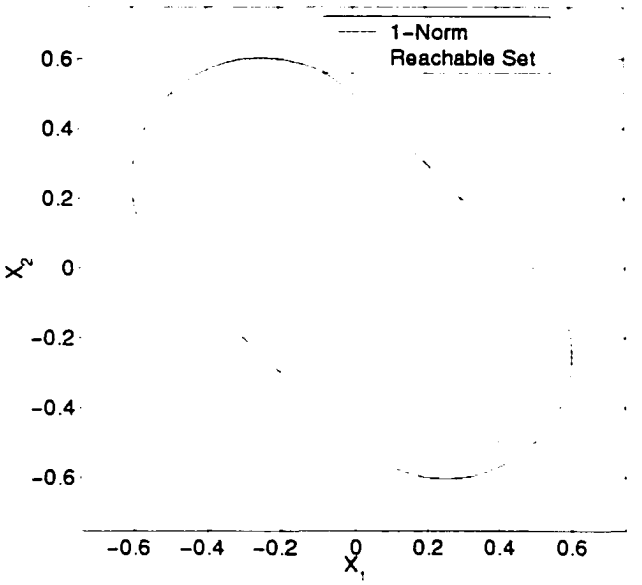

Figure 4.4a: Comparison of the System 1-Norm and Actual Reachable Set with Unit Peak Input for System (4.3) (Open Valve)

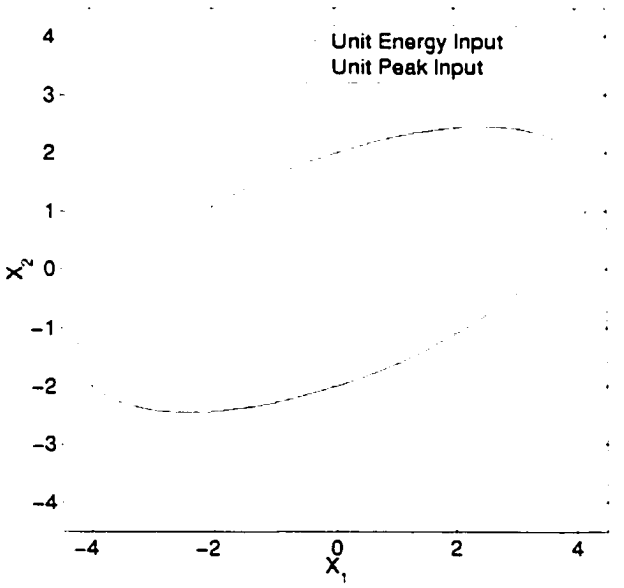

Figure 4.4b: Comparison of the Reachable Set with Unit Energy Input and the Reachable Set with Unit Peak Input for System (4.3) (Open Valve)

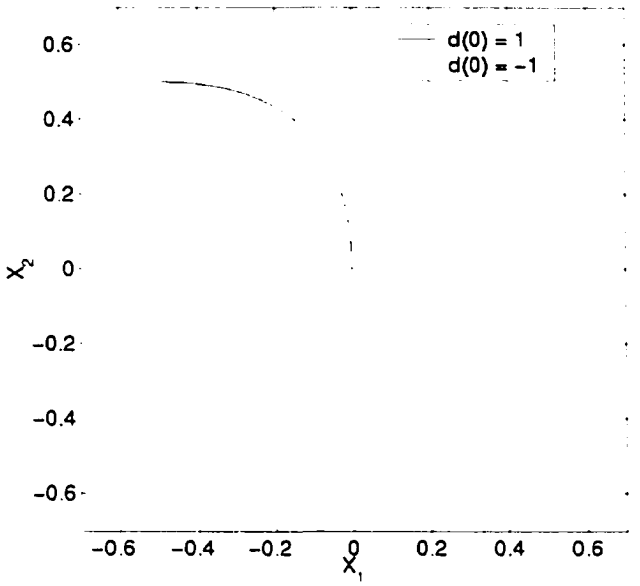

Figure 4.5: Simulation Results for System (4.3) with Disturbance (4.1b) and (4.7) (Open Valve)

The next step is to design a controller in the form (2.29), based on the techniques in Section 2.9. For this particular case, it is important to be careful when designing controllers. No controller will actually reduce the peak-to-peak gain of this system. It is possible to reduce the volume of the reachable set, however, and that is our goal.

The controller based on (2.29) that removes the most volume from the reachable set and remains stable uses the symmetric matrices

$$Q = \begin{bmatrix} 2 & 4 \\ 4 & 10 \end{bmatrix}, \quad P = \begin{bmatrix} 1 & 1 \\ 1 & 2 \end{bmatrix}. \tag{4.8}$$

Based on the system (4.2), and referring back to Section 2.11 on piecewise linear models, we can now write this system in the piecewise linear form (2.51). Thus, the model for this system with the control is as follows

$$\dot{x} = A_i x + Dd, \quad |d| \le 1$$
$$A_0 = \begin{bmatrix} -1 & -1 \\ 0 & 0 \end{bmatrix}, \quad x \in X_0 = \left\{ x \middle| x^T PBx_2 < 0 \right\} \quad (u = 0) \qquad (4.9)$$
$$A_1 = \begin{bmatrix} -1 & -1 \\ 0 & -2 \end{bmatrix}, \quad x \in X_1 = \left\{ x \middle| x^T PBx_2 \ge 0 \right\} \quad (u = u_{\max} = 1)$$

This system generates the reachable set shown in Figure 4.6. This plot shows the reachable set for the open valve case and the control case based on (4.9) for comparison. One can see that there is little change in the reachable set and none in the peak-to-peak value of 0.7071.

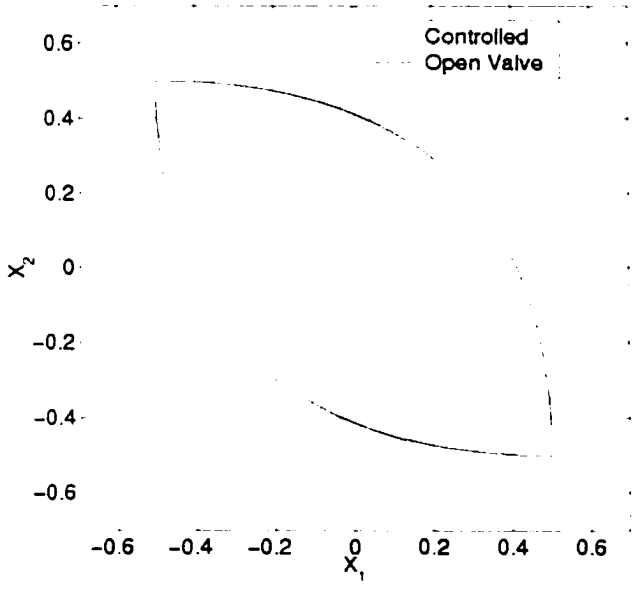

Figure 4.6: Comparison of Reachable Sets for Open Valve Case and Control Case for System (4.2)

To sum up, Table 4.1 shows the results so far for the 2D example #1. Values for both the system 1-norm and the reachable set are reported for cases when (4.6) points in the direction of the principle axes. We also report the maximum radii for both of these solutions. In the case of the reachable set, the maximum radius is the peak-to-peak gain.

Table 4.1 Results for 2D Example #1

Control Version	Reachable Set			System 1-Norm		
	$\|x_1\|_\infty$	$\|x_2\|_\infty$	Peak-to-Peak Gain	$\|x_1\|_\infty$	$\|x_2\|_\infty$	Maximum Radius
Open Valve	5.00e-1	5.00e-1	7.07e-1	5.00e-1	5.00e-1	7.07e-1
1	5.00e-1	5.00e-1	7.07e-1	n/a	n/a	n/a

4.3 2D Example #2

This 2D example requires a slight change in coordinates to fit within the properties for piecewise linear semi-active systems described in Section 2.11. To accomplish this, we must use the transformation matrix in the properties from Section 2.11. Instead of identity, it will be set to

$$T = \begin{bmatrix} 0 & 1 \\ 1 & 0 \end{bmatrix}.$$

As in the last 2D example, this example does not show all of the characteristics of higher dimensional systems but does exemplify some of them. Specifically, its eigenvalues show some similar characteristics to the higher dimensional models shown in later sections of this chapter. When the valve is open, the system exhibits stable under-damped dynamics that converge to the origin. In this 2D model, this means that the system has a pair of under-damped complex eigenvalues whose real part is negative. When the valve is closed, the system must have one eigenvalue that is identically zero, and all other eigenvalues must be stable. In the 2D case, this means that the system must have one zero eigenvalue and one negative real eigenvalue.

The system is described by the following dynamics.

$$\dot{x} = \begin{bmatrix} -1 & -10 \\ 1 & 0 \end{bmatrix} x + \begin{bmatrix} 10 \\ 0 \end{bmatrix} (u_{\max} - u) x_2 + \begin{bmatrix} 1 \\ 0 \end{bmatrix} d, \quad |d| \le 1. \tag{4.10}$$

As in the last section, this is in the form of the semi-active system with a linear approximation in (2.23). For this system, we are taking the valve closed case to be $u=0$ and the valve open case to be $u=u_{max}=1$. When $u=1$, the system eigenvalues are $-5 \pm 3.12i$, and when $u=0$, the system eigenvalues are 0 and -1. This corresponds to a natural frequency of 3.16 rad/s and a damping ratio of 0.16.

Again, we will begin by discussing this system for the case where the valve is held open. This will give us a baseline for comparisons when we design and implement a control logic such as (2.29). When the valve is held open, we set $u=u_{max}=1$ for all time. This leads to a simplified system as follows.

$$\dot{x} = \begin{bmatrix} -1 & -10 \\ 1 & 0 \end{bmatrix} x + \begin{bmatrix} 1 \\ 0 \end{bmatrix} d, \quad |d| \le 1, \tag{4.11}$$

or equivalently,

$$\dot{x} = A_1 x + Dd, \quad |d| \le 1. \tag{4.12}$$

From here, we can follow the same path of analysis taken for the 2D example #1 from the previous section.

First, we will apply the system 1-norm to (4.11). This will give us an upper bound on the open valve system's reachable set everywhere except at the local extremum points where the system 1-norm result is tight. To do this, we need to augment (4.11) as we did in (4.5) and (4.6). Once this is done, we can calculate the system 1-norm value in all directions to find the bounding shape. This result is shown in Figure 4.7. The maximum radius on this plot is 1.2762 at the point (1.2760,0.0225) and the minimum

radius is 0.4059 at the point (-0.0036,0.4059). Since this is a symmetric plot, these extrema occur again 180° from these points.



Figure 4.7: System 1-Norm Results for System (4.11) (Open Valve)

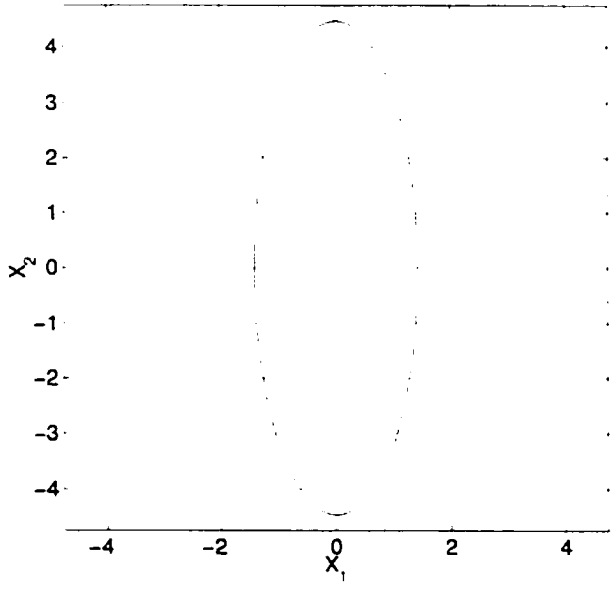

Figure 4.8: Bound on Output Peak for Unit-Energy Input for System (4.11) (Open Valve)

We can also find the reachable set for the case where the input energy is bounded by unity. This method was reviewed in Section 3.3. It involves solving a Lyapunov function and plotting the ellipse generated by the solution. The results from this analysis for the system in (4.11) are shown in Figure 4.8. The maximum radius is 4.4721 on the y-axis, and the minimum radius is 1.4142 on the x-axis. Again, we can see that the change from a unit peak bound on the input to a unit energy bound on the input makes a huge difference in the reachable set.

The last step in the analysis of the open valve system is the generation of the reachable set from the disturbance of the form (4.1b). For the 2D example #2, we will use

$$k_n = x \tag{4.13}$$

in the disturbance law. This gives us the disturbance law (4.1a). Using the disturbance law (4.1a) to generate the disturbance for the system (4.11) gives the reachable set shown in Figure 4.9a. This system does not have any equilibrium points other than the origin. The system's flow direction at the boundary is indicated on the figure. We can see that this system has two symmetric maximum radii. These constitute the peak-to-peak gain of the system and take a value of 1.2762 at $\theta = 3.124, -1.755e-2$.

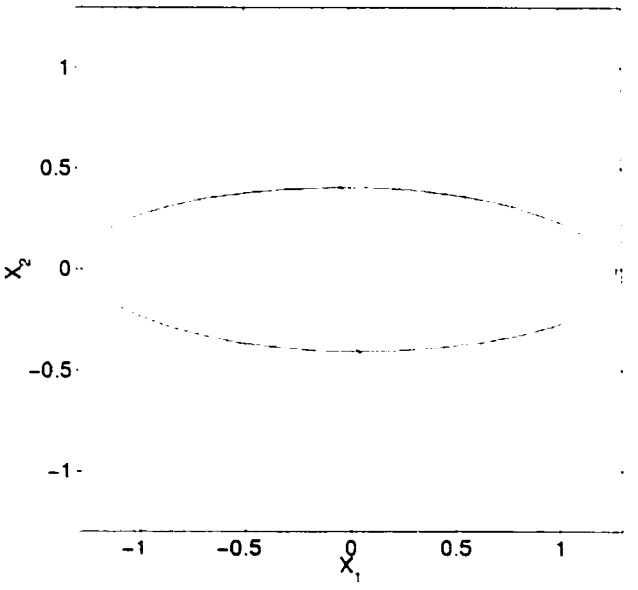

Figure 4.9a: Reachable Set for the System (4.11) with Unit Peak Input (Open Valve)

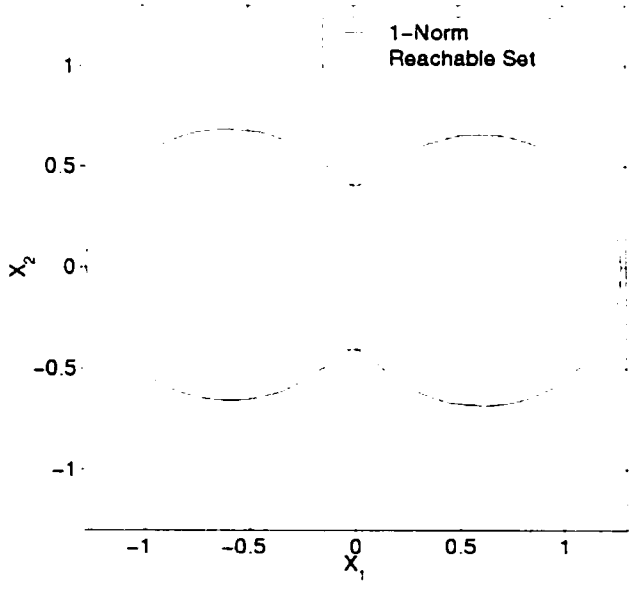

Figure 4.9b: Comparison of the System 1-Norm and Actual Reachable Set with Unit Peak Input for System (4.11) (Open Valve)

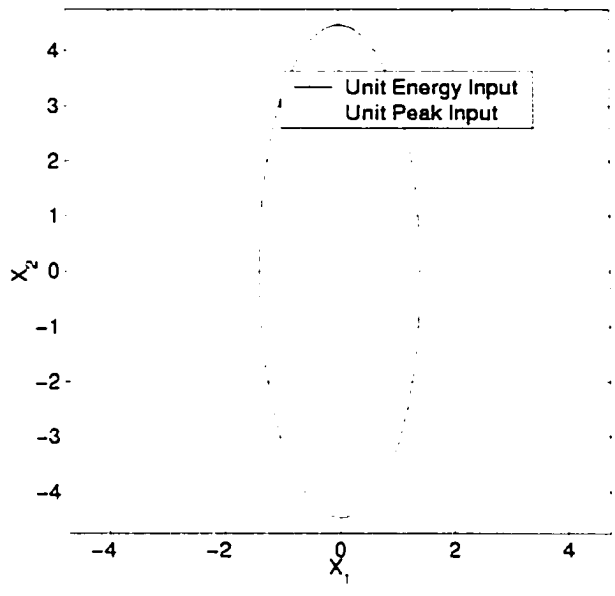

Figure 4.9c: Comparison of the Reachable Set with Unit Energy Input and the Reachable Set with Unit Peak Input for System (4.11) (Open Valve)

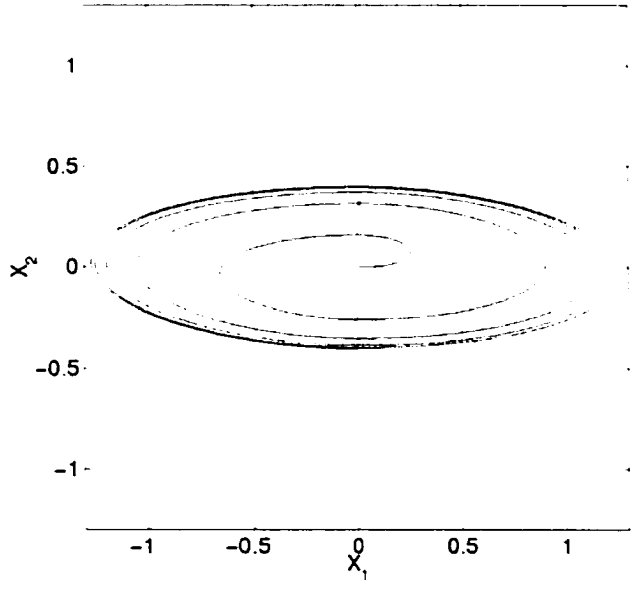

Figure 4.10: Simulation Results for System (4.11) with Disturbance (4.1) (Open Valve)

Figures 4.9b and 4.9c compare the reachable set with unit peak input to previous results. We can see in the case of Figure 4.9b that the system 1-norm gives tight results for the local extrema. Figure 4.10 shows the system trajectories for a simulation with $x(0)=0$ and a disturbance (4.1a). The system spirals out from the origin towards the reachable set in Figure 4.9a.

For this system, there is a large group of stable controllers that will improve the peak-to-peak gain of the system. This is in contrast to the 2D example #1, for which no controller would improve the peak-to-peak gain of the system. Again, we will start with the controller design shown in Section 2.9, and we will design three controllers this way. The values for the symmetric matrix P in each of these three controllers are shown in Table 4.2. The associated values of the Q matrices will be given in Appendix I.

Table 4.2: Values used for Positive Definite Symmetric P Matrix in Candidate Controllers for 2D example #2

Control Version	P(1,1)	P(1,2)	P(2,2)
1	5.05e-2	5.00e-2	5.55e-1
2	1.00e-1	5.00e-2	1.05e0
3	1.63e2	3.75e1	2.10e3

Now that we have the P matrices for the controllers, we can define the piecewise linear model that will describe the controlled system. Based on the system (4.10), and referring back to Section 2.11, our model for the controlled system is

$$\begin{aligned} &\dot{x} = A_i x + Dd, \quad |d| \le 1 \\ &A_0 = \begin{bmatrix} -1 & 0 \\ 1 & 0 \end{bmatrix}, \quad x \in X_0 = \left\{ x \middle| x^T PBx_2 < 0 \right\} \quad (u = 0) \\ &A_1 = \begin{bmatrix} -1 & -10 \\ 1 & 0 \end{bmatrix}, \quad x \in X_1 = \left\{ x \middle| x^T PBx_2 \ge 0 \right\} \quad (u = u_{\max} = 1) \end{aligned} \qquad (4.14)$$

Using the disturbance (4.1a), we can generate the reachable sets for these three controllers. This is shown in Figure 4.11, along with the reachable set from Figure 4.9 for reference. We can see that the addition of the controller significantly reduces the volume of the reachable set and the value of the peak-to-peak gain.

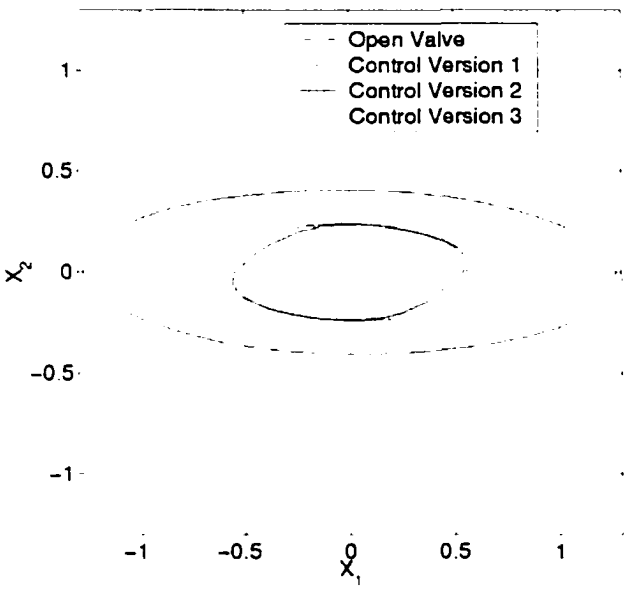

Figure 4.11: Reachable Sets for Controlled Cases for 2D Example #2

Table 4.3 shows the results for these three controllers and for the open valve case. Values for the system 1-norm and the reachable set are reported for cases when (4.6) points in the direction of the principal axes. We also report the maximum radii for both of these solutions. In the case of the reachable set, the maximum radius is the peak-to-peak gain.

Recall from our discussion of the control logic in Section 2.9 that the Lyapunov quickest descent control design creates two switching planes across which the value of u changes. Looking at (4.14), we can see that the control is actually checking to see where the state is in relation to the planes defined by the normals PB and $[0 \quad 1]^T$. As an

interesting exercise in this simple 2D case, we can arbitrarily choose the switching plane *PB* without using the Lyapunov control techniques in Section 2.9. If we do this and define each new control logic by the angle between the two switching planes, we can generate Figure 4.12, which shows how the peak-to-peak value for the controlled system changes as the angle between the switching planes is increased to 90°.

Table 4.3: Results for 2D example #1

Control Version	Reachable Set			System 1-Norm		
	$\|x_1\|_\infty$	$\|x_2\|_\infty$	Peak-to-Peak Gain	$\|x_1\|_\infty$	$\|x_2\|_\infty$	Maximum Radius
Open Valve	1.28e0	4.06e-1	1.28e0	1.28e0	4.06e-1	1.34e0
1	5.76e-1	2.38e-1	5.78e-1	n/a	n/a	n/a
2	5.59e-1	2.34e-1	5.62e-1	n/a	n/a	n/a
3	5.55e-1	2.33e-1	5.58e-1	n/a	n/a	n/a

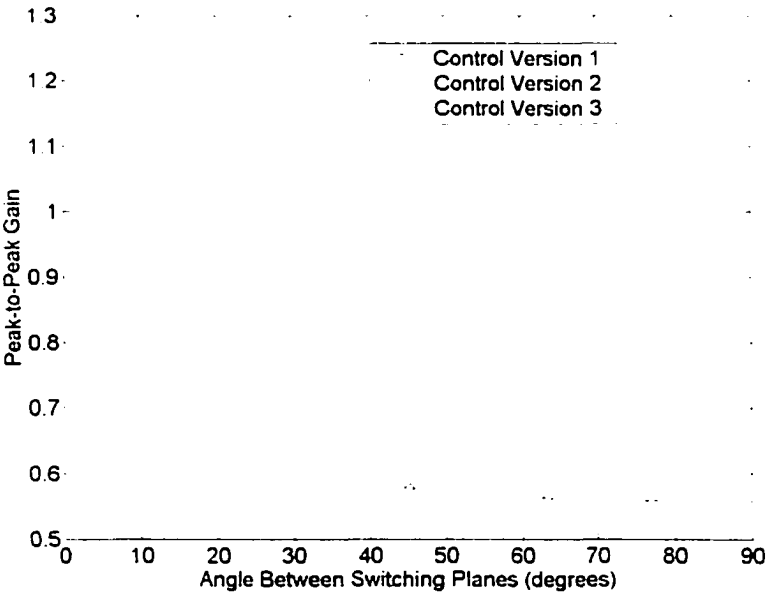

Figure 4.12: Peak-to-Peak Gain Relative to Angle Between Switching Planes for 2D Example #2

In the case where the angle is 0°, we can see that the peak-to-peak gain is equivalent to the open valve case. The three controllers that we designed above are also marked on Figure 4.12.

4.4 3D Example

This example is the smallest dimension that includes separate actuator dynamics, as described by the semi-active control framework in Chapter 2 (Epp and Stalford, 2002). It will be used as the stepping-stone from 2D analysis to higher dimensions.

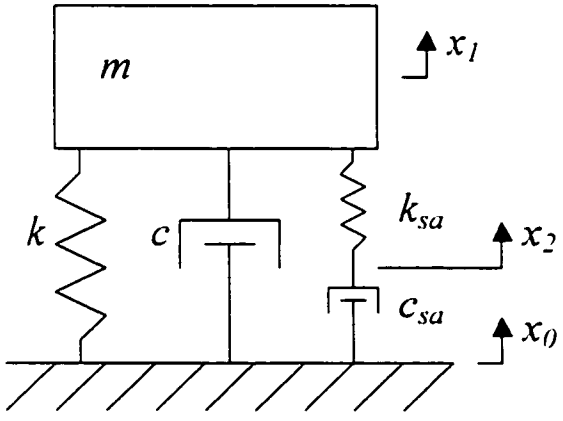

Figure 4.13: Example problem -- Linear system with switched semi-active element

This example consists of a second order linear system and a single semi-active actuator shown in Figure 4.13, with base acceleration as the disturbance. This is the simplest system with separate actuator dynamics that fits into the class of semi-active control problems considered here. Based on the coordinates shown in Figure 4.13, relative coordinates are defined as

$$\begin{aligned} z_1 &= x_1 - x_0 \\ z_2 &= \dot{x}_1 - \dot{x}_0 \end{aligned} \qquad z_3 = x_1 - x_2 . \tag{4.15}$$

In this example, z_1 and z_2 are the states associated with the linear system, and z_3 is the state associated with the switched semi-active element. Using these coordinates, the system can be written in the form of the semi-active system with a linear approximation in (2.23) as

$$\dot{z} = A_1 z + 5000B(u_{\max} - u)z_3 + Dd,\ |d| \le 1$$
$$A_1 = \begin{bmatrix} 0 & 1 & 0 \\ -224.72 & -4.50 & -2247.20 \\ 0 & 1 & -5000 \end{bmatrix},\ B = \begin{bmatrix} 0 \\ 0 \\ 1 \end{bmatrix},\ D = \begin{bmatrix} 0 \\ -10 \\ 0 \end{bmatrix}. \qquad (4.16)$$

The design of this model was originally based on the dynamics of an air-suspended heavy truck model. For this system, we are taking the valve closed case to be $u=0$ and the valve open case to be $u=u_{max}=1$.

For the case where $u=0$, the system has the eigenvalues $-2.25\pm49.67i$ and 0. The natural frequency of the underdamped mode is 49.72 rad/s, and the damping ratio is 0.045. This means that the initial condition in the direction of the eigenvector corresponding to the zero eigenvalue remains fixed as time progresses. The system spirals in toward the origin in the plane made by the other two eigenvectors of the open valve system.

For the open valve case where $u=1$, the system has the eigenvalues $-2.47\pm14.79i$ and –4999.6. The natural frequency of the underdamped mode is 15.00 rad/s, and the damping ratio is 0.165. This means that in one direction all trajectories are decaying to the origin very quickly (0.138 ms half-life), and in the other two directions the trajectories are spiraling in toward the origin. The specific directions are determined by the eigenvectors.

For illustration, Figure 4.14 shows simulation response for the system with an initial condition at (1,1,2) for both cases without disturbance. Note that for all simulation plots the axis limits are chosen to be tight to the maximum states. One can see that when $u=0$ the system is not actually stable to the origin but to some other point dependent on the initial condition because it has a zero eigenvalue. This equilibrium point will occur on the line $-224.72z_1 - 2247.20z_2 = 0$ and its position on this line will be determined by the initial conditions for the closed valve system.

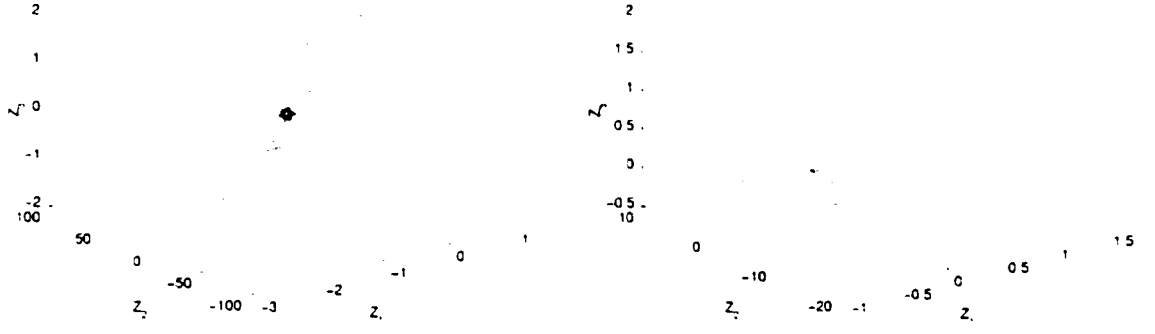

(Closed Valve) **(Open Valve)**

Figure 4.14: Simulated 3D system response with an initial condition of (1,1,2) and no disturbance

As seen previously for the 2D cases, we will begin by looking at the 3D system in the case where the valve is held open. In this case, we set $u=u_{max}=1$ for all time. This leads to a simplified system as follows.

$$\dot{z} = \begin{bmatrix} 0 & 1 & 0 \\ -224.72 & -4.50 & -2247.20 \\ 0 & 1 & -5000 \end{bmatrix} z + \begin{bmatrix} 0 \\ -10 \\ 0 \end{bmatrix} d, \quad |d| \le 1. \tag{4.17}$$

or equivalently

$$\dot{z} = A_1 z + Dd, \quad |d| \le 1. \tag{4.18}$$

Again, we recall that there are several techniques that can be applied to this simplified system, as discussed in Section 3.2. The first of these is the system 1-norm, which requires a slight modification of the system (4.18). We must add an output term as follows

$$\begin{aligned} \dot{z} &= A_1 z + Dd, \quad |d| \le 1 \\ y &= Cz \end{aligned} \tag{4.19}$$

where

$$C = [\sin(\theta)\cos(\phi) \quad \sin(\theta)\sin(\phi) \quad \cos(\theta)], \quad 0 \le \phi < 2\pi, \quad 0 \le \theta \le \pi. \tag{4.20}$$

This will generate the system 1-norm result in every direction and give us an over estimate of the reachable set. As for the 2D cases, this estimate will be exact at the points of local extremum. Figure 4.15 shows the system 1-norm results for the system (4.17). The maximum radius for this plot is 2.5859 at the point (1.1962e-2,2.5859,4.6821e-4), the minimum radius is 4.3912e-7 at the point (3.6e-11,1.2e-7,4.0e-7), and the saddle point radius is 0.1749 at the point (0.1733,-2.3084e-2,-2.6613e-6). These radii reoccur in a symmetric fashion about the origin.

Also, we can calculate the peak system response to unit-energy input. Note that this is a change in the bound on the input from what has been discussed so far. The resulting ellipsoidal bound on the reachable set is very large compared to the estimate from the system 1-norm. This illustrates the differences that occur when using an energy norm to bound the input rather than a peak norm as is used for most of the work. The resulting bounds on the reachable set for unit peak input are shown in Figure 4.16a.

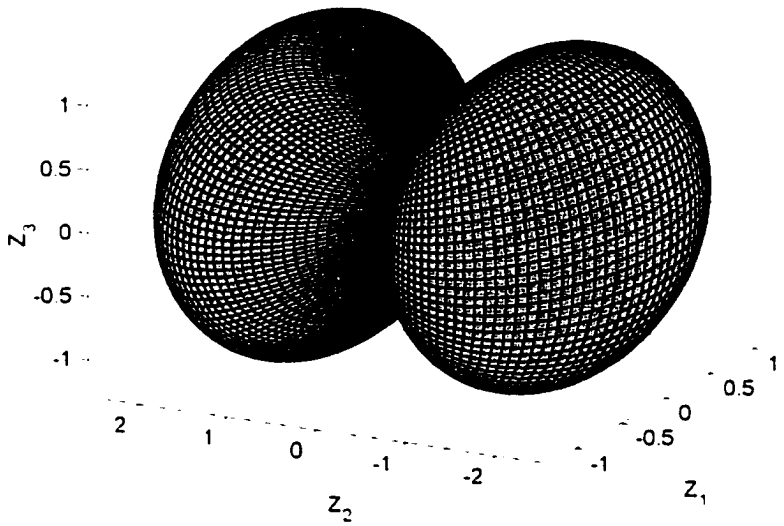

Figure 4.15: System 1-Norm Result for System (4.17) (Open Valve)

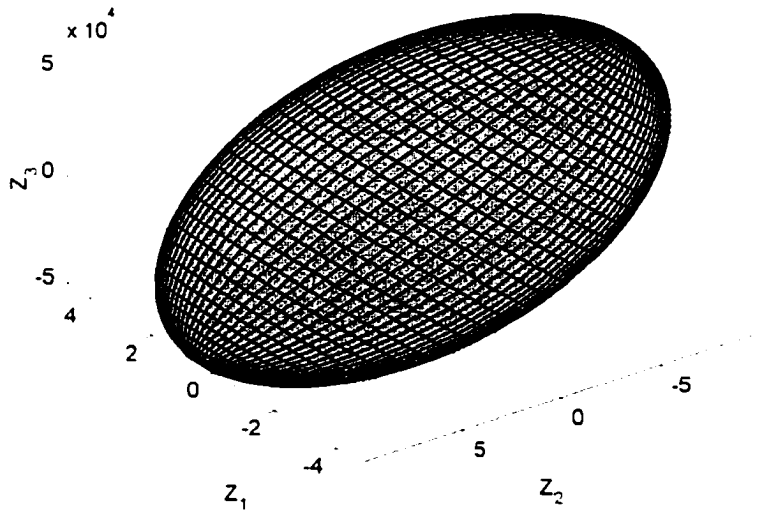

Figure 4.16a: Bound on Output Peak for Unit-Energy Input for System (4.17) (Open Valve)

The controllability Gramian that generates this plot is

$$W_c = \begin{bmatrix} 4.50e-2 & 0 & 4.04e-7 \\ 0 & 1.01e1 & 2.02e-3 \\ 4.04e-7 & 2.02e-3 & 4.04e-7 \end{bmatrix}.$$

The maximum radius for this plot is 50048 at the point (-4.4946e-1,-1.0,5.0048e4), the minimum radius is 0.31443 at the point (-2.5217e-12,-3.1443e-1,-6.2824e-5), and the saddle point radius is 4.7137 at the point (4.7137,-8.4958e-9,4.2332e-5). These radii reoccur in a symmetric fashion about the origin.

Finding the reachable set from simulated response to some disturbance for 3D systems is much more difficult than for the 2D problems discussed previously. Finding this reachable set, or at least a tight bound on the peak-to-peak gain of this system, is one of the goals of this dissertation. What we can do for the open valve case is transform the system into a modal space and find tight bounds on each of the modes. These bounds can then be transformed back into the original system space and combined. This does not give the exact reachable set but rather a tight covering. This is similar to a technique used by Gayek (1986), but in that work he used a box to bound each mode and transformed these into an *n*-dimensional box in the system space bounding the reachable set. For the 3D problem, this procedure is relatively simple. Since one of the modes in this open valve case is under-damped, we can find a very tight covering using techniques discussed in the 2D problems. The only other mode is a decay that eventually reaches equilibrium with the disturbance acting on it. This leads to an elongated coin shape. This is plotted in Figure 4.16b for the open valve system (4.17). Note that the thickness in the direction of the stable real eigenvalue is on the order of 1e-7, so it is difficult to see.

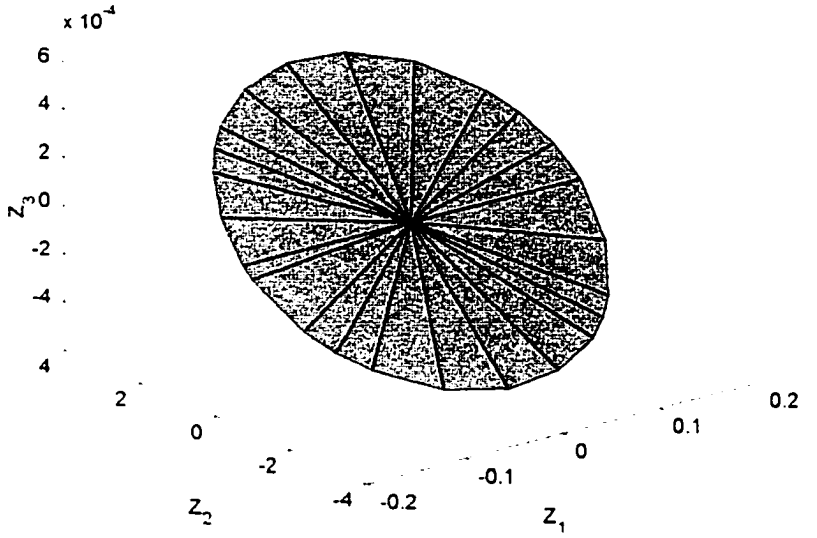

Figure 4.16b: Tight Covering of the Reachable Set for System (4.17)

(Open Valve)

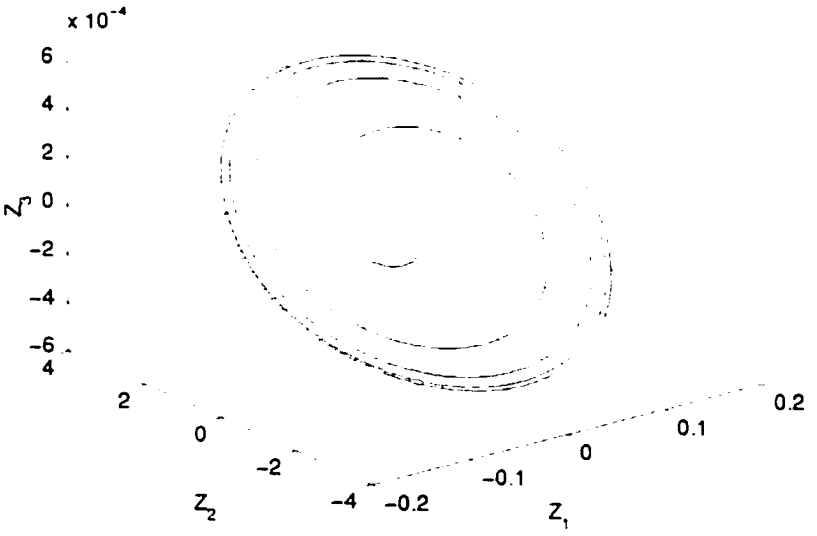

Figure 4.17a: Simulated Response of System (4.17) with a Disturbance (4.1a) (Open Valve)

For illustration, we have plotted the response of system (4.17) to a disturbance (4.1a) in Figure 4.17a. Notice that the system finds some limit cycle, but unlike the 2D case that limit cycle does not bound the space in all directions. For this figure, the initial condition of the system is at the origin.

The Lyapunov based quickest descent method described in Chapter 2 is used to construct six candidate stable semi-active controllers for this 3D example. These controllers will be used to illustrate the methods in future chapters and to show results. The P matrices used for each of these controllers are shown in Table 4.4. The corresponding Q matrices will be reported in Appendix I.

Table 4.4: Values used for Positive Definite Symmetric P Matrix in Candidate Controllers for 3-D Example

Control Version	P(1,1)	P(1,2)	P(1,3)	P(2,2)	P(2,3)	P(3,3)
1	3.79e0	1.89e-3	-5.46e-4	1.52e-2	-6.84e-3	1.03e-1
2	1.94e1	5.15e-4	1.54e-3	8.79e-2	-3.94e-2	1.17e-1
3	3.09e3	1.89e0	-5.45e-1	1.52e1	-6.86e0	1.30e1
4	3.44e3	1.70e0	-4.70e-1	1.68e1	-7.59e0	3.42e0
5	3.23e5	1.90e2	-5.32e1	1.59e3	-7.15e2	3.21e2
6	1.34e2	2.22e0	-9.88e-1	5.51e-1	-2.47e-1	1.11e-1

With these matrices, we can now use the system (4.16) along with the results in Section 2.11 on piecewise linear models to construct the piecewise linear system description for the controlled version of (4.16).

$$\dot{x} = A_i x + Dd, \quad |d| \le 1$$

$$A_0 = \begin{bmatrix} 0 & 1 & 0 \\ -224.72 & -4.50 & -2247.20 \\ 0 & 1 & 0 \end{bmatrix}, \quad x \in X_0 = \left\{ x \middle| x^T PBx_3 < 0 \right\} \quad (u = 0)$$

$$A_1 = \begin{bmatrix} 0 & 1 & 0 \\ -224.72 & -4.50 & -2247.20 \\ 0 & 1 & -5000 \end{bmatrix}, \quad x \in X_1 = \left\{ x \middle| x^T PBx_3 \ge 0 \right\} \quad (u = u_{\max} = 1)$$

(4.21)

Since we cannot find a peak-to-peak gain value for the controlled systems, we will report the maximum simulated performance of these controllers with the disturbance (4.1a). As an example of this simulated response, Figure 4.18 shows the simulated response of (4.21) with Control Version 6. The maximum radius of the simulations will serve as a lower bound on the peak-to-peak gain for the system. The system 1-norm results for this 3D example are given in Table 4.5, and Figure 4.17b shows these values spread over all of the control laws. This figure is not very important at this stage, but we will add new results to it in each of the next three chapters to give a clear picture of the results. Since we are confident that the control law performance will be better than the open valve performance, we can use the open valve peak-to-peak gain as a good indicator of the quality of further results. Basically, if some upper bound for the control law performance is greater than the open valve performance, we know it is conservative. The maximum simulation responses are given in Table 4.6.

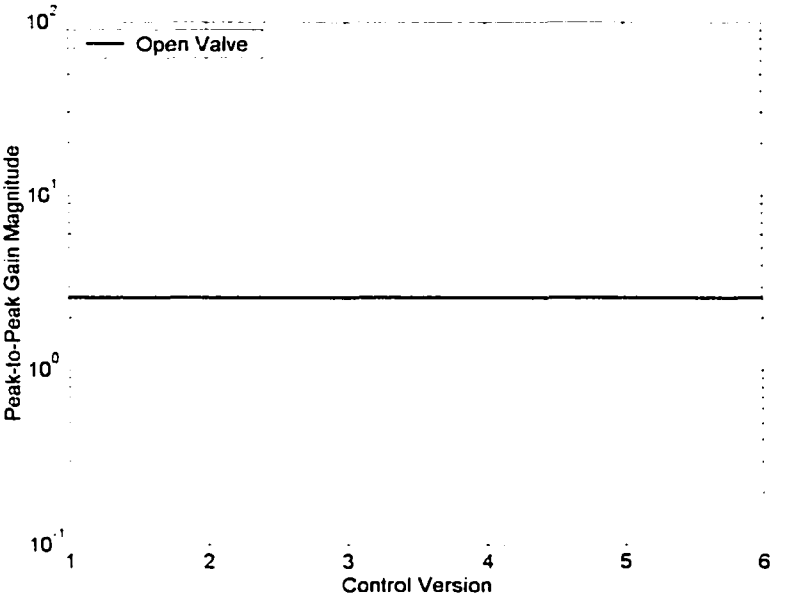

Figure 4.17b: Results Summary for the 3D example

Table 4.5: System 1-Norm Results for 3D example (Open Valve)

Control Version	System 1-Norm			
	$\|z_1\|_\infty$	$\|z_2\|_\infty$	$\|z_3\|_\infty$	Maximum Radius
Open Valve	1.73e-1	2.58e0	5.60e-4	2.59e0

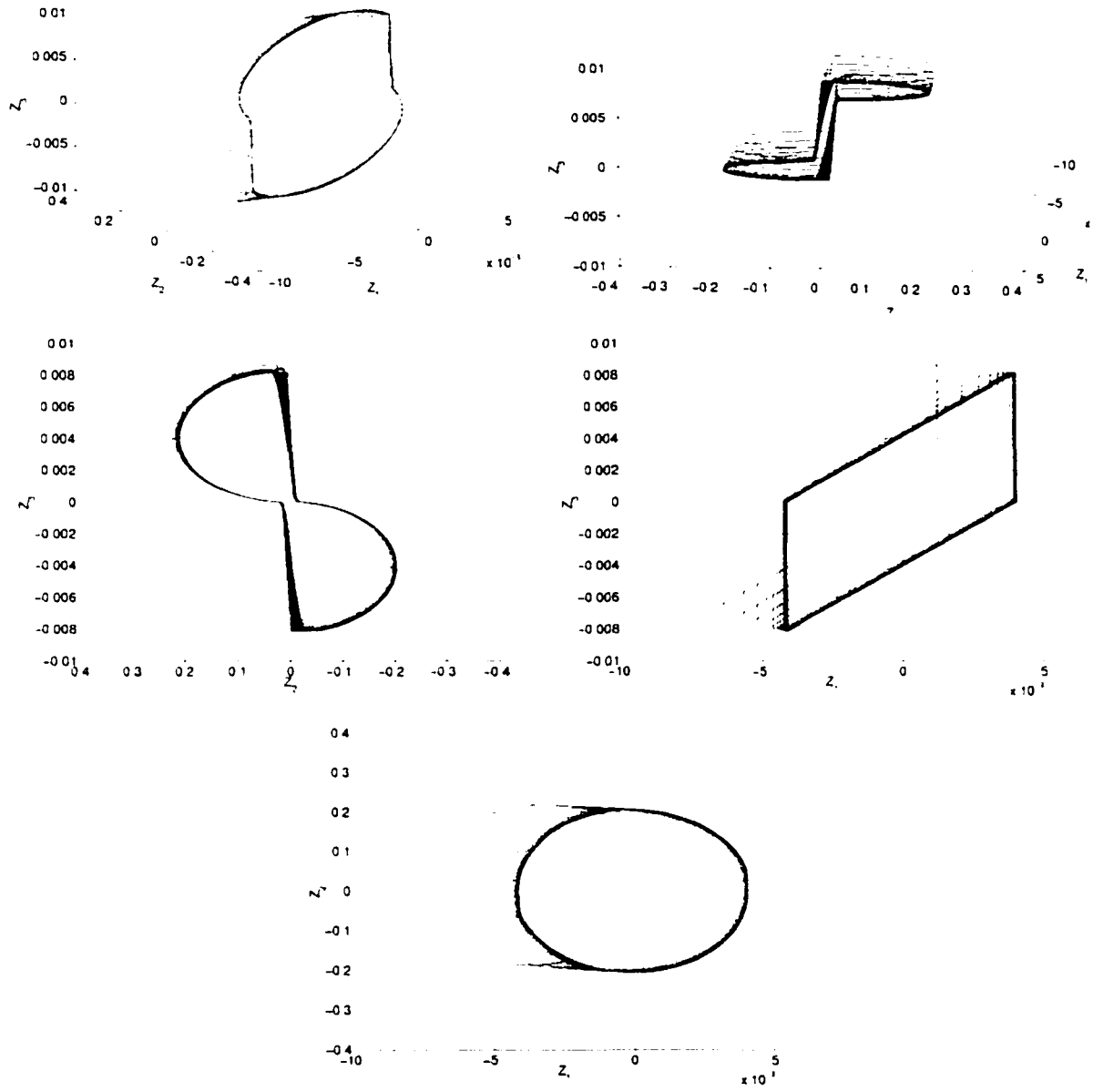

Figure 4.18: 5 Views of the Simulated Response of (4.21) with Control Version 6 and Disturbance (4.1a)

Table 4.6: Maximum Simulated Radius Results for 3D example with Candidate Controllers

Control Version	Simulated Response			
	$\|z_1\|_\infty$	$\|z_2\|_\infty$	$\|z_3\|_\infty$	Maximum Radius
Open Valve	1.72e-1	2.57e0	5.14e-4	2.59e0
1	4.03e-2	3.58e-1	1.12e-2	3.60e-1
2	3.77e-2	3.47e-1	1.14e-2	3.49e-1
3	2.09e-2	2.77e-1	1.05e-2	2.77e-1
4	4.08e-3	2.20e-1	8.70e-3	2.20e-1
5	4.08e-3	2.20e-1	8.70e-3	2.20e-1
6	4.14e-3	2.23e-1	8.77e-3	2.23e-1

We can clearly see from Table 4.6 that the addition of the control to the system has significantly reduced the maximum system response.

4.5 7D Example

This example is the most complicated to be treated here. The assumption is that if the method works for this problem, higher dimensions should also be attainable. This problem is one that has been treated previously by Kuehn (2000), both experimentally and theoretically. This system is a model of a scaled three-story building that was used for experimental testing of semi-active actuators in 1998-2000. Figure 4.19 shows the author next to the scale building, and Figure 4.20 shows a schematic drawing of the building. In Figure 4.19 the semi-active actuator is installed between the second and third floors. This position for the actuator is not modeled here; rather, we model the system with the actuator between the ground and the first floor.



Figure 4.19: Picture of a Three-Story Scale Building whose Model is Used Here for an Example

The red diagonal strut in Figure 4.20 is attached to decrease the torsional motion of the building so that it mostly acts in one plane. The disturbance was introduced into the building in the x-direction from Figure 4.20 as a base excitation to simulate a seismic event.

A single semi-active actuator was then added to this scale building diagonally in the xz-plane to resist the disturbance motion. The location is shown in Figure 4.21, which is a projection of Figure 4.20 into the xz-plane.

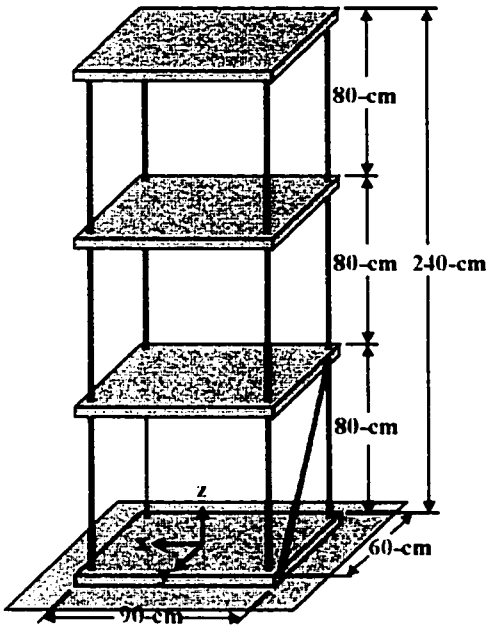

Figure 4.20: Schematic Drawing of a Three-Story Scale Building whose Model is Used Here for an Example

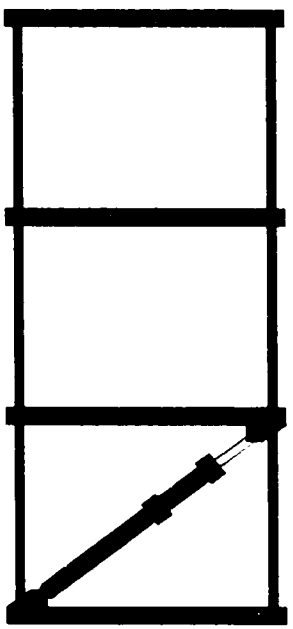

Figure 4.21: Semi-active Actuator Installation Position

This system now fits into the framework described in Chapter 2 and can be modeled as such. The model used in Kuehn (2000) is fully nonlinear as in equation

(2.17). For most of the analysis that follows, we will use a linearized version of this model based on equation (2.23). This linearized system is

$$\dot{x} = Ax + B(u_{\max} - u)x_7 + Dd, \quad \|d\|_\infty \le 1 \tag{4.22}$$

with the following matrices:

$$A = \begin{bmatrix} 0 & 0 & 0 & 1 & 0 & 0 & 0 \\ 0 & 0 & 0 & 0 & 1 & 0 & 0 \\ 0 & 0 & 0 & 0 & 0 & 1 & 0 \\ -1071 & 1095 & 0 & -0.61 & 0.43 & 0 & 2998 \\ 1071 & -2130 & 1248 & 0.61 & -0.83 & 0.287 & -2998 \\ 0 & 1035 & -2399 & 0 & 0.40 & -0.55 & 0 \\ 0 & 0 & 0 & -28.45 & 0 & 0 & -8000 \end{bmatrix}, \tag{4.23}$$

$$B = \begin{bmatrix} 0 \\ 0 \\ 0 \\ 0 \\ 0 \\ 0 \\ 8000 \end{bmatrix}, \tag{4.24}$$

and

$$D = \begin{bmatrix} 0 \\ 0 \\ 0 \\ -1000 \\ 0 \\ 0 \\ 0 \end{bmatrix}. \tag{4.25}$$

For this system, we are taking the valve closed case to be $u=0$ and the valve open case to be $u=u_{max}=1$. The eigenvalues, corresponding natural frequencies, and damping ratios for the four modes in the case where $u=0$ are

$$\lambda_1 = -0.52 \pm 296i, \quad \omega_n = 295.8\,^{rad}/_{\sec}, \quad \zeta = 0.0018$$
$$\lambda_2 = -0.41 \pm 55.1i, \quad \omega_n = 55.0\,^{rad}/_{\sec}, \quad \zeta = 0.0074$$
$$\lambda_3 = -0.07 \pm 19.7i, \quad \omega_n = 19.7\,^{rad}/_{\sec}, \quad \zeta = 0.0034$$
$$\lambda_4 = 0$$

and when $u=1$ they are

$$\lambda_1 = -2.14 \pm 59.9i, \quad \omega_n = 59.9\,^{rad}/_{\sec}, \quad \zeta = 0.036$$
$$\lambda_2 = -3.60 \pm 42.1i, \quad \omega_n = 42.2\,^{rad}/_{\sec}, \quad \zeta = 0.085$$
$$\lambda_3 = -0.59 \pm 14.1i, \quad \omega_n = 14.1\,^{rad}/_{\sec}, \quad \zeta = 0.042$$
$$\lambda_4 = -7989$$

The first thing to notice is that the system has three underdamped modes in both cases. The motion associated with these modes will tend to decay towards the origin while cycling around it when there is no disturbance. When there is a disturbance present, these modes will decay to some stable attracting manifold in a spiraling motion. In the case where $u=0$, there is a zero eigenvalue, which means that, barring a disturbance in the corresponding eigenvector direction, the motion in that direction will be zero. For the case when $u=1$, the system will decay exponentially along the eigenvector associated with the negative real eigenvalue. If there is no disturbance in this direction, the system will decay to the stable manifold of the other eigenvalues. If there is a disturbance in this direction, the system will decay to some modified version of the stable manifold formed by the other eigenvalues.

Admittedly, this does not give a very clear picture of the system dynamics. Unfortunately, with systems of dimension higher than 3 we are unable to graphically show the system dynamics, greatly reducing our understanding of the motion.

As in the previous examples, we will start here by looking at the system where the valve is held open. In this case, we have $u=u_{max}=1$ for all time. This leads to the model

$$\dot{x} = A_1 x + Dd, \quad |d| \le 1, \tag{4.26}$$

where the matrices A_1 and D are defined as (4.23) and (4.25).

The first thing that we will do with this open valve system is to look at the system 1-norm results. Unlike all the other examples, the system 1-norm results for this 7D problem cannot be viewed graphically. Table 4.7 shows the system 1-norm results in the Cartesian directions and the maximum radius.

Table 4.7: System 1-Norm Results for the 7D example (Open Valve)

Control Version	System 1-Norm							
	$\|z_1\|_\infty$	$\|z_2\|_\infty$	$\|z_3\|_\infty$	$\|z_4\|_\infty$	$\|z_5\|_\infty$	$\|z_6\|_\infty$	$\|z_7\|_\infty$	Maximum Radius
Open Valve	4.27e1	3.36e1	1.55e1	5.78e2	4.95e2	2.59e2	2.05e0	8.06e2

Next, we can calculate the reachable set with unit-energy input as discussed in Section 3.3. To do this, we must solve the Lyapunov equation (3.22b). Since this is a 7D problem we cannot visualize the resulting elliptical bound, but we can calculate the local extremum radii from the singular values, S, of the resulting controllability Gramian matrix. We also report the eigenvector matrix, U, which gives us directions that correspond to these radii.

$$R = \left(\sqrt{S}\right)^{-1} = \begin{bmatrix} 2.09e-3 & 0 & 0 & 0 & 0 & 0 & 0 \\ 0 & 6.21e-3 & 0 & 0 & 0 & 0 & 0 \\ 0 & 0 & 9.16e-3 & 0 & 0 & 0 & 0 \\ 0 & 0 & 0 & 3.02e-2 & 0 & 0 & 0 \\ 0 & 0 & 0 & 0 & 2.57e-1 & 0 & 0 \\ 0 & 0 & 0 & 0 & 0 & 5.46e-1 & 0 \\ 0 & 0 & 0 & 0 & 0 & 0 & 3.56e1 \end{bmatrix}$$

$$U = \begin{bmatrix} -2.94e-3 & -2.75e-3 & -2.96e-2 & 7.46e-1 & -6.06e-1 & 2.72e-1 & 3.71e-4 \\ 3.02e-3 & -2.36e-2 & -2.33e-2 & 6.00e-1 & 4.42e-1 & -6.66e-1 & -2.85e-4 \\ 1.33e-3 & -1.01e-2 & -1.05e-2 & 2.83e-1 & 6.61e-1 & 6.95e-1 & -1.06e-4 \\ 7.46e-1 & -6.09e-1 & -2.69e-1 & -3.31e-2 & -2.79e-3 & 1.75e-3 & 3.55e-3 \\ 6.04e-1 & 4.48e-1 & 6.57e-1 & 4.24e-2 & -2.88e-3 & 8.07e-4 & 1.04e-5 \\ 2.80e-1 & 6.54e-1 & -7.03e-1 & -3.27e-3 & -6.20e-4 & 3.17e-4 & -8.08e-7 \\ -2.65e-1 & 2.16e-1 & 9.51e-4 & 4.13e-5 & 4.31e-4 & -2.24e-4 & 1.0 \end{bmatrix}$$

Comparing the magnitudes of these radii with the magnitudes in Table 4.7 illustrates the difference between a unit-peak bound on the disturbance and a unit-energy bound. Note however, that the radii reported are not in the same directions. This comparison just gives a general idea of the relative size of the two bounds.

Kuehn (2000) designed 19 controllers all based on the quickest descent Lyapunov derivation shown in Section 2.9. Many of these controllers were somewhat redundant in their level of performance, so only the first 10 of these will be used. These controller cases will be used later as the final test of the methods explored. Instead of showing the whole P matrix for each of these controllers, we will only show the vector PB in Table 4.8, which is really all that is needed to capture the information in the control logic (2.29). The full P matrices and the corresponding Q matrices will be documented in Appendix I.

Table 4.8: Values used for *PB* Vector in Candidate Controllers for 7-D Example

Control Version	*PB*
1	[0.899, –5.47, 7.29, 0.161, –0.0766, 0.0301, 0.287]^T
2	[0.900, -5.47, 7.29, 0.162, -0.0766, 0.0301, 0.369]^T
3	[1.67, -174, 328, 2.17, -3.90, 3.11, 7.29]^T
4	[9.23, -208, 378, 2.62, -4.12, 3.06, 8.10]^T
5	[0.144, -47.0, 51.9, 2.72, -1.90, -2.13, 5.60]^T
6	[74.9, -116, 4.12, 5.09, -1.20, -2.77, 7.56]^T
7	[6.52, -13.9, 2.11, 2.39, 1.73, 1.05, 0.792]^T
8	[1.93, -15.2, 1.46, 1.92, 1.34, 0.830, 0.699]^T
9	[6.52, -13.9, 2.11, 2.39, 1.73, 1.05, 0.874]^T
10	[1.93, –15.2, 1.46, 1.92, 1.34, 0.830, 0.781]^T

Table 4.9: Simulation Results for 7D Example with Candidate Controllers

Control Version	$\|z_1\|_\infty$	$\|z_2\|_\infty$	$\|z_3\|_\infty$	$\|z_4\|_\infty$	$\|z_5\|_\infty$	$\|z_6\|_\infty$	$\|z_7\|_\infty$	Simulated Maximum Radius
Open Valve	4.47e1	3.32e1	1.48e1	5.26e2	5.28e2	3.06e2	1.71e0	7.99e2
1	6.79e0	6.60e0	3.08e0	8.93e1	9.19e1	4.72e1	5.06e0	1.29e2
2	6.97e0	6.67e0	3.11e0	9.08e1	9.36e1	4.78e1	5.15e0	1.32e2
3	1.57e1	1.13e1	5.24e0	2.01e2	1.63e2	8.24e1	6.00e0	2.66e2
4	1.55e1	1.14e1	5.31e0	2.02e2	1.61e2	7.98e1	6.03e0	2.66e2
5	1.19e1	9.19e0	4.24e0	1.62e2	1.27e2	6.52e1	6.29e0	2.08e2
6	1.23e1	1.04e1	4.76e0	1.72e2	1.46e2	7.27e1	5.12e0	2.29e2
7	3.08e0	4.67e0	3.90e0	7.47e1	1.14e2	2.01e2	4.50e0	2.27e2
8	3.27e0	3.37e0	3.28e0	6.20e1	9.98e1	1.65e2	5.30e0	1.81e2
9	1.87e0	2.52e0	3.82e0	5.98e1	1.19e2	1.90e2	3.91e0	2.19e2
10	1.64e0	1.93e0	3.11e0	5.53e1	9.93e1	1.62e2	3.89e0	1.77e2

The maximum simulated system response for each case of the 7D system with the disturbance logic (4.1b) with (4.13) is shown in Table 4.9. Kuehn used this disturbance in some of his results and showed that it excited the system in question significantly more than the other disturbance logics he tried. Kuehn did not directly show the actual maximum system radius in the work, as he used a modified radius that accounted for his

performance preferences. Here we are solely interested in the maximum undistorted system radius in terms of the peak-to-peak gain.

4.6 Summary

In this chapter we have developed four example models that will be used to illustrate the techniques to be discussed later in this dissertation. For each model, we discussed the open valve case as a baseline for the system performance. This was done on the assumption that any qualifying controllers used would improve the system performance over the open valve case. For the open valve case, we looked at the system 1-norm results, which give upper bounds on the reachable set, except at extremum points, where it is exact. We then looked at the reachable set for the case where the input had a unit-energy bound rather than the unit-peak bound that we are really interested in. These results show the differences in the two disturbance bounds when they are compared to the system 1-norm. For the 2D examples, we were able to generate the reachable set by judicious choice of disturbance and these were reported. For the higher dimensional examples, simulation results were reported for a particular type of disturbance. Finally, Lyapunov type controllers were designed for each system, and the controlled system's performance was reported along with the open valve results.

These models will be used in later chapters to illustrate and show results for each of the methods discussed. The 2D models in particular will be used to illustrate the application of the methods to these problems and to show how the methods are applied with a concrete example. The 3D model will then be used as a first step in extending the

methods to higher dimensions. The 7D model will be used as a final higher dimensional test of the methods.

At this point, we have only actual reachable set solutions for the 2D problems. The goal in this dissertation is to find some tight bound on the reachable set for the higher dimensional piecewise linear systems. To this end, we can learn several things from the 2D problems discussed here:

1. The addition of the Lyapunov controller (2.29) to the system decreases the volume of the reachable set in all cases. In the 2D example #2 it also decreased the peak-to-peak gain. We can see this in Figures 4.6 and 4.11.
2. The reachable set with unit peak input and the reachable set with unit energy input gives significantly differing results. We can see this in Figures 4.4b and 4.9c.
3. In the 2D cases, the simulation with disturbance (4.1a) asymptotically approaches the reachable set.

CHAPTER 5

CLASSICAL LYAPUNOV BOUNDS AND A NEW EXTENSION

In this chapter, we will look at results for a classical Lyapunov method for bounding the reachable set and a new extension of this method. This new method uses intersecting ellipsoidal regions for the Lyapunov function, while the classical method uses a single ellipsoid. The classical Lyapunov bound is based on the work by Kuehn and Stalford (2000) and Kuehn (2000), and the extension is based on unpublished notes by Stalford (2001). In both these cases, the ellipsoidal regions are restricted by the constraint that the symmetric P matrix describing the region must satisfy (2.26), or (AII.39) for the piecewise case, for some positive definite Q matrix. The results indicate that this imposes a very conservative constraint on the method of intersecting regions. We will actually relax this constraint in the methods of Chapter 6.

Lyapunov methods for finding a bound on the reachable set have been used for many years. La Salle and Lefschetz (1961) were among the first to use Lyapunov arguments to find an elliptical upper bound on what they called the region of ultimate boundedness. This is simply the reachable set of a system. Grantham (1981) also used Lyapunov arguments to find a bound on the reachable set. Neither of these works dealt with semi-actively controlled systems. More recently, Reithmeier and Leitmann (2001) and Kuehn and Stalford (2000) used Lyapunov techniques to treat semi-active structural systems. In these papers, the authors used continuous Lyapunov functions that were

directly related to the control derivation as bounds for the reachable set. Unfortunately, the bounds on the reachable set found in this way are very conservative. One possible method to improve this is to use piecewise Lyapunov functions as the boundary.

Piecewise Lyapunov functions have been used in the literature both in quadratic forms and in linear forms. Brockett (1977) tried to improve the circle criterion for predicting stability using piecewise quadratic Lyapunov functions defined as above with two regions. He showed how his method can reduce the assumptions made on the transfer function of the system and still show stability. Xie (1995) also used quadratic Lyapunov functions defined in this way to show stability of an uncertain linear system using linear matrix inequalities. Molchanov and Pyatnitskii (1986) used piecewise linear Lypapunov functions that were defined with the max operator as above to obtain criteria of uniform absolute stability for nonlinear nonstationary systems. In their book, Garofalo and Glielmo (1996) devoted a whole chapter to the use of piecewise linear Lyapunov functions for robust control. Milani (2001) used piecewise affine Lyapunov functions for stability analysis of discrete linear systems with saturating controls. His analysis showed that piecewise affine functions were strictly more effective for Lyapunov stability analysis of that particular type of system.

The two Lyapunov methods discussed here are described in detail in Appendix II. In this chapter, we present numerical results for the peak-to-peak gain based on both of these methods for some of the examples discussed in Chapter 4.

5.1 Results for Example Systems

The results from the application of the methods described above and in Appendix II will be shown for the 2D examples and for the 3D example. Since the 2D example #1 has only one controller designed, we will not apply the piecewise Lyapunov method to that specific example. This is essentially because the piecewise Lyapunov method relies on the already designed controllers for candidate Lyapunov functions. The 7D method will be omitted because the results presented for the smaller problems do not show a significant improvement, and it was deemed unnecessary to attempt to apply these methods to the higher dimensional problem.

For the 2D example #1, we can only apply the classical bounding method described in Section AII.1. The results for this are shown in Table 5.1 below. We can see from the table that the classical bounding method is about four times too high for this simple problem.

Table 5.1: Summary of previous results for the 2D example #1

Control Version	Actual Peak-to-Peak Gain	System 1-Norm Maximum Radius	Classical Bounding Method Radius
Open Valve	7.07e-1	7.07e-1	n/a
1	7.07e-1	n/a	2.62e0

In the application of this method to the 2D example #2, we use the control laws designed in Chapter 4 for this system as the trial functions for the extension of the classical method shown in this Chapter. All of the P matrices in Table 4.2 are normalized by their maximum singular value so that the minimum radius of all the ellipsoids will be equivalent. Every combination of these Lyapunov functions is then tried and a new

bounding radius is calculated for the ball B_{r_2}. Table 5.2 shows the reachable set results, system 1-norm results, and the new results from this chapter when a single Lyapunov function is considered. We can see that the classical bounding method seems to have no relation to the actual peak-to-peak gain and is mostly very conservative (up to 3 orders of magnitude). Most importantly, we cannot use these values to judge the relative merit of the designed controllers. The one thing that we can say from these results is that the bound formed by the Lyapunov function is one that is guaranteed to be inescapable.

Table 5.2: Results for the 2D Example #2

Control Version	Actual Peak-to-Peak Gain	System 1-Norm Maximum Radius	Classical Bounding Method Radius
Open Valve	1.28e0	1.28e0	n/a
1	5.78e-1	n/a	1.06e2
2	5.78e-1	n/a	2.23e0
3	5.62e-1	n/a	6.55e2

Table 5.3 shows the results of the analysis with piecewise Lyapunov functions as well as simulation results for the new control laws based on the analysis in Sections AII.2 to AII.4. In Table 5.3, the control version column indicates which P matrices from Table 4.2 were used with the modified control law. For instance, the row that indicates a control version of 1+3 means that we used the P matrices from Control Version 1 and Control Version 3 and combined them as was developed earlier in this chapter. Notice first, that the simulated response of the system with a bounded disturbance from Chapter 4 does not change significantly when we use multiple Ps in the control law from the case where a single P is used in the control law. We can see that this new method does not seem to be particularly effective for improving the bound on the attractor set over the

classical method. It does, however, improve in a few cases. This seems to indicate that the method is an improvement only when very judicious choices for the P matrices are combined.

Table 5.3: Intersecting P Method Results for the 2D example #2

Control Version	Intersecting *P* Simulated Maximum Radius	Intersecting *P* Maximum Radius
1+2	5.63e-1	1.77e2
1+3	5.59e-1	1.77e2
2+3	5.59e-1	2.30e1
1+2+3	5.59e-1	7.94e1

Table 5.4: Results for the 3D Example

Control Version	Simulated Maximum Radius	System 1-Norm Maximum Radius	Classical Bounding Method Radius
Open Valve	$2.59 \cdot 10^{0}$	$2.59 \cdot 10^{0}$	n/a
1	3.60e-1	n/a	1.85e3
2	3.49e-1	n/a	1.40e2
3	2.77e-1	n/a	2.15e3
4	2.20e-1	n/a	1.60e6
5	2.20e-1	n/a	4.55e5
6	2.23e-1	n/a	4.96e3

The results for the 3D case indicate much the same thing. Table 5.4 shows the results for a single Lyapunov function. The resulting upper bounds range from 140 to 1.6 million. These bounding radii values are 2-6 orders of magnitude higher than the system 1-norm results or the simulation results for any of the control versions. Also, the classical technique favors controller 2 over controller 6 by a huge factor, when in fact the simulation results put controller 6 ahead of 2. This further supports the fact that this

classical technique for bounding the system response is not practically useful. It is conservative and cannot differentiate between controllers. Figure 5.1 shows this graphically, comparing it to the open valve system 1-norm results from the last chapter.

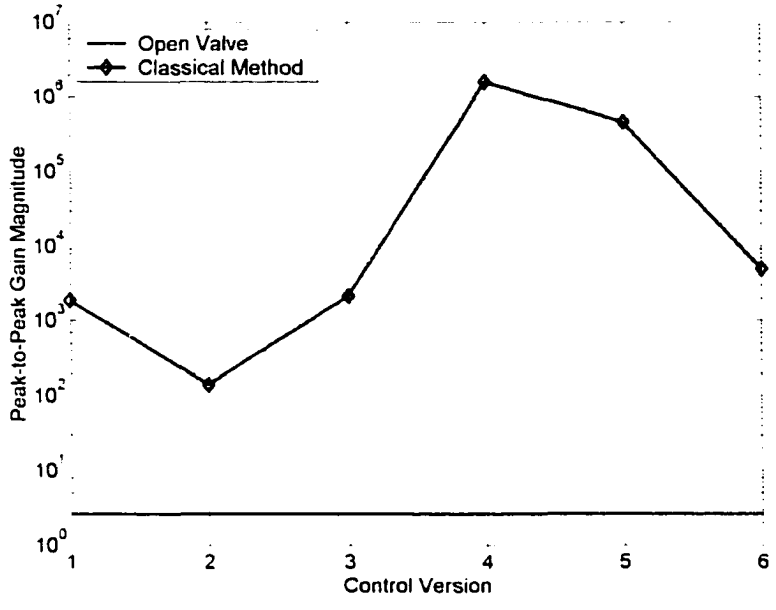

Figure 5.1: Results Summary for the 3D Example

Table 5.5 shows the new results for piecewise Lyapunov functions. Again, the simulation results with combined Ps are not much different than the simulation results for the best control version in the combination. Unfortunately, this is accompanied by a result for the attractor set that is somewhere between that of the best control version and the rest of the control versions in combination. Take control versions 1 and 4 for example. We can see from Table 5.5 that the simulation from the control version 1+4 is very close to that for control version 4 in Table 5.4. The attractor set bound for control version 1+4 is 5.33e3, which is between the attractor set bound for control version 1 of 1.85e3 and for control version 4 of 1.60e6. The conclusion is the same as for the case

with a single Lyapunov function: this technique is not practically useful because it is conservative and cannot differentiate between controllers.

Table 5.5: Intersecting P Method Results for the 3D Example

Control Version	Intersecting P Maximum Radius	Intersecting P Simulated Maximum Radius
1+2	7.65e2	3.59e-1
1+3	2.08e3	3.34e-1
1+4	5.33e3	3.60e-1
1+5	7.79e2	3.40e-1
1+6	1.95e2	2.26e-1
2+3	1.32e3	2.77e-1
2+4	2.92e3	2.66e-1
2+5	7.15e2	2.20e-1
2+6	1.58e2	2.77e-1
3+4	6.91e3	2.77e-1
3+5	2.77e3	2.20e-1
3+6	2.77e3	2.20e-1
4+5	1.12e6	2.20e-1
4+6	2.15e6	2.20e-1
5+6	7.15e5	2.20e-1
1+2+6	1.41e2	2.31e-1
1+3+6	2.08e3	2.31e-1
2+5+6	7.15e2	2.20e-1
4+5+6	1.12e6	2.20e-1

The final example is the 7D scale building. The performance index here is not exactly the same as that used by Kuehn (2000) for the same system. The classical bounding technique result reported here is the undistorted radius of the system. When Kuehn reported this information, he used a performance matrix to scale the states relative to each other according to his desired system performance. While this is easily done and is a very useful way to view the results, for simplicity, as well as ease of comparison

later, we will use undistorted radius. The results for this method are presented in Table 5.6.

Table 5.6: Results for 7D example

Control Version	Simulated Maximum Radius	System 1-Norm Maximum Radius	Classical Bounding Method Radius
Open Valve	7.99e2	8.06e2	n/a
1	1.29e2	n/a	1.82e4
2	1.32e2	n/a	2.14e3
3	2.66e2	n/a	1.54e6
4	2.66e2	n/a	2.04e5
5	2.08e2	n/a	2.87e5
6	2.29e2	n/a	3.50e5
7	2.27e2	n/a	4.77e6
8	1.81e2	n/a	3.58e6
9	2.19e2	n/a	5.60e5
10	1.77e2	n/a	4.20e5

As in previous examples, it can be seen in Table 5.6 that the classical bounding method is very conservative and does not reflect differences in control strategy. In this example, the classical bounding technique was anywhere from 1-4 orders of magnitude larger than the simulation results. It also chose control 2 as the best case, and control 7 as the worst performer. This is in contrast to the simulation, which indicated that the best control was number 1 and the worst performers were controls 3 and 4.

Since the method using piecewise Lyapunov functions does not show significant improvements over the results using the classical bounding method, unless P matrices are chosen very judiciously, we will not apply the method to the 7D case.

5.2 Summary

In this chapter, we have reviewed the results of two methods for bounding the reachable set. The first method relies on a single continuous Lyapunov function to bound the reachable set, and the second relies on piecewise Lyapunov functions, all based on the constraint $Q > 0$. In both cases, we are looking for the region outside which the derivative of the Lyapunov function can be guaranteed to be negative. Results are presented for both methods for the example problems from Chapter 4.

The method using a single Lyapunov function gives results that are most often very conservative and do not reflect the actual peak-to-peak gain in the 2D cases. The results for the 7D problem, for example, are up to 6 orders of magnitude higher than the highest simulated system response. Because of this conservatism, this method is also unable to distinguish between controllers on the basis of performance.

The method of piecewise Lyapunov functions showed promise when first developed. The subsequent results for the method indicate that actually finding a combination that improves the attractor set is difficult with the restriction of satisfying (AII.39) in each region. This method is also unable to distinguish the relative performance of the control laws. This restriction is relaxed in the next chapter, and an optimization method is used to find the piecewise ellipsoid boundaries.

CHAPTER 6

LINEAR MATRIX INEQUALITIES (LMI) METHOD AND EXAMPLES

In this chapter, the problem of finding a bound on the peak system response to persistent bounded disturbances (i.e. peak-to-peak gain) for the semi-active controlled system described earlier is transformed into a convex optimization problem with linear matrix inequality constraints (LMI method). This method has only become fruitful within the last two or three decades, because the solution of such problems typically relies on numerical interior point methods executed on a computer. Also, efficient interior point methods for solving these problems have only been available since the early 1980's (Boyd et al., 1994). Several computer codes are currently available to solve these problems, including at least two written to run with Matlab. The LMI Control Toolbox is used exclusively here in solving LMI type problems (Gahinet, et al., 1995).

The LMI method has been applied to system and control theory quite extensively (Boyd et al., 1994). It has been applied most often to robust control problems (problems with H_2 and H_∞ performance measures) and problems that can be written in terms of Lyapunov equations and their derivatives (system stability). Multiobjective robust control problems can be solved with the LMI method as well. The problem of finding an upper bound on the peak-to-peak gain of a piecewise linear semi-active control system can be written in terms of Lyapunov functions and their derivatives, and as such can be treated with the LMI method.

Linear matrix inequalities are inequalities that must hold on the whole space of the problem in question, because it is the positive definiteness that is checked. Thus, they do not directly lend themselves to solving problems where the system is piecewise linear as in (3.23c) and (3.28a,b). As we will see in Section 6.3, in a piecewise linear system the system space is subdivided into regions, and different inequality conditions are defined in each region. To pose this type of problem as an LMI, we must reconstruct the problem in terms of inequalities that hold on the whole system space. This process (Section 6.3) involves a procedure called the S-procedure, which is shown in Proposition 6.1. Unfortunately, this process is normally conservative, which means that the solution to the LMI for bounding the peak-to-peak gain of the semi-active control system with a linear approximation in the actuator (Section 2.11) will be conservative.

This chapter presents the development of the LMI method to find a bound on the maximum system states for a semi-active controlled system with a bounded disturbance (peak-to-peak gain). First, we discuss some related problem developments in the literature. Next, the development of the LMI method for finding a bound on the reachable set with unit peak input for a linear system is shown. Finally, the results are extended to piecewise linear systems for use in the semi-active problem.

6.1 Background

The LMI formulation has been fruitful in attacking a number of difficult performance problems. For example, using the LMI approach, Abedor, Nagpal, and Poola (1996) developed upper bounds on peak-to-peak gain for linear time invariant (LTI) systems like (3.24a). The method that they discussed resulted in a continuous

feedback controller that minimized the peak-to-peak gain for an LTI system. This is different than the problem in this dissertation in that he did not treat piecewise linear systems, discontinuous dynamics, or semi-active control.

Hassibi and Boyd (1998), Johansson and Rantzer (1998), and Rantzer and Johansson (2000) derived various L_2 performance bounds for piecewise linear and affine systems like (3.28a,b). These authors treated systems that incorporated discontinuous dynamics. However, they did not treat peak-to-peak gain performance for their systems. Although they did not treat peak-to-peak gain, Hassibi and Boyd (1998) did mention that the problem could be solved using the LMI method. Xie, Shishkin, and Fu (1997) developed lower bounds on uncertainty limits for robust stability of linear uncertain systems like (3.23b). The paper described the LMI application to a system modeled as a convex hull of linear system and tried to find the stability limit of the system relative to the uncertain terms in the system matrix.

Pettersson and Lennartson (1997a, 1997b) used continuous, piecewise C^1 quadratic Lyapunov functions to establish stability for autonomous hybrid and nonlinear systems modeled as weighted sums of linear systems. After significant effort modeling these systems, the authors treated these systems as significantly simpler uncertain systems like (3.24b) when the LMI method was applied. Working with a single Lyapunov function, P, Pancake, Corless, and Brickman (2000) developed sufficient conditions which guaranteed a certain peak-to-peak gain for polytopic uncertain/nonlinear systems modeled as weighted sums of linear stable systems. In a method very similar to the previous paper, when they applied the LMI method, the system was reduced to an uncertain system like (3.24b).

None of these papers treat the peak-to-peak gain problem for systems modeled as piecewise linear dynamics like (3.28a). Even though none of these works treated the problem we are interested in, certain concepts from several papers are used in the developments in the rest of this chapter.

Before we describe the development of the LMI formulation for our problem, two pieces of information are needed. First, a definition of linear matrix inequalities and quadratic functions, which will be used throughout, will be given.

Definition 6.1 (Linear Matrix Inequalities)

Non-Strict Inequalities: A non-strict linear matrix inequality (LMI) has the form $P(x) \geq 0$, where P is a symmetric n x n matrix populated by the variables $x \in \Re^n$. The non-strict inequality symbol in the case of linear matrix inequalities means that the matrix is at least positive semi-definite (i.e. $x^T Px \geq 0, \quad x \neq 0$).

Strict Inequalities: A strict linear matrix inequality (LMI) has the form $P(x) > 0$, where P is a symmetric n x n matrix populated by the variables $x \in \Re^n$. The strict inequality symbol in the case of linear matrix inequalities means that the matrix is positive definite (i.e. $x^T Px > 0, \quad x \neq 0$).

The distinction between strict and non-strict inequalities is important. The reader will notice later in this chapter that many of the LMIs defined have both strict and non-strict components. When we solve these problems, we solve problems where all the inequalities are assumed to be strict. Fortunately, this also automatically satisfies the case where some inequalities are non-strict. However, it does not allow the case where the inequalities reduce to equalities. For the problems in this chapter, this essentially adds a slight amount of conservatism to the already conservative LMI formulations.

To avoid confusion, we will always use the form $x^T Px > 0$ in the following derivations and examples. The reader should remember that when the LMI method is applied with the Matlab LMI Control Toolbox, the constraint is actually on the positive definiteness of the matrix P rather than on the quadratic equation $x^T Px$. They are equivalent conditions, but the meaning becomes slightly clearer if we present the quadratic function condition.

Definition 6.2 (Quadratic Function)

A scalar function F is said to be a quadratic function of $x \in \Re^n$ if there exists a symmetric n x n matrix T and an n-vector u and a scalar v such that F satisfies

$$F(x) = x^T Tx + 2u^T x + v, \quad x \in \Re^n \tag{6.1}$$

Second, a commonly encountered technique in the next several sections called the *S*-procedure will be described. This procedure is helpful when we encounter the constraint that some quadratic function is negative whenever some other quadratic functions are negative. In these cases, the *S*-procedure can be used to form a conservative LMI that is an approximation of the constraint.

Proposition 6.1 (*S*-procedure)

(a) Let $F_0, \ldots, F_p$, $p \geq 1$ be quadratic functions. Suppose there exists scalars $\tau_1, \ldots, \tau_p \geq 0$ such that

$$F_0(x) - \sum_{i=1}^{p} \tau_i F_i(x) \geq 0, \quad \forall x \in \Re^n, \tag{6.2}$$

then $F_0(x) \geq 0$ for all x such that $F_i(x) \geq 0$, $i = 1, \ldots, p$.

(b) (Converse only holds for p=1.) Let F_0, F_1 be quadratic functions. Suppose there exists x_0 such that $F_1(x_0) \geq 0$, and suppose that $F_0(x) \geq 0$ for all x such that $F_1(x) \geq 0$. Then there exists τ_1 such that

$$F_0(x) - \tau_1 F_1(x) \geq 0, \quad \forall x \in \Re^n . \tag{6.3}$$

Proof

For (a) and (b) see Yakubovich, 1977.

This result will be used when we encounter constraints in the form of a quadratic function that holds only on a region of the system space that can be described by a quadratic function. The *S*-procedure will allow us to write this as a single linear matrix inequality constraint whose positive definiteness can be checked on the whole space. It is interesting to note that because the converse of the *S*-procedure only holds for p=1, the resulting linear matrix inequality is a conservative estimate when p>1. This is the case in Section 6.3, where we apply the LMI method to piecewise linear systems. If we use the S-procedure in a problem, we will rewrite a set of inequalities in the form (6.2) and say that if we can satisfy (6.2), then the individual inequalities are satisfied. If $p > 1$, then we cannot say that if all of the individual inequalities are satisfied that (6.2) will be satisfied. So the use of the S-procedure disallows some possible solutions that would in fact fit within the individual inequality constraints and becomes a conservative estimate of the individual inequalities.

6.2 Single P LMI Method

Both the LMI formulation that follows and the convex optimization problem associated with it will be used to find a bound on the reachable set for the open valve

system. Recall that the system 1-norm can be used to find a tight bound in the peak-to-peak gain for the stable LTI system (3.23d). This gives us a means of judging the conservatism in the LMI results for the open valve case. This section will develop the LMI formulation to find a bound on the reachable set for the LTI system (3.23d) where the disturbance is bounded by

$$|d| \le 1. \tag{6.4}$$

The reachable set that we are looking for is defined in Definition 3.6. Another way to look at this reachable set is to see that all trajectories that start outside this set are heading in towards this set. This is in fact the way that the LMI is set up. Next, the reachable set is bounded by an elliptical function and this bound is guaranteed using Lyapunov arguments. This is a formalization of the discussion at the end of Chapter 3.

Proposition 6.2 (Elliptical Bound on Reachable Set with Unit Peak Input)

Consider an LTI system of the form (3.24a) with the disturbance bound (6.4). Suppose there exists a quadratic function $V(x) = x^T Px$, with $P > 0$ and $\frac{dV(t)}{dt} \le 0$ for all x and d such that $V(x) > 1$. Then the ellipsoid defined by

$$\varepsilon = \{x | x^T Px \le 1\} \tag{6.5}$$

contains the reachable set of the dynamic system with a unit peak input.

Proof

This has been well known for many years. See Krasovski (1959), La Salle and Lefschetz (1961), Yoshizawa (1966), and Grantham (1981) for more discussions and proof. This proposition basically says that if the system's energy is

decreasing everywhere outside the ellipsoid ε, and the system starts inside the ellipsoid, it will be unable to get outside.

Finally, the problem can be couched in terms of LMIs. The following proposition and corollary give the LMI formulation for finding an elliptical bound on the reachable set with unit peak input for the system (3.24a). This formulation will be used in the next section, where it will be extended and applied to piecewise linear systems of the form (3.29), as described in Section 2.11.

Proposition 6.3 (Estimate for the reachable set)

Consider the dynamic system (3.24a) with disturbance (6.4). Suppose there exists a symmetric matrix $P > 0$ and scalars $\alpha, \beta > 0$ such that for all x and d

$$\begin{bmatrix} x \\ d \\ 1 \end{bmatrix}^T \begin{bmatrix} A^T P + PA + \alpha P & PD & 0 \\ D^T P & -\beta I & 0 \\ 0 & 0 & \beta - \alpha \end{bmatrix} \begin{bmatrix} x \\ d \\ 1 \end{bmatrix} \leq 0 . \tag{6.6}$$

Then the ellipse in (6.5) bounds the reachable set for the system in (3.24a) with a unit peak input (Boyd et al., 1994). Note that this also implies that all minors are ≥ 0.

Proof

It suffices to show that the conditions in Proposition 6.2 hold. Given LMI (6.6) we define scalar functions

$$\begin{aligned} F_0 &= -\begin{bmatrix} x \\ d \end{bmatrix}^T \begin{bmatrix} A^T P + PA & PD \\ D^T P & 0 \end{bmatrix} \begin{bmatrix} x \\ d \end{bmatrix} \\ F_1 &= \begin{bmatrix} x \\ 1 \end{bmatrix}^T \begin{bmatrix} P & 0 \\ 0 & -1 \end{bmatrix} \begin{bmatrix} x \\ 1 \end{bmatrix} \\ F_2 &= \begin{bmatrix} d \\ 1 \end{bmatrix}^T \begin{bmatrix} -I & 0 \\ 0 & 1 \end{bmatrix} \begin{bmatrix} d \\ 1 \end{bmatrix} \end{aligned} . \tag{6.7}$$

or equivalently

$$\begin{aligned} F_0 &= -x^T\left(A^T P + PA\right)x - 2PDd = -\frac{dV(t)}{dt} \\ F_1 &= x^T Px - 1 = V(x) - 1 \\ F_2 &= -d^T d + 1 \end{aligned} \quad . \tag{6.8}$$

Rewriting (6.6) gives

$$x^T\left(A^T P + PA + \alpha P\right)x + 2PDd - \beta d^T Id + \beta - \alpha \le 0 . \tag{6.9}$$

which can be rearranged to give

$$x^T\left(A^T P + PA\right)x + 2PDd + \alpha\left(x^T Px - 1\right) + \beta\left(1 - d^T Id\right) \le 0 . \tag{6.10}$$

Substituting (6.8) gives

$$-F_0 + \alpha F_1 + \beta F_2 \le 0 , \tag{6.11}$$

or, rearranging,

$$F_0 - \left(\alpha F_1 + \beta F_2\right) \ge 0 . \tag{6.12}$$

Applying (a) of Proposition 6.1 gives the result

$$F_0(x,d) \ge 0, \quad \text{for all } x \text{ and } d \text{ such that } \quad F(x)_1 \ge 0, \quad F_2(d) \ge 0 . \tag{6.13}$$

This is equivalent to the conditions and conclusions in Proposition 6.2.

Proposition 6.3 can be simplified with the following corollary.

Corollary 6.1

Consider the dynamic system given in (3.24a) with disturbance (6.4). Suppose there exists a symmetric matrix $P > 0$ and scalar $\alpha > 0$ such that for all x and d

$$\begin{bmatrix} x \\ d \end{bmatrix}^T \begin{bmatrix} A^T P + PA + \alpha P & PD \\ D^T P & -\alpha I \end{bmatrix} \begin{bmatrix} x \\ d \end{bmatrix} \le 0 . \tag{6.14}$$

Then the ellipse in (6.5) bounds the reachable set for that system (Boyd et al., 1994).

Proof

Since we must have $\alpha \geq \beta$ for all minors of Proposition 6.3 to hold, it follows that if Proposition 6.3 holds for some (α, β) then it holds for all (α, β_0) with $\alpha \geq \beta_0 \geq \beta$. Therefore, we can assume without loss of generality that $\beta = \alpha$, and rewrite (6.6) as (6.14).

The LMI in Corollary 6.1 is quadratic in the variables α and P, so we must make it linear by fixing α. This means that to find some minimal solution that satisfies these inequalities we will have to do a search over possible values of α, which significantly increases the computational effort to solve such problems. When the LMIs in Corollary 6.1 are combined with a convex optimization criterion, we end up with a method to minimize the size of the ellipsoid that bounds the reachable set for the system in (3.24a) for the disturbance bound in (6.4) for some fixed α. As pointed out above, we then must optimize the objective with respect to α to find some global optimal solution.

Proposition 6.4 (Optimization I)

Solving the following minimization problem

Maximize λ
Subject to the LMI constraints in Corollary 6.1
and $P > \lambda I$,

minimizes the maximum radius of the ellipse (6.6), which is a conservative bound on the reachable set of the dynamic system (3.24a) with unit peak input.

Proof

Refer to Boyd et al. 1994, pp. 44.

Proposition 6.4 allows us to find some upper elliptical bound on the dynamics of an LTI system for a unity bounded disturbance. This is useful when considering such systems,

as is the system 1-norm, which gives a tight bound on the peak-to-peak gain. For our problem however, this LMI method must be extended to apply to piecewise linear systems like (3.29) so that we can apply it to the system in Section 2.11. The next section will extend Corollary 6.1 to find a continuous, piecewise C^1 Lyapunov function that will be an upper bound on the reachable set for a piecewise linear system with a unit peak input.

6.3 Piecewise LMI Method

As mentioned at the end of Chapter 3, and as shown below, the extension of the Corollary 6.1 to include piecewise linear systems and continuous, piecewise C^1 Lyapunov functions requires additional terms in the $\dot{V}$ inequality. Since the LMI method can check only for positive definiteness of a matrix, we must have matrix conditions that hold on the whole space. From (3.33) we can see that the conditions for the continuous, piecewise C^1 Lyapunov function to bound the reachable set need only to hold on regions defined by the control law. To reconcile this with the LMI method, we will have to add a term to the Lyapunov function that will convert the regional condition to a condition that needs to be satisfied on the whole space. Note that a term was already added in the last section to combine the Lyapunov function condition and the derivative condition. These extra terms will be evident when one compares (6.24) to (6.14) and (3.33). The extra term is added to the inequality constraints using the S-procedure discussed earlier.

Another conservatism in the problem is the estimation of the reachable set with ellipsoidal boundaries. By constraining the solutions for a boundary to be ellipsoidal we are probably adding significant conservatism, since the actual reachable set is probably

not ellipsoidal in shape. This was evident in the last two chapters and is the case here as well. We can remedy this somewhat by using a large number of partitions for describing the piecewise linear system and solving an LMI problem on each of these smaller regions. However, this does not seem to be able to converge to a tight bound, as we shall see in the following results section.

For the LMI application to piecewise linear systems of the form (3.29), we must predetermine the regions X_i. For the problem of the semi-active controlled system from Section 2.11, the system space will be split into two major regions corresponding to the open valve case and the closed valve case. The system will be linearized independently on each of these regions as shown in Section 2.11, and solutions for the upper bound on the reachable set will be found with the LMI method. These solution functions will be constrained to be continuous across region boundaries so that a continuous, piecewise C^1 Lyapunov function will be constructed that bounds the system response for unit peak input. For the LMI analysis, each of the two regions, $X_{u=0}$ and $X_{u=1}$ (denoting valve closed and valve open respectively) will be further split into a specific type of new polytopic region called generalized simplex regions, which will be collectively denoted as $X_j, j = 1,\ldots,N$.

Definition 6.3 (Vertex Directions at Infinity)

> If a vertex of a polytope is located at infinity, we will use the unit vector that points from the origin towards that vertex at infinity to define that vertex. That unit vector is defined as the vertex direction at infinity.

Definition 6.4 (Generalized Simplex Regions)

A generalized simplex region is defined as the convex hull of a finite number of corner points, v_k, $k = 0,\ldots,p$, in $\Re^n$, where every point x in the region can be written as

$$x = \sum_{k=0}^{q} z_k v_k + \sum_{k=q+1}^{p} z_k v_k \tag{6.15}$$

with $z_k \geq 0$, $\sum_{k=0}^{q} z_k = 1$, and $p=n$. The column vectors v_k, $k = 0,\ldots,q$ are finite vertices, while v_k, $k = q+1,\ldots,p$ define vertex directions at infinity. (Rantzer and Johansson, 2000)

Most of the problems that we discuss will have regions that radiate out from the origin. This means that we will mostly be dealing with the second term on the right hand side in equation (6.15). To clarify this, we will use the 2D example #2 from Section 4.3 and assume that the control law vector PB is $\begin{bmatrix}1 & 0\end{bmatrix}^T$ in the control law (2.29). From the control law we know that we will at least have to divide the space into four regions that corresponding to the four quadrants where the control law is defined. For each of these regions, we will further split each region into two smaller regions. We can write any point in a region as a linear combination of the finite vertices and the unit vectors that describe the directions of the boundaries for that region when the vertices are at infinity. The regions, denoted as X_i, $i = 1,\ldots,8$, the vertex v_0 at the origin, and vectors that define the vertex directions at infinity, v_k, $k = 1,\ldots,8$ for these regions are shown in Figure 6.1. Based on the control law, the regions that are shaded grey where $A=A_{u=0}$ (closed valve), and the regions are white where $A=A_{u=1}$ (open valve). So, referring back

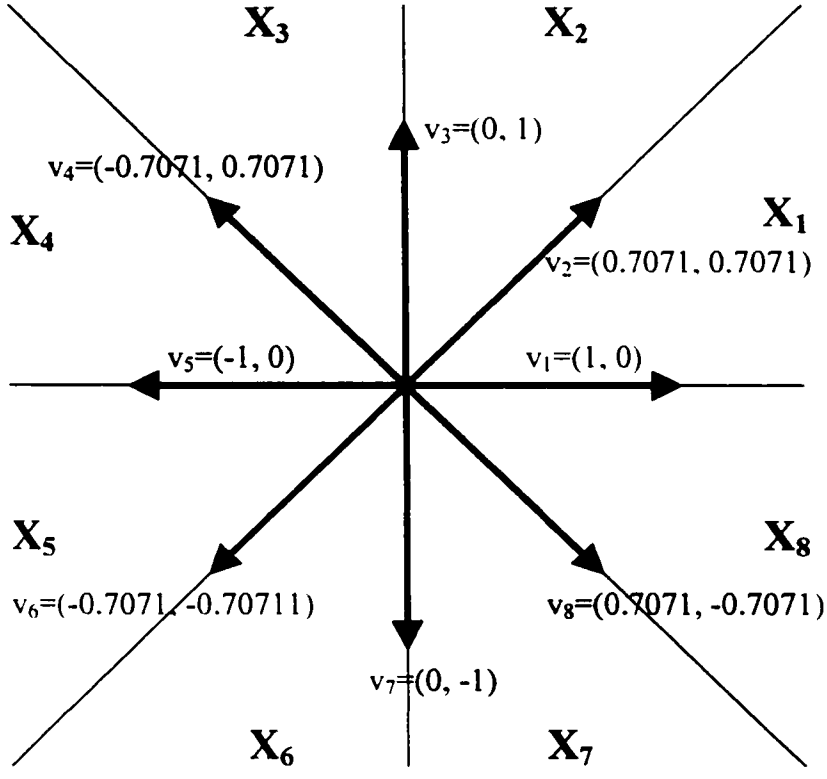

Figure 6.1: Regions and vertex directions for the 2D example #2.

Grey area are where $A=A_{u=0}$ and white areas are where $A=A_{u=1}$.

to (6.15), and setting the coefficient for v_0 to zero, the point (1, 0.3) in Figure 6.1 can be written as a positive linear combination of the vectors

$$\begin{bmatrix} 1 \\ 0.3 \end{bmatrix} = 0.7 \cdot v_1 + 0.4243 \cdot v_2 .$$

If we used any vectors except these two we would end up with negative coefficients and not satisfy Definition 6.4.

For the discretization of the system space used in the following derivation, we will assume that v_0 is always at the origin and v_k, $k = 1,\ldots,p$ are vertex directions at infinity. Each of these new regions will be assigned an A_j chosen from $A_{u=0}$ and $A_{u=1}$, depending on whether X_j is part of $X_{u=0}$ or $X_{u=1}$. Refer back to Figure 6.1 to see how

this works for the 2D example #2 with a simple control law. Now, since the LMI method requires all of the inequalities to be quadratic functions, we must approximate the regions X_j in terms of a quadratic function as follows.

Proposition 6.5 (Quadratic estimate for regions)

Given a generalized simplex region X, there exists a non-zero matrix E such that

$$Ex \geq 0, \quad x \in X, \tag{6.16}$$

where the vector inequality in (6.16) means that all the terms are non-negative. Furthermore, for some matrix U with non-negative elements, an ellipsoidal outer approximation of X is given by

$$x^T E^T U E x \geq 0, \quad x \in X. \tag{6.17}$$

Proof

Refer to Johansson and Rantzer (1998).

Note that the values in U are solved for in the LMI process. We do not specify them beforehand. We must also include LMI constraints to guarantee that each component in U is positive.

If we wanted to construct these regions in the simplest way possible, we could simply use the regions defined by the control law (2.29). If we do this, we do not need to use the simplex regions defined previously. It is relatively simple to write inequalities to define these regions. For instance, for our simple 2D example #2, if we wanted to define the area in Figure 6.1 , quadrant II, where $A = A_{u=0}$ we would write

$$\begin{bmatrix} 0 & 1 \\ -1 & 0 \end{bmatrix} x \geq 0, \quad x \in X_{QuadII}.$$

which is equation (6.16). This allows us only to define as many regions for the LMI solution as are defined by the control law. To increase the number of regions we need to define each region in some unified way that will be simple to keep track of and use. This is the simplex region defined above.

To construct these matrices from the simplex regions in Definition 6.4, we first start with a matrix of column vectors of all vertices except the one at the origin.

$$Vert = \begin{bmatrix} v_1 & \dots & v_p \end{bmatrix}. \tag{6.18}$$

For each simplex region, we construct an extraction matrix $\varepsilon_i \in \Re^{p \times n}$ of X_i in the following way. The kth row of ε_i is zero for all k such that $v_k \notin X_i$, and the remaining rows are equal to the rows of an identity matrix. Then we can set

$$E_i = \varepsilon_i^T \varepsilon_i (Vert \cdot \varepsilon_i)^{-1} \tag{6.19}$$

(Rantzer and Johansson, 2000). Rantzer and Johansson (2000) showed that this matrix will satisfy (6.16).

For the 2D example #2, this can be done in the following way. First using the regions in Figure 6.1 we write the matrix of column vectors skipping v_0

$$Vert = \begin{bmatrix} v_1 & \dots & v_8 \end{bmatrix}.$$

Then, if we are interested in the region X_2 we can write the extraction matrix as

$$\varepsilon_2 = \begin{bmatrix} 0 & 0 \\ 1 & 0 \\ 0 & 1 \\ 0 & 0 \\ 0 & 0 \\ 0 & 0 \\ 0 & 0 \\ 0 & 0 \end{bmatrix}.$$

which leads to

$$E_2 = \begin{bmatrix} 1.4142 & 0 \\ -1 & 1 \end{bmatrix}.$$

which will satisfy (6.16) everywhere in region X_2.

We also need to construct some method for ensuring that the Lyapunov function that will be found is continuous across region boundaries. This will be accomplished with the following proposition.

Proposition 6.6 (Continuous, piecewise C^1 Lyapunov function)

Given two regions X_1 and X_2, there exist two non-zero matrices F_1 and F_2 such that

$$F_1 x = F_2 x, \quad x \in X_1 \cap X_2 . \tag{6.20}$$

Then, for some symmetric matrix T, a continuous, piecewise C^1, quadratic Lyapunov function consisting of P_1 and P_2 in the regions X_1 and X_2 respectively can be written as

$$P_j = F_j^T T F_j, \quad j = 1,2. \tag{6.21}$$

Proof

Refer to Johansson and Rantzer (1998).

This allows us to have one set of variables in the matrix T and still have different Lyapunov functions in each region defined by the control algorithm. The LMI process will solve for the variables in T, and we will then construct the continuous, piecewise C^1 Lyapunov function from (6.21). Again, the simplest way to define these regions is in terms of the control law partitions. It is reasonably easy to come up with matrices that

satisfy (6.20) in this case. In fact, we can use the same matrices as we did for the simple case of (6.16). So, for our 2D example #2 we could set

$$F_{QuadI} = \begin{bmatrix} 0 & 1 \\ 1 & 0 \end{bmatrix}, \quad F_{QuadII} = \begin{bmatrix} 0 & 1 \\ -1 & 0 \end{bmatrix}.$$

Then, on the boundary between quadrant I and quadrant II we would have (6.20) satisfied.

Some problems benefit if we augment these F matrices with an identity matrix. It is obvious that this will still satisfy (6.20). Again, if we want to be able to subdivide the space further, it behooves us to find some unified and simple way to generate these matrices. That is the purpose of the simplex regions.

For the simplex regions in Definition 6.4 we can set

$$F_i = \varepsilon_i (Vert \cdot \varepsilon_i)^{-1}. \tag{6.22}$$

Rantzer and Johansson (2000) showed that this will satisfy (6.20). Some problems benefit from the added flexibility when the matrix in (6.22) is augmented with an identity matrix

$$F_{i,aug} = \begin{bmatrix} \varepsilon_i (Vert \cdot \varepsilon_i) \\ I \end{bmatrix}. \tag{6.23}$$

This obviously still satisfies (6.20).

For the 2D example #2 using the regions 2 and 3 and using (6.22) we can get

$$F_2 = \begin{bmatrix} 0 & 0 \\ 1.4142 & 0 \\ -1 & 1 \\ 0 & 0 \\ 0 & 0 \\ 0 & 0 \\ 0 & 0 \\ 0 & 0 \end{bmatrix}, \quad F_3 = \begin{bmatrix} 0 & 0 \\ 0 & 0 \\ 1 & 1 \\ -1.4142 & 0 \\ 0 & 0 \\ 0 & 0 \\ 0 & 0 \\ 0 & 0 \end{bmatrix},$$

and when $x \in X_1 \cap X_2$

$$F_2 x = F_3 x = \begin{bmatrix} 0 \\ 0 \\ 1 \\ 0 \\ 0 \\ 0 \\ 0 \\ 0 \end{bmatrix}.$$

The LMI in (6.14) will next be extended to treat the piecewise linear system (3.29). As far as this author knows, this is the first time that this method has been used to find an upper bound on the reachable set for piecewise linear systems of the form (3.29) with a unit peak input. One of the references (Hassibi and Boyd, 1998) mentioned this possibility but did not treat it (refer to Section 3.6). Since each P_j must hold only within its respective region, X_j, the S-procedure can be used to construct the LMI as follows.

Proposition 6.7 (Piecewise solution for the reachable set with unit peak input)

Suppose we have matrices E_j and F_j that satisfy (6.16) and (6.20) respectively. If there exist symmetric matrices T, U_j, and W_j such that U_j and W_j have nonnegative entries and $\alpha_j \geq 0$ such that

$$
\begin{aligned}
&P_j = F_j^T T F_j \\
&\begin{bmatrix} x \\ d \end{bmatrix}^T \begin{bmatrix} A_j^T P_j + P_j A_j + \alpha_j P_j + E_j^T U_j E_j & P_j D \\ D^T P_j & -\alpha_j I \end{bmatrix} \begin{bmatrix} x \\ d \end{bmatrix} \le 0 \\
&x^T \left(P_j - E_j^T W_j E_j \right) x > 0
\end{aligned}
\tag{6.24}
$$

for all j, then the continuous, piecewise C^1 boundary defined by the P_j in each region, X_j, bounds the reachable set for the system (3.29) with a unit peak input.

Proof

Applying Proposition 6.1 to (6.24) gives

$$
\begin{aligned}
&P_j = F_j^T T F_j \\
&\begin{bmatrix} x^T \\ d^T \end{bmatrix}^T \begin{bmatrix} A_j^T P_j + P_j A_j + \alpha_j P_j & P_j D \\ D^T P_j & -\alpha_j I \end{bmatrix} \begin{bmatrix} x \\ d \end{bmatrix} \le 0 \\
&x^T P_j x > 0
\end{aligned}
\tag{6.25}
$$

for all x such that

$$
\begin{aligned}
x^T E_j^T U_j E_j x \ge 0 \\
x^T E_j^T W_j E_j x \ge 0
\end{aligned}
\tag{6.26}
$$

Note that the coefficient generally used when applying Proposition 6.1 is set to unity as we allow U_j and W_j to absorb that variable. From Corollary 6.1 and Proposition 6.5 we can see that (6.25) guarantees that the reachable set for the system (3.29) with a unit peak input is bounded by

$$
\varepsilon = \left\{ x \middle| x^T P_j x \le 1 \right\} \tag{6.27}
$$

in an approximation for the region X_j from Proposition 6.5.

As pointed out in discussion following Corollary 6.1 this is not an LMI unless we fix α_j.

The inequality in (6.14) is a combination of three inequalities with the relationship shown in (6.13) and (6.8). They are combined using the S-procedure to

produce one inequality constraint so that the LMI method can be applied. All of the original inequalities' conditions are applied to the entire space, as is the combined inequality in (6.14). For the case with piecewise linear dynamics that we are now considering, the combined inequalities in (6.14) need to hold only on a subspace described by another inequality. To do this and to apply the LMI method, we must again augment the inequality constraint with another term so that the inequality can hold on the whole space. This term is the $E_j^T U_j E_j$ term in (6.24). This conversion from an inequality on a subspace to an inequality on the whole space adds a significant amount of conservatism to the constraint. This was not evident in the case of (6.14) because the constituent inequalities all held on the same space as the final combined inequality.

Finally, a single bounding sphere is added to the LMI to get the largest radius of the continuous, piecewise C^1 constructed from the P_j in each region.

Proposition 6.8 (Bounding Radius)

If the following holds with some symmetric matrix V_j with non-negative elements

$$x^T P_h x \equiv x^T (\delta I) x$$

$$x^T (P_h - P_j + E_j V_j E_j) x \le 0, \tag{6.28}$$

then $\frac{1}{\sqrt{\delta}}$ is an outer bound for the maximum radius of the continuous, piecewise C^1 Lyapunov function generated by the P_j. Thus, it is an outer bound on the peak-to-peak gain of the system.

Proof

Applying Proposition 6.1 to (6.28) gives

$$x^T P_h x \equiv x^T (\delta I) x$$

$$x^T P_j x \geq x^T P_h x. \tag{6.29}$$

for all x where

$$x^T E_j V_j E_j x \geq 0. \tag{6.30}$$

Again, note that the coefficient generally used when applying Proposition 6.1 is set to unity as we allow V_j to absorb that variable. From Proposition 6.5 we can see that this guarantees that δ is the bound of the singular values for the continuous, piecewise C^1 Lyapunov function on an approximation for the set X_j.

The combination of Proposition 6.7 and Proposition 6.8 with a convex optimization criterion results in a method to minimize the size of a continuous, piecewise C^1 ellipsoid that bounds the reachable set for the system (3.29) with a unit peak input.

Proposition 6.9 (Optimization II)

Solving the minimization problem

Maximize δ
Subject to the LMI constraints in Proposition 6.7 and Proposition 6.8,

minimizes the maximum radius of the continuous, piecewise C^1 ellipse formed from (6.27), which is an upper bound on the reachable set with a unit peak input for the system (3.29).

Proof

This is obvious since Proposition 6.7 guarantees that the reachable set is bounded by the continuous, piecewise C^1 ellipse formed from (6.27), and Proposition 6.8 guarantees that $\frac{1}{\sqrt{\delta}}$ is an upper bound for the maximum radius of the same continuous, piecewise C^1 ellipse.

To find some global optimal solution, we must solve this optimization problem with fixed α_j and then search for an optimal solution over all α_j.

To further improve the linear approximation of a nonlinear system, a piecewise affine approximation such as (3.28b) can be used as in Section 2.10. This allows better approximations in regions that do not include the origin. The derivation of the LMI formulation for this piecewise affine system is very similar to the simpler derivation above. For this more general LMI analysis, we still use general simplex regions, but here we put no restrictions on where the vertices will be. When this method of piecewise affine systems is used to find a continuous, piecewise C^1 Lyapunov bound for the system's reachable set, it is very important to choose the regions $X_j, j = 1,\ldots,N$ so that there is a solution in every region. It is easily possible to choose a set of regions that will disallow a single continuous, piecewise C^1 Lyapunov function that encircles the origin and is continuous across region boundaries. If there is not a solution everywhere (in every region), the LMI will not be feasible.

If we replace the state vector x with a new state vector $\bar{x} = [x \quad 1]^T$, we can rewrite (3.28b) in the form of (3.29). This allows us to use all of the derivations above for the affine system description with a few interesting results (Johansson and Rantzer, 1998) (Rantzer and Johansson, 2000). Using this affine description and the new state vector will lead to the possibility of quadratic Lyapunov functions that are not centered on the origin. This allows far greater flexibility than the previous method.

This does not, however, help the problem at hand. From the numerical work in the next section, we find that the limiting factors for the LMI solution are the regions where $u=0$. In these regions, the system dynamics are already linear and so cannot be

improved by using an affine approximation (refer to Section 2.10). The only parts of the space that can benefit from the affine linearization are those where $u=1$, but those regions are not limiting the effectiveness of the LMI solution.

6.4 Results for Example Systems

We will present the results found with the application of the LMI methods to the example problems described in Chapter 4. In every case the control logic is based on the quickest descent logic from Section 2.9, and the specifics of each case are given in Chapter 4. A summary of the simulation results from Chapter 4, the system 1-norm and classical bounding results from Chapters 4 and 5, and the results from the extension of the classical bounding method from Chapter 5 will be included for later comparisons.

In each case we will apply the techniques from Proposition 6.4 to the open valve system where $u=1$ is held constant throughout. This should give us a bound that is outside of the results for the system 1-norm of the same open valve case. Next, we will split the system space into regions and apply the techniques in Proposition 6.7 to the semi-active system with the various trial control laws discussed in Chapter 4. We expect to get boundaries from this that are inside the result for the open valve system 1-norm, as the performance of all controllers seem to easily improve over this case from simulation studies. In fact, the results obtained are reasonably conservative for the controlled cases until we apply very fine partitioning of the state space. In most cases, as the number of partitions increases the values from the LMI methods decrease. The limitation is that as the number of regions increases, the computation time also increases dramatically. The

LMI Control Toolbox for Matlab is not optimized for very large sets of LMI constraints. We will discuss the actual problem size as each example problem is discussed.

Since the control case designed in Section 4.2 is reasonably uninteresting, we will focus on the open valve case where $u=1$ is held constant. Table 6.1 summarizes the previous results for this system and presents the new bound on the maximum system radius, with a unit peak input generated from the application of the LMI method. We can see that the LMI method bound gives the same value as the simulation and the system 1-norm for this system.

Table 6.1: Results for 2D example #1

Control Version	Simulated Maximum Radius	System 1-Norm Maximum Radius	LMI Maximum Radius 4 Partitions
Open Valve	7.07e-1	7.07e-1	7.07e-1
1	7.07e-1	n/a	7.08e-1

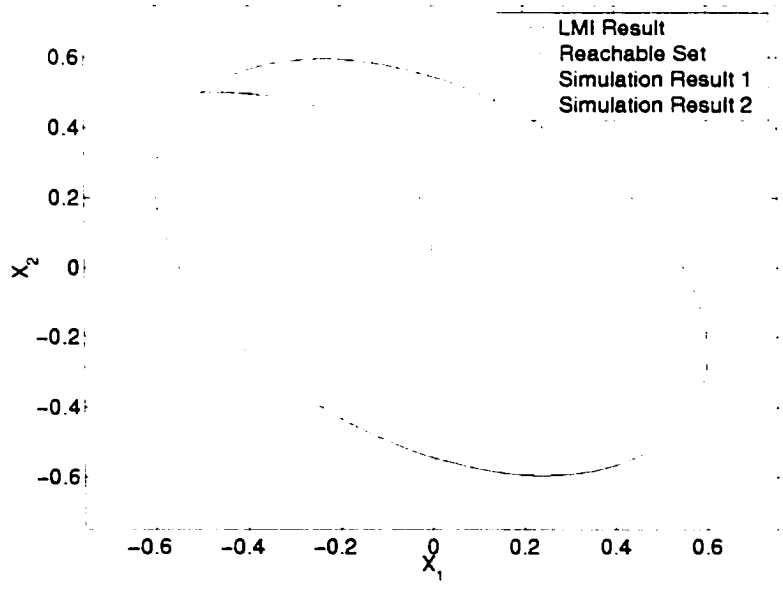

Figure 6.2: Ellipsoid bound on the reachable set found with the LMI method for the 2D example #1 compared to earlier results

Figure 6.2 shows the actual inescapable ellipse that the LMI method generates as a bound on the reachable set for the open valve case. The figure includes simulation results generated for the example with an initial condition at the origin and using the disturbance logic discussed in Section 4.1, along with the actual reachable set that was shown in Section 4.2 for comparison and the simulation results from Figure 4.5. Obviously, from this plot we can say that the LMI method does a very good job for this system at the extreme points of the reachable set. However, it is unable to capture the true shape of the reachable set.

The 2D example #2 is much more interesting because we designed several control laws for it and will be able to see how the LMI method ranks these controllers relative to the simulation studies and actual reachable sets found in Chapter 4. For reference, the previous results are summarized in Table 6.2. As seen in earlier chapters, none of the methods so far have been particularly successful in finding a good bound on the peak-to-peak gain in the controlled cases.

Table 6.2: Summary of previous results for the 2D example #2

Control Version	Actual Peak-to-Peak Gain	System 1-Norm Maximum Radius	Classical Bounding Method Radius	Intersecting Ps Bounding Radius
Open Valve	1.28e0	1.28e0	n/a	n/a
1	5.78e-1	n/a	1.06e2	n/a
2	5.62e-1	n/a	2.23e0	n/a
3	5.58e-1	n/a	6.55e2	n/a
2+3	5.58e-1	n/a	n/a	2.30e1

We first apply the LMI method to the case where $u=1$ is held constant using the method in Proposition 6.4 and get a maximum radius of 1.36. This compares well with

the actual peak-to-peak gain value from the system of 1.28. Next, we apply the LMI method to the controlled cases using a variety of partition numbers. The initial 4-partition problem gives disappointing maximum radius results of 1.42 and 1.43 for controllers 1 and 2 respectively. These values are significantly high relative to the actual peak-to-peak values shown in Table 6.2.

We next try 12 partitions and 30 partitions using the simplex regions defined in Section 6.3. Interestingly, the LMI results decrease with an increase in the number of regions used. Just increasing the regions from 4 to 12 halves the maximum radius given by the LMI method. The final values obtained with 30 regions are all within between 0.1% and 40% of the peak-to-peak gain results. These results are shown in Table 6.3. Unfortunately, these values are not consistent with the relative magnitudes of the peak-to-peak results for the various control laws. This means that even though the LMI solution gives a reasonable bound on the maximum system radius, we still cannot use it to judge the relative performance of controllers.

Table 6.3: LMI results for 2D example #2

Control Version	Actual Peak-to-Peak Gain	LMI Maximum Radius 4 Partitions	LMI Maximum Radius 12 Partitions	LMI Maximum Radius 30 Partitions
Open Valve	1.28e0	1.36e0	1.36e0	1.36e0
1	5.78e-1	1.42e0	6.98e-1	5.79e-1
2	5.62e-1	1.43e0	6.68e-1	5.97e-1
3	5.85e-1	1.40e0	8.59e-1	7.69e-1

These additional regions cannot be used without a penalty in computer time. With N regions we are solving an optimization problem with a combined LMI constraint dimension of 17*N+2 for this 2D case. This mean that, in the case of 30 partitions, we

have an LMI constraint total dimension of 512, or looked at another way, we are checking the positive definiteness of a 512 x 512 matrix as a constraint for the optimization problem. If this isn't bad enough, remember that we also have to search over all α_j to find some globally optimal solution, so the optimization problem needs to be solved many times. We usually start the evaluation of the LMI problem at 50 equally spaced values for α_j between 0.01 and 100. We then take the best result and use an optimization routine in Matlab to find a final solution.

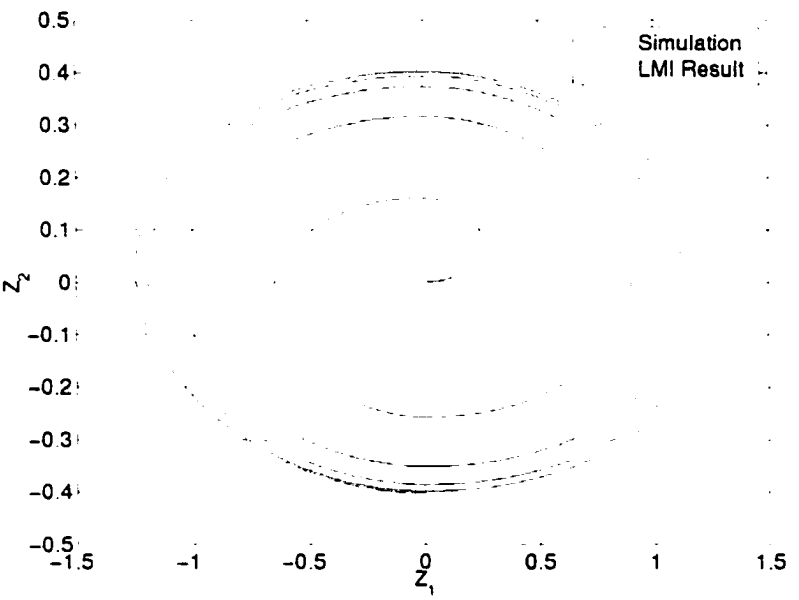

Figure 6.3a: Ellipsoid bound on the reachable set found with the LMI method for the open valve 2D example #2 along with simulation results

Figure 6.3a shows the solution for the open valve case and Figure 6.3b shows the solutions for the 4 and 12 partition LMIs along with the simulation for the control version 1. This gives us some idea of what the elliptical regions for which the LMI method solves look like. We can see that the LMI not only does a reasonable job bounding the maximum system radius, but reasonably approximates the overall shape of the system

dynamics when higher numbers of dimensions are used. We can also see from this figure how much the results are improved when more regions in the LMI are used.

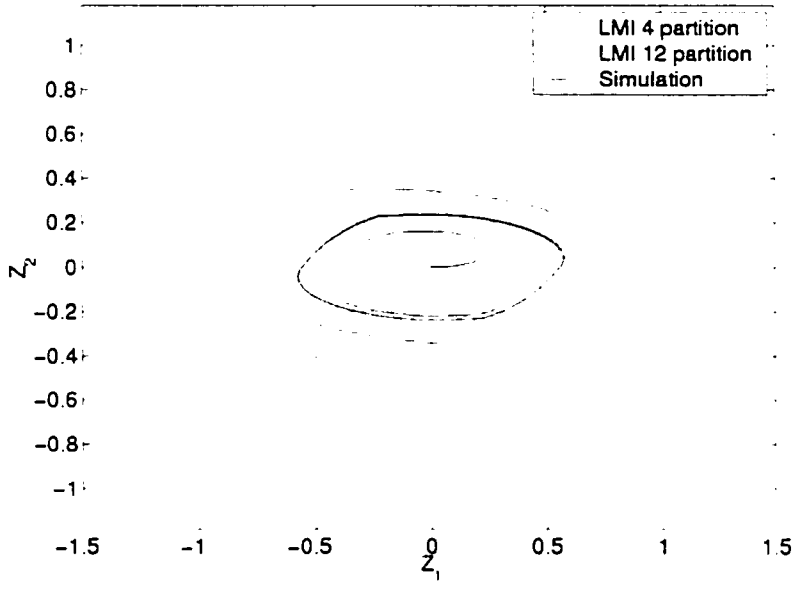

Figure 6.3b: Ellipsoid bound on the reachable set found with the LMI method for the controlled 2D example #2 along with simulation results for control version 1

Table 6.4: Summary of Previous Results for the 3D example

Control Version	Simulated Maximum Radius	System 1-Norm Maximum Radius	Classical Bounding Method Radius	Intersecting Ps Bounding Radius
Open Valve	$2.59 \cdot 10^0$	$2.59 \cdot 10^0$	n/a	n/a
1	3.60e-1	n/a	1.85e3	n/a
2	3.49e-1	n/a	1.40e2	n/a
3	2.77e-1	n/a	2.15e3	n/a
4	2.20e-1	n/a	1.60e6	n/a
5	2.20e-1	n/a	4.55e5	n/a
6	2.23e-1	n/a	4.96e3	n/a
1+2+6	2.31e-1	n/a	n/a	1.40e2

The LMI method is next applied to the 3D example problem. Table 6.4 summarizes the previous results for this example. From this table we can see that none of the previous methods were very good at bounding the system's reachable set. In fact, none of these methods indicate that the semi-active control system outperforms the benchmark value from the open valve system 1-norm.

As for the 2D examples, we first apply the LMI method to the open valve system case in this 3D example. The resulting maximum system radius is 2.87. This is a reasonable bound, as the exact maximum system radius is 2.59. Next, we apply the LMI using 4 partitions based on the various control laws to the cases with a controller. This results in bounds that are around 1 order of magnitude larger than the simulation results and mostly larger than the system 1-norm result for the open valve case. We then increase the number of simplex partitions in an effort to find better bounds on the reachable set.

In an effort to further explore the relationship between region selection and size with the attained results, we also used quadrahedral regions for some of the LMI problems. Four planes that meet at the origin to form a quadrahedral region, which has a base at infinity, define these regions. This type of region fits into Propositions 6.4 and 6.6. This essentially allows a rectangular grid on the surface of the Lyapunov function rather than a triangular mesh as in the simplex case. Results for this discretization method were found for various mesh sizes in all of the control versions. We also briefly explored the use of non-uniform meshing in the regions with some success.

Figures 6.4 thru 6.9 summarize the 3D example LMI results for all cases that were solved. These figures show the number of regions, type of regions, and resulting peak-to-

peak bound. The regions were evenly distributed on the whole system space in the case of the simplex regions.

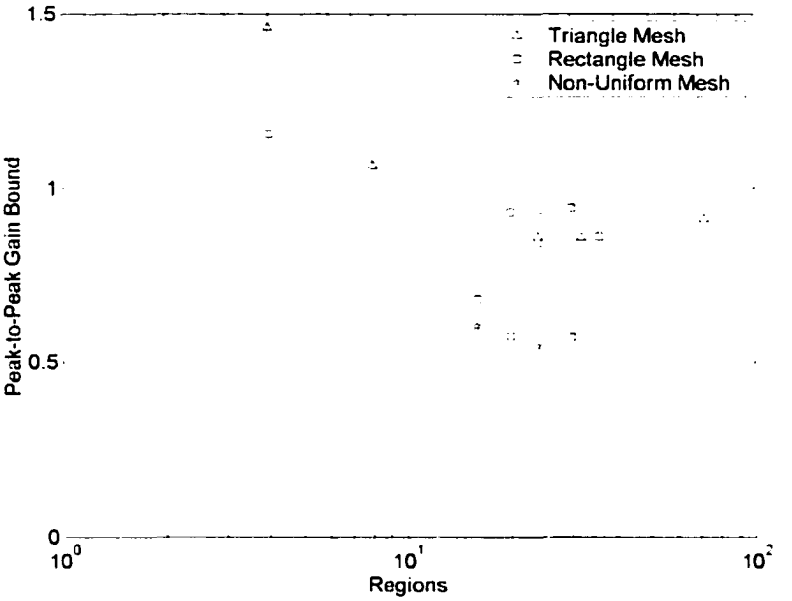

Figure 6.4: LMI Results for Control Version 1

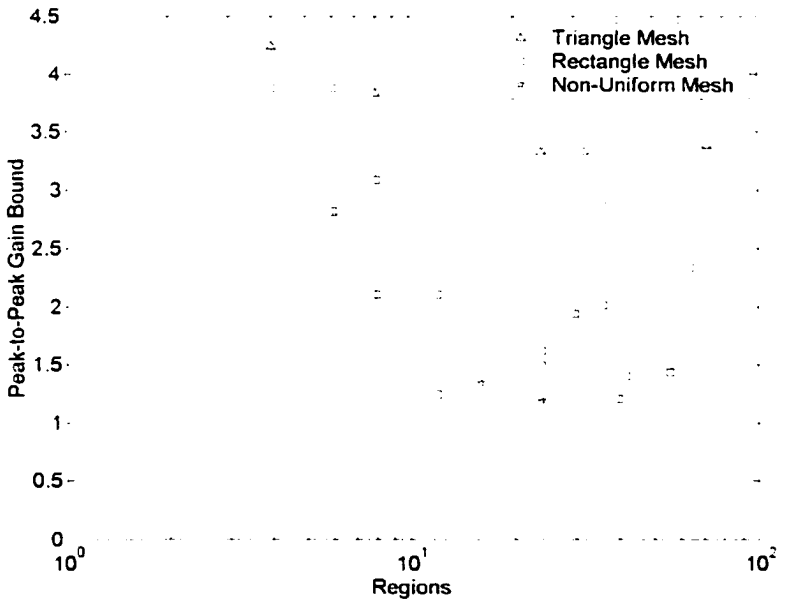

Figure 6.5: LMI Results for Control Version 2

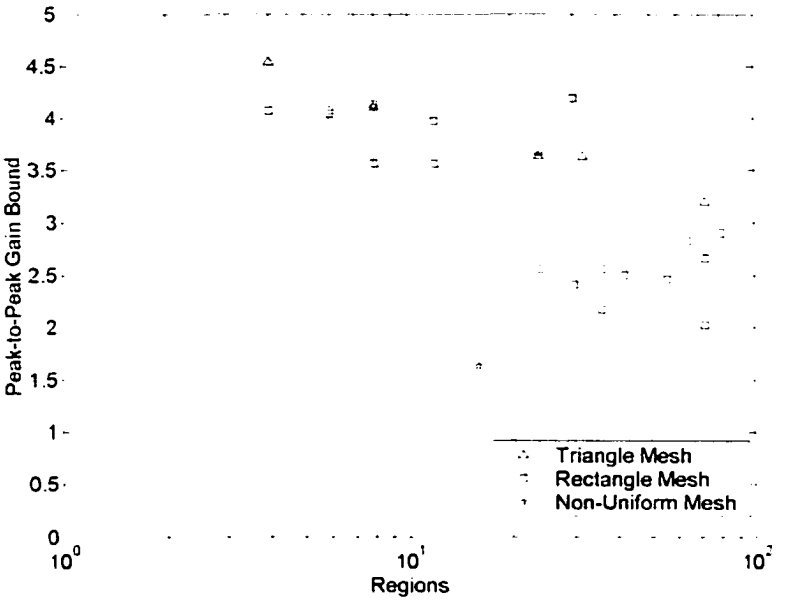

Figure 6.6: LMI Results for Control Version 3

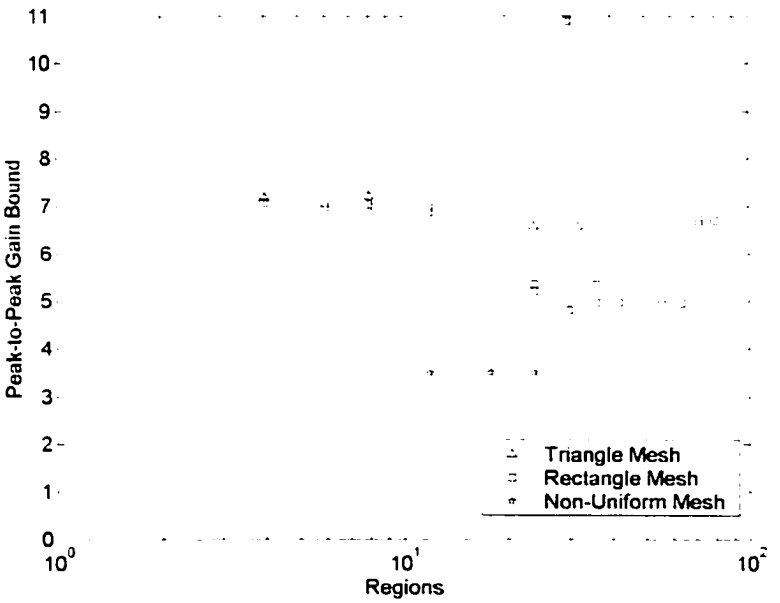

Figure 6.7: LMI Results for Control Version 4

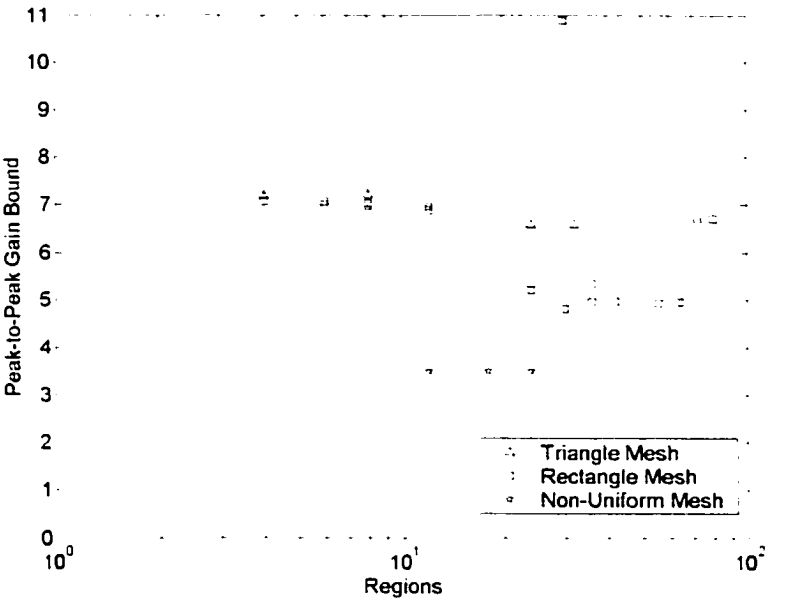

Figure 6.8: LMI Results for Control Version 5

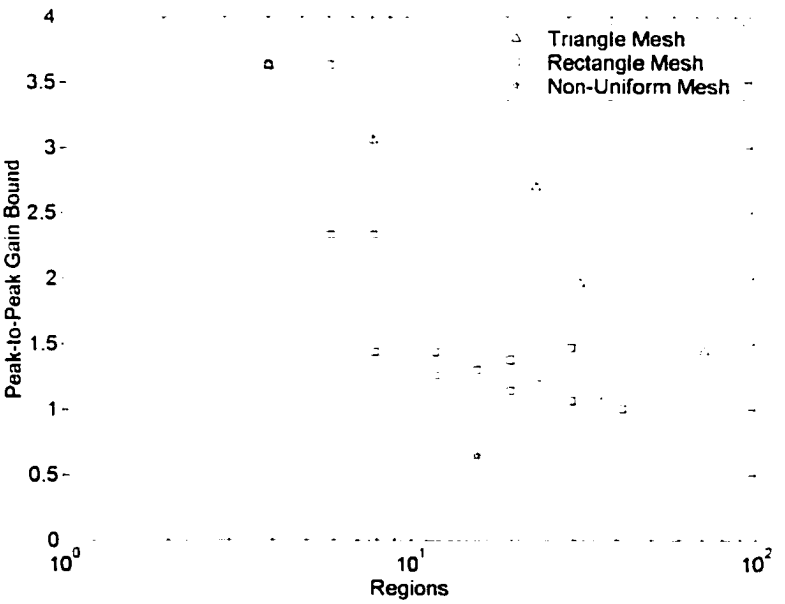

Figure 6.9: LMI Results for Control Version 6

For the quadrahedral case, the regions in the open valve area were increased independently of the regions in the closed valve area, but the meshing in each region was

still uniform. However, not every combination of region size was tried. Finally, several non-uniform simplex meshes were tried with very good results.

As in the 2D example #2, the size of the overall optimization problem increases sharply with the number of partitions. This is partly because the LMI constraint has an order 29*N+3 in the simplex region case and 41*N+3 in the quadrahedral case, but also because we have to search for an optimal solution over the range of α_j. Some of the optimization problems that solve the LMI problems and search over values of α_j for some global optimal solution take up to several hours. To illustrate this, Figure 6.10 shows the time to solution compared to number of regions for control version 6 with quadrahedral regions. This is typical of all the LMI solutions tried. Figure 6.10 shows that there is approximately an exponential increase in the time to solution as the number of regions are increased.

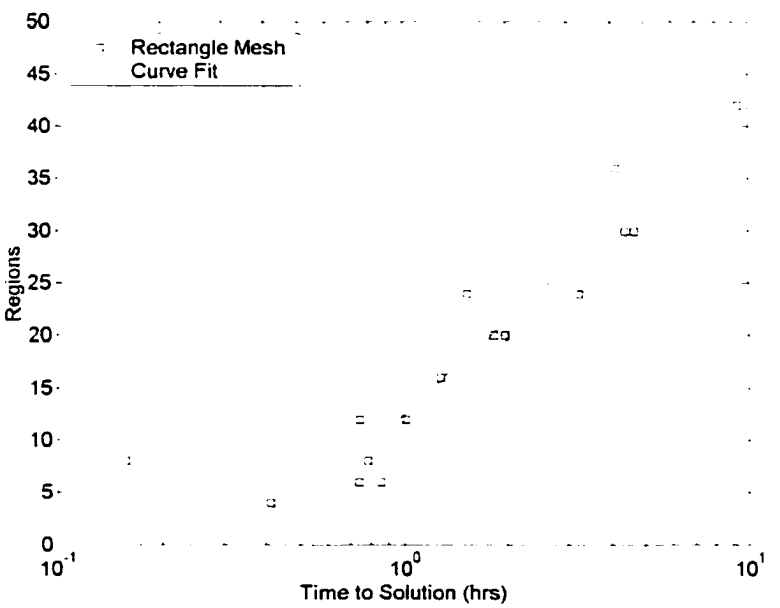

Figure 6.10: Time to Solution for Quadrahedral Discretization of Control Version 6 for 3D Example

In fact, disregarding the outlying data point at t=0.157 hrs, an exponential curve fit of the data results in the equation $t = 0.374 \cdot 10^{N/29.367}$, where N is the number of regions and t is the time to solution in hours. To put this in perspective, extrapolating with the curve fit in Figure 6.10 indicates that it would take approximately 1 year to find a solution with 128 regions.

Table 6.5 shows the best LMI results along with details of mesh method and size. Notice that the least upper bound in every case is found when the partitions in the closed region are finer than those in the open region. We can conclude from this that the LMI method needs more divisions in the closed region to find a better answer.

Table 6.5: LMI Results for 3D Example

Control Version	Simulated Maximum Radius	Best LMI Solutions			
		Peak-to-Peak Gain Bound	Closed Valve Regions	Open Valve Regions	Type of Region
Open Valve	2.59e0	2.87e0	2	2	n/a
1	3.60e-1	5.45e-1	16	8	non-unif
2	3.49e-1	1.19e0	16	8	non-unif
3	2.77e-1	1.63e0	8	8	non-unif
4	2.20e-1	3.50e0	16	8	non-unif
5	2.20e-1	3.57e0	16	8	non-unif
6	2.23e-1	6.48e-1	8	8	non-unif

Figure 6.11 shows the best LMI results compared graphically to the results from the last two chapters. We can see that the LMI results are a huge improvement over the classical bounding technique and the results indicate that the semi-active system performance is better than the open valve performance in some cases.

Also, if we compare the results from Table 6.5 to the simulation studies in Table 6.4, we can see that the LMI method results and the simulation results do not agree on the relative control performance.

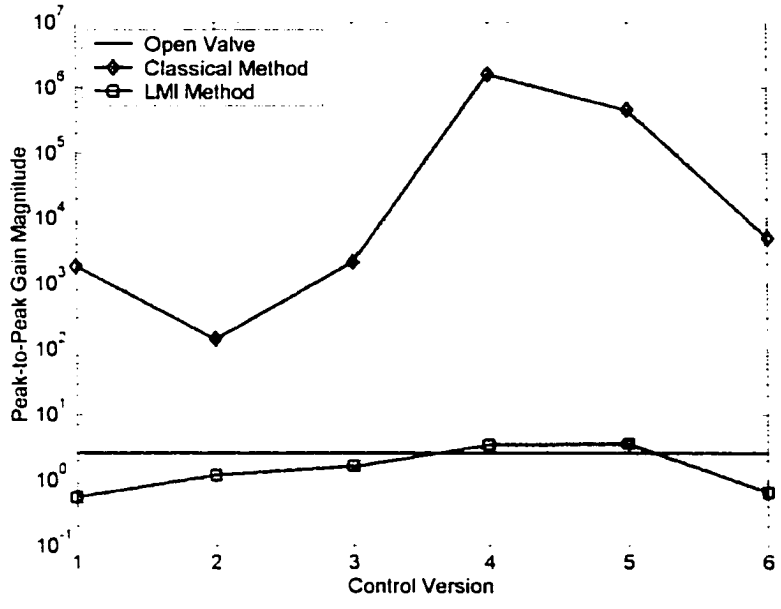

Figure 6.11: Results Summary for the 3D Example

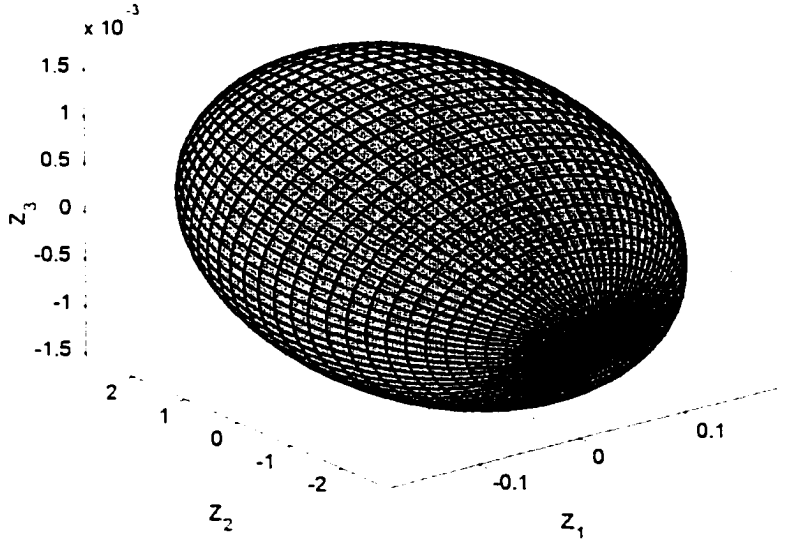

Figure 6.12: LMI result for 3D example in Open Valve Case.

Next we will graphically show the LMI results for particular cases. Figure 6.12 shows the LMI result for an upper bound on the reachable set of the 3D system with the valve held open. We can see from the results in Table 6.5 that the LMI results in this case are reasonably close to the tight bounds given by the system 1-norm.

Figure 6.13 shows the LMI bound for control version 1 with 4 partitions. The breaks in the surface were purposely left in to allow the reader to better visualize this 3D shape. The breaks correspond to the switching planes of the controller, which are also used to define the regions used in the LMI analysis with 4 regions. The coloring of the surface indicates the calculated values on the surface for $\dot{V}$.

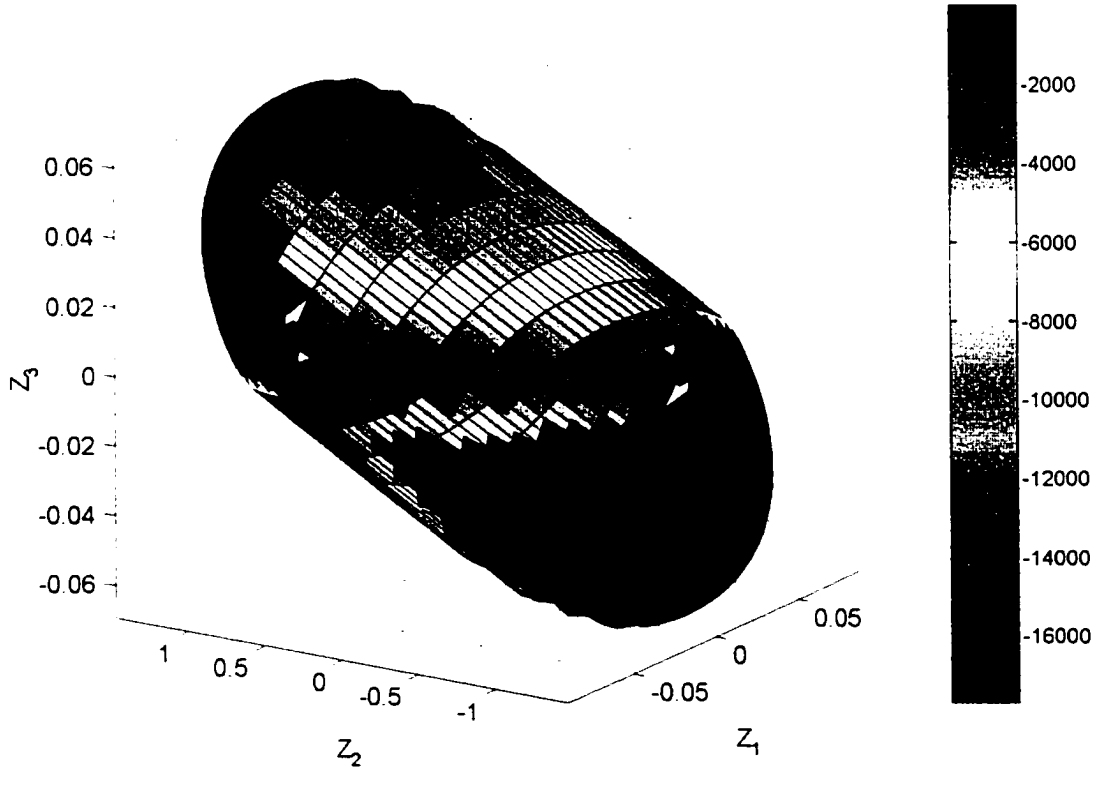

Figure 6.13: LMI result for 3D example with control version 1 with 4 partitions showing the value of $\dot{V}$ in the surface color.

As can be seen, the values for the Lyapunov derivative are in fact negative on the whole surface with the maximum calculated value at a node being $\dot{V} = -1.2$. It is interesting to note that the part of the surface that is entirely red is the region where the control law has set $u=0$. We can deduce from the fact that $\dot{V}$ is negative but close to zero in the region where $u=0$, that these symmetric regions are the limiting factor in determining some tight upper bound on the system's reachable set.

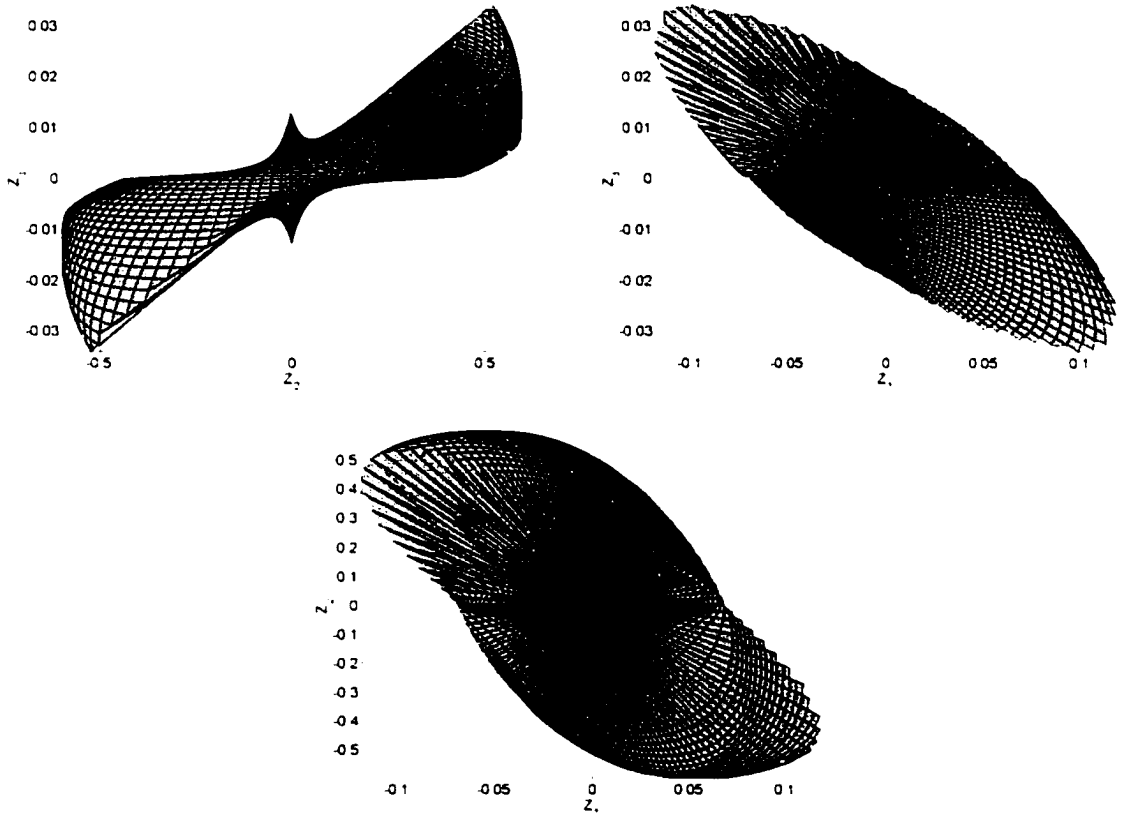

Figure 6.14: Best LMI result for 3D example with control version 1

Figure 6.14 shows the best result obtained for control version 1 in the 3D example and Figure 6.15 shows the best result for control version 6. Three orthogonal views are shown rather than a 3D view since the figure is somewhat irregular. Recall from the derivation of the LMI problem that we are only minimizing the maximum radius of the

surface. We can see the effect of this in the figure where there are some irregularities in the surface. The LMI does not care about these irregularities as long as they are not at the maximum radius.

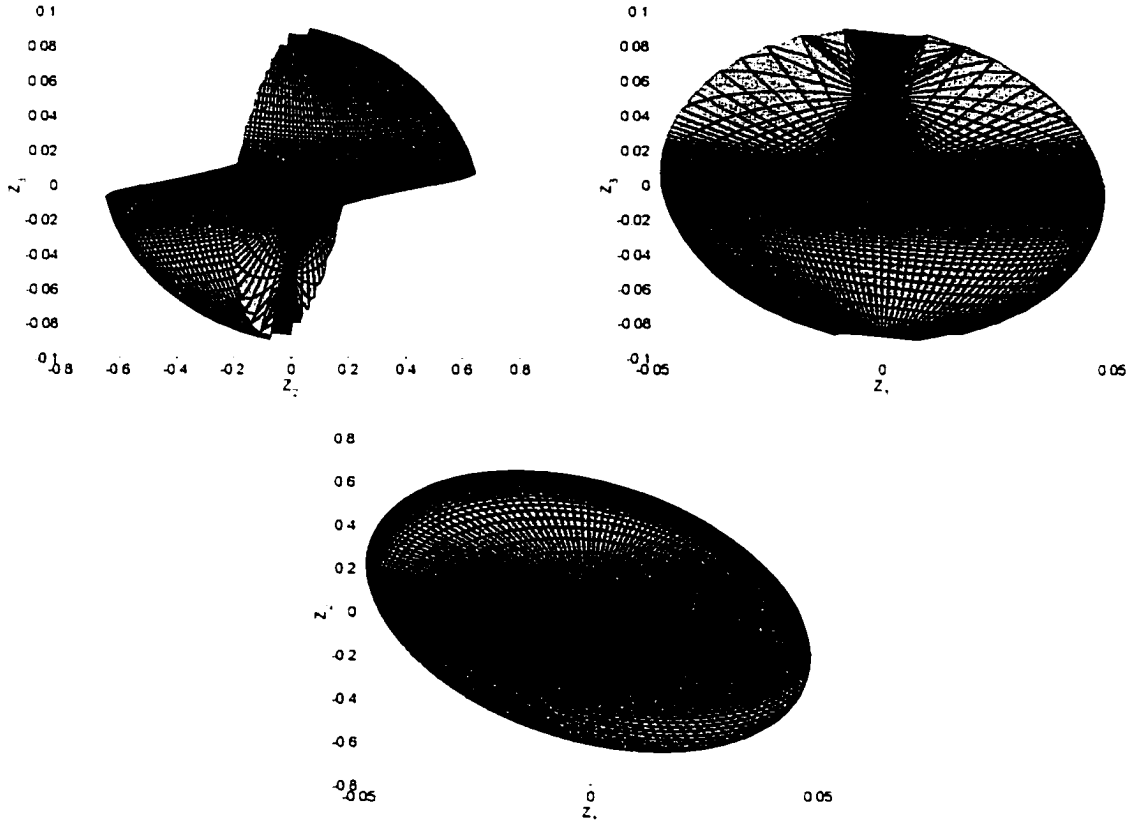

Figure 6.15: Best LMI result for 3D example with control version 6.

It is possible, since the LMI method is limited to using quadratic Lyapunov functions, that the actual shape of the reachable set is not easily approximated by such functions. This is also a reasonable explanation for the reduction of the maximum radius with the LMI method when more regions are used. In other words, a continuous, piecewise C^1 quadratic boundary has a much better chance of tightly approximating the actual reachable set.

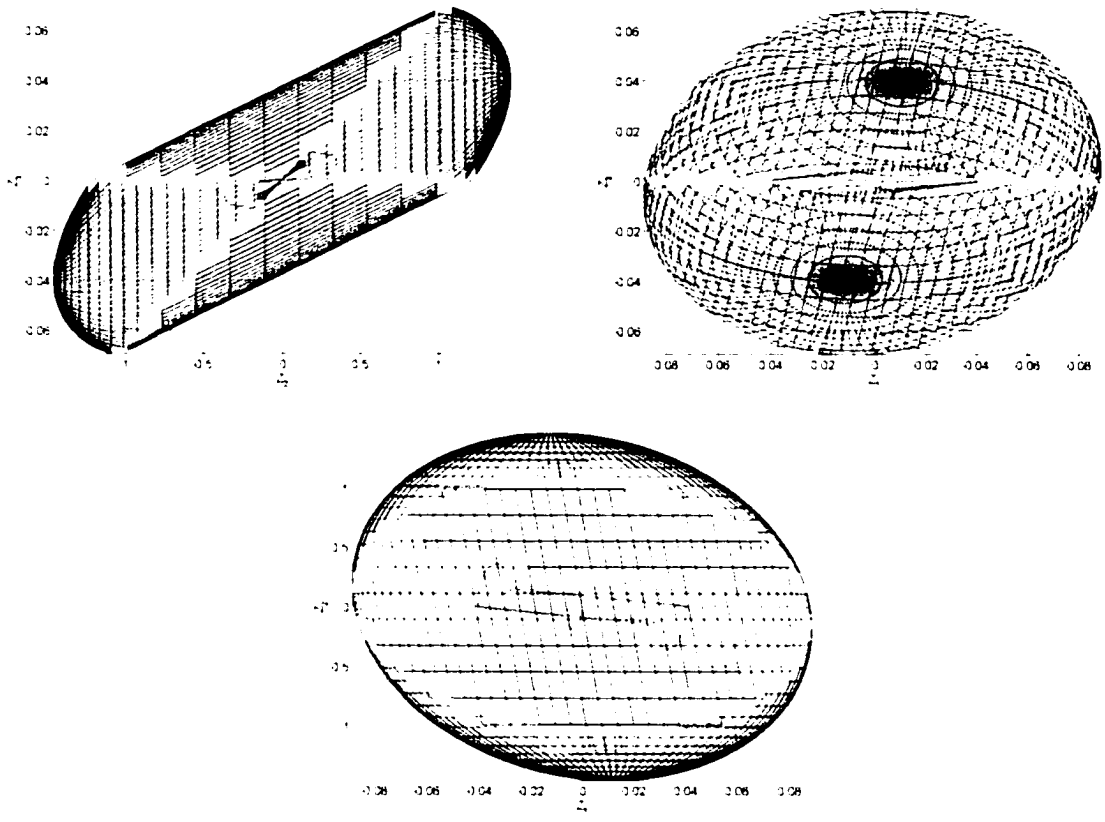

Figure 6.16: LMI result for 3D example with control version 1 with 4 partitions showing the simulation results for comparison.

To tie the LMI results back to the simulation studies, Figure 6.15 shows the LMI bound as a black mesh with the simulation results plotted in blue for the control case 1. We can see that there are parts of the system space to which this particular simulation does not ever get. This does not, however, mean that there is not some disturbance that would drive the system into these regions. Since the 4 partition LMI result plotted is obviously a conservative bound on the reachable set, we can assume that there are some regions inside the LMI bound to which the system will never get with the bounded disturbance. We can say the 4 partition LMI result is conservative since the 8 partition solution is significantly smaller.

Finally, Table 6.6 summarizes the previous results and presents the LMI results, with 4 partitions for the 7D example. The application of the LMI method to the open valve case leads to a reasonable upper bound of 8.91, which is not much larger than the exact answer from the system 1-norm of 8.06. Higher numbers of regions were not tried here because of difficulties describing simplex regions in 7 dimensions.

Table 6.6: Summary of previous results and LMI results for 7D example

Control Version	Simulated Maximum Radius	System 1-Norm Maximum Radius	Classical Bounding Method Radius	LMI Maximum radius 4 Partitions
Open valve	7.99e2	8.06e2	n/a	8.91e2
1	1.29e2	n/a	1.82e4	6.34e2
2	1.32e2	n/a	2.14e3	4.62e2
3	2.66e2	n/a	1.54e6	8.18e2
4	2.66e2	n/a	2.04e5	6.92e2
5	2.08e2	n/a	2.87e5	9.58e2
6	2.29e2	n/a	3.50e5	5.57e2
7	2.27e2	n/a	4.77e6	3.09e3
8	1.81e2	n/a	3.58e6	2.26e3
9	2.19e2	n/a	5.60e5	3.07e3
10	1.77e2	n/a	4.20e5	2.23e3

When the LMI method is applied to the controlled cases with the partitions based on the control law, we get results that range from 100% higher to 1 order of magnitude higher than the simulation results. Also, the controllers indicated by the simulation results indicated to be best were not the same as the ones indicated by the LMI method. The results for the 7D case show the same trends as those for the lower dimensional cases.

6.5 Summary

A general method has been developed for computing tighter bounds for peak-to-peak performance bounds for piecewise linear systems. It computes bounds that are up to 4.5 times better than the benchmark open valve peak-to-peak gain. But the improvements depend on the number and type of regions used in the partitions. In every one of the control cases for the 3D problem, better results are obtained when the mesh in the closed region are finer than those in the open region and evidence indicates that non-uniform meshing improve the results as well. The results found with the LMI method improve the bound on the reachable set in every case over those generated by the classical bounding method from Chapter 4.

The best LMI results for the 3D example are able to improve the upper bound for the peak-to-peak gain over the upper bound from the system 1-norm. This improvement over past methods comes with a significant increase in computation time. For N regions, the LMI dimension is 41*N+3, and, for a typical time vs. regions plot in Figure 6.10, a curve fit indicates that the time will increase as $t = 0.374 \cdot 10^{N/29.367}$. We can conclude that the LMI method in this chapter is able to predict that the semi-active controlled system will outperform the open valve case in some of the cases tried, but my available computing power is not sufficient to solve these problems quickly. It is clear from Figures 6.4 to 6.9 that convergence to a limiting upper bound was not achieved for any of the control versions for the various meshes tried. Based on the limited results, it appears that finer mesh sizes are needed for convergence, which may require more computing speed than currently available.

This is the first time that the Lyapunov control law from Chapter 2 has been shown to have good L_1 performance as well as the guaranteed stability that it was designed for. The LMI method was able to show that the control law from Chapter 2 could improve the bound on the system peak-to-peak gain 4.5 times over the open valve benchmark.

CHAPTER 7

TIGHT BOUNDS AND REACHABLE SET SOLUTIONS FOR 3D SEMI-ACTIVE CONTROL PROBLEMS

In the two previous chapters, several methods were presented for finding upper bounds on the peak-to-peak gain of the semi-active system described in Chapter 2. Those methods gave upper bounds on the reachable set for this system, with results that vary from 10^5 times larger than the open valve result to 4.5 times smaller. The LMI method of Chapter 6 was able to predict that the semi-active controlled system outperforms the open valve system, but the methods in Chapter 5 were not. We demonstrated for the 2D examples that semi-active control improves peak-to-peak performance by constructing the reachable sets in those cases. The exact answers for the reachable sets in the 2D cases illustrate that the peak-to-peak gain for the semi-active system is significantly better than that of the open valve case. Unfortunately, up to this point we have not been able to establish this type of result for the 3D or 7D systems. All we have for those cases so far, is the fact that simulation studies indicate significantly better performance for semi-active control than for the open valve case and that the LMI method predicts some improvement.

In this chapter, we will provide tight bounds for the reachable sets of the 6 control laws developed for the 3D case. This will be done by the method described below and expanded in Section 7.2.

1. Determine equilibrium points for open and closed valve dynamics (corresponding to maximal disturbances in the range $|d| \leq 1$).
2. Determine which of these equilibrium points will hold when the semi-active control is applied to the system.
3. Show that the equilibrium points in step 2 are reachable from the origin. Also, establish that points on the x_1-axis between the system equilibrium points are reachable.
4. From initial conditions on the x_3 plane near the x_1-axis, construct "worst case" trajectories that cycle/wind around that axis, forming a surface to use as the reachable set candidate R.
5. Establish that R is closed and continuous.
6. Show numerically that the semi-active system trajectories either follow the surface or point into the interior of R. This demonstrates that $\dot{V} \leq 0$ on the surface.
7. Show that the surface R is attractive to points outside.
8. Show that the surface R is reachable from points on the interior.

Once these 8 properties are established, we can claim that the surface constructed, R, is the reachable set, denoted as R^*. The above method is developed for the 3D semi-active control problems and may need some modifications and/or additions in any extension to 4D or higher dimensional problems.

The rest of this chapter is organized as follows. The first section gives a detailed description of the method used to generate the candidate reachable set. This parallels the above procedure. Control version 5 is used as the example throughout. Finally, results

are given for each of the control versions in separate sections, with similar control versions grouped together. Therein, any details that differ from the main development procedure are discussed. In the last section, we summarize the chapter and draw some conclusions.

7.1 Method for Constructing Reachable Set for 3D Semi-Active Control Problems

In this section, the method used to construct the candidate reachable sets R is described in detail. After two preliminary sections, the later sections follow the procedure outlined above. We will argue that the set R is in fact the actual reachable set R^*. Control version 5 will be used as the example throughout.

7.1.1 Summary of Semi-Active Control System Dynamics

Recall that we have the piecewise linear model of the semi-active system defined by the control law from Chapter 4, which is summarized as follows.

$$\dot{x} = A_i x + Dd, \quad |d| \le 1$$

$$A_0 = \begin{bmatrix} 0 & 1 & 0 \\ -224.72 & -4.50 & -2247.20 \\ 0 & 1 & 0 \end{bmatrix}, \quad x \in X_0 = \left\{x \middle| x^T PBx_3 < 0\right\} \quad (u = 0) \qquad . \qquad (7.1)$$

$$A_1 = \begin{bmatrix} 0 & 1 & 0 \\ -224.72 & -4.50 & -2247.20 \\ 0 & 1 & -5000 \end{bmatrix}, \quad x \in X_1 = \left\{x \middle| x^T PBx_3 \ge 0\right\} \quad (u = u_{\max} = 1)$$

The semi-active control law defines two switching planes referred to throughout this chapter. For control version 5, the normalized switching planes are

$$B^T P^T x = -0.166x_1 - 2.22x_2 + x_3 = 0 \qquad (7.2)$$

and

$$x_3 = 0. \tag{7.3}$$

Each of the regions X_0 and X_1, defined by the control, are further subdivided into regions based on the switching planes (7.2-7.3) as follows. For (7.2) we have

$$\begin{aligned} X_0^+ &= \{x | B^T P^T x < 0, x_3 > 0\} \\ X_0^- &= \{x | B^T P^T x > 0, x_3 < 0\}. \end{aligned} \tag{7.4}$$

and for (7.3) we will have

$$\begin{aligned} X_1^+ &= \{x | B^T P^T x \geq 0, x_3 \geq 0\} \\ X_1^- &= \{x | B^T P^T x \leq 0, x_3 \leq 0\}. \end{aligned} \tag{7.5}$$

This allows the problem to be split at the $x_3 = 0$ plane. We will use this in the next subsection for symmetry arguments.

Since the system dynamics (7.1) are linear in each region, a piecewise solution to this system of equations can be found. If we fix the disturbance as constant over some time interval, we can rewrite the solution of the piecewise linear dynamics in (7.1) as

$$\begin{bmatrix} \dot{x} \\ \dot{d} \end{bmatrix} = e^{\bar{A}\Delta t} \begin{bmatrix} x_0 \\ d_0 \end{bmatrix} \tag{7.6}$$

where

$$\bar{A} = \begin{bmatrix} A_i & D \\ 0 & 0 \end{bmatrix}. \tag{7.7}$$

This allows us to find an exact solution to the system dynamics over any time interval, where the disturbance is constant and no switching planes are crossed.

An interesting thing to note about this system is that when the valve is closed, the system trajectories all have the characteristic $x_3 = x_1 + c$, where c is a constant determined by the initial conditions.

7.1.2 System Radial Symmetry

Our arguments will take advantage of the radial symmetry property of the control law regions. Recall that this was shown in Proposition 2.3 when the piecewise linear dynamics generated from the control law was first introduced. Since we have already shown that the control law regions are radially symmetric, the next step is to show that the system dynamics in (7.1) are also radially symmetric. This is done in the following Proposition.

Proposition 7.1 (Radial Symmetry of the Semi-Active Dynamics)

The reachable set R^* of the semi-active control system in (7.1) is radially symmetric.

Proof:

Let $x_r \in R^*$. We claim that $-x_r \in R^*$. Let $(x(t), d(t)), 0 \le t \le t_f$ be a trajectory/disturbance pair satisfying the semi-active control system such that $x(0) = 0$ and $x(t_f) = x_r$. If $t_f = \infty$, we assume that $x(t) \to x_r$ as $t \to \infty$. Since the pair $(-x(t), -d(t))$ satisfies the control system

$$-\dot{x} = A_i(-x) + D(-d), \quad -x \in X_i, \tag{7.8}$$

it follows that $-x_r \in R^*$.

Finally, this leads to the following Corollary, which is used throughout the chapter.

Corollary 7.1

The reachable set R^* can be subdivided into two parts where, for each part,

1. $x \in R^{*+}$ iff $-x \in R^{*-}$

2. $R^{\bullet+} \cup R^{\bullet-} = R^{\bullet}$

3. $0 \in R^{\bullet+} \cap R^{\bullet-}$

This allows us to simply construct the system reachable set in the region $x_3 \geq 0$ and to use the radially symmetric set as the reachable set in the rest of the space. We still must show that the overall reachable set is closed and continuous to guarantee that trajectories cannot get out.

7.1.3 Open and Closed Valve Dynamics

The first thing to explore in the pursuit of a candidate reachable set is the location of the equilibrium points for the closed and open valve system dynamics. This information will then be used to find the equilibrium points for the semi-active systems being considered. In these systems, the equilibrium points are determined by the system dynamics and the disturbance value. We must include all equilibrium points that exist for any value of the disturbance. To do this, we need to look at the equilibrium points for each region. This is because if we are only considering open or closed valve dynamics, the equilibrium points are linearly dependent on the disturbance. This means that if the extreme equilibrium points are inside the candidate reachable set R, all of the interior equilibrium points are included as well. For this piecewise linear system, we have two types of equilibrium points to deal with. The first are the open valve region equilibrium points. The two extreme values are (0.0445, 0, 0), corresponding to d=-1, and (-0.0445, 0, 0), corresponding to d=1. For the closed valve system, the equilibrium points form a line whose position depends on the disturbance. For this case, we find that the equilibrium points occur in the $x_2=0$ plane and are given by the two lines

$$x_3 = -\frac{1}{10}x_1 + \frac{1}{224.72} \quad \text{for } d = -1$$
$$x_3 = -\frac{1}{10}x_1 - \frac{1}{224.72} \quad \text{for } d = 1 \tag{7.9}$$

Note that the closed valve equilibrium points include the two points that are also the open valve equilibrium points.

For both the open and closed valve systems, recall that the eigenvalues were given in Section 4.4 along with the corresponding natural frequencies and damping ratios. To help understand how each of these systems reacts to a disturbance, we can look at the modal canonical form of each system and analyze the effect of the disturbance for each mode. For the open valve case, the modal canonical form is

$$\dot{q} = \begin{bmatrix} -2.47 & 14.79 & 0 \\ -14.79 & -2.47 & 0 \\ 0 & 0 & -4999.6 \end{bmatrix} q + \begin{bmatrix} -10.02 \\ 1.68 \\ 0.0022 \end{bmatrix} d . \tag{7.10}$$

From this we can see that there are two distinct modes. The first is the underdamped mode discussed previously. This mode moves in a clockwise fashion about the equilibrium point. Figure 7.1 shows a view of this first mode for the open valve system in the state space. This figure is a side view of the last portion of the simulation shown in Figure 4.14. We can see that the system never attains large values of x_3 for any reasonable value of x_2. This is important since the second mode decays quickly to this mode.

The second mode is an exponential decay to an equilibrium value determined by the disturbance but very close to the origin. In state space, this means that the system decays exponentially to the trajectory shown in Figure 7.1.

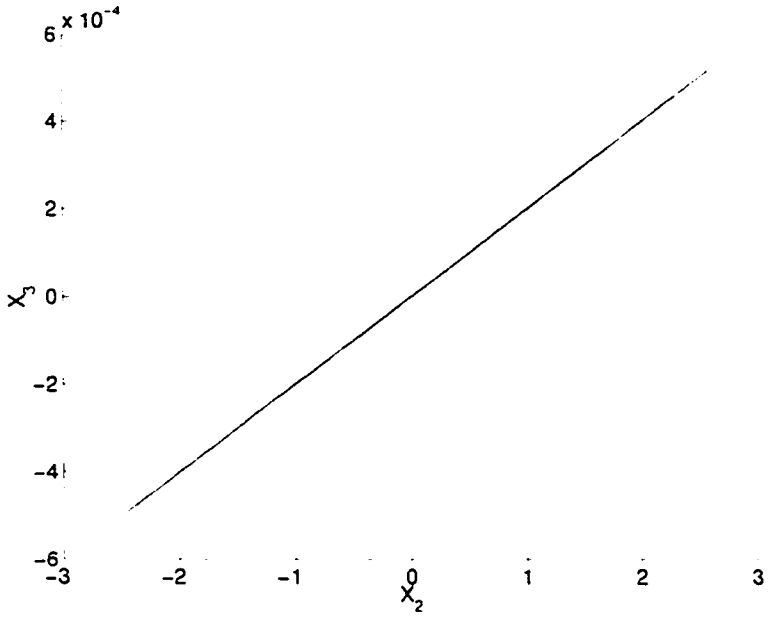

Figure 7.1: Side View of the First Open Valve Mode in State Space Coordinates

A check of the eigenvalues indicates that the plane made by the modal states q_1 and q_2 corresesponds very closely to the actual system plane made by the x_1 and x_2 states. This can be seen in Figure 4.14. The system will exhibit this behavior with a disturbance, but it will be centered on an equilibrium point other than the origin due to the disturbance. Note also that the equilibrium point will move from (-0.0445, 0, 0) to (0.0445, 0, 0) as the disturbance changes from d=1 to d=-1.

For the closed valve case, the modal canonical form is

$$\dot{q} = \begin{bmatrix} 0 & 0 & 0 \\ 0 & -2.25 & 49.67 \\ 0 & -49.67 & -2.25 \end{bmatrix} q + \begin{bmatrix} 0 \\ 10.00 \\ -0.45 \end{bmatrix} d . \tag{7.11}$$

As in the open valve case, there are two distinct modes. The first is a marginally stable mode indicating non-vibratory motion. This mode can easily be seen from the original

system dynamics as $\dot{x}_1 = \dot{x}_3$. This indicates that the two states are related as $x_3 = x_1 + c$ where c is a constant determined by initial conditions. Simply, this means that the system will always exhibit a 45° relationship between $\dot{x}_1$ and $\dot{x}_3$ with some offset from the origin determined by the initial conditions. In this plane, $x_3 = x_1 + c$, the system will exhibit the characteristics of its other mode, namely underdamped oscillation in a clockwise fashion. This behavior can be seen in Figure 4.14. With a disturbance, the system will exhibit this behavior around some equilibrium point determined from (7.9) rather than around the origin.

Several important things to note follow. First, both the open and closed valve systems exhibit clockwise rotational motion when the dynamics are projected into the x_1x_2-plane. Second, it is not hard to come up with a scheme for the disturbance switching in either case that will direct the system trajectory to circle around the outside of the equilibrium points in a closed loop. A simple version of this would have the disturbance d=1 when $x_2 \leq 0$ and d=-1 otherwise. This in fact leads to a trajectory in the open valve case that asymptotically approaches the system 1-norm value reported in Table 4.5 for the open valve case. Lastly, it is important to note that the only way to change the constant in the closed valve relationship $x_3 = x_1 + c$ is to change the initial conditions for the closed valve trajectories. The semi-active control law does this by moving into the open valve dynamics for a certain period of time. When the system again moves into the closed region, it is with a new initial condition. A simple example of this is a spring with a resettable free length.

7.1.4 Equilibrium Points for the Semi-Active System

Now that we know the equilibrium points and dynamics for each system individually, the semi-active control versions can be considered. In the semi-active case only open valve equilibrium points that occur inside the open valve region are kept. This happens similarly for both the closed valve equilibrium points and for the dynamics. Recall from the control law definition in (7.1), that when the system is on one of the switching planes (7.2-7.3), the control chooses the open valve. Since both of the open valve equilibrium points occur on the boundary $x_3 = 0$, and this will not change with the control version, the open valve equilibrium points are included in the semi-active system for all control versions. In the case of the closed valve equilibrium points, one must check to see where they correspond to a closed region in the semi-active system. It is interesting to note that no control version can have closed valve dynamics on the $x_2=0$ plane and have finite peak-to-peak gain. This is because the equilibrium points for the closed valve system go in a line to infinity on this plane.

Figures 7.2 and 7.3 show generic plots of the x_1x_3-plane versions for the two cases in the six control versions considered here. Figure 7.2 indicates a typical plot for control versions 1, 3, 4, 5, and 6. The value of the angle α is positive and the closed valve equilibrium points in the closed valve region are all closer to the origin in the x_1 direction than the open valve equilibrium points. Figure 7.3 shows a generic plot for control version 2. Notice that, in this case, the angle α is negative indicating that the closed valve equilibrium points are further from the origin. Table 7.2 shows the actual angles for each of the control laws in this view.

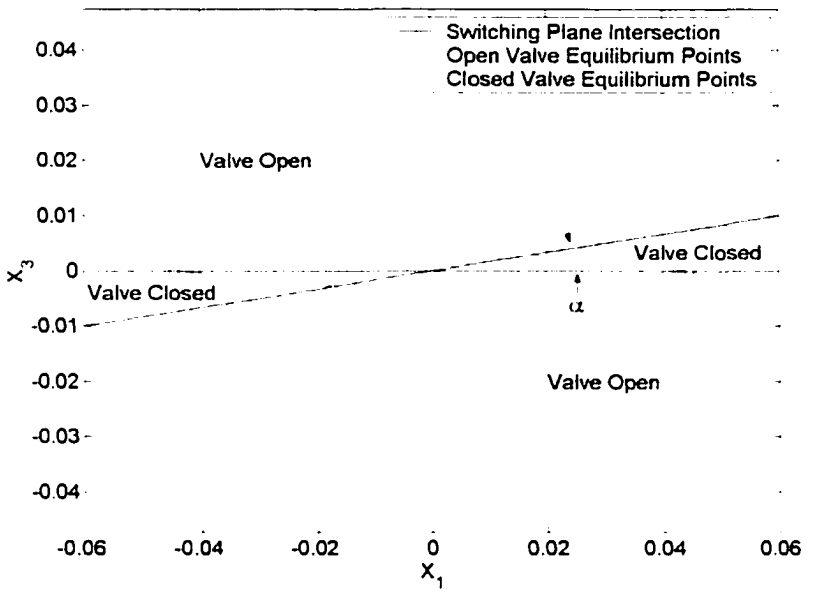

Figure 7.2: Intersection of Switching Planes (7.2-7.3) with the x_1x_3-Plane for Control Versions 1,3,4,5,6

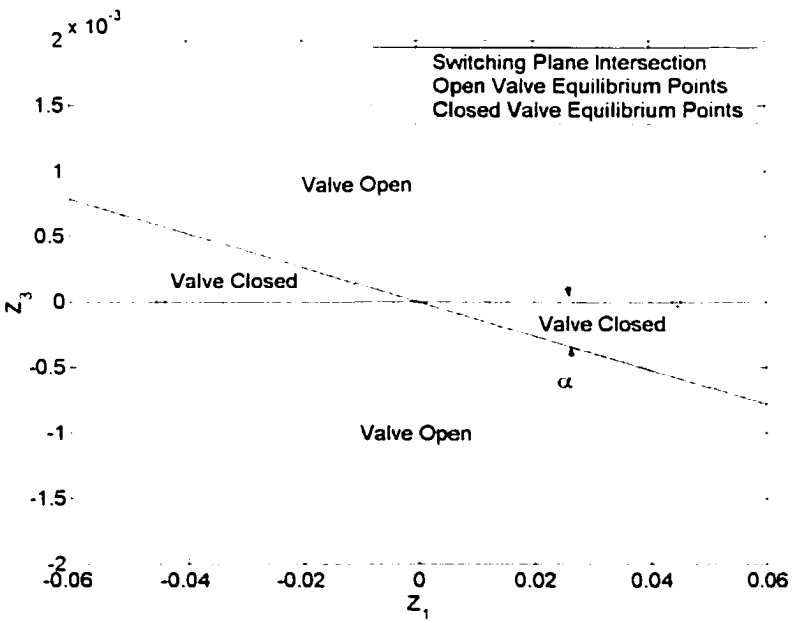

Figure 7.3: Intersection of Switching Planes (7.2-7.3) with the x_1x_3-Plane for Control Version 2

Table 7.1: Values for the Angle α in the Figures 7.2-7.3 for Control Versions 1-6 in Degrees

α_1	α_2	α_3	α_4	α_5	α_6
0.30	-0.75	2.39	7.82	9.40	83.58

7.1.5 Reachability of the Semi-Active Equilibrium Points

In control versions 1, 3, 4, 5, and 6, all of the closed and open valve equilibrium points present in the semi-active system are reachable. In control version 2, the open valve equilibrium point is reachable from the origin, but the closed valve equilibrium points, which are beyond these points, are not. The simplest way to establish the reachablility of the first group is through an example. Control version 5 will be used to illustrate one method for getting from the origin to the extreme equilibrium point. In a later section this will be discussed for each control version individually, and the reachability of the closed valve equilibrium points will be discussed.

For control version 5, the process of getting to the equilibrium point from the origin is as follows.

1. Start at the origin. Apply a d=-1 to move the system into the closed valve region X_0^*.
2. Continue applying d=-1 until the system reaches x_2=0, at which point the disturbance is switched to d=1. Continue in the region X_0^*.
3. When the boundary between X_0^* and X_1^* is reached the system switches to the open valve dynamics.

4. Continuing with the d=1 until switching to d=-1 will get you exactly back to the intersection of the two switching planes (7.2-7.3). Solving for the correct time to switch disturbances is an optimization problem. The system will remain in X_1^- throughout.
5. When the system gets to the intersection of the switching planes (7.2-7.3), maintaining d=-1 will move the system into the region X_1^-, asymptotically heading for the trajectory in Figure 7.1, and will move the system towards x_2=0. The system will reach the point where x_2=0 when it exactly reaches the x_1-axis. At this point, continued application of d=-1 will move the system into the closed valve region X_0^-.
6. The procedure then repeats cyclic steps 2-5 indefinitely.

This procedure will move the system asymptotically toward the extreme open valve equilibrium point at (0.0445, 0, 0). The system will reach the equilibrium point asymptotically as $t \to \infty$. Later, it will become important to show that the x_1-axis is also reachable at points less than the extreme equilibrium points and that points on the intersection of the switching planes (7.2-7.3) are also reachable. Fortunately, the procedure above goes through points on both of these lines, thus showing that they are reachable. The dynamics in the procedure are illustrated in Figure 7.4. This figure shows several views of the trajectories as they move out towards the equilibrium point for control version 5. As pointed out earlier, the only way for the system to cycle from one level curve in the closed valve dynamics to another is to switch to open valve dynamics briefly. This can be seen in the second plot in Figure 7.4. The trajectories angling up to the right are the closed valve dynamics. When those trajectories reach some maximum x_1

value, the system switches to open valve dynamics and cycles over to a level curve in the closed region moving the system farther out in the x_1 direction.

Referring back to Figure 7.2, control version 5 can get to any of the closed valve equilibrium points by first using the procedure outlined above until the appropriate time and then playing a different disturbance. The system can also reach the extreme point (-0.0445, 0, 0), since we have Proposition 7.2. The main difference is that all of the disturbances are switched to the opposite extreme values. This will drive the system to the extreme opposite equilibrium point in a similar fashion to that in Figure 7.4. This basically means that all of the equilibrium points in control version 5 must be inside the reachable set R^* for the system, since we can get to them all from the origin. This is also true for the x_1-axis and the intersection of the switching planes (7.2-7.3) with values $-0.0445<x_1<0.0445$.

Similar procedures will drive the system to extreme equilibrium points for control versions 1, 3, 4, and 6. For control version 2, the system is not able to get to the closed valve equilibrium points, since they are farther out than the extreme open valve equilibrium point.

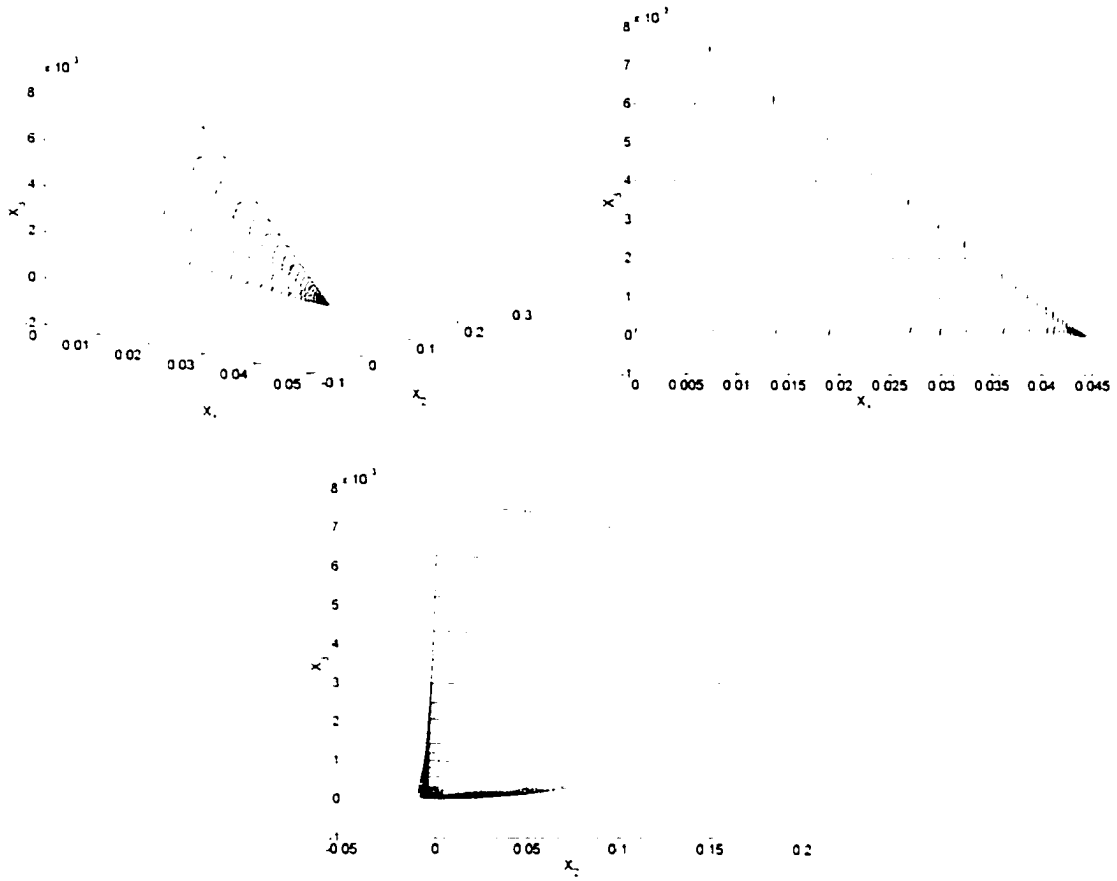

Figure 7.4: Three Views of the Dynamics to get Semi-Active Control Version 5 from the Origin to the Extreme Equilibrium Point (0.0445, 0, 0)

7.1.6 Constructing Individual Parts of the Candidate Reachable Set, R

With the equilibrium points fully known and reachable, we can move on to constructing a surface in each of the four control regions (X_0^+, X_0^-, X_1^+, X_1^-) to use as a candidate reachable set R for control version 5. Since we can show that the system is radially symmetric (see Section 7.1.2), we can find solutions in regions X_0^-, X_1^-. The solutions in the other regions will simply be the radially symmetric versions of these

surfaces. We must, however ensure that these surfaces are closed and continuous in the end. The way we do this is to look for a surface generated by the solution of the system dynamics (7.6-7.7) where, for any disturbance $|d| \leq 1$, all the possible system trajectories either follow the surface or move inside. This is done in each region with the constraint that the surfaces in each region are closed and continuous at the region boundaries.

The process of finding a surface begins in the closed valve region where $x_3>0$ (region X_0^*). Since there is a very fast mode that decays quickly to a value close to $x_3=0$ in the open valve dynamics (see Figure 7.1 and discussion), we will assume that the system switches to the closed loop dynamics at the line of the intersection between the two switching planes (7.2-7.3). From the last section, we know that points on this line are reachable if $-0.0445<x_1<0.0445$. Therefore, we will start on the line of the intersection between these extreme values. From this starting line, we follow the outer system trajectories until they meet with a switching plane that moves from closed to open dynamics.

Figure 7.5 shows an example of the resulting surface for the region X_0^* for control version 5. This surface is generated with the system trajectories in X_0^*, starting from the intersection of the two switching planes (7.2-7.3) and with the disturbance d=-1. The part of the surface that is generated by system trajectories is labeled part CL. Edge B is where the simulations begin. Edge A is where the simulation trajectories end on the switching plane. The tip of the cone corresponds to the intersection of the closed loop equilibrium points and the $x_3=0$ plane. The base of the cone touches the $x_3=0$ plane at the other place where the closed valve equilibrium points intersect the $x_3=0$ plane. The back plate, labeled part BP, is simply a plane formed by the closed valve trajectory

intersecting the equilibrium point at that end of the cone. It is the plane that is generated from $x_3 = x_1 + c$ where c=-0.0445. Regardless of the disturbance, we know that the closed valve trajectories will all fall on this plane. Edge C is where the part BP intersects with the switching plane. As discussed earlier, this is the plane generated by a closed loop trajectory with an initial condition at (-0.0445, 0, 0). Note that the gridlines on the surface are trajectories that have been combined to generate a surface.

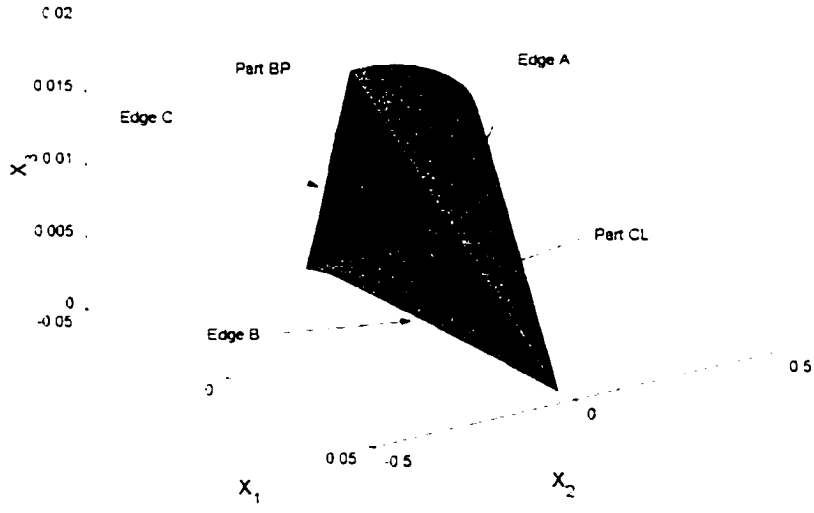

Figure 7.5: Surface Generated from System Trajectories in the Closed Valve Region X_0^* for Control Version 5

The surface in Figure 7.5 intersects the switching plane (7.2) with velocity vectors that will move the system into the region X_1^* at edges A and C. The next step in the process of building R is to start at these edges and find a surface in the open valve region that this system is moving into and that bounds the system response. Again, the surface is such that all the system trajectories will be on the surface or headed inside the surface.

Figure 7.6 shows the surface generated for the open valve region X_1^*. In this figure, the surface is labeled part OP and edges A and C correspond to the edges with the same names in Figure 7.5. The system leaves the open valve region when the trajectories get to the switching plane (7.3) corresponding to edge B*. It can be seen in this figure that the open valve trajectories tend to move the system back toward the x_3 plane, regardless of where the trajectories originate.

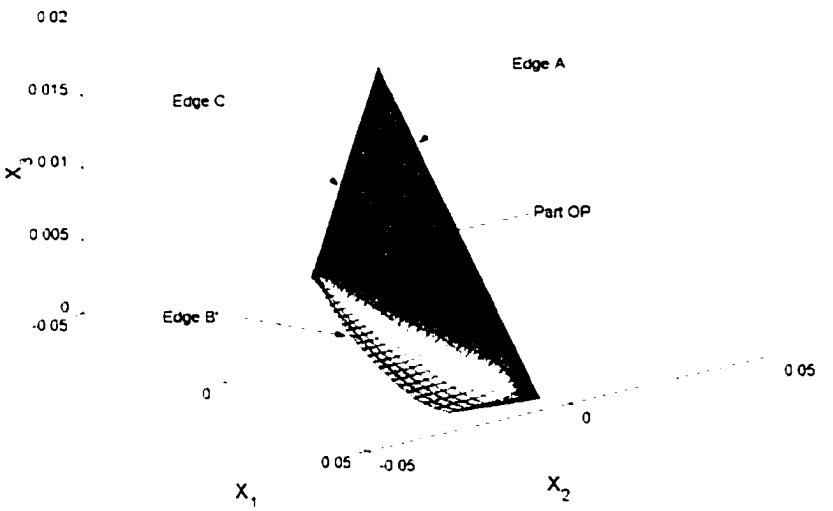

Figure 7.6: Surface Generated from System Trajectories in the Open Valve Region X_1^* for Control Version 5

To close the whole surface we need to have edges B and B* in Figures 7.5 and 7.6 match in the following way. When we use the radially symmetric versions of CL and OP to complete the candidate reachable set, we end up trying to match the edge B in Figure 7.5 with the radially symmetric version of edge B* in Figure 7.6. If we can match up these edges, we will have a closed and continuous surface for the candidate reachable set. This is accomplished by an iterative process. Starting with B*, which was generated as

discussed above, the process is repeated with the radially symmetric version of B' as a new edge B. This new edge B is used to then regenerate CL , BP, and OP and finally B'. This process is repeated until the radially symmetric version of B' matches edge B. It turns out that large changes in edge B only generate small changes in edge B'. This means that the iterations converge very quickly (3 iterations for control version 5). The final results from this process are shown in Figure 7.7 for control version 5. It can be seen that the two edges match very well.

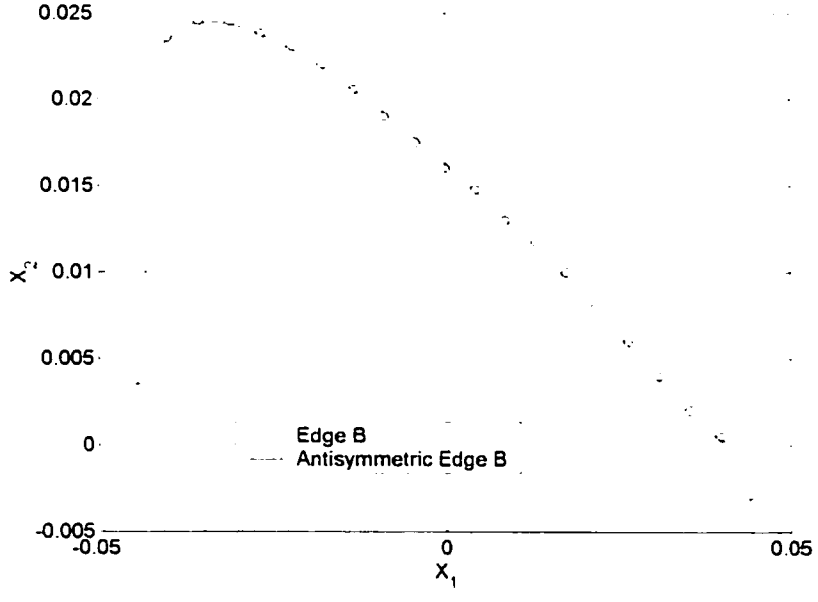

Figure 7.7: Final Values for B and B' on the x_3=0 Plane after 3 Iterations for Control Version 5

Since the system is radially symmetric across the $x_3 = 0$ plane, we can stop here and use radially symmetric versions of CL and OP for the regions X_1^- and X_0^-. Figure 7.8 shows all the pieces available at this point to construct the candidate reachable set for control version 5. No scale is shown, since this is an exploded view where the pieces are not in their correct positions relative to each other. The next thing to be done is to show

that the surface made by joining all of these parts is closed and continuous. We will label the parts symmetric to CL, OP, and BP as CL', OP', and BP' respectively. We will use a similar convention for the edges labeled in Figures 7.5 and 7.6.

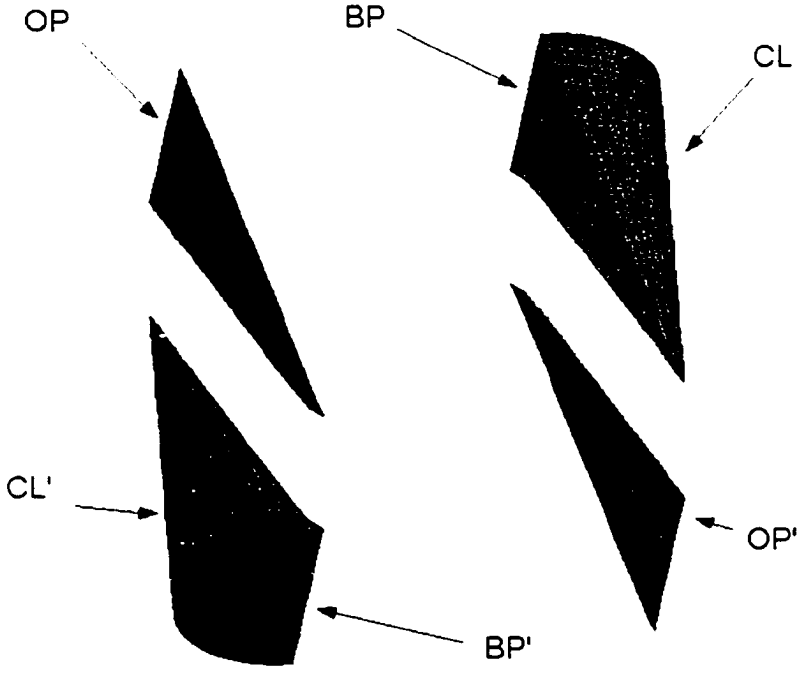

Figure 7.8: Exploded View of Component Parts for Candidate Reachable Set of Control Version 5

7.1.7 Check that the Candidate Reachable Set is Closed and Continuous

Once we have the pieces shown in Figure 7.8, we need to assemble the completed candidate reachable set. To do this, all the parts need to be closed and continuous at their intersections. From the way they were created, we can already say that parts CL and BP are continuous at their intersection. This is because the same closed valve trajectory was used to create the base of "cone" CL and plane BP. It can also be seen that parts CL and

OP are continuous at edge A, since the initial conditions used to generate OP along this edge are the final conditions of the trajectories used for CL at this edge. The surface is continuous at edge C since the intersection of plane BP and the switching plane (7.2) was used for initial conditions when generating that part of OP. Finally, the tip of "cone" CL is closed. This tip is not in fact a point but rather a flat region resembling a screwdriver that essentially occurs on the x_3=0 plane between planes (7.2) and x_2=0.

A detailed view of this tip with the assembled surface is shown in Figure 7.9. The trajectory runs from an initial point on the intersection of the switching planes (7.2-7.3) to the equilibrium point. At the equilibrium point, the trajectory turns around and follows the same path back to the initial condition. The result is that we have a continuous surface in regions X_1^* and X_0^*. These parts form a closed surface except for an opening pointed in the $-x_3$ direction. To close this surface, we use the radially symmetric surface in the regions X_1^* and X_0^*, which, by the same argument, is continuous and closed in those regions except for an opening pointed in the $-x_3$ direction. Since we have used an iterative process to ensure that edge(B*)=-edge(B), the joined surfaces will be closed at the intersection where x_3=0.

Once this is done, we have a closed continuous surface that is radially symmetric and that can be used as a candidate reachable set for the semi-active system. This closed surface is shown in Figure 7.10. There are several more things to explore before we can claim that this candidate reachable set is in fact the actual reachable set for the semi-active control system. Since we are looking for the peak-to-peak gain from the reachable set, this value and the extreme values in the coordinate directions are indicated in Table 7.2 for the candidate reachable set in Figure 7.10.

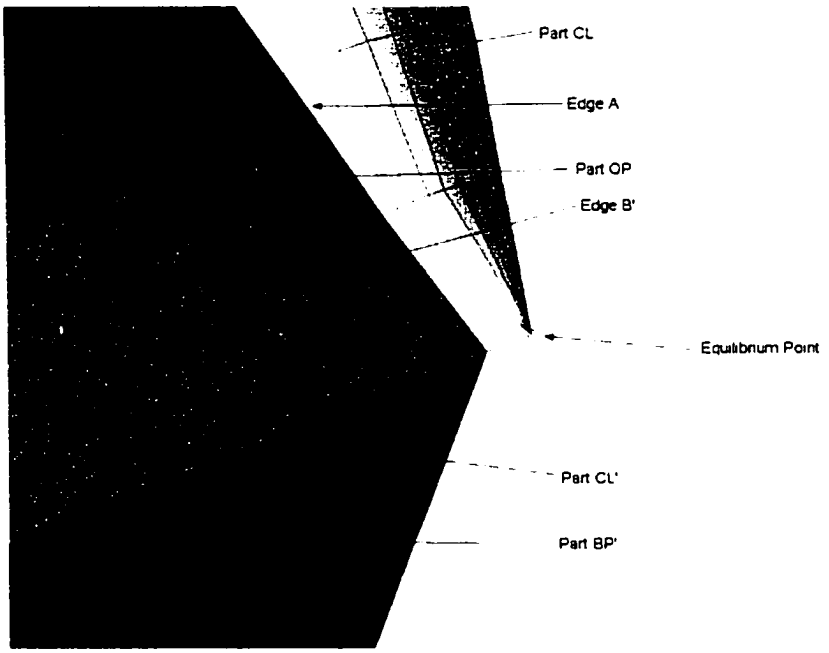

Figure 7.9: Close Up View of Tip of Candidate Reachable Set

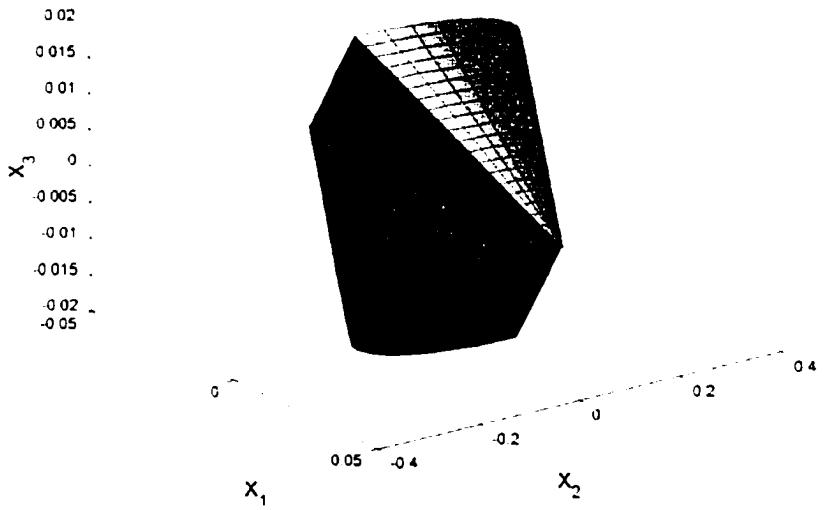

Figure 7.10: Assembled View of the Candidate Reachable Set for the Semi-Active Control Problem with Control Version 5

Table 7.2: Extreme values for the Candidate Reachable Set for Control Version 5 shown in Figure 7.10

$\|x_1\|_\infty$	$\|x_2\|_\infty$	$\|x_3\|_\infty$	Peak-to-Peak Gain
4.45e-2	3.75e-1	1.51e-2	3.77e-1

7.1.8 Check that All Trajectories Follow the Surface or Point Inwards

The next step in showing that the candidate reachable set R is in fact the actual reachable set R^* is to show that for any disturbance in the range $|d| \le 1$ all possible trajectories that originate on the surface R either follow the surface or move to the interior. This means that if we consider R to be a Lyapunov function V, then for any disturbance in the allowable range $\dot{V} \le 0$ on the surface. If this can be shown, then there is no way for a system trajectory to escape this surface, as long as the surface is closed and continuous. We showed that R is in fact closed and continuous in the previous section.

Now, we will show that if we check the trajectory direction for both extremes of the disturbance, we can say that this bounds the possible trajectory directions of the system. If we consider the surface of the candidate reachable set to be a Lyapunov function V for the system in (7.1), we can say that the time derivative of this function is

$$\dot{V} = \nabla V \bullet \dot{x}. \tag{7.12}$$

The only part of this that depends on the disturbance is $\dot{x}$. In fact, it depends linearly on the disturbance. This means that $\dot{V}$ is also linearly dependent on the disturbance. So, if we can find some indication of $\dot{V}$ for disturbances d=1 and d=-1, we can say that the

value of $\dot{V}$ will vary linearly in disturbance between these two values. Thus, all we need to do is to check the extremes of $\dot{V}$. A good first indication that this is true is shown in Figure 7.11. This figure shows a cross-section of the candidate reachable set for control version 5 along with the trajectories that would be generated with the other disturbances at several points on the surface as it goes around.

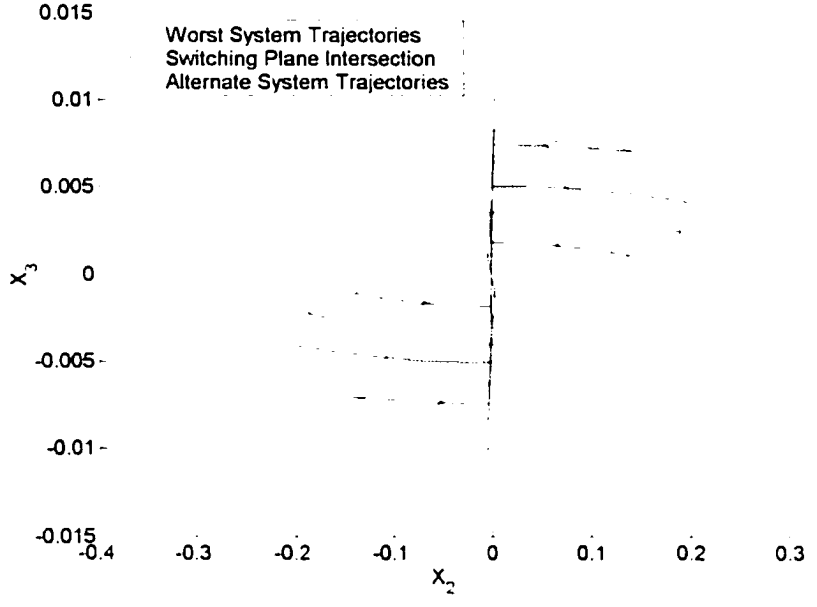

Figure 7.11: Cross-Section of the Candidate Reachable Set for Control Version 5 at the Plane $x_1=0$

We will also use numerical techniques to check the angle that the surface normal and the system trajectory make with each other on the whole surface. This value is normalized so that if the angle is 0°, then the trajectory is following the surface. Also, if the angle is $<0^o$, then the trajectory is moving to the interior. Conversely, if the angle is $>0^o$, then the trajectory is moving to the exterior. We will first use the disturbance used to create the surface itself. Since this was used to make the surface, the angle should be 0° everywhere on the surface for this disturbance. The real test will come when we use

the opposite disturbance. If the surface is in fact the reachable set R^*, all the angles with this opposite disturbance should be $\leq 0''$.

The surface normal is calculated by a convolution method that finds the normal at every vertex with eight neighbors on the discrete grid that forms the surface. If we say that the surface is represented by an $n \times m$ matrix of 3-vectors denoted collectively as X, we must first calculate intermediate values X_v and X_u by convolving X with the following matrices.

$$X_v : \frac{1}{12}\begin{bmatrix} -1 & 0 & 1 \\ -4 & 0 & 4 \\ -1 & 0 & 1 \end{bmatrix}$$
$$X_u : \frac{1}{12}\begin{bmatrix} -1 & -4 & -1 \\ 0 & 0 & 0 \\ 1 & 4 & 1 \end{bmatrix}^{\cdot} \tag{7.13}$$

Then the surface normal at some point is given by

$$\hat{n} = \frac{X_v \times X_u}{\|X_v \times X_u\|}. \tag{7.14}$$

We then calculate the angle between this normal and the system trajectory at the same point on the surface. This is then normalized as indicated earlier. The results of this process for control version 5 are shown in Table 7.3 and Table 7.4. Table 7.3 shows the results using the disturbance that generated the surface in the first place. As such, we would expect all the values to be identically zero. This is not quite true due to the approximate nature of the numerical normal vector, but we can see that the values are all very close to zero. In Table 7.4 the opposite disturbance was used. We expected to get values for the angle that ranged from zero into negative numbers. This would indicate

that the system was either following the surface or moving towards the interior. As can be seen in the table, all of the values do in fact follow the expectation.

Table 7.3: Angle of System Trajectory with Candidate Reachable Set Surface for Control Version 5 with Disturbance that Generated Surface R

Edge or Surface	Minimum Angle (degrees)	Maximum Angle (degrees)
Interior of CL	-0.00	+0.01
Edge A on CL	-0.00	+0.01
Edge B on CL	-0.00	+0.00
Edge at Tip on CL	-0.00	+0.00
Edge at Base on CL	-0.00	+0.00
Interior of OP	-1.13	+0.04
Edge A on OP	-0.00	+0.37
Edge B' on OP	-0.00	+0.00
Edge C on OP	-0.05	+0.00
Interior BP	-0.00	+0.00
Edge of BP	-0.00	+0.00
Edge C on BP	-0.00	+0.00

Table 7.4: Angle of System Trajectory with Candidate Reachable Set Surface for Control Version 5 with Opposite Disturbance

Edge or Surface	Minimum Angle (degrees)	Maximum Angle (degrees)
Interior of CL	-12.25	-0.02
Edge A on CL	-0.03	-0.02
Edge B on CL	-2.06	-0.02
Edge at Tip on CL	-12.26	-0.02
Edge at Base on CL	-11.43	-0.02
Interior of OP	-89.46	-0.01
Edge A on OP	-71.33	-14.70
Edge B' on OP	-3.45	-0.01
Edge C on OP	-56.99	-12.88
Interior BP	-0.00	+0.00
Edge of BP	-0.00	+0.00
Edge C on BP	-0.00	+0.00

Some inaccuracies will be evident particularly at the edges, since we are using a numerical technique to find the normal vector that relies on the surrounding values at some point. The mesh used for each surface had 300 divisions in the direction of the system trajectories and 150 divisions in the direction perpendicular to the system trajectories. This accounts for the non-zero values in the third column of Table 7.3. Notice that the largest errors occurred on an edge. The data in Tables 7.3 and 7.4 are a very good indication that all trajectories are either moving along the surface or moving to the interior. This gives us a very powerful argument for the contention that the candidate reachable set R is in fact the actual reachable set R^*.

7.1.9 Show that the Semi-Active System Converges to R from Outside

In an effort to show that the system will converge to the candidate reachable set if the initial conditions of the system are outside of the candidate reachable set, it is helpful to divide the system space into component parts. Fortunately, due to the radial symmetry in the problem we will not have to look directly at all of these divisions. Let us first look at the region between planes $x_3 - x_1 = -0.0445$ and $x_3 - x_1 = 0.0445$ formed by parts BP and BP', intersecting the equilibrium points of the open valve system. Recall that system dynamics anywhere with a constant disturbance can be given by the equations (7.6-7.7). Let us say that a trajectory on the surface of the candidate reachable set can be found by the equation (7.6) with some maximal disturbance d_0=1 or -1 over some time interval Δt and the appropriate matrix for $\bar{A}$. Let some initial condition outside of the surface but with the same maximal disturbance be indicated as

$$\begin{bmatrix} x_0 + \Delta x_0 \\ d_0 \end{bmatrix}.$$

Then, if the matrix exponential in (7.6) is evaluated, the trajectory generated will not move parallel to the surface of the candidate reachable set but rather decay toward it. If the disturbance is increased with the same ratio as the initial condition for the specific location, then the trajectory will parallel the surface. Since the surface is generated by maximal disturbances, the disturbance cannot be increased. Therefore, any initial condition between the planes $x_3 - x_1 = -0.0445$ and $x_3 - x_1 = 0.0445$ and outside the candidate reachable set surface will decay towards the surface.

Another way to look at this is based on the equilibrium points of the system. On the surface of the candidate reachable set, the trajectories are created by choosing either d=1 or d=-1. These two cases correspond to two different equilibrium points for the system. This means we can look at the choice of disturbance from the point of view of the equilibrium points. Which of the two possible equilibrium points will generate the worst trajectory?

Once we have chosen the equilibrium point to use, we know that the system will decay to this equilibrium point asymptotically as $e^{\alpha t}$, where α is the real part of the system's eigenvalues. This results in exponential decay if α is negative. Recall that for the open valve system the eigenvalues are

$$\lambda_1 = -2.47 \pm 14.79i$$
$$\lambda_2 = -4999.6$$

and the closed valve eigenvalues are

$$\lambda_1 = -2.25 \pm 49.67i$$
$$\lambda_2 = 0$$

For the closed valve region there is only one complex eigenvalue that results in a decay $e^{-2.25t}$ towards the chosen equilibrium point. Recall that, if the system starts at some point $\left(x_1^0,\ x_2^0,\ x_3^0\right)$ outside the CL surface in the region X_0^+, then the system must stay on the plane $x_3^0 - x_1^0 = c$ and spiral to one of the two equilibrium points on that plane depending on the disturbance. This is true for all trajectories in the X_0^+ and X_0^- regions between the planes of parts BP and BP'. In the open valve regions, there are two eigenvalues that generate decay toward the chosen equilibrium point in two ways. The negative real eigenvalue creates a very fast decay e^{-5000t}, which moves the system towards the level shown in Figure 7.1, and the complex eigenvalue creates another decay $e^{-2.47t}$ in the oscillatory motion parallel to the plane in Figure 7.1. Thus we can see decay in the regions X_1^+ and X_1^- as well.

Using these decaying trajectories, we can construct the surfaces OP, OP', CL, and CL'. Since these surfaces connect to form a closed, continuous, bounded surface R, we can say that any trajectory outside this surface will decay towards this surface. In fact, if the same choices for the disturbance are used for the trajectory outside as were used to generate the candidate reachable set, the trajectory will asymptotically approach the surface. This case is the slowest convergence to the surface, as it will only approach the surface as $t \to \infty$. If the disturbances are used in any other order, the system will approach the surface faster and possibly enter the surface rather than approach it asymptotically.

Figure 7.12 shows a typical trajectory of this kind for control version 5. The initial condition in space is (0, 0.3, 0), which is outside the candidate reachable set but

inside the region X_0^*. The disturbance is the same maximal one used to generate the candidate reachable set for control version 5.

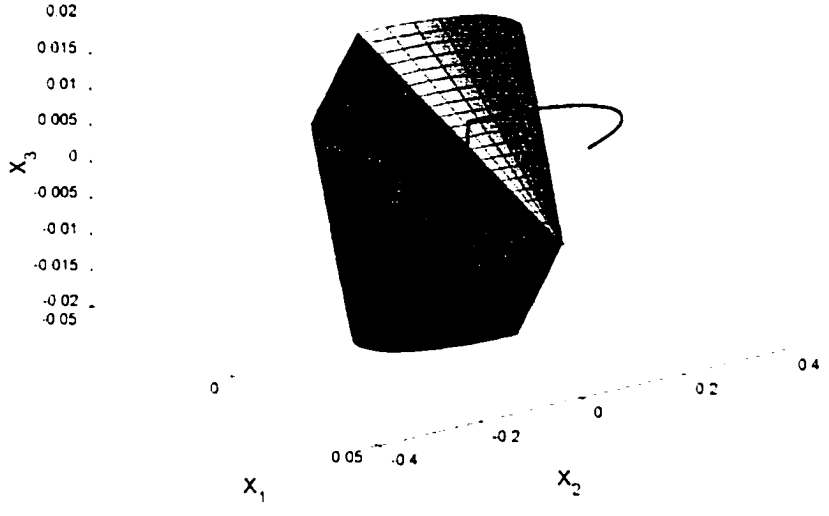

Figure 7.12: Typical Trajectory with Initial Condition Outside Candidate Reachable Set and Between Planes Formed by Parts BP and BP' at the Equilibrium Points for Control Version 5

Using any other disturbance makes the trajectory decay towards the attractor set faster. The asymptotic convergence in the open valve region is very fast due to the large negative real eigenvalue. From the figure, one can see that the trajectory approximately follows the surface shape while decaying quickly to the surface itself.

Since the system is radially symmetric, we only need to look at the other side of one of the planes $x_3 - x_1 = -0.0445$ and $x_3 - x_1 = 0.0445$. The other area will simply act in an radially symmetric manner. We will look at the area on the far side of $x_3 - x_1 = -0.0445$ from the origin ($x_3 - x_1 \leq -0.0445$). In the closed valve area with

$x_3>0$ (X_0^+) we know from the switching plane equation (7.2) for control version 5 that we are in the region where $x_2 > -0.0745x_1 + 0.450x_3$. With these conditions, the equation for $\dot{x}_2$ is always negative, regardless of the disturbance. This means that the system will always move into the open valve region X_1^+, regardless of the value of the disturbance from the closed valve region X_0^+. Once the system is in the open valve region, it quickly decays to the closed valve region X_0^-. In this region, the system looks like an extension of the part CL$^+$ into this region. All of this means that the extreme trajectories in the regions where $x_3 - x_1 \leq -0.0445$ tend to move in a spiral fashion towards the candidate reachable set in region X_0^-.

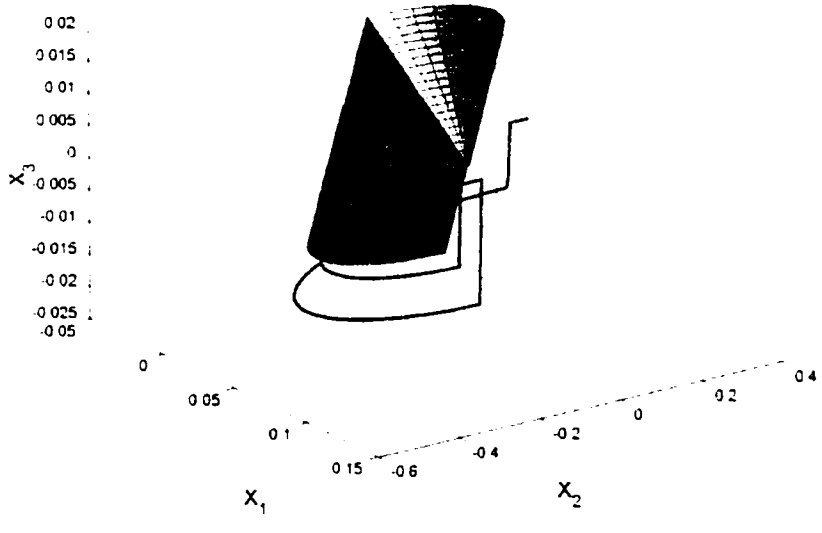

Figure 7.13: Typical Trajectory for the System when x_3-x_1<-0.0445.

This behavior can be seen in Figure 7.13 with the system initial condition at (0.075, 0.1, 0.01). The system moves out of the closed valve region it starts in and gets stuck spiraling in to R in the extension of the cone shaped CL$^+$. All the other possible

trajectories in this region converge to the interior of this extension of CL' for the same reason that they decay to CL' itself. This behavior is seen symmetrically in the region $x_3 - x_1 \geq 0.0445$.

7.1.10 Getting to the Candidate Reachable Set Boundary from Inside

Getting to the boundary of the candidate reachable set from the inside is actually reasonably easy. One method hinges on the fact that we already know that the system can get to the open valve equilibrium points. Unfortunately, it takes an infinite amount of time to get there. Since this is the case, we also know that we can get very close to the equilibrium point in finite time. Starting from anywhere in the candidate reachable set, if a zero disturbance is played the system decays to the origin. Once at the origin we can play the disturbance used in Section 7.1.5 to get out to one of the equilibrium points. At this point, we just need to use the disturbance that generated the candidate reachable set surface. If we use this exact disturbance, the system will stay on the surface of the candidate reachable set and move toward a stable limit cycle centered at the origin. If we do this from both equilibrium points, which we know are reachable, we cover the surface made up of CL, OP, CL', and OP'.

Figure 7.14 shows how this is done, with the trajectory starting at one of the equilibrium points and moving towards the limit cycle around the origin. The trajectory is shown on the surface of the candidate reachable set. Note that to actually reach these points we would have to head towards the equilibrium point from the origin as in Figure 7.4. We would have to stay on this course for infinite time to get infinitely close to get to the equilibrium point. Then we switch to the trajectory shown in Figure 7.14 and must

stay on this trajectory for an infinite time as well to get to the limit cycle around the origin. Since we cannot go to infinite time twice, we can only approach this trajectory asymptotically. To complete the surface we would have to do this from the other equilibrium point as well. In this fashion, the system can get from any point inside the candidate reachable set to anywhere on the surface.

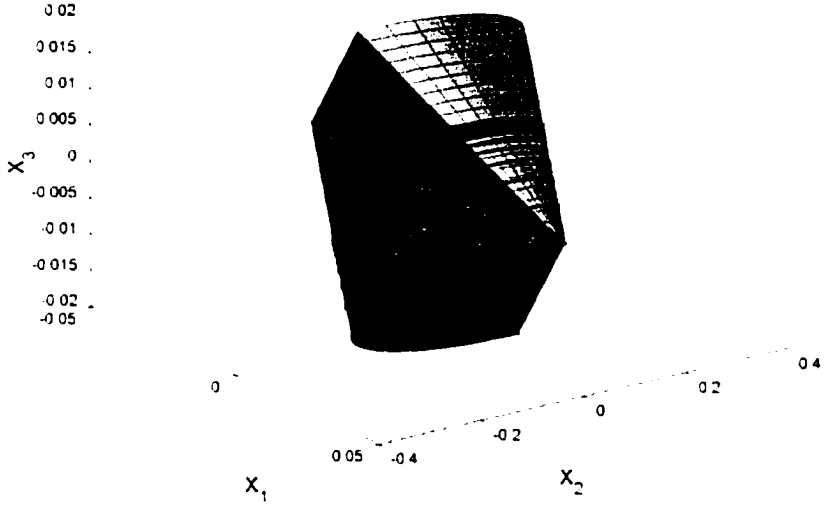

Figure 7.14: Trajectory from an Equilibrium Point Along the Surface of the Candidate Reachable Set

7.1.11 Claim that the Candidate Reachable Set is the Actual Reachable Set

We made many conclusions in sections 7.1.3 to 7.1.10. First, the open valve equilibrium points are always available in the semi-active system dynamics, and we can reach these points from the origin asymptotically. Part of the line made by the closed valve equilibrium points is available in the semi-active system, but only values that are closer to the origin than the open valve equilibrium points are reachable from the origin.

We also see that we can construct surfaces in each of the four regions defined by the control law that follows the "worst case" system dynamics. Essentially, this means that anywhere on this surface the system will only be able to follow the surface or move to the inside. We can argue that when these surfaces were pieced together, the final surface generated to enclose the system dynamics is closed and continuous everywhere. Numerical tests of this closed continuous surface validate the claim that all system trajectories either move along the surface or towards the interior. Finally, we can argue that that the surface is attractive to points outside and can be reached from points inside. With the information and arguments in Sections 7.1.3 to 7.1.10 summarized above, we can now claim that the candidate reachable set R is in fact the actual reachable set R^*.

7.2 Control Versions 5 and 4

Control versions 5 and 4 have very similar dynamics. In fact, the resulting reachable sets are indistinguishable from each other. Control version 5 was used as an example throughout Section 7.1. There are very few differences between the results for control version 5 shown in Section 7.1 and the results for control version 4. The main differences are outlined below.

The normalized switching planes for control version 4 are

$$B^T P^T x = -0.137x_1 - 2.22x_2 + x_3 = 0 \tag{7.15}$$

and

$$x_3 = 0. \tag{7.16}$$

Notice that these are almost exactly the same as those for control version 5 in (7.2-7.3). This is why the two control versions are so closed.

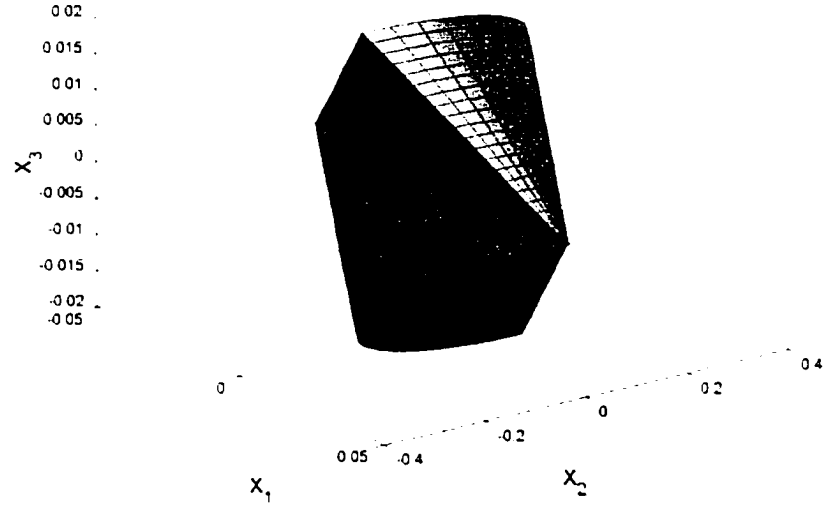

Figure 7.15: Assembled View of the Candidate Reachable Set for the Semi-Active Control Problem with Control Version 4

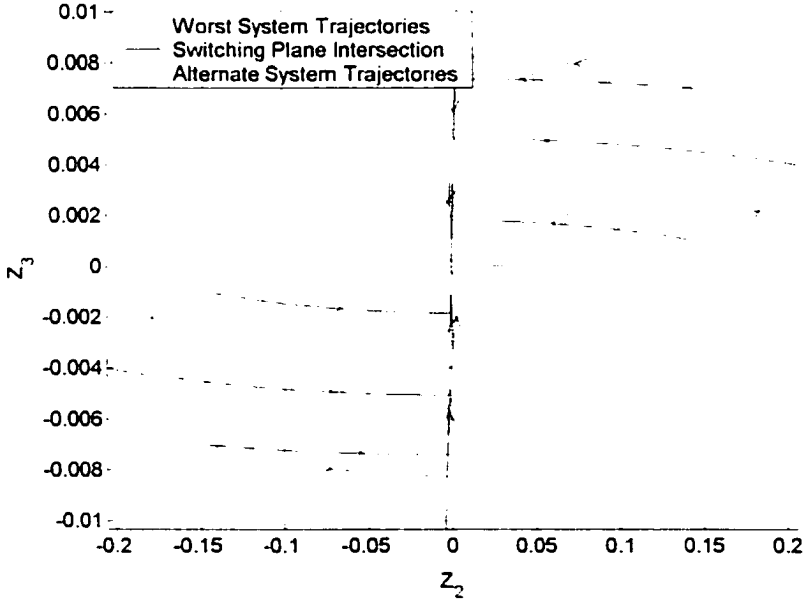

Figure 7.16: Cross-Section of the Candidate Reachable Set for Control Version 4 at the Plane $x_1=0$

The surface generated by the methods in Section 7.1 for control version 4 is shown in Figure 7.15. The cross-section of this set is shown in Figure 7.16. If we compare this to the surface generated for control version 5 in Figure 7.10, they are indistinguishable.

Tables 7.5 and 7.6 indicate the results from comparing the numerical normal vector to the system trajectories of control version 4. Recall that a negative angle means that the system trajectory is moving into the surface, and a positive angle means that the system is moving out of the surface. If we use the disturbance that generated our candidate reachable set shown in Figure 7.15, we expect to get 0° everywhere. This is shown in Table 7.5. As discussed before, due to the grid sized used and the numerical calculation of the normal vector, some variation of the angles in Table 7.5 can be seen. If the opposite extreme disturbance is used, we expect angles that are mostly negative. This is in Table 7.6.

Table 7.5: Angle of System Trajectory with Candidate Reachable Set Surface for Control Version 4 with Disturbance that Generated Surface R

Edge or Surface	Minimum Angle (degrees)	Maximum Angle (degrees)
Interior of CL	-0.00	+0.06
Edge A on CL	-0.00	+0.01
Edge B on CL	-0.00	+0.00
Edge at Tip on CL	-0.00	+0.06
Edge at Base on CL	-0.00	+0.00
Interior of OP	-0.16	+0.82
Edge A on OP	-0.00	+0.89
Edge B` on OP	-0.00	+0.02
Edge C on OP	-0.02	+0.00
Interior BP	-0.00	+0.00
Edge of BP	-0.00	+0.00
Edge C on BP	-0.00	+0.00

Table 7.6: Angle of System Trajectory with Candidate Reachable Set Surface for Control Version 4 with Opposite Disturbance

Edge or Surface	Minimum Angle (degrees)	Maximum Angle (degrees)
Interior of CL	-12.23	-0.00
Edge A on CL	-0.58	-0.00
Edge B on CL	-1.97	-0.03
Edge at Tip on CL	-13.82	-0.04
Edge at Base on CL	-11.43	-0.03
Interior of OP	-89.70	-0.01
Edge A on OP	-71.20	-14.89
Edge B* on OP	-3.69	-0.01
Edge C on OP	-82.34	-14.80
Interior BP	-0.00	+0.00
Edge of BP	-0.00	+0.00
Edge C on BP	-0.00	+0.00

Using the same arguments that we made for control version 5 in Section 7.1, we claim here that the candidate reachable set R in Figure 7.14 is in fact the actual reachable set R^*.

Finally, Table 7.6b summarizes the peak-to-peak gain results that we can get from the largest radius of the reachable set for control versions 5 and 4, along with some other relevant data.

Table 7.6b: Summary of Extreme values for the Reachable Sets of Control Versions 5 and 4

Control Version	$\|x_1\|_\infty$	$\|x_2\|_\infty$	$\|x_3\|_\infty$	Peak-to-Peak Gain
5	4.45e-2	3.75e-1	1.51e-2	3.77e-1
4	4.45e-2	3.75e-1	1.51e-2	3.77e-1

7.3 Control Versions 3 and 1

Control versions 3 and 1 both have very similar dynamics, which are slightly different than those of control versions 5 and 4. Fortunately, they still share many of the same characteristics with the previous control laws. We will point out the differences and summarize the results for the reachable sets of control laws 3 and 1.

As before, we will begin with the normalized switching planes, the root of determining the semi-active system dynamics. For control version 3, the switching planes are given by

$$B^T P^T x = -0.0417x_1 - 0.524x_2 + x_3 = 0 \tag{7.17}$$

and

$$x_3 = 0. \tag{7.18}$$

For control version 4 the switching planes are given by

$$B^T P^T x = -0.0053x_1 - .0664x_2 + x_3 = 0 \tag{7.19}$$

and

$$x_3 = 0. \tag{7.20}$$

Notice that for these two control versions, the switching planes are somewhat different. Regardless, these two systems exhibit very similar dynamics.

The differences between these control versions and those in Section 7.2 are related to the steepness of the switching plane (7.17) or (7.19) for the construction of the part OP for the candidate reachable sets. In the case of control versions 5 and 4, the open valve dynamics moved the system away from the switching plane and into the open valve region X_1^*. For control versions 3 and 1, the open valve dynamics do not move away from the switching plane until it reaches a much smaller value of x_3. Since this is the

case, the worst case trajectory used to create the candidate reachable set surface OP begins from edge A and C in a sliding mode, which moves the system down the switching plane. This sliding mode is created by applying d=1 in both the open and closed regions X_1^* and X_0^*. Eventually, the system reaches a point where this disturbance moves the system away from the sliding mode into the open region X_1^*. Other than these differences, construction of this candidate reachable set is the same as in Section 7.1. This is more clearly shown by the following figures.

The candidate reachable sets for control versions 3 and 1 are shown in Figures 7.17-7.20. Figure 7.17 shows the candidate set for control version 3. Notice that even with the sliding mode for part OP the reachable set is nearly indistinguishable from that of control versions 5 and 4. Figure 7.18 shows the cross-section of the candidate reachable set for control version 3. The sliding mode in part OP is shown between points A and B. At B the system finally moves into region X_1^*. Figures 7.19 and 7.20 show the same two views for control version 1. Notice that in the case of control version 1, the system does not move off of the sliding mode until it gets very close to the intersection of the switching planes (at the origin in Figure 7.20). This is because the switching plane in that case is not as steep as in control version 3. This can be seen in the candidate reachable set in Figure 7.19.

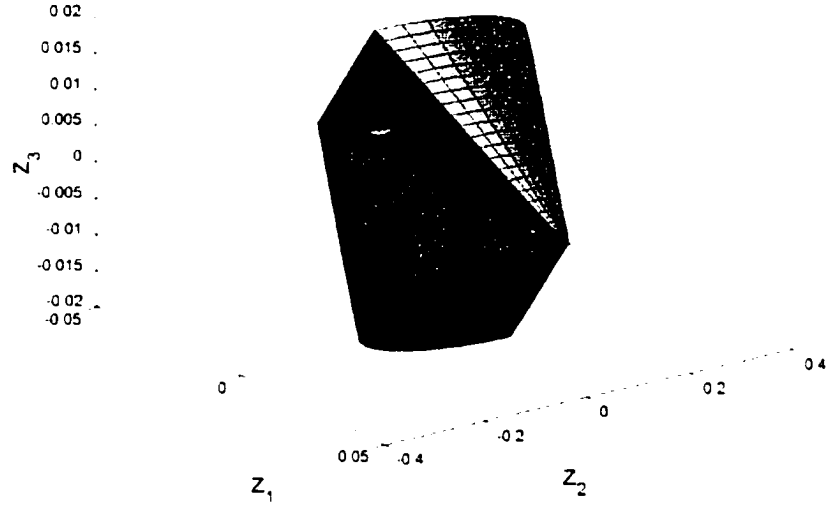

Figure 7.17: Assembled View of the Candidate Reachable Set for the Semi-Active Control Problem with Control Version 3

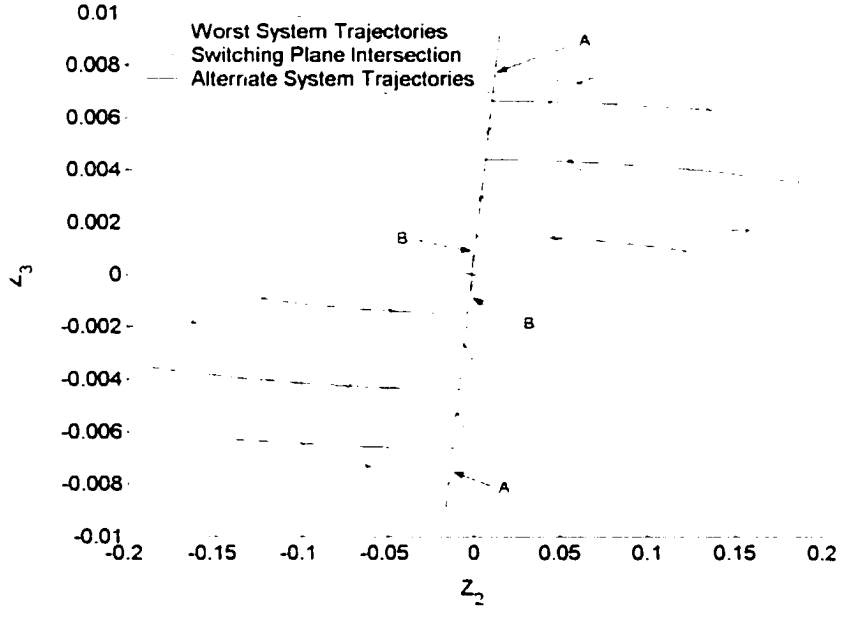

Figure 7.18: Cross-Section of the Candidate Reachable Set for Control Version 3 at the Plane $x_1=0$ (Sliding Mode Between A and B)

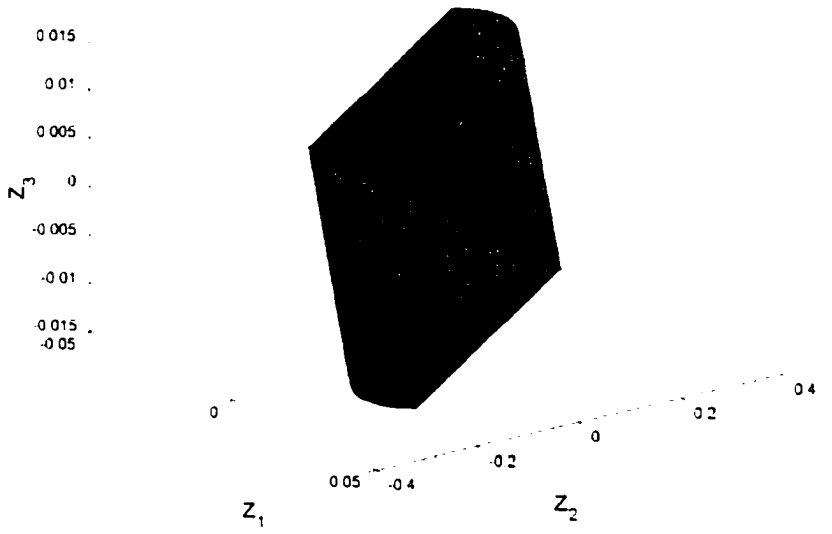

Figure 7.19: Assembled View of the Candidate Reachable Set for the Semi-Active Control Problem with Control Version 1

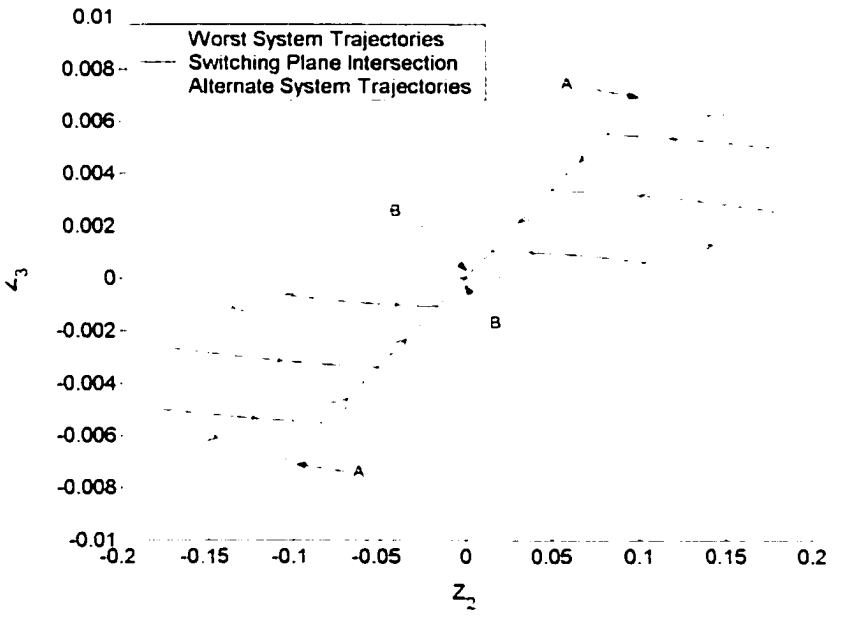

Figure 7.20: Cross-Section of the Candidate Reachable Set for Control Version 1 at the Plane $x_1=0$ (Sliding Mode Between A and B)

Tables 7.7 to 7.10 indicate the results of comparing the numerical normal vector and the system trajectories in control versions 3 and 1. Recall that a negative angle means that the system trajectory is moving into the surface, and a positive angle means that the system is moving out of the surface. If we use the disturbance that generated our candidate reachable set shown in Figures 7.17 and 7.19, we expect to get 0° everywhere. This is shown in Table 7.7 for control version 3 and in Table 7.9 for control version 1. As discussed before, due to the grid size used and the numerical calculation of the normal vector, some variation of the angles in Tables 7.7 and 7.9 can be seen. If the opposite extreme disturbance is used, we expect angles that are mostly negative. This is in Table 7.8 and 7.10 for control versions 3 and 1 respectively.

Table 7.7: Angle of System Trajectory with Candidate Reachable Set Surface for Control Version 3 with Disturbance that Generated Surface R.

Edge or Surface	Minimum Angle (degrees)	Maximum Angle (degrees)
Interior of CL	-0.00	+0.10
Edge A on CL	-0.00	+0.15
Edge B on CL	-0.00	+0.00
Edge at Tip on CL	-0.00	+0.10
Edge at Base on CL	-0.00	+0.00
Interior of OP	-0.10	+0.17
Edge A on OP	-0.10	+0.20
Edge B' on OP	-0.00	+0.03
Edge C on OP	-0.00	+0.06
Interior BP	-0.00	+0.00
Edge of BP	-0.00	+0.00
Edge C on BP	-0.00	+0.00

Table 7.8: Angle of System Trajectory with Candidate Reachable Set Surface for Control Version 3 with Opposite Disturbance

Edge or Surface	Minimum Angle (degrees)	Maximum Angle (degrees)
Interior of CL	-12.23	-0.02
Edge A on CL	-0.19	-0.02
Edge B on CL	-2.06	-0.03
Edge at Tip on CL	-13.50	-0.17
Edge at Base on CL	-11.43	-0.08
Interior of OP	-89.84	-0.01
Edge A on OP	-77.88	-40.98
Edge B' on OP	-3.73	-0.01
Edge C on OP	-47.64	-38.86
Interior BP	-0.00	+0.00
Edge of BP	-0.00	+0.00
Edge C on BP	-0.00	+0.00

Table 7.9: Angle of System Trajectory with Candidate Reachable Set Surface for Control Version 1 with Disturbance that Generated Surface R

Edge or Surface	Minimum Angle (degrees)	Maximum Angle (degrees)
Interior of CL	-0.00	+0.07
Edge A on CL	-0.00	+0.00
Edge B on CL	-0.00	+0.00
Edge at Tip on CL	-0.00	+0.07
Edge at Base on CL	-0.00	+0.00
Interior of OP	-0.14	+0.00
Edge A on OP	-0.14	+0.25
Edge B' on OP	-0.00	+0.00
Edge C on OP	-0.00	+0.02
Interior BP	-0.00	+0.00
Edge of BP	-0.00	+0.00
Edge C on BP	-0.00	+0.00

Table 7.10: Angle of System Trajectory with Candidate Reachable Set Surface for Control Version 1 with Opposite Disturbance

Edge or Surface	Minimum Angle (degrees)	Maximum Angle (degrees)
Interior of CL	-12.23	-0.03
Edge A on CL	-0.80	-0.24
Edge B on CL	-1.85	-0.02
Edge at Tip on CL	-30.78	-0.05
Edge at Base on CL	-11.42	-0.58
Interior of OP	-89.70	-0.01
Edge A on OP	-89.65	-5.36
Edge B* on OP	-3.51	-0.01
Edge C on OP	-10.52	-5.36
Interior BP	-0.00	+0.00
Edge of BP	-0.00	+0.00
Edge C on BP	-0.00	+0.00

For control versions 3 and 1, the system behavior inside and outside the candidate reachable sets still follows the general trends indicated in Section 7.1 for control version 5. The only difference is that the system will slide down the switching surface for some time when it switches from a closed region to an open region. The plots are indistinguishable from those in Figures 7.12 and 7.13.

Using the same arguments made for control version 5 in Section 7.1, we can claim that the candidate reachable sets R in Figure 7.17 for control version 3 and in Figure 7.19 for control version 1 are in fact the actual reachable sets R^* for these two control versions.

Finally, Table 7.11 summarizes the peak-to-peak gain results we can get from the largest radius of the reachable set for control versions 5 and 4, along with some other relevant data. These values almost identical to those from control versions 5 and 4, since they are based on the system trajectory starting at equilibrium point (0.0445, 0, 0) and travel the largest arc back to the switching plane. This trajectory forms the base of the

cone CL. This trajectory does not change significantly from version to version. The only difference is the x_3 value for control version 1. This is smaller than the others since the switching plane in this case is so much less steep. This does not affect the peak-to-peak gain, however.

Table 7.11: Summary of Extreme values for the Reachable Sets of Control Versions 3 and 1

Control Version	$\|x_1\|_\infty$	$\|x_2\|_\infty$	$\|x_3\|_\infty$	Peak-to-Peak Gain
3	4.45e-2	3.75e-1	1.51e-2	3.77e-1
1	4.45e-2	3.75e-1	1.38e-2	3.77e-1

7.4 Control Version 6

Control version 6 exhibits dynamics that are again similar to control version 5, with some exceptions. Due to the switching plane locations, the flat tip of CL in the candidate reachable set is very wide in this control law. The procedures outlined in Section 7.1 are unchanged for this control version, but they result in a candidate reachable set that is distinctly different from that of control version 5. This leads to the most significant variation of the resulting peak-to-peak gain from the results for control version 5. This control version does not use a sliding surface for part of OP as did versions 3 and 1.

As before, we will begin with the normalized switching planes, the root of determining the semi-active system dynamics. For control version 3, the switching planes are given by

$$B^T P^T x = -8.88x_1 - 2.22x_2 + x_3 = 0 \tag{7.21}$$

and

$$x_3 = 0. \tag{7.22}$$

Comparing this to (7.2) and (7.3) for control version 5, we can see that the only difference is in the first term in (7.21).

The candidate reachable set for control version 6 is constructed in the same fashion as that of control version 5 in Section 7.1. The shape that emerges is somewhat different than that for control version 5, since the switching planes are different. Figure 7.21 shows the candidate reachable set for control version 6. The tip of part CL is very pronounced in this control law and stands out immediately. This tip actually reduces the effectiveness of this control because it delays the point where the trajectory switches regions back to closed valve. Because the switch to the closed valve region is delayed, the closed trajectory travels farther out than in the case of any other control version.

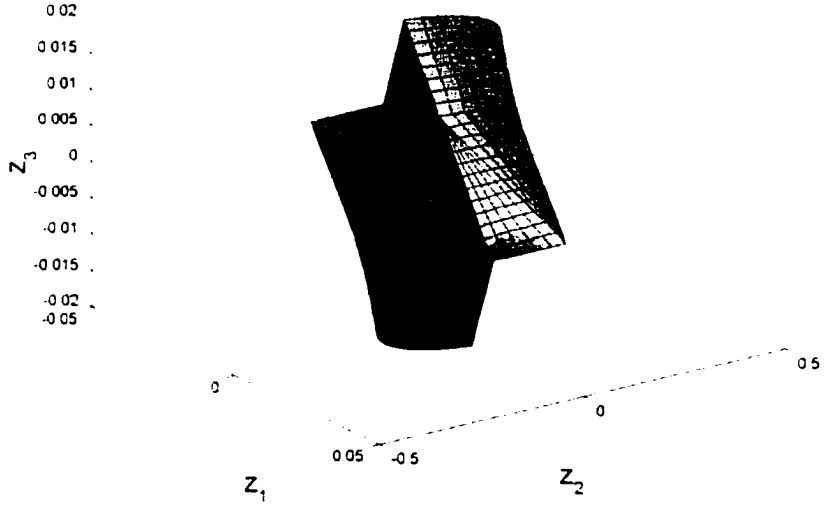

Figure 7.21: Assembled View of the Candidate Reachable Set for the Semi-Active Control Problem with Control Version 6

Figure 7.22 shows the cross-section of this candidate reachable set at the plane x_1=0. One can see that part OP is not constructed with a sliding surface as in control versions 3 and 1, but rather in the fashion of control versions 5 and 4.

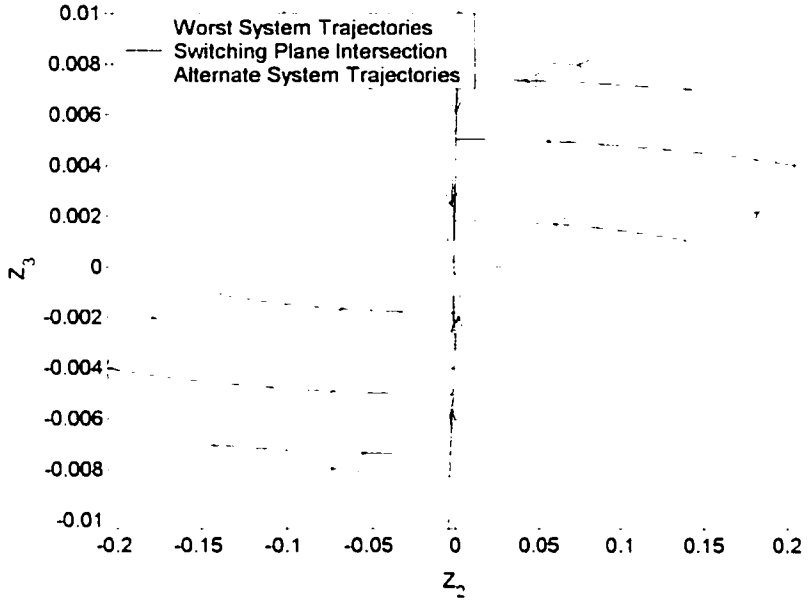

Figure 7.22: Cross-Section of the Candidate Reachable Set for Control Version 6 at the Plane x_1=0

Tables 7.11 and 7.12 indicate the results of comparing the numerical normal vector and the system trajectories of control version 6. Recall that a negative angle means that the system trajectory is moving into the surface, and a positive angle means that the system is moving out of the surface. If we use the disturbance that generated our candidate reachable set shown in Figures 7.21, we expect to get 0° everywhere. This is shown in Table 7.11b. As discussed before, due to the grid size used and the numerical calculation of the normal vector, there is some variation of the angles in Tables 7.11b. If the opposite extreme disturbance is used, we expect angles that are negative or zero. This is shown in Table 7.12.

Table 7.11b: Angle of System Trajectory with Candidate Reachable Set Surface for Control Version 6 with Disturbance that Generated Surface R.

Edge or Surface	Minimum Angle (degrees)	Maximum Angle (degrees)
Interior of CL	-0.00	+0.04
Edge A on CL	-0.00	+0.01
Edge B on CL	-0.00	+0.00
Edge at Tip on CL	-0.00	+0.07
Edge at Base on CL	-0.00	+0.00
Interior of OP	-0.12	+0.75
Edge A on OP	-0.00	+0.62
Edge B' on OP	-0.01	+0.02
Edge C on OP	-0.01	+0.00
Interior BP	-0.00	+0.00
Edge of BP	-0.00	+0.00
Edge C on BP	-0.00	+0.00

Table 7.12: Angle of System Trajectory with Candidate Reachable Set Surface for Control Version 6 with Opposite Disturbance

Edge or Surface	Minimum Angle (degrees)	Maximum Angle (degrees)
Interior of CL	-12.12	-0.00
Edge A on CL	-0.32	-0.00
Edge B on CL	-2.65	-0.02
Edge at Tip on CL	-15.20	-0.01
Edge at Base on CL	-10.39	-0.05
Interior of OP	-89.77	-0.01
Edge A on OP	-69.55	-15.78
Edge B' on OP	-3.60	-0.01
Edge C on OP	-85.87	-12.23
Interior BP	-0.00	+0.00
Edge of BP	-0.00	+0.00
Edge C on BP	-0.00	+0.00

Using the same arguments made for control version 5 in Section 7.1, we claim that the candidate reachable set R in Figure 7.21 is in fact the actual reachable set R^*.

Finally, Table 7.13 summarizes the peak-to-peak gain results we can get from the largest radius of the reachable set for control 6, along with some other relevant data. This control version generates the largest peak-to-peak gain of all the versions we are considering.

Table 7.13: Summary of Extreme values for the Reachable Sets of Control Version 6

Control Version	$\|x_1\|_\infty$	$\|x_2\|_\infty$	$\|x_3\|_\infty$	Peak-to-Peak Gain
6	4.45e-2	4.06e-1	1.51e-2	4.08e-1

7.5 Control Version 2

Control version 2 exhibits two main differences from control version 5. First, the switching plane slope is such that the candidate reachable set is constructed with a sliding mode for the part OP as was done for control versions 3 and 1. In fact, the slope of the switching plane is somewhere between the slopes in those two control versions. The other major difference is that the system equilibrium points exhibit behavior unlike any of the other control laws. This is shown in Figure 7.3. The closed valve equilibrium points present in the semi-active control system are farther from the origin than the open valve equilibrium point. This raises an interesting question. Can we reach these closed valve equilibrium points from the origin?

If we can show that these points are not reachable from the origin, we will have a very interesting case. If we can further show that the system will stop at these equilibrium points when the initial conditions are far away, we will have found a case in

which the reachable set and the attractor set for the system are different. We have not seen this in any of the other control versions so far.

Since the system is radially symmetric, we can look at only the equilibrium points where $x_1>0$ and be assured that our findings will also apply to the rest of the equilibrium points in a radially symmetric fashion. We can in fact limit the region of consideration to the region where $x_3 - x_1 \geq -0.0445$, since the closed valve equilibrium points are all outside this plane. Note that this is the plane that the semi-active system trajectory makes when it starts at the open valve equilibrium point (0.0445, 0, 0). We have been using this plane to construct BP' for all the other control versions. If we can show that the system cannot reach the closed valve equilibrium points farther from the origin than this plane, we can use this plane to construct the candidate reachable set for control version 2 as we have for all other control versions.

As before, the normalized switching planes are the root of determining the semi-active system dynamics. For control version 3 the switching planes are given by

$$B^T P^1 x = 0.0131x_1 - 0.335x_2 + x_3 = 0 \tag{7.23}$$

and

$$x_3 = 0. \tag{7.24}$$

This is the only control version that has a positive coefficient in the first term of the switching plane (7.23). This term is the reason the system has closed valve equilibrium points farther from the origin than the open valve equilibrium points.

We will begin by proposing a candidate reachable set R, constructed as in Section 7.1 with the modification for the sliding surface from control versions 3 and 1. Let us

assume that the closed valve equilibrium points are not in the proposed reachable set and see if we can reach them from R. This is shown in Figure 7.23.

From arguments in 7.1.9, which still hold here, we know that the system cannot escape this candidate reachable set in the region between planes $x_3 - x_1 \geq -0.0445$ and $x_3 - x_1 \geq 0.0445$. Since this is the case, the only way for the system to get out to the closed valve equilibrium points is to move through part of the reachable set candidate that intersects planes $x_3 - x_1 \geq -0.0445$ or $x_3 - x_1 \geq 0.0445$. Thus, we will look at the tip of cone CL and the base of cone CL' as the two local areas where the system could get out to the equilibrium points. Figure 7.24 shows a cross-section of this candidate reachable set at the plane x_1=0. This shows the sliding surface that was used to construct the candidate reachable set.

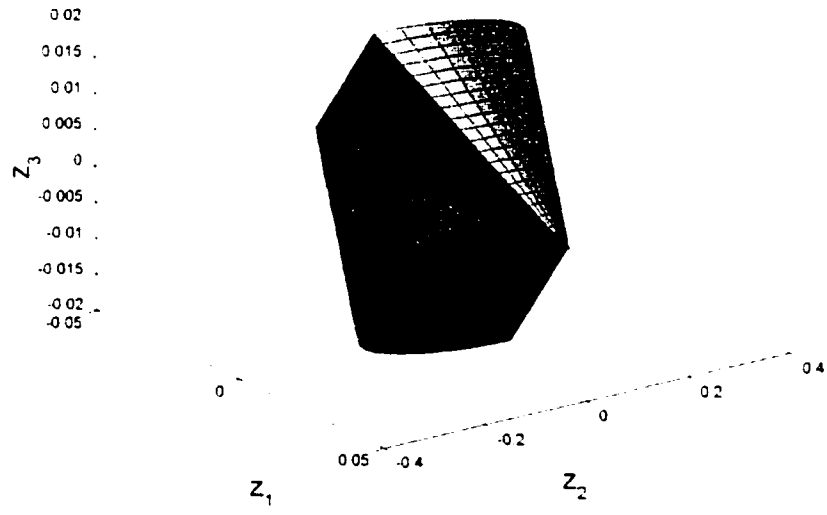

Figure 7.23: Assembled View of the Candidate Reachable Set for the Semi-Active Control Problem with Control Version 2

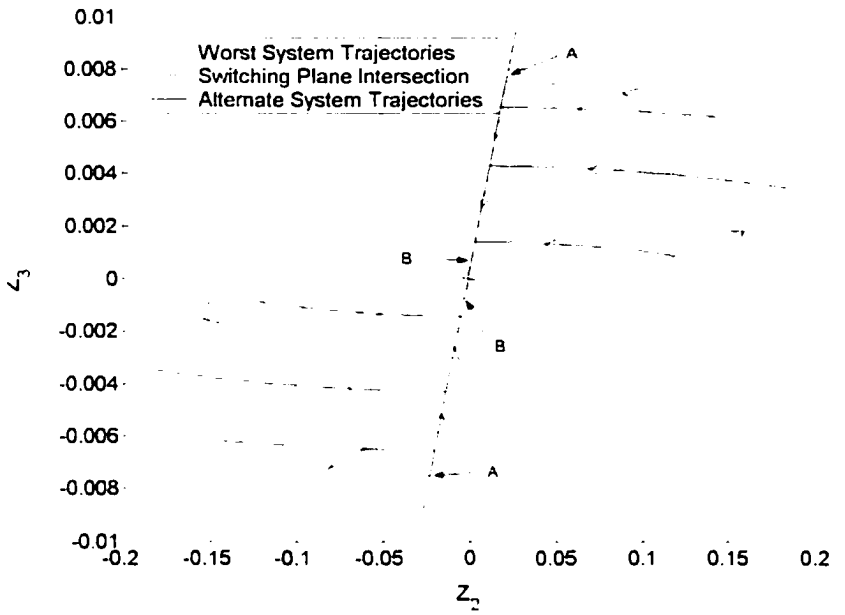

Figure 7.24: Cross-Section of the Candidate Reachable Set for Control Version 2 at the Plane $x_1=0$ (Sliding Mode Between A and B)

The tip of the candidate set in Figure 7.23 is at the open valve equilibrium point. Since we know that we can reach that point from the origin (albeit in infinite time), we will assume that the system can start there and try to get out to the closed valve equilibrium points. The general view of the tip of this candidate reachable set is very similar to that shown in Figure 7.9 for control version 5. Assuming that the system starts anywhere on this tip, the system cannot get farther out in the x_1 direction. This is because for either open or closed dynamics the system equation $\dot{x}_1 = x_2$ holds, and the tip of the candidate reachable set is in region $x_2 \geq 0$ with $x_2 = 0$ at the equilibrium point indicated in Figure 7.9. This means that there is no possibility that the system can escape the reachable set candidate through the tip, as shown in Figure 7.23.

The remainder of the reachable set that intersects the plane $x_3 - x_1 = -0.0445$ is all in region $x_3 \leq 0$. This indicates that we will be dealing with regions X_0^- and X_1^-.

To show that there is no possibility that the system can leave this candidate reachable set through its intersection with plane $x_3 - x_1 = -0.0445$, we will use the plane itself. First, in region X_0^- we know that the closed valve system dynamics are curves on the level sets $x_3 - x_1 = c$, and that the system cannot move between these level curves without going into an open valve region. Thus, there is no way for the system to move off of the level curve $x_3 - x_1 = -0.0445$ in the closed region X_0^-. Finally, we have region X_1^- as the only possible way for the system to get out to the closed valve equilibrium points that are outside plane $x_3 - x_1 = -0.0445$. Fortunately, if we take the normal vector to this plane and check the dot product of that normal with the system dynamics in region X_1^- we get the result

$$\begin{aligned} \dot{V} &= \hat{n} \bullet \dot{x} \\ \dot{V} &= \begin{bmatrix} 1 \\ 0 \\ -1 \end{bmatrix} \bullet \begin{bmatrix} x_2 \\ -224.72x_1 - 4.50x_2 - 2247.20x_3 \\ x_2 - 5000x_3 \end{bmatrix} \\ \dot{V} &= 5000x_3 \end{aligned} \tag{7.25}$$

Since we are considering that region X_1^-, x_3 is always negative, and $\dot{V}$ in (7.25) will also always be negative. This means that the system cannot get past the plane $x_3 - x_1 = -0.0445$ in the X_1^- region. With this, we have covered every possible place locally where the system could possibly try to get out of the candidate reachable set and reach the closed valve equilibrium points. Globally, we know that these are the only possible places for the system to escape R. This means that those equilibrium points are not reachable from the origin and are thus not included in the reachable set. They would, however, be included in the attractor set, but we are not really looking for that.

Tables 7.14 and 7.15 indicate the results from comparing the numerical normal vector and the system trajectories in the case of control version 2. Recall that a negative angle means that the system trajectory is moving into the surface, and a positive angle means that the system is moving out of the surface. If we use the disturbance that generated our candidate reachable set shown in Figures 7.23, we expect to get 0° everywhere. This is shown in Table 7.14. As discussed before, due to the grid size used and the numerical calculation of the normal vector, there is some variation of the angles in Table 7.14. If the opposite extreme disturbance is used, we expect angles that are negative or zero. This is shown in Table 7.15.

Table 7.14: Angle of System Trajectory with Candidate Reachable Set Surface for Control Version 2 with Disturbance that Generated Surface R

Edge or Surface	Minimum Angle (degrees)	Maximum Angle (degrees)
Interior of CL	-0.00	+0.11
Edge A on CL	-0.00	+0.08
Edge B on CL	-0.00	+0.01
Edge at Tip on CL	-0.00	+0.00
Edge at Base on CL	-0.01	+0.00
Interior of OP	-0.8	+0.12
Edge A on OP	-0.3	+0.20
Edge B' on OP	-0.00	+0.03
Edge C on OP	-0.01	+0.04
Interior BP	-0.00	+0.00
Edge of BP	-0.00	+0.00
Edge C on BP	-0.00	+0.00

Table 7.15: Angle of System Trajectory with Candidate Reachable Set Surface for Control Version 2 with Opposite Disturbance

Edge or Surface	Minimum Angle (degrees)	Maximum Angle (degrees)
Interior of CL	-11.51	-0.01
Edge A on CL	-0.34	-0.05
Edge B on CL	-2.04	-0.02
Edge at Tip on CL	-9.32	-0.09
Edge at Base on CL	-21.38	-0.15
Interior of OP	-89.90	-0.01
Edge A on OP	-68.94	-25.66
Edge B' on OP	-5.43	-0.01
Edge C on OP	-46.22	-34.96
Interior BP	-0.00	+0.00
Edge of BP	-0.00	+0.00
Edge C on BP	-0.00	+0.00

Using the same arguments made for control version 5 in Section 7.1, we claim here that the candidate reachable set R in Figure 7.23 is in fact the actual reachable set R^*.

Finally, Table 7.16 summarizes the peak-to-peak gain results we can get from the largest radius of the reachable set for control version 2, along with some other relevant data. Here again, we get the same values as we have for the control versions 5, 4, 3, and 1.

Table 7.16: Summary of Extreme values for the Reachable Sets of Control Version 2

Control Version	$\|z_1\|_\infty$	$\|z_2\|_\infty$	$\|z_3\|_\infty$	Peak-to-Peak Gain
2	4.45e-2	3.75e-1	1.51e-2	3.77e-1

7.6 New Simulation Results

In Chapter 4 we presented simulation results generated using a disturbance law of the form discussed in Section 4.1. These simulation results were used as a lower bound on the system reachable set in the subsequent chapters. Now, in light of the reachable sets found for the 3D semi-active control cases, we can say that those simulations were conservative lower bounds. In this section, we revisit the simulation of the 3D systems using a disturbance sequence that drives the system farther towards the reachable set and again use these simulation values as lower bounds for the system reachable set.

The specific disturbance that we use is based on the sequence that drives the system asymptotically to the open valve equilibrium points. This is described for control version 5 in Section 7.1.5. To actually get all the way to the equilibrium point would take infinite time, which is not realistic for a simulation. We only use 35 cycles of the sequence described in Section 7.1.5 to move the system towards the equilibrium point (0.0445, 0, 0). When we have gone 35 cycles, the system is on the switching plane intersection. At that point we apply a disturbance d=1, and the system follows a trajectory in the closed valve region X_0^- that is close to the base of cone CL' from the reachable set. The simulation will stop when this trajectory gets back to one of the switching planes. This is shown in Figure 7.25 for control version 5.

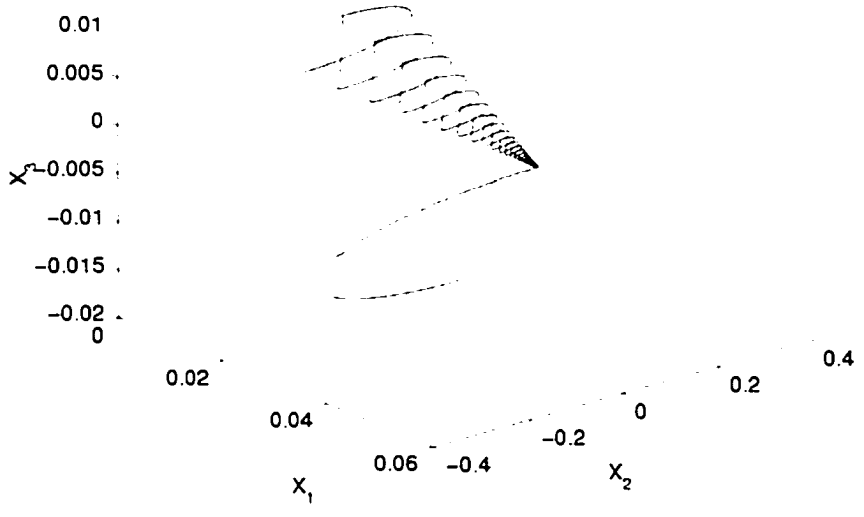

Figure 7.25: Simulated Trajectory for Control Version 5

This procedure is carried out for all 6 control versions and the results are shown in Table 7.17. The time to get to 35 cycles as the system heads out to the equilibrium point is about 2.26 sec. in every case. The values obtained in this length of time are very close to the reachable set maxima.

Table 7.17: New Simulation Values for the 3D Example

Control Version	$\|z_1\|_\infty$	$\|z_2\|_\infty$	$\|z_3\|_\infty$	Maximum Radius
1	4.44e-2	3.75e-1	1.51e-2	3.76e-1
2	4.44e-2	3.75e-1	1.51e-2	3.76e-1
3	4.44e-2	3.75e-1	1.51e-2	3.76e-1
4	4.44e-2	3.75e-1	1.51e-2	3.76e-1
5	4.44e-2	3.75e-1	1.51e-2	3.76e-1
6	4.44e-2	4.05e-1	1.51e-2	4.06e-1

7.7 Summary

The challenge in this chapter was to build reachable sets for the 3D semi-active control system and to show that the candidate reachable sets constructed were in fact the reachable sets. The first part of the chapter outlined the method for constructing the candidate reachable sets based on worst case system trajectories and the system equilibrium points. The points x_1=+/- 0.0445 with x_2=x_3=0 are equilibrium points for both the open and closed valve dynamics. As a result, these points are equilibrium points for all of the 3D control versions. These points are asymptotically reachable from the origin and the points with the maximum radius on the surface (peak-to-peak gain points) are reachable from these equilibrium points. These equilibrium points were instrumental in using the 8-step method to construct the candidate reachable sets for all 6 control laws. Arguments presented make it clear that the candidate reachable sets constructed were in fact the actual reachable sets for the system. Reachable sets were constructed for all 6 control versions presented in Chapter 4 for the 3D semi-active control system.

The most interesting of the control versions was number 2, in which there were some equilibrium points for the semi-active control system not in the set of reachable points from the origin. This means that the reachable set and the attractor set were different in this case. In fact, the attractor set must be larger than the reachable set to encompass the equilibrium points outside. However, since the goal of this dissertation is to find the peak-to-peak gain for semi-active systems, we are really interested only in the reachable sets.

The final section in this chapter revisited the simulation results found for the 3D semi-active system in Chapter 4. Those results were produced with a disturbance that, in

hindsight, did not in fact drive the system very close to the reachable set. A new disturbance was used, and the new simulation results were found to be much closer to the reachable set for all cases. These results were shown in Section 7.6.

When we compared the actual peak-to-peak gains found in this chapter with the estimates from the last three chapters, we can see how conservative those estimates actually were. Figure 7.26 shows this comparison graphically, and Table 7.18 indicates the values. As was expected, the actual peak-to-peak gain value for all of the semi-actively controlled systems was significantly less than the peak-to-peak gain of the open valve system. Interestingly, none of the example problem results from the last three chapters could consistently predict this. Neither did any of the estimation methods predict the lack of variation in actual peak-to-peak gain from control version to control version.

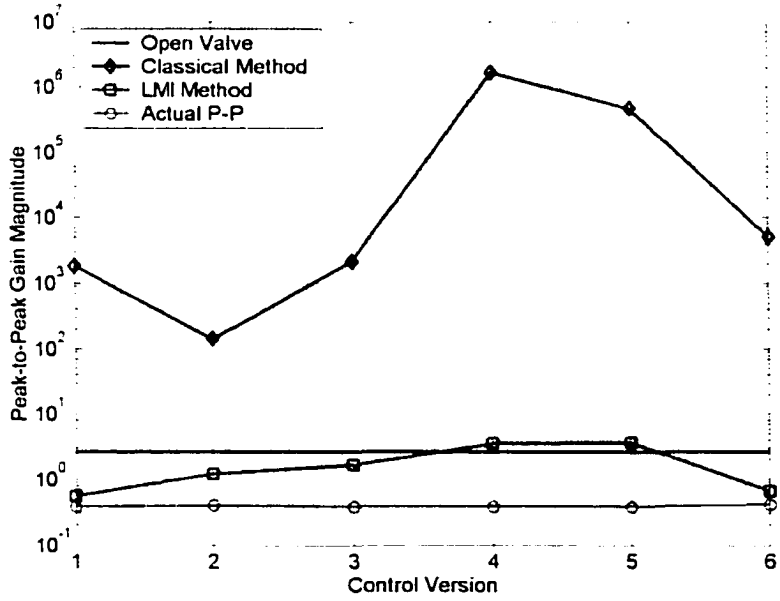

Figure 7.26: Results Summary for the 3D Example

Table 7.18: Results Summary for the 3D Example

Control Version	System 1-Norm	Classical Bounding Method	Best LMI Results (# of regions)	Actual Peak-to-Peak Value
Open Valve	2.59e0	N/A	2.87 (4)	2.59e0
1	N/A	1.85e3	5.45e-1 (24)	3.77e-1
2	N/A	1.40e2	1.19e0 (24)	3.77e-1
3	N/A	2.15e3	1.63e0 (16)	3.77e-1
4	N/A	1.60e6	3.50e0 (24)	3.77e-1
5	N/A	4.55e5	3.57e0 (24)	3.77e-1
6	N/A	4.96e3	6.48e-1 (16)	4.08e-1

With the actual peak-to-peak gain finally known for the 3D example, we can comment on the relative effectiveness of the various control versions. There does not seem to be significant variation in the peak-to-peak gain for the 3D example control versions except in the case of version 6. Thus, we can really only eliminate control version 6 using the peak-to-peak gain information. The final choice of a control version from the remaining 5 versions would have to come down to some performance measure in addition to the peak-to-peak gain. Examples could include the original simulation or some other analytical performance measure based on an energy method.

As mentioned in Chapter 6, this is the first time that the Lyapunov control law from Chapter 2 has been shown to have good L_1 performance. The results from the current chapter indicate that, for the 3D example dynamics, this control law improves the actual peak-to-peak gain of the system 6.5 times over the peak-to-peak gain of the open valve case.

CHAPTER 8

LMI METHOD REVISITED

The surfaces of the reachable sets of Chapter 7 had the quadratic form of a cone surface. In this chapter, we model these surfaces using a quadratic form with quadratic, linear, and constant terms. These models are first constructed by looking at the least square error in position and later with the addition of the least square error in gradient.

Next, we revisit the LMI method and develop a new formulation for the LMI constraints in Chapter 6 based on the quadratic form with constant, linear, and quadratic terms. In order to make the formulation of Chapter 6 a subset of this new formulation, we add a small ε parameter in the $\dot{V} \leq 0$ inequality so that the LMI method has feasible solutions for quadratic models with the linear and constant terms set to zero.

For the quadratic models where the linear and constant terms are not zero, we use one of the constraints in the new LMI formulation to cast doubts on the possibility that the LMI method will be able to exactly "copy" the reachable sets from Chapter 7. However, the new LMI method is still able to find upper bounds on these reachable sets. In fact, the new LMI formulation gives results that are similar to those of Chapter 6.

8.1 Quadratic Modeling

The Lyapunov function is extended to include nonzero constant and linear terms. We will also show how the Lyapunov time derivative changes with this new function.

Throughout this dissertation, continuous, piecewise quadratic Lyapunov functions of the form

$$V_i(x) = x^T P_i x = 1, \quad P_i > 0, \quad x \in X_i, \tag{8.1}$$

where

$$V(x) = V_i(x), \quad x \in X_i, \tag{8.2}$$

have been used to try to model the reachable sets of the semi-active control systems. To extend this quadratic model to include linear and constant terms, the function in (8.1) will be expanded to

$$V_i(x) = x^T P_i x + 2q_i^T x + r_i = 1, \quad V_i > 0, \quad x \in X_i, \tag{8.3}$$

where P_i is a symmetric nxn matrix, q_i is an $nx1$ vector, and r_i is a scalar. This new function will allow much more flexibility in the modeling of the reachable set surfaces in Chapter 7.

For the function (8.3) to be a Lyapunov function (see Appendix II), we must have

$$\dot{V}_i \le 0. \tag{8.4}$$

The interior of the new piecewise Lyapunov function in (8.3) can be differentiated with respect to time to get the following.

$$\dot{V}_i = \nabla V \bullet \dot{x}. \tag{8.5}$$

When this is expanded, and the system equation of the form (2.51) is substituted, (8.5) becomes

$$\dot{V}_i = \left(2x^T P_i + 2q_i^T\right) \bullet \left(A_i x + Dd\right), \tag{8.6}$$

which can be further expanded to

$$\dot{V}_i = 2x^T P_i A_i x + 2x^T P_i D d + 2q_i^T A_i x + 2q_i^T D d. \tag{8.7}$$

If the surface of the reachable set R^* exactly fits functions of the form (8.3), then the time derivative $\dot{V}_i$ should actually be zero everywhere on the surface. We can see that as the surface is scaled, the derivative $\dot{V}_i$ becomes more negative. Thus, if any point on R^* is described by the state/disturbance pair $\left(x^0,\ d^0\right)$, we can scale the estimate for R^* by scaling x^0 by λ. This results in a scaled Lyapunov function of the form

$$V_i\left(\lambda x^0\right) = \lambda^2\left(x^0\right)^T P_i x^0 + 2\lambda q_i^T x^0 + r_i,\quad V_i > 0,\quad x \in X_i, \tag{8.8}$$

which is no longer equal to one. This Lyapunov function has a time derivative

$$\dot{V}_i = 2\lambda^2\left(x^0\right)^T P_i A_i x^0 + 2\lambda\left(\left(x^0\right)^T P_i D d^0 + q_i^T A_i x^0\right) + 2q_i^T D d^0. \tag{8.9}$$

One issue that needs to be addressed is the continuity of the piecewise C^1 Lyapunov functions. To treat continuity in these surfaces, we must add some constraints to the process of finding surfaces that will bound the reachable set. One method for combining all of the requirements and constraints involved is the LMI method. However, we must first fit the reachable set surface from Chapter 7 using the quadratic model with nonzero linear and constant terms.

8.2 Modeling the Reachable Set of Control Version 5 of the 3D Example

In this section, we use a least square error to fit the Lyapunov function model in (8.2-8.3) to the reachable set surface for control version 5 from the 3D example problem covered in the last chapter. First, we model the surface of the reachable set using only a penalty on the position error. This is done with a coarse discretization (6 regions) of the surface and then with a finer discretization (62 regions). The residual from the model is reduced by two orders of magnitude when going from the coarse discretization to the

finer one. Then, we combine the penalty on the position error with the penalty on the gradient error to improve the modeling of the surface curvature. With this new error distribution, we trade an increase in the residual error for a decrease in $\dot{V}_i$ on the surface. Note that there is no constraint that guarantees these models are continuous across region boundaries.

From the work in the last section we have numerical descriptions of the surface of the reachable set for control version 5 that we can use for this work. We can use these data to solve for the components in P_i, q_i, and r_i in the function (8.3) by using a simple least squares method. To show how well the functions estimate the surface, we will use the residual. The residual for the estimated Lyapunov functions can be found by calculating the value

$$\text{residual} = x^T P_i x + 2q_i^T x + r_i - 1 \tag{8.10}$$

with the estimates for P_i, q_i, and r_i found with the least squares method. If the function estimates are perfect, the residual should be equal to zero. Since this will not be the case, the closer to zero the residual is, the better the estimate of the surface.

To start, we will use a single function (8.3) to represent each of the surfaces CL, OP, BP and each of their radially symmetric components. Figure 8.1 shows each of the regions to be estimated by (8.3) outlined in black. Figure 8.2 shows the residual as a color on the surface of the reachable set after the least squares method has been used to find approximate values for P_i, q_i, and r_i in each region. The residual values on Figure 8.2 range from 2.6710e-3 to –6.6592e-4.

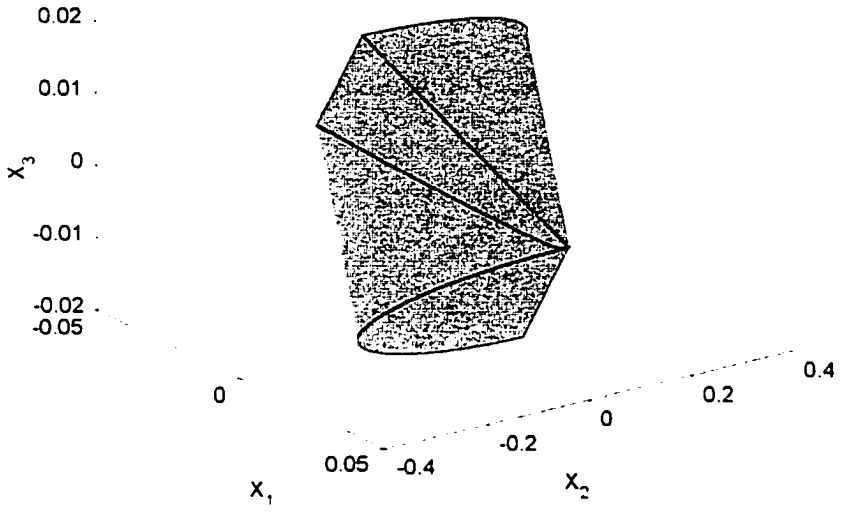

Figure 8.1: Coarse Discretization of Reachable Set for Quadratic Estimation

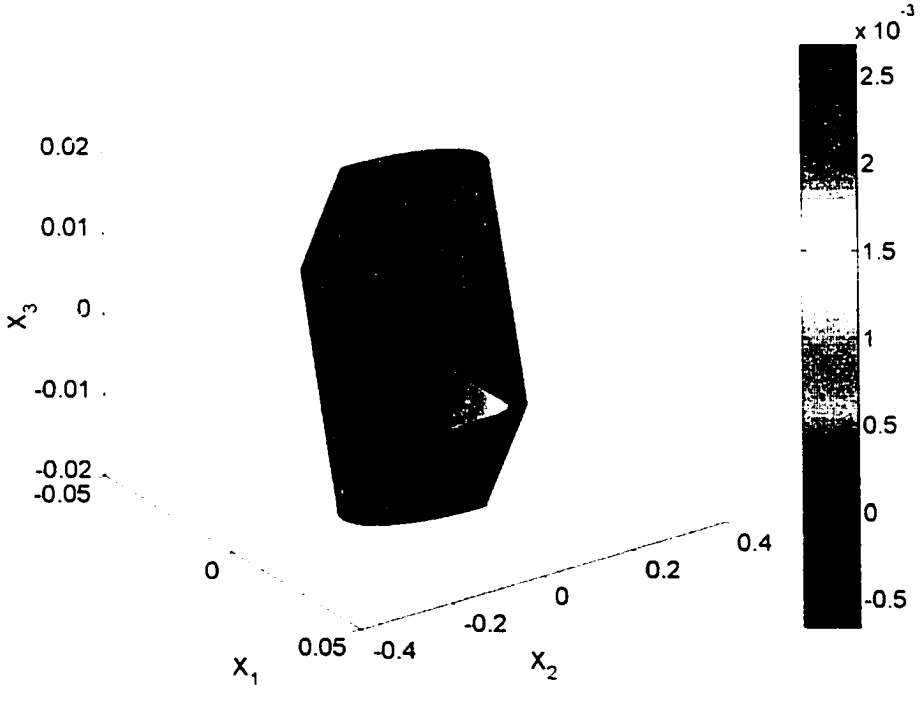

Figure 8.2: Residual Values for Least Squares Quadratic Estimate with Coarse Discretization

One can see that the residual extremes occur where part OP meets part CL' and its radially symmetric intersection. The values of the residual that were closest to zero occurred on plates BP and BP'. The absolute value of these residuals is less than 1e-15. This is expected, since flat plates are easily modeled by functions of the form (8.3).

For illustration, the results from this coarse discretization for region CL are

$$V_{CL}(x) = x^T \begin{bmatrix} 1.00e0 & 1.86e-1 & 1.83e2 \\ 1.86e-1 & 8.81e-1 & 7.53e-1 \\ 1.83e2 & 7.53e-1 & 1.78e3 \end{bmatrix} x + 2 \begin{bmatrix} 1.38e-2 \\ 2.96e-3 \\ 8.10e0 \end{bmatrix}^T x + (1.00e0). \tag{8.11}$$

and for region CL' they are

$$V_{CL'}(x) = x^T \begin{bmatrix} 1.00e0 & 1.86e-1 & 1.83e2 \\ 1.86e-1 & 8.81e-1 & 7.53e-1 \\ 1.83e2 & 7.53e-1 & 1.78e3 \end{bmatrix} x + 2 \begin{bmatrix} -1.38e-2 \\ -2.96e-3 \\ -8.10e0 \end{bmatrix}^T x + (1.00e0). \tag{8.12}$$

Notice that the only differences in the results are the values in q_{CL} and $q_{CL'}$. These values are negative in the CL' case and positive in the CL case. This is expected, since we know that we must have $V(x) = 1$ everywhere on this surface. If we plug $-x$ into the function for V_{CL}, we need to change q_{CL} to $-q_{CL}$ to maintain the function equal to one. Similar behavior is evident in the rest of the region solutions as follows.

$$V_{OP}(x) = x^T \begin{bmatrix} 1.00e0 & 1.24e0 & -6.00e0 \\ 1.24e0 & -1.09e0 & -8.34e1 \\ -6.00e0 & -8.34e1 & 7.60e1 \end{bmatrix} x + 2 \begin{bmatrix} -3.82e-3 \\ -6.77e-2 \\ 8.21e-2 \end{bmatrix}^T x + (1.00e0) \tag{8.13}$$

$$V_{OP'}(x) = x^T \begin{bmatrix} 1.00e0 & 1.24e0 & -6.00e0 \\ 1.24e0 & -1.09e0 & -8.34e1 \\ -6.00e0 & -8.34e1 & 7.60e1 \end{bmatrix} x + 2 \begin{bmatrix} 3.82e-3 \\ 6.77e-2 \\ -8.21e-2 \end{bmatrix}^T x + (1.00e0) \tag{8.14}$$

$$V_{HI'}(x) = x^T \begin{bmatrix} 1.00e0 & 0.00e0 & -4.00e-1 \\ 0.00e0 & 0.00e0 & 0.00e0 \\ -4.00e-1 & 0.00e0 & -2.00e-1 \end{bmatrix} x + 2 \begin{bmatrix} 1.34e-2 \\ 0.00e0 \\ 1.33e-2 \end{bmatrix}^T x + (1.00e0) \qquad (8.15)$$

$$V_{HI''}(x) = x^T \begin{bmatrix} 1.00e0 & 0.00e0 & -4.00e-1 \\ 0.00e0 & 0.00e0 & 0.00e0 \\ -4.00e-1 & 0.00e0 & -2.00e-1 \end{bmatrix} x + 2 \begin{bmatrix} -1.34e-2 \\ 0.00e0 \\ -1.33e-2 \end{bmatrix}^T x + (1.00e0) \qquad (8.16)$$

Notice that all of these models exhibit the radially symmetric property of the reachable sets.

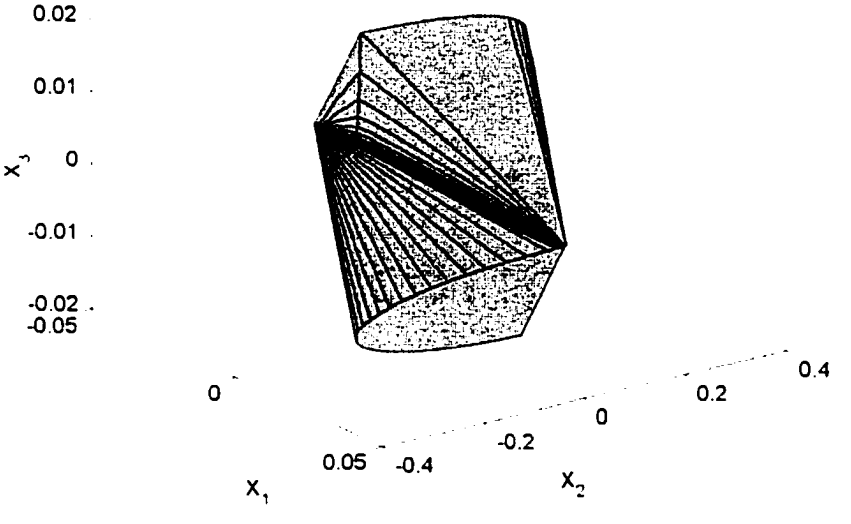

Figure 8.3: Finer Discretization of Reachable Set for Quadratic Estimation

To reduce the residual from the estimation, we next divide each of the regions in Figure 8.1 further, with most size refinement occurring at the intersection where the highest residuals are observed in Figure 8.2. The finer discretization is shown in Figure 8.3. Regions CL and CL' are each divided into many smaller regions, with the final size of these regions dependent on the residual value from Figure 8.2. Parts OP and OP' are

both split in two directions, as can be seen in Figure 8.3. Since parts BP and BP' essentially have a zero residual, these parts are not subdivided further.

The residual results are shown in Figure 8.4 for this finer discretization of the surface. It is somewhat hard to see, but the worst area of the residual is still the region just at the intersection of parts CL' and OP and the radially symmetric intersection. The values of the residual in this figure range from 1.8953e-5 to –6.3012e-5. These values are a vast improvement over those of the coarser discretization previously shown.

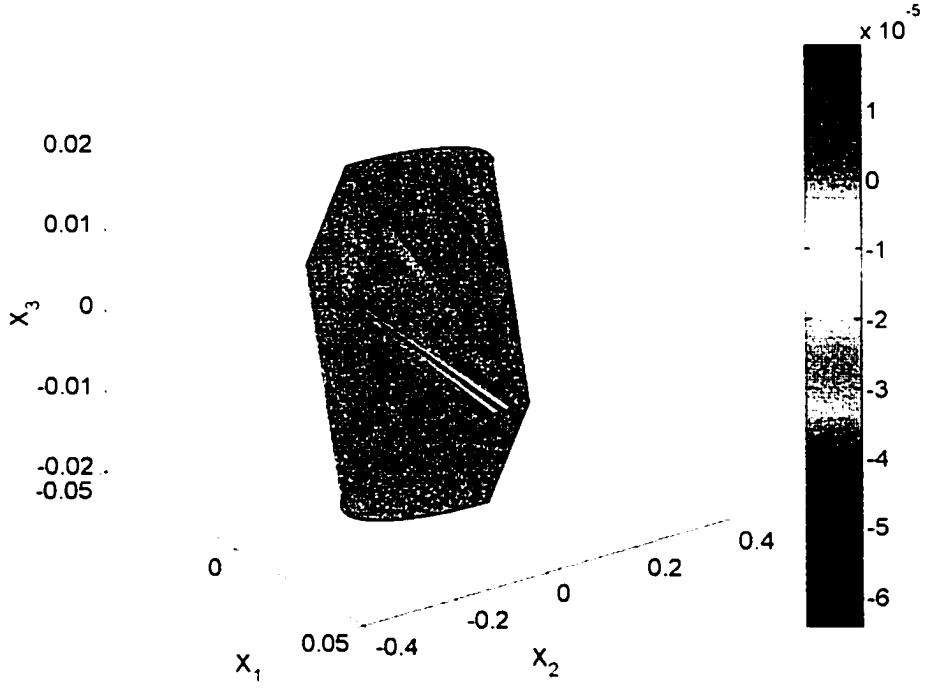

Figure 8.4: Residual Values for Least Squares Quadratic Estimate with Refined Discretization

The value of $\dot{V}$ is calculated on the surface of the refined discretization model. These results are shown in Figure 8.5. The values on the plot range from –136 to 77.8. These values of the Lyapunov derivative are not very close to zero, as expected.

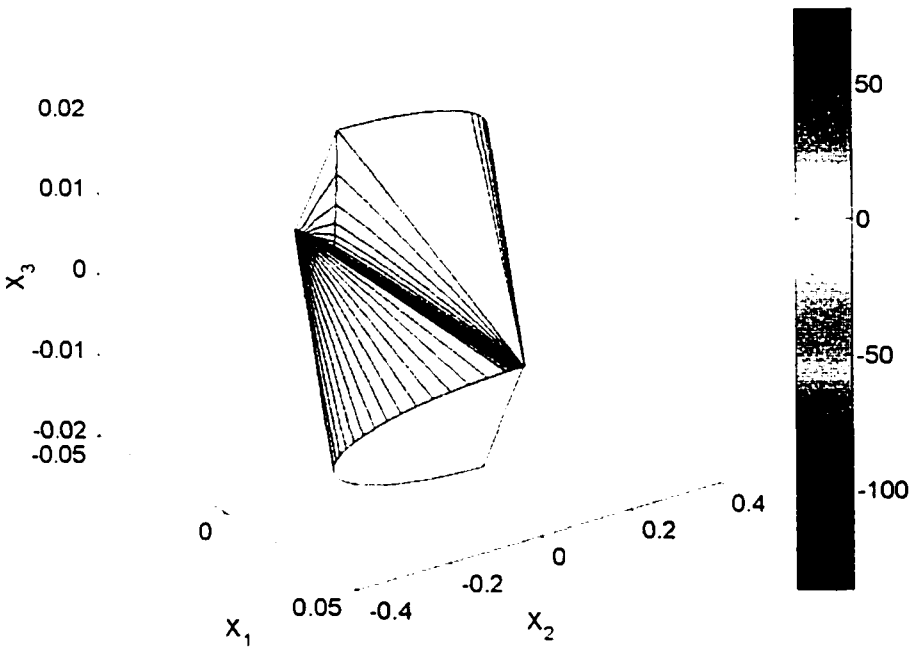

Figure 8.5: Lyapunov Derivative for Least Squares Quadratic Estimate with Refined Discretization (min –1.3601e2 max 7.7762e1)

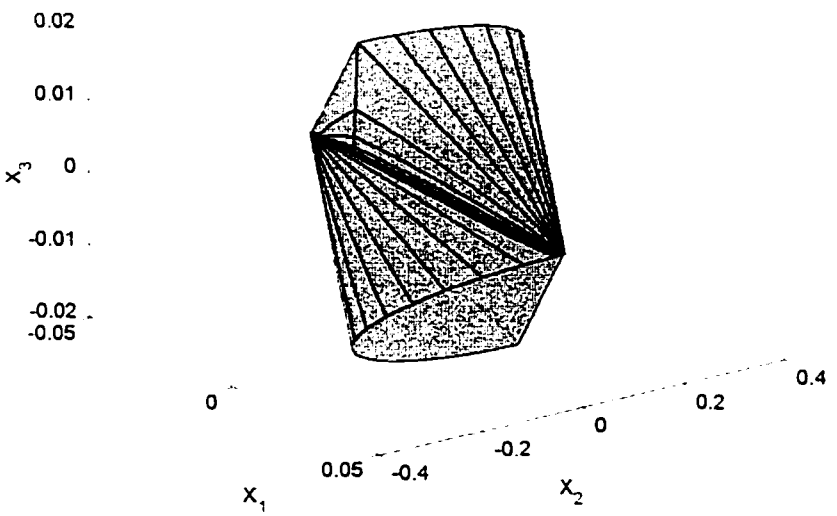

Figure 8.6: Discretization of Reachable Set for Quadratic Estimation with Gradient Error Included

Since the Lyapunov derivative $\dot{V}_i$ is not penalized in Figure 8.5, a new least squares fit is found for the reachable set that includes both the position error and an error on the surface gradient. This is done to investigate how an improvement in the gradient approximation will affect the residual for the modeled surface. Figure 8.6 shows the discretization used for this approximation. The discretization is uniform over each of the pieces, rather than skewed as in Figure 8.3.

The residual for this approximation is shown in Figure 8.7, and the Lyapunov derivative is shown in Figure 8.8. We can see that by including the error in the gradient as one of the errors in the least squares approximation, we do indeed reduce the range of the Lyapunov derivative over the surface. This comes at the price of a significant increase in the residual values over the surface.

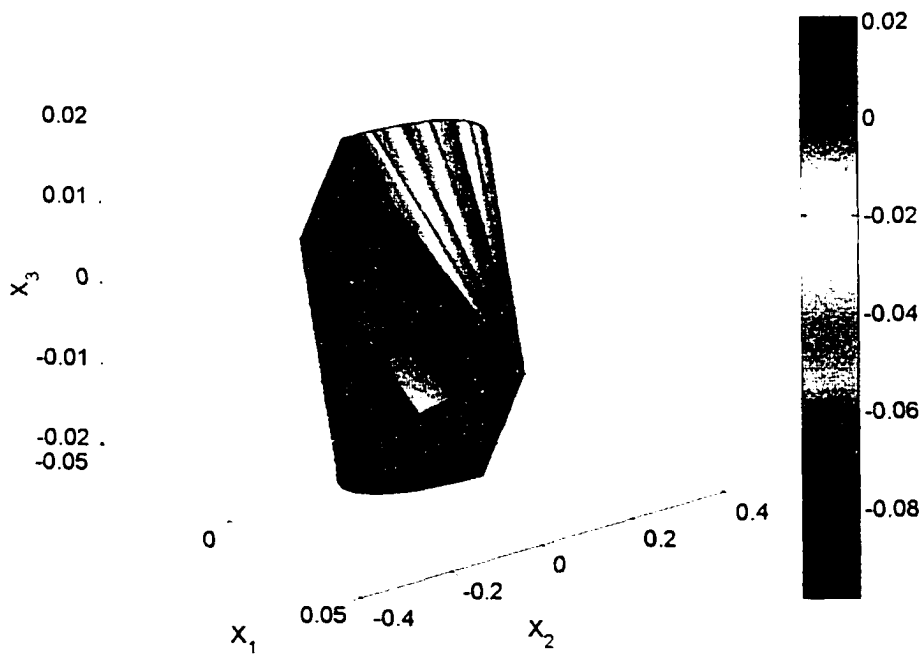

Figure 8.7: Residual Values for Least Squares Quadratic Estimate with Gradient Error Included

The results in this section indicate that the approximation of the reachable set for model (8.3) improves with a finer mesh. They also indicate that, with the addition of an error penalty on the surface gradient, there is a tradeoff between position estimate and gradient estimate for these reachable set surfaces for model (8.3).

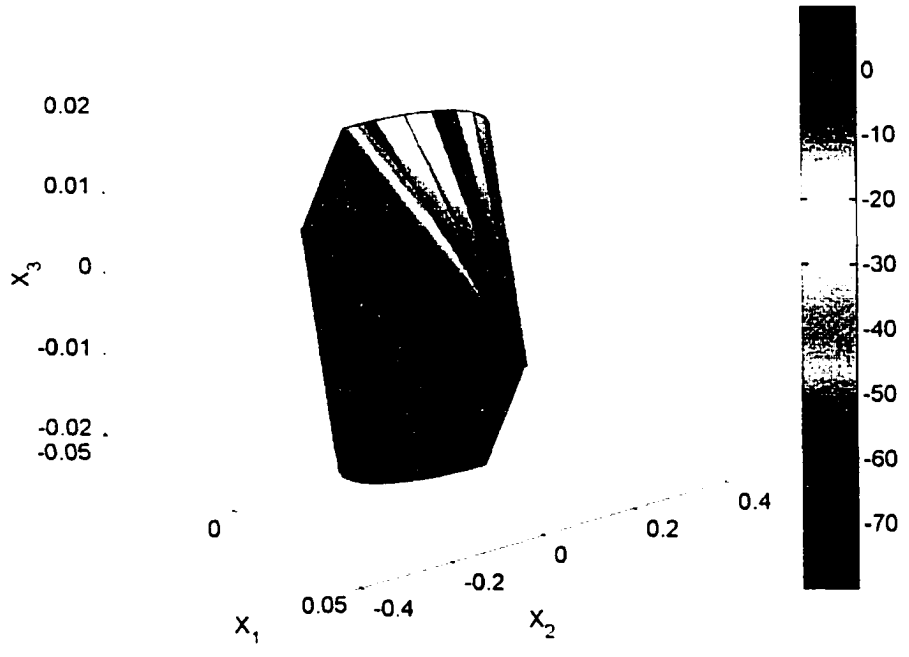

Figure 8.8: Lyapunov Derivative for Least Squares Quadratic Estimate with Gradient Error Included (min –1.3601e2 max 7.7762e1)

The next step is to apply the LMI method in an attempt to find a tight upper bound on the reachable set that is continuous across the control boundaries (7.2) and (7.3) for the 3D example problems. This will be developed in the next section.

8.3 Extension of LMI Method Formulated in Chapter 6

In Chapter 6 the LMI formulation was based on quadratic models with no linear or constant terms. Since the surfaces of the reachable set are quadratic-like models with

nonzero linear and constant terms, we extend the LMI formulation to such models. In addition, we add a small positive ε parameter in the new formulation so that quadratic models with zero linear and constant terms are feasible. In this way, the LMI formulation of Chapter 6 is a subset of the new formulation. Without the small ε parameter, the Chapter 6 solutions are not feasible for this new formulation.

Recall from the end of Section 6.3 that we can in fact expand the LMI to incorporate quadratic functions with nonzero linear and constant terms. This is done by expanding the state vector to $\bar{x} = [x \quad 1]^T$ and rewriting all of the LMI arguments with this new state vector (Johansson and Rantzer, 1998 and 2000) (Hassibi and Boyd, 1998). Using this new state vector we can write the Lyapunov function (8.3) as

$$V_i(x) = \begin{bmatrix} x \\ 1 \end{bmatrix}^T \begin{bmatrix} P_i & q_i \\ q_i^T & r_i \end{bmatrix} \begin{bmatrix} x \\ 1 \end{bmatrix} = \bar{x}^T \bar{P} \bar{x} . \tag{8.17}$$

Paralleling the development in Section 6.3, we begin by defining the regions of the control law in the form

$$\bar{E}\bar{x} = \begin{bmatrix} E & e \end{bmatrix} \begin{bmatrix} x \\ 1 \end{bmatrix} \geq 0, \quad x \in X , \tag{8.18}$$

where X is defined as in Chapter 6. We also need to define the relation that holds on the boundaries between regions as follows.

$$\bar{F}_1 x = \begin{bmatrix} F_1 & f_1 \end{bmatrix} \begin{bmatrix} x \\ 1 \end{bmatrix} = \begin{bmatrix} F_2 & f_2 \end{bmatrix} \begin{bmatrix} x \\ 1 \end{bmatrix} = \bar{F}_2 x, \quad x \in X_1 \cap X_2 . \tag{8.19}$$

Then, for some symmetric matrix $\bar{T}$, a piecewise quadratic Lyapunov function consisting of $\bar{P}_1$ and $\bar{P}_2$ in the regions X_1 and X_2 respectively can be written as

$$\bar{P}_j = \bar{F}_j^T \bar{T} \bar{F}_j , \quad j = 1,2 . \tag{8.20}$$

Thus, as in Chapter 6, we have collected all the variables in one matrix $\bar{T}$.

With these preliminaries, the parallel to Proposition 6.7 can be presented. There is essentially no change in the form, but the state vector has been augmented as suggested above. Again, we are making extensive use of the *S*-procedure from Chapter 6 to combine the inequality constraints with region constraints. It introduces conservativeness to the problem, but this is unavoidable.

Proposition 8.1 (Piecewise solution for the reachable set with unit peak input – expanded)

Suppose we have matrices $\bar{E}_j$ and $\bar{F}_j$ that satisfy (8.18) and (8.19) respectively. If there exist symmetric matrices $\bar{T}$, $\bar{U}_j$, and $\bar{W}_j$ such that $\bar{U}_j$ and $\bar{W}_j$ have nonnegative entries, and $\alpha_j \geq 0$ such that

$$\begin{aligned}
&\bar{P}_j = \bar{F}_j^T \bar{T} \bar{F}_j \\
&\begin{bmatrix} \bar{x} \\ d \end{bmatrix}^T \begin{bmatrix} \bar{A}_j^T \bar{P}_j + \bar{P}_j \bar{A}_j + \alpha_j \bar{P}_j + \bar{E}_j^T \bar{U}_j \bar{E}_j & \bar{P}_j \bar{D} \\ \bar{D}^T \bar{P}_j & -\alpha_j I \end{bmatrix} \begin{bmatrix} \bar{x} \\ d \end{bmatrix} \leq 0, \\
&\bar{x}^T \left(\bar{P}_j - \bar{E}_j^T \bar{W}_j \bar{E}_j \right) \bar{x} > 0
\end{aligned} \tag{8.21}$$

where

$$\bar{A}_j = \begin{bmatrix} A_j & 0 \\ 0 & 0 \end{bmatrix}$$
$$\bar{D} = \begin{bmatrix} D & 0 \end{bmatrix}^T$$

for all j, then the piecewise continuous boundary defined by $\bar{P}_j$ in each region, X_j bounds the reachable set for the system (3.29) with a unit peak input. The proof here parallels the proof for Proposition 6.7.

If we substitute the matrices from (8.17) thru (8.19) into (8.21) we can expand the inequalities to

$$\begin{bmatrix} x \\ 1 \\ d \end{bmatrix}^T \begin{bmatrix} A_i^T P_i + P_i A_i + \alpha_i P_i + E_i^T U E_i & A_i q_i + \alpha_i q_i + E_i^T U e_i & P_i D \\ q_i^T A_i + \alpha q_i^T + e_i^T U E_i & \alpha r_i + e_i^T U e_i & q_i^T D \\ D^T P_i & D^T q_i & -\alpha_i I \end{bmatrix} \begin{bmatrix} x \\ 1 \\ d \end{bmatrix} \le 0 \quad (8.22)$$

and

$$\begin{bmatrix} x \\ 1 \end{bmatrix}^T \begin{bmatrix} P_i - E_i^T W E_i & q_i - E_i^T W e_i \\ q_i^T - e_i^T W E_i & r_i - e_i^T W e_i \end{bmatrix} \begin{bmatrix} x \\ 1 \end{bmatrix} > 0. \quad (8.23)$$

To see if the formulation in Chapter 6 is a subset of these LMIs, we need to set e_i and f_i to zero. To show this, we will look at the expanded versions of the LMIs shown in (8.22) and (8.23). These now can be reduced to

$$\begin{bmatrix} x \\ 1 \\ d \end{bmatrix}^T \begin{bmatrix} A_i^T P_i + P_i A_i + \alpha_i P_i + E_i^T U E_i & A_i q_i + \alpha_i q_i & P_i D \\ q_i^T A_i + \alpha q_i^T & \alpha r_i & q_i^T D \\ D^T P_i & D^T q_i & -\alpha_i I \end{bmatrix} \begin{bmatrix} x \\ 1 \\ d \end{bmatrix} \le 0 \quad (8.24)$$

and

$$\begin{bmatrix} x \\ 1 \end{bmatrix}^T \begin{bmatrix} P_i - E_i^T W E_i & q_i \\ q_i^T & r_i \end{bmatrix} \begin{bmatrix} x \\ 1 \end{bmatrix} > 0. \quad (8.25)$$

One of the limitations of the LMI Control Toolbox for Matlab is that it can only treat strict inequalities. This is a limitation when the only solution to the LMI problem involves a positive or negative semi-definite solution rather than a positive or negative definite solution. When we use the reduced LMIs in (8.24) and (8.25), and the LMI problem in Proposition 8.1 with Proposition 6.8, and the minimization problem in Proposition 6.9, we find that these problems are not feasible with the Matlab toolbox. The method tries to generate a negative semi-definite LMI in (8.24) and a positive semi-definite LMI in (8.25). The solution essentially tries to sets q_i and r_i in $\bar{P}$ to zero, which means it is trying to go toward the solution forms of Chapter 6, where only a second

order term was present in the Lyapunov function. If q_i is zero, we would need $r_i<0$ to satisfy the strict version of the $\dot{V}$ inequality (8.24) and $r_i>0$ to satisfy the V inequality (8.25).

If we let both q_i and r_i go to zero the problem cannot be solved by the Matlab toolbox. This can be seen in the following inequalities. Setting q_i and r_i to zero and rewriting (8.24) and (8.25) gives

$$\begin{bmatrix} x \\ 1 \\ d \end{bmatrix}^T \begin{bmatrix} A_i^T P_i + P_i A_i + \alpha_i P_i + E_i^T U E_i & 0 & P_i D \\ 0 & 0 & 0 \\ D^T P_i & 0 & -\alpha_i I \end{bmatrix} \begin{bmatrix} x \\ 1 \\ d \end{bmatrix} \le 0 \tag{8.26}$$

and

$$\begin{bmatrix} x \\ 1 \end{bmatrix}^T \begin{bmatrix} P_i - E_i^T W E_i & 0 \\ 0 & 0 \end{bmatrix} \begin{bmatrix} x \\ 1 \end{bmatrix} > 0. \tag{8.27}$$

Since the Matlab toolbox requires strict inequalities, we can see that neither of the inequalities in (8.26) and (8.27) can be solved. They both will have at least one zero eigenvalue. If we remove the zero rows and columns from these inequalities we reduce the problem back to the one in Chapter 6.

In an effort to achieve a feasible solution using the new formulation a small ε is introduced into the $\dot{V}$ inequality of the LMI (8.24). The LMI in equation (8.24) now becomes

$$\begin{bmatrix} x \\ 1 \\ d \end{bmatrix}^T \begin{bmatrix} A_i^T P_i + P_i A_i + \alpha_i P_i + E_i^T U E_i & A_i q_i + \alpha_i q_i & P_i D \\ q_i^T A_i + \alpha q_i^T & \alpha r_i - \varepsilon & q_i^T D \\ D^T P_i & D^T q_i & -\alpha_i I \end{bmatrix} \begin{bmatrix} x \\ 1 \\ d \end{bmatrix} \le 0. \tag{8.28}$$

This is equivalent to changing equation (8.4) to

$$\dot{V}_i \le \varepsilon. \tag{8.29}$$

which will approach equation (8.4) as $\varepsilon \to 0$. With this slight modification, the LMI formulation in Chapter 6 is now a true subset of the expanded formulation.

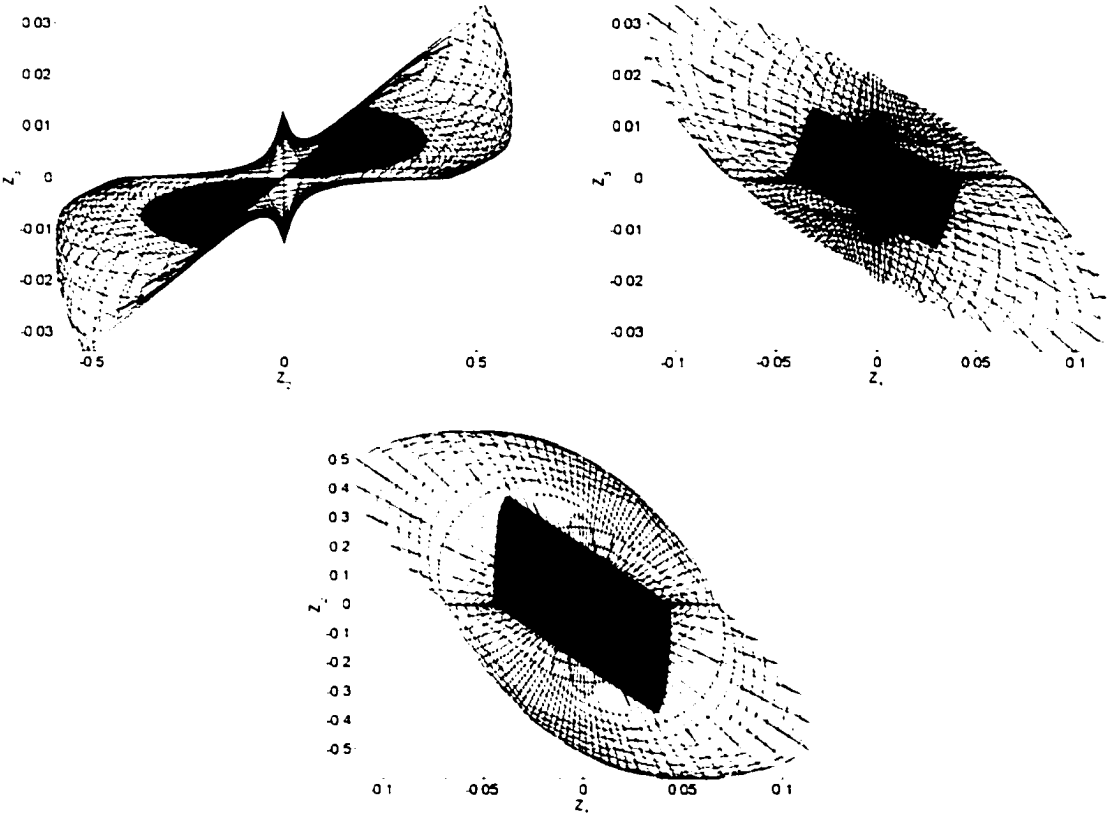

Figure 8.9: Three Views of the Comparison Between the Reachable Set from Chapter 7 (Red) and LMI Solution from Chapter 6 (Black Mesh) for the 3D Example with Control Version 1

For reference, the difference between the reachable set in Chapter 7 and the LMI solutions from Chapter 6 is illustrated in Figure 8.9. It shows the reachable set solution for the 3D example with control version 1 and the best LMI solution for the same problem from Chapter 6. As discussed in Chapter 6, the LMI solution is somewhat conservative. We can also see that the shape of the LMI solution does not conform to the

shape of the reachable set solution very well. The LMI is, however, able to match the concave nature of the reachable set.

8.4 Can the LMI Method Provide a Tight Fit to the Reachable Set for Control Version 5?

A key constraint of the LMI method is that the matrix $\bar{P}_j - \bar{E}_j \bar{W}_j \bar{E}_j > 0$ be positive definite for a matrix W_j, whose terms are all positive. In this section, we show that the LMI method does not provide a tight fit to the reachable sets of Chapter 7 for a number of fine meshes. For smaller and smaller meshes of the reachable set surface, we show that there is always a large negative eigenvalue present in the matrix $\bar{P}_j - \bar{E}_j \bar{W}_j \bar{E}_j > 0$. We believe that this could be due to a concave curvature intrinsic property of the reachable set surface.

The matrix $\bar{P}_j$ will come directly from the least squares models found in the last section. The boundary descriptions $\bar{E}_j$ will also come from the discretization used to generate the models in the last section. With these matrices, we can see if the inequality $\bar{P}_j - \bar{E}_j \bar{W}_j \bar{E}_j > 0$ has any chance of being satisfied. This will tell us if the LMI could give tight results. The results for the coarse model shown in Figure 8.1 are shown in Table 8.1. For each of the regions CL, OP, and BP, we show the minimum eigenvalue for the coarse model generated in the last section. The next column shows the best result that can be found for the minimum eigenvalue of the matrix $\bar{P}_j - \bar{E}_j \bar{W}_j \bar{E}_j$. For the LMI in (8.21) to have a solution, we know that the minimum eigenvalue of the matrix $\bar{P}_j - \bar{E}_j \bar{W}_j \bar{E}_j$ must be positive so that the LMI $\bar{P}_j - \bar{E}_j \bar{W}_j \bar{E}_j > 0$ is true. Table 8.2 shows

the same results for the finer discretization shown in Figure 8.3, and Table 8.3 shows this for the models where the gradient error was also used (Figure 8.6). For reference, the number of divisions used in each region is also shown in Tables 8.1 to 8.3. Again, we are only showing the minimum eigenvalues over all models for any piece of the region.

Table 8.1: Results for Feasibility of $\bar{P}_l - \bar{E}_l\bar{W}_l\bar{E}_l > 0$ for Coarse Model

Region	Min Eigenvalue for $\bar{P}_l$	Min Eigenvalue for $\bar{P}_l - \bar{E}_l\bar{W}_l\bar{E}_l$	Number of Divisions
CL	-17.68	-0.1459	1
OP	-54.50	-0.00198	1
BP	0.00	0.00	1

Table 8.2: Results for Feasibility of $\bar{P}_l - \bar{E}_l\bar{W}_l\bar{E}_l > 0$ for Finer Model

Region	Min Eigenvalue for $\bar{P}_l$	Min Eigenvalue for $\bar{P}_l - \bar{E}_l\bar{W}_l\bar{E}_l$	Number of Divisions
CL	-0.148	-0.000853	20
OP	-2571700	-819910	20
BP	0.00	0.00	1

Table 8.3: Results for Feasibility of $\bar{P}_l - \bar{E}_l\bar{W}_l\bar{E}_l > 0$ for Model with Gradient Error

Region	Min Eigenvalue for $\bar{P}_l$	Min Eigenvalue for $\bar{P}_l - \bar{E}_l\bar{W}_l\bar{E}_l$	Number of Divisions
CL	-2010	-723	15
OP	-1316	-493	20
BP	0.00	0.00	1

Finally, to see if even smaller regions will help us get $\bar{P}_l - \bar{E}_l\bar{W}_l\bar{E}_l > 0$, the discretization for part of region OP was discretized even further. Figure 8.10 shows the whole surface with part of surface OP showing the finest discretization we have tried. The part of the surface that was discretized is indicated in red. Least square models with

the gradient error and position error were found for each of these small regions, and the minimum eigenvalues were calculated for $\bar{P}_j$. Then, the minimum eigenvalues attainable for $\bar{P}_j - \bar{E}_j \bar{W}_j \bar{E}_j$ were found. Recall that $\bar{W}_j$ is a variable matrix, but all the terms in this matrix must be positive. The results for this finest discretization of surface OP are shown in Table 8.4.

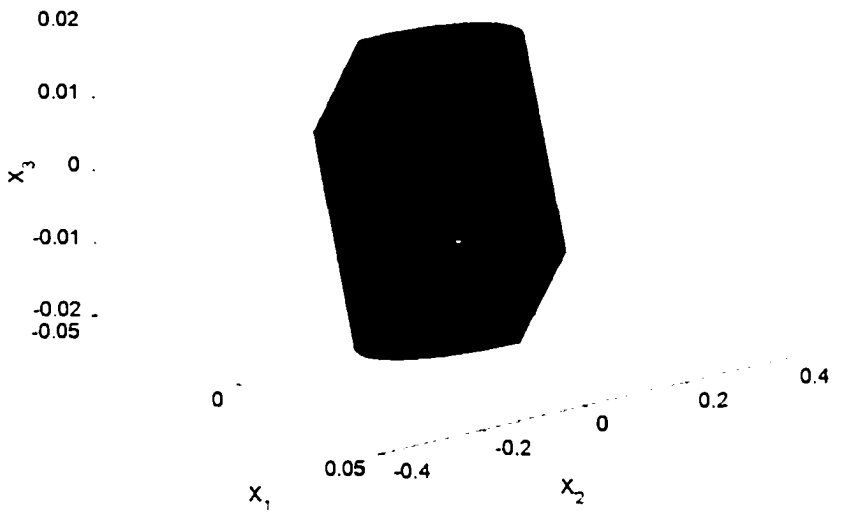

Figure 8.10: Finest Discretization of the OP Region

Table 8.4: Results for Feasibility of $\bar{P}_j - \bar{E}_j \bar{W}_j \bar{E}_j > 0$ for Finest Discretization of OP Region

Min Eigenvalue for $\bar{P}_j$	Min Eigenvalue for $\bar{P}_j - \bar{E}_j \bar{W}_j \bar{E}_j$	Number of Divisions
-534.9	-228.4	50

Based on the above results, we have doubts that the LMI method is going to find a bounding surface that exactly copies the reachable set. This is because a very tight fit would have the form of the models found from the least square modeling in the previous

section. Since any tight fit would have this form, and the inequality $\bar{P}_j - \bar{E}_j \bar{W}_j \bar{E}_j > 0$ cannot be satisfied on these surfaces, we believe that the LMI will never be able to construct a bounding surface that exactly copies the reachable set surface as do the models in the last section. This conclusion is reached since it appears that the OP surface has an intrinsic negative curvature that the term $\bar{E}_j \bar{W}_j \bar{E}_j$ cannot overcome with smaller and smaller mesh sizes.

8.5 Solution of the Expanded LMI Problem

The new LMI method formulation with the small ε parameter has feasible solutions not unlike those of Chapter 6 for 4 regions. As we go to a large number of regions, we see that the new model continues to find feasible solutions that are near the solutions of Chapter 6. The solutions are slightly smaller, as expected, since we are now solving for the region outside of which $\dot{V}(x) < \varepsilon$ rather than $\dot{V}(x) < 0$. The solutions set q_i to zero and r_i to some positive value <ε in every region, regardless of the number of regions.

To apply the expanded LMI we first look at the simplest case where the regions X_i are defined only by the control law for the 3D example with control version 5. This means that we have 4 regions represented, as explained in Chapter 6. Since these 4 regions are defined by planes that go through the origin, we know that the vectors e_i and f_i are zero. Some of the terms in (8.21) are cancelled, and the LMIs reduce to (8.24). In their paper, Johansson and Rantzer (1998) indicated that this is in fact the case when the dynamics are not piecewise affine. Since we are using piecewise linear dynamics, we have not used any region boundaries that would give e_i and f_i non-zero values. We will

also treat the case from Chapter 6 where 24 regions were used. As in the 4 region case, the planes defining the regions all go through the origin, so e_i and f_i will be identically zero. The best solutions found for the six control versions of the 3D example are shown in Table 8.5, along with the ε used. Table 8.5 also shows the results of using this process for the case from Chapter 6 with 24 regions.

Table 8.5: Extended LMI Results for 3D Example

Control Version	ε	Extended LMI Maximum Radius 4 Partitions	Extended LMI Maximum Radius 24 Partitions	LMI Results from Chapter 6 24 Partitions
1	1e-6	1.4606	0.8263	0.86
1	1e-8	1.4616	0.8266	
1	1e-10	1.4608	0.8270	
1	1e-12	1.4622	0.8319	
2	1e-6	4.2387	3.3424	3.33
2	1e-8	4.2398	3.3491	
2	1e-10	4.2412	3.3517	
2	1e-12	4.2410	3.3623	
3	1e-6	4.5399	3.6326	3.64
3	1e-8	4.5396	3.6325	
3	1e-10	4.5400	3.6326	
3	1e-12	4.5408	3.6421	
4	1e-6	7.1689	6.5859	6.59
4	1e-8	7.1712	6.5851	
4	1e-10	7.1684	6.5853	
4	1e-12	7.1681	6.5872	
5	1e-6	7.1799	6.5864	6.59
5	1e-8	7.1773	6.5876	
5	1e-10	7.1820	6.5863	
5	1e-12	7.1830	6.5871	
6	1e-6	3.6386	2.6761	2.70
6	1e-8	3.6344	2.6792	
6	1e-10	3.6344	2.6835	
6	1e-12	3.6371	2.6847	

Notice that these results are the same or slightly smaller than the results for the LMI problem in Chapter 6 with 4 regions and 24 regions, as reported in Table 6.5. We

can conclude that the LMI problem solution wants to move towards the solutions from Chapter 6. In other words, the extended LMI problem indicates that the addition of the linear and constant terms in the Lyapunov function do not significantly improve the LMI results of Chapter 6.

To verify that the small ε does not affect the solutions significantly, we looked at the 24 partition result with $\varepsilon = 1e-8$ for control version 1. The maximum value of $\dot{V}$ on this surface is calculated to be 6.66e-9. Using the scaling in equation (8.9) we were able to bring this maximum down to zero with a scaling of $\lambda = 1.0000134$. Recall from Section 8.1 that this scales the radius of the state vector. This is equivalent to scaling the radius of the state vector so we can directly scale the results in Table 8.5. The value for control version 1 with $\varepsilon = 1e-8$ does not change to the significant digits reported since $0.8266\lambda = 0.8266 \times 1.0000134 = 0.8266$.

8.6 Conclusions

In this chapter we used quadratic models that included quadratic, linear and constant terms to model the surface of the reachable sets from Chapter 7. These models were fit to the surfaces using a least square error for the position and for the surface gradient. The residual and $\dot{V}$ were shown on the surface of each of these models.

An extended LMI formulation based on the work in Chapter 6 was developed that included the quadratic Lyapunov terms from Chapter 6 as well as nonzero linear and constant terms. A small ε was added to the formulation to ensure that the LMI formulation in Chapter 6 was a subset of the new formulation, essentially changing $\dot{V} < 0$ to $\dot{V} < \varepsilon$.

We showed that the LMI method may not be able to exactly copy the surface of the reachable sets from Chapter 7. This was shown by examining the positive definite criterion of the Lyapunov function. There was always a negative eigenvalue associated, regardless of the mesh size used to discretize the surface.

The upper bounds on the reachable set that are generated by this new LMI formulation resulted in values close to those found in Chapter 6. The solutions of the new formulation set the linear term in the Lyapunov function to zero and the constant term to a small value less than ε. In some cases the results here were even slightly better than those in Chapter 6 (4% improvement in the case of control version 1). Even with this improvement we can see from the results in Chapter 6 and those in this chapter that the largest improvement in the bounds can be achieved by increasing the region discretization rather than by adding nonzero linear and constant terms.

CHAPTER 9

APPLICATION OF MICRO-ELECTRO-MECHANICAL SYSTEM (MEMS) SENSORS TO SEMI-ACTIVE SYSTEMS

Recently, advances in MEMS sensors have led to reliable, accurate, small sensors that are starting to be seen in many industrial applications. Because they are becoming more widely used, sensors based on MEMS technology are also becoming more cost effective. This chapter is a brief overview of the possible application of some MEMS sensors to hydraulic semi-active systems.

The general requirements for sensors applied to semi-active structural control systems are discussed. The main issue for sensors in these systems is packaging that is resistant to the environment they are used in. We also discuss the types of measurements that are appropriate for these systems and whether available sensors can directly measure these or if they must be estimated. Several examples of appropriate sensors will be given. Finally, some background related to new sensor design at Sandia National Laboratories will also be discussed.

9.1 General Sensing Requirements for Semi-Active Control Systems

Since the author's experience with semi-active systems is in hydraulic semi-active control for structures, this section will focus on that problem. Specifically, the following discussion will be applicable to hydraulic semi-active actuators installed on highway

bridges and buildings for vibration reduction (Patten, et al. 1997) (Stalford and Kuehn, 1999) (Kuehn, 2000).

Referring back to the modeling in Chapter 2, we can see what measurements are needed if the goal is to measure all the states in a semi-actively controlled structure. We would need to measure the semi-active state, which is differential pressure in the case of hydraulic semi-active actuators. We also would need to measure the states used in the structural model. For a bridge this would likely be the displacement and velocity of nodal points from a finite element model of the bridge deck. In a building the states would be position and velocity of the floors relative to each other. In either case, the structural states will likely be positions and velocities.

In most cases it is impractical to measure all of the states in the structure and the semi-active actuator. This is particularly true with large detailed models where there are too many states to practically measure. Instead, a state estimator is typically used to estimate the complete state from whatever sensors are available. For structures such as bridges and buildings this allows us to install strain gages and accelerometers and use their output to estimate the positions and velocities of the structure. Strain gages and accelerometers measure a value at a point in the structure rather than measuring a value between two points as position or velocity transducers would have to. This means that they are actually easier to use to measure structural motions since they are typically smaller and only need one installation point rather than two.

Regardless of the sensors chosen to take measurements of the semi-active structural system, there are several general requirements for any sensor used. They must be robust to the environment, low power, and reliable.

First, the sensor must be robust to the environment it will be used in. This includes several aspects. The sensor must withstand physical invasions by the environment. On a bridge, for example, the sensor is likely going to be subjected to weather, road debris kicked up by traffic and very possibly the attention of some small animals. Sensors associated with the semi-active actuator need to be resistant to hydraulic oil. This is particularly true for the pressure sensors, which are constantly in contact with the oil. Another environmental issue is the ambient temperature. Sensors used for long term structural monitoring or control must not be affected by temperature variations that accompany the changing seasons. All of these issues are related to packaging. The right packaging on a sensor will allow it to function reliably in the environment it is placed.

Packaging also allows for various methods of attaching the sensor to the structure it is measuring. This becomes very important, for example, when considering how to integrate a pressure sensor into the semi-active actuator. Ideally, one would like to put the pressure sensor inside the piston in the actuator and run the wires out through the actuator rod. To do this we need a very small pressure sensor that can withstand the pressure inside the actuator and that can be sealed inside the piston. The requirements for packaging on the accelerometers are less stringent as the method of attachment is not predetermined, but they still must be protected from the environment.

Very often, when control systems are installed on structures it is to protect the structures in natural disasters such as earthquakes. In natural disasters, there is very often widespread loss of electrical power. This means that any system that is specifically designed to counteract such natural disasters must have its own power supply that is

protected from outage during these events. Since the system must effectively be self-powered, sensors with low power requirements are very important in the overall system design. Low power consumption is also important in cases where the structure is in remote locations as is common for highway bridges.

Sensor reliability is also very important in structural systems. This is for two reasons. First, if the system is activated very infrequently, there must be some reasonable assurance that the system will work when it is called upon. This is particularly true in systems that are meant to protect buildings from earthquake damage since earthquakes are reasonably infrequent. Also, as in the low power requirement, many structural systems are remotely located and more reliable hardware directly translates into a lower maintenance cost.

As in almost every commercial application, system cost is a concern when implementing semi-active structural control systems. Minimizing the cost of the sensors used helps to reduce the overall system cost.

9.2 Currently Available MEMS Sensors

Two types of MEMS sensors are readily available to fit the requirements we have set forth. Mature MEMS based pressure sensors and accelerometers are widely available. Since these sensors typically have all their components integrated on a single piece of silicon, they are significantly more reliable than conventional transducers, which have multiple components in them. This integrated structure of MEMS sensors also allows for a minimum of power usage by these sensors. MEMS sensors are readily available in packaging that is hardened to the environment they will be used in. There is actually a

large range of packaging available for these sensors. Finally, and possibly most important, now that both MEMS pressure sensors and MEMS accelerometers have reached full commercialization (Grace, 2000), their cost is lower than competing conventional transducers. In this section we will look at two example sensors that would be good choices for semi-active control systems and discuss the benefits of using these MEMS sensors.

The first example sensor we will look at is a MEMS pressure sensor from ICSensors. The pressure sensor model 87N is a high performance, low profile, temperature compensated pressure sensor that would work very well as an integrated sensor in a semi-active actuator. Two of the available package options are shown in Figure 9.1 for this sensor.

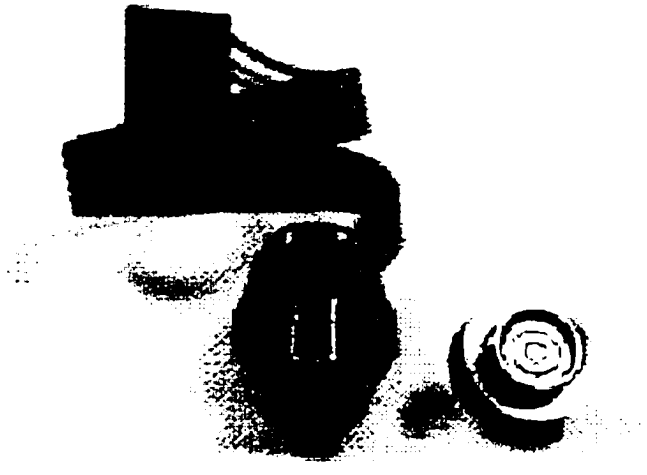

Figure 9.1: ICSensor Pressure Sensor Model 87N in Two Package Configurations

The packaging of this sensor is specifically designed for harsh environments. It can be used with any gas or fluid that does not attack 316 stainless steel, which includes

hydraulic oil. Thus the sensor is sufficiently protected for our use. The actual pressure sensing element in inside the stainless steel case and is coupled to the stainless steel diaphragm on the case by silicon oil. Referring to Figure 9.1, the package on the right has a weldable ring that can be used to connect it permanently in place and as a seal. This package would lend itself to installation in the piston of the semi-active actuator as it is 0.545 inches in diameter and only 0.25 inches tall, excluding the connecting pins on the back.

Since this sensor uses a MEMS integrated pressure sensing element it is very reliable and cost efficient. The sensor requires only 6.2 mW of power for operation, making it very economical to operate.

Similar pressure sensors that could also be applied to the semi-active actuator are Advanced Custom Sensors, Inc. model 7213, BEI Edcliff Instruments Division model 6-07, and Invensys model SenSym ICT. All of these sensors have 316 stainless steel packaging with either weld rings or o-ring grooves which would allow easy packaging into the semi-active actuator piston.

The second example we will look at is an accelerometer from Crossbow that can be used to take measurements anywhere on the semi-actively controlled structure. The LP series accelerometers come in a variety of acceleration ranges and can come in a single axis or tri axis configuration. Several options are available for packaging, but the standard nylon package shown in Figure 9.2 is sufficient for protection outdoors as long as the sensor is not completely immersed in water. The packaging here also allows for the sensor to be screwed down to the structural element it is measuring.

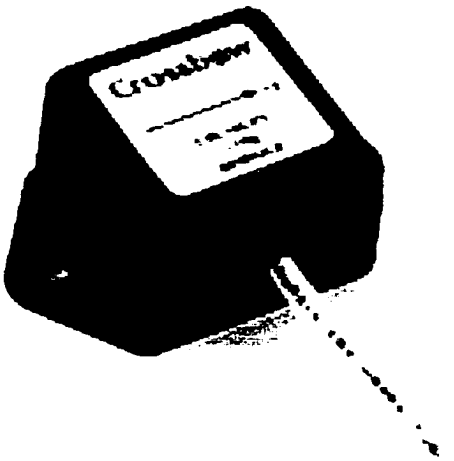

Figure 9.2: Crossbow LP Series Accelerometer in Nylon Package

The largest benefit of using this type of accelerometer is that compared to traditional piezoelectric and piezoresistive accelerometer technologies, the MEMS sensor offers equivalent performance at a significantly lower cost. Although this sensor is not specifically compensated for changes in temperature, it is reasonably insensitive to them. The sensor also requires only 25 mW per axis to operate. One of the nice features of this sensor is that the output conditioning amplifies the output so that it is in the range 0.5 V to 4.5 V for the full scale. This minimizes the signal conditioning necessary after reading the sensor.

Similar accelerometers that could also easily be used for the semi-active structural system are the ICSensors model 3150, and the Silicon Designs, Inc model 2012. Both have packages that are resistant to weather and can be attached with screws. All these sensors are MEMS based and exhibit low power requirements and good reliability.

9.3 Efforts Toward Useful Pressure Sensors and Accelerometers at Sandia National Laboratories

There has been significant work at Sandia National Laboratories in the area of MEMS sensors. This work has covered topics in both the design and fabrication areas. Some of the work that has been done relates to pressure sensors and accelerometers that we are interested in for this chapter.

Pressure sensors are one of the oldest commercial applications of MEMS technology. The work at Sandia National Labs related to pressure sensors in the literature seems to focus on modeling and improving the sensing technology rather than improving the application packaging. This is evident in some recent papers. Eaton, et al. (1999) reported a new analytical solution for diaphragm deflection and compared the result with FEA results and experimental data. The analytical result was qualitatively similar to the experimental data, and predicts special behavior that is specific to micromachined diaphragms in pressure sensors. In another paper, Eaton, et al. (1995) went through some points in the design and testing of a surface micromachined pressure sensor array. Some fabrication issues were also covered in that paper. In an interesting paper, again by Eaton, et al. (1998), a commercially available bulk micromachined pressure sensor was compared to an experimental surface micromachined pressure sensor. In terms of sensing performance, the bulk micromachined sensor was the clear leader. However, the surface micromachined sensor was significantly smaller and could be integrated with CMOS with less difficulty. The paper concludes that more work on increasing the surface micromachined sensor technology is required.

There is also some focus on accelerometer technology in the literature from Sandia National Laboratories. As with the pressure sensors, most of the effort is focused on developing new sensor technologies. Roessig, et al. (1997) discussed the design and testing of a surface micromachined resonant accelerometer, which has a resonator that responds to changes in acceleration by changing its frequency of vibration. This paper covered both the first and second generation designs of this sensor. Another new accelerometer design is discussed in a paper by Lemkin, et al. (1997). The 3-axis $\Sigma\Delta$ accelerometer designed was tested and showed a 25 dB increase in dynamic range relative to several earlier designs including the Analog Devices ADXL05.

Finally, some related work has also been done in the area of MEMS sensor reliability. Two recent papers were published on MEMS reliability in vibration environments and shock environments (Tanner, et al. 2000a & 2000b). In the first paper, MEMS microengine was subjected to a vibration environment with a peak acceleration of 120 g that spanned frequencies from 20-2000 Hz. Out of 22 devices tested, 2 showed vibration related failures. The failures occurred due to moving debris shorting potential gaps in the system and from rubbing induced adhesion. The work for this paper also identified a non-vibration failure mode in the electrical features of the microengine. The second paper subjected the same microengine design to shock loading with pulse widths of 1 to 0.2 ms in the range from 500 g to 40000 g. At impulse levels above 4000 g debris from the die edges started moving to positions where shorts were caused when the systems were tested after the shock event. At levels above 20000 g, failures started to appear in the thinner flexural components.

9.4 Summary

In this chapter we have given a brief overview of the possible application of some MEMS sensors to hydraulic semi-active systems. A general outline of the relevant issues for sensors applied to these systems was presented. The most important issues are packaging, power, reliability and cost. MEMS sensors are typically low power, reliable, and low cost so they are perfect for this application. Sensors were presented that had appropriate packaging for environments typical of semi-active structural systems. The ICSensor model 87N pressure sensor is a high performance, low profile, temperature compensated pressure sensor that would work very well as an integrated sensor in a semi-active actuator. The Crossbow LP series accelerometers are packaged to be weather resistant and are significantly less expensive than comparable conventional transducers. Both of these sensors would be appropriate for application to semi-active structural control systems.

Although both pressure sensor and accelerometer technologies are commercially mature, work is still in progress towards improving these technologies. Sandia National Laboratories has made significant progress in the areas of sensor element technology and new fabrication methods. Work has also been performed in the area of MEMS reliability to show that MEMS sensors are reasonably insensitive to shock and vibration.

CHAPTER 10

CONCLUSIONS

The open problem of finding tight bounds for the peak-to-peak gain of piecewise linear systems is treated in this dissertation. The class of piecewise linear systems treated is based on semi-active control systems with nonlinear actuator dynamics. Knowing this peak-to-peak gain for semi-active structural control systems is a very important factor in the design of these systems, and has essentially been unexplored by designers. This is due to the lack of methods for finding peak-to-peak gains for such nonlinear discontinuous systems. This dissertation explores several general methods as well as one special method for finding an upper bound on the reachable set of semi-active control systems that are modeled as piecewise linear systems with unit peak inputs. The maximum radius of each set is an upper bound on the peak-to-peak gain.

Modeling techniques for simplifying the semi-active system with bilinear actuator dynamics to piecewise linear systems are explored. We begin by outlining the quickest descent method of semi-active control law design, which occasionally has been used in the semi-active literature. This control method creates piecewise linear dynamics in the system based on hyperplanes that define the regions of continuous dynamics. The final system has a piecewise linear description for the dynamics.

Several representative example problems are then introduced to help evaluate the tightness of the peak-to-peak performance gain bounds. These problems range from 2D to 7D and are all semi-active control problems with control laws designed using the steepest descent design method. The resulting piecewise linear system models are then

presented and are used in further chapters to examine the effectiveness of various techniques. There are some simulation methods available to create system trajectories in the 2D cases that will asymptotically approach the reachable set of these systems from below. Since this is true, the examples we focus on are the 3D and 7D ones. The tight lower bounds on the 2D reachable sets with unit peak input are presented with the example descriptions. Some general information on these types of systems can be inferred from the 2D examples. The most important point is that the peak-to-peak gain of the semi-active system is significantly lower than that of the open valve (no semi-active control) system. This general characterization is also supported by simulation studies. It is a relatively simple matter of applying a system norm to the open valve system to find the peak-to-peak gain. For the 3D example this value is 2.59, and for the 7D example it is 806.

We can find lower bounds for the reachable set in the 3D and higher dimensional cases by using simulation with any disturbance of our choosing. For the 3D example in this dissertation, simulation results were obtained using a disturbance that tried to maximize the velocity of the system away from the origin. These lower bound results ranged from 0.22 to 0.36 for the six control versions of the 3D example.

The first method for finding an upper bound for the reachable set of these semi-active systems is based directly on the construction of the steepest descent control law. This control law relies on a Lyapunov function to find a stabilizing controller for the system. The method is constrained by the Lyapunov equation, $-Q = A^T P + PA$, where $Q > 0$. The Lyapunov function from the control design can also be used to find an upper bound on the system. Unfortunately, when this method is applied to the example

problems, the results show that this method is very conservative due to the requirement $Q > 0$. Depending on the control law, the upper bound for the peak-to-peak gain for the 3D semi-active system range from 140 to 1.6 million. When these results are combined with the lower bound simulation results for the 3D problem, the resulting range for the peak-to-peak gain can be up to 7 orders of magnitude. The results for the 7D example range from 2140 to 4.77 million. These values turn out to be extremely conservative upper bounds on the peak-to-peak gain for the example problems. An extension of this method is explored which combines the Lyapunov functions from the various example controllers with $Q_i > 0$ is explored, but the results do not show significant improvement.

The first major contribution in this dissertation is the development of a Linear Matrix Inequalities (LMIs) method to treat upper bounds on the peak-to-peak gain for piecewise linear systems. This method uses convex optimization to find piecewise Lyapunov functions to bound the reachable set of the semi-active system. One of the benefits of this method over the classical method is that it is no longer directly tied to the control design with $Q > 0$. However, this method essentially solves individual problems in each continuous region of the semi-active system, with the constraint that the resulting Lyapunov functions be continuous at the boundaries. Because the optimization must be solved on the whole space, this means that the LMIs for each region must be expanded so that they can be solved on the whole space. This adds significant conservatism to the method. Even with this conservatism, the results obtained using this method indicate a significant improvement over the classical method and show, in most cases, that the semi-active system outperforms the open valve system for the 3D example. These results are found to be highly dependent on the region mesh size and arrangement.

The 3D results for the LMI method range from 0.55 to 3.57 compared to the open valve peak-to-peak gain of 2.59. The best case for this example was control version 1. For that control version the LMI method with 24 regions was able to bring the upper bound on the peak-to-peak gain down to 0.55, which is 4.5 times lower than the open valve peak-to-peak gain and only 50% above the actual peak-to-peak gain from Chapter 7. The best results for control versions 2,3 and 6 were up to three times smaller, but no bigger, than the open valve benchmark. These results were found using non-uniform simplex meshing with 16 to 24 regions. Control versions 4 and 5 were the only two that remained above the benchmark open valve peak-to-peak gain. These two versions were both within a factor of 1.5 of this benchmark. The results for the 7D example range from 462 to 3070, although we only use a limited number of regions.

From the LMI results for the 3D example we conclude that more regions are required to get a tighter bound on the reachable set. Unfortunately, the addition of regions for this method is limited due to computation time. The computation time for the LMI results increased dramatically with the addition of finer regions and dimension of the piecewise linear system. In the 3D example with control version 6 we saw that the time increases exponentially with an increase in the number of regions. We fit a curve to a plot of time versus number of regions for this example and extrapolated times for higher number of regions. For 60 regions the curve fit predicted that the LMI method could find a solution in 2 days, and for 128 regions the curve fit predicted a solution in approximately 1 year. This increase in time is a great limiting factor in the application of this method. However, as computing power increases, this problem will be reduced. A two order of magnitude increase in computer speed will decrease the time to solve the

128 region case from 1 year to 4 days. In obtaining the results a number of different region mesh sizes were tried without ever achieving convergence of the upper bound on the peak-to-peak performance.

Finally, since the numerical methods seem to give conservative bounds, a special method is developed for the 3D semi-active control system. This is the second major contribution of this dissertation. The method is based on an understanding of the system dynamics. Starting from a set of initial conditions based on this knowledge, worst case system trajectories are used to construct surfaces in each of the regions defined by the control law. These surfaces are constructed so that they form a closed, continuous, bounded surface in the whole space when they are joined at the region boundaries. It is shown that this surface is reachable from the origin and is attractive to points outside. Very tight bounds are found for the reachable sets of the 3D example with this method. This method shows that the peak-to-peak gains for the six semi-active control cases for the 3D example range from 0.377 to 0.408. This means that these peak-to-peak gains are around one order of magnitude less than the peak-to-peak gain of the open valve system. The final results for the 3D example are 2 to 10 times smaller than the results from the LMI method and up to seven orders of magnitude less than the results from the classical method.. These results illustrate that the LMI method is capable of achieving fairly tight bounds provided sufficient computing speed is available to handle a sufficient number of regions.

The results that were found for the peak-to-peak gains of the class of semi-active control problems treated indicate, for the first time, the excellent performance nature of such Lyapunov control laws. Since such laws are designed to guarantee stability, it is a

major new conclusion that these laws are also able to provide guaranteed bounds on the peak-to-peak gain of the system that are up to 6.5 times lower than the open valve case for the 3D example problem.

It is possible to model the reachable sets found with the special method as quadratic functions locally, where these quadratic functions have nonzero quadratic, linear, and constant terms. This is done for several mesh sizes, and the resulting models can be used to approximate the reachable sets from the last chapter without a large transference of data. The LMI method is extended to incorporate these new model forms into the set of possible solutions. A small ε was added to guarantee that the results from Chapter 6 are a subset of the extended LMI formulation. It is shown that using the LMI method will not be able to generate a tight fit to the reachable sets by checking one of the inequality constraints on the quadratic models generated with nonzero linear and constant terms. When we solve the LMI problem for upper bounds on the reachable set, the solutions converge back to those from Chapter 6 where the linear and constant terms are zero. We conclude that only minimal improvements are possible with this new LMI formulation that incorporates linear and constant terms with the quadratic term for the Lyapunov function.

In this dissertation, several new methods for finding tighter bounds for the peak-to-peak gain of piecewise linear systems are explored. Two of these methods are significant improvements over previous work in the literature. The first new method is based on linear matrix inequalities and can be applied to n-dimensional systems. The second new technique uses graphical methods to find the actual reachable sets for the 3D example.

REFERENCES

Abedor, J., Nagpal, K., Poola, K., "A Linear Matrix Inequality Approach to Peak-to-Peak Gain Minimization", International Journal of Robust and Nonlinear Control, Vol. 6, pp. 899-927, 1996.

Allen, J., Kinney, R., Sarsfield, J., Daily, M., Ellis, J., Smith, J., Montague, S., Howe, R., Boser, B., Horowitz, R., Pisano, A., Lemkin, M., Clark, W., Juneau, T., "Integrated Micro-Electro-Mechanical Sensor Development for Inertial Applications," Position Location and Navigation Symposium, 1998.

Asarin, E., Olivier, B., Dand, T., Maler, O., "Approximate Reachability Analysis of Piecewise-Linear Dynamical Systems," *Hybrid Systems: Computation and Control*, Springer-Verlag, 2000.

Balakrishnan, V., Boyd, S., "On Computing the Worst-Case Peak Gain of Linear Systems," *Systems and Control Letters*, Vol. 19, No. 4, 1992.

Besinger, F., Cebon, D., Cole, D., "Force Control of a Semi-Active Damper," *Vehicle System Dynamics*, Vol. 24, pp. 695-723, 1995.

Boyd, S., El Ghaoui, L., Feron, E., Balakrishnan, V., *Linear Matrix Inequalities in System and Control Theory*, SIAM Studies in Applied Mathematics, Vol. 15, SIAM, 1994.

Brockett, R., "On Improving the Circle Criterion," 26th Conference on Decision and Control, 1977.

Corless, M., and Leitmann, G., "Destabilization via Active Stiffness," *Dynamics and Control*, Vol. 7, pp. 263-268, 1997.

Doyle, J., Francis, B., Tannenbaum, A., *Feedback Control Theory*, Macmillan Publishing Company, 1992.

Dyke, S., Spencer, B., Sain, M., and Carlson, J., "An Experimental Study of MR Dampers for Seismic Protection," *Smart Materials and Structures*, Vol. 7, pp. 693-703, 1998.

Dyke, S., Spencer, B., Sain, M., and Carlson, J., "Modeling and Control of Magnetorheological Dampers for Seismic Response Reduction," *Smart Materials and Structures*, Vol. 5, pp. 565-575, 1996.

Eaton, W., Bitsie, F., Smith, J., Plummer, D., "A New Analytical Solution for Diaphragm Deflection and its Application to a Surface-Micromachined Pressure Sensor," International Conference on Modeling and Simulation of Microsystems, 1999.

Eaton, W., Smith, F., "Characterization of a Surface Micromachined Pressure Sensor Array," *Micromachining and Microfabrication Symposium, Proceedings of SPIE*, 1995.

Eaton, W., Smith, F., Monk, D., O'Brien, G., Miller, T., "Comparison of Bulk- and Surface- Micromachined Pressure Sensors," *Micromachined Devices and Components, Proceedings of SPIE*, 1998.

Ebrahimpour, A., Patten, W., Sack, R., Hancock, K., Shui, H., "Semi-active Control of Floor Systems," CIVIL-COMP93, *Developments in Structural Engineering Computing*, 1993.

Epp, D., Stalford, H., "Less Conservative Performance Bounds with the LMI Method for a Class of Semi-Active Control Problems with Nonlinear Actuator Dynamics," American Control Conference, 2002.

Fashoro, M., Hajek, O., Loparo, K., "Reachability Properties of Constrained Linear Systems," *Journal of Optimization Theory and Applications*, Vol. 73, No. 1, pp. 169-195, 1992.

Fialho, I., Georgiou, T., "Worst Case Analysis of Nonlinear Systems," *IEEE Transactions on Automatic Control*, Vol. 44, No. 6, 1999.

Fisher, M., Vincent, T., Summers, D., "Under-Estimates of Reachable Sets for Linear Control Systems," *Dynamics and Control*, Vol. 5, pp. 241-251, 1995.

Gahinet, P., Nemirovsky, A., Laub, J., Chilali, M., *LMI Control Toolbox for Use with Matlab*, The Mathworks Inc., 1995.

Garofalo, F.(Ed.), Glielmo, L.(Ed.), *Robust Control via Variable Structure and Lyapunov Techniques*, Springer, 1996.

Gavin, H., Doke, N., "Resonance Suppression through Variable Stiffness and Damping Mechanisms," *SPIE Conference on Smart Systems for Bridges, Structures, and Highways*, SPIE Vol. 3671, pp. 43-51, 1999.

Gayek, J., "A Survey of Techniques for Approximating Reachable and Controllable Sets," *IEEE Conference on Decision and Control*, 1991.

Gayek, J., "Approximating Reachable Sets for a Class of Linear Control Systems," *International Journal of Control*, Vol. 43, pp. 441-453, 1986.

Grace, R., "The New MEMS and Their Killer Apps," *Sensors*, guest editorial, Vol. 17, No. 7, 2000.

Grantham, W., "Estimating Reachable Sets," *Journal of Dynamic Systems, Measurement, and Control*, Vol. 103, pp. 420-422, 1981.

Halkin, H., "The Principle of Optimal Evolution," *International Symposium of Nonlinear Differential Equations and Nonlinear Mechanics*, Academic Press, pp. 284-302, 1963.

Hassibi, A., Boyd, S., "Quadratic Stabilization and Control of Piecewise-Linear Systems", Proceedings of the American Control Conference, June 1998.

Hrovat, D., Barak, P., and Rabbins, M., "Semi-active versus Passive or Active Tuned Mass Dampers for Structural Control," *Journal of Engineering Mechanics*, Vol. 109, pp. 691-705, 1983.

Hrovat, D., Margolis, D., Hubbard, M., "An Approach Toward the Optimal Semi-Active Suspension," *Transactions of the ASME*, Vol. 110, pp. 288-296, 1988.

Hu, B., Eberhard, P., "Response Bounds for Linear Damped Systems," *Journal of Applied Mechanics*, Vol. 66, pp. 997-1003, 1999.

Johansson, M., Rantzer, A., "Computation of Piecewise Quadratic Lyapunov Functions for Hybrid Systems", IEEE Transactions on Automatic Control, Vol. 43, No. 4, pp. 555-559, April 1998.

Karnopp, D., Crosby, M., and Harwood, R., "Vibration Control Using Semi-active Force Generators," *Journal of Engineering for Industry*, Vol. 96, pp. 619-626, 1974.

Kasturi, P., and Dupont, P., "Constrained Optimal Control of Vibration Dampers," *Journal of Sound and Vibration*, Vol. 215, pp. 499-509, 1998.

Khalil, H., *Nonlinear Systems*, Macmillan Publishing Company, 1992.

Kitching, K., Cole, D., Cebon, D., "Performance of a Semi-Active Damper for Heavy Vehicles," *Journal of Dynamic Systems, Measurement, and Control*, Vol. 122, pp. 498-506, 2000.

Kobori, T., Takahashi, M., Nasu, T., Niwa, N., and Ogasawara, K., "Seismic Response Controlled Structure with Active Variable Stiffness System," *Earthquake Engineering and Structural Dynamics*, Vol. 22, pp. 925-941, 1993.

Krasovski, N., *Problems of the Theory of Stability of Motion*, Stanford University Press, 1963; translation of the Russian edition, 1959.

Kuehn, J., *Semi-Active Structural Control Systems with Nonlinear Actuator Dynamics: Design, Stability Analysis, and Experimental Verification*, Ph.D. Dissertation, University of Oklahoma, 2000.

Kuehn, J., Stalford, H., "Stability of a Lyapunov Controller for a Semi-Active Structural Control System with Nonlinear Actuator Dynamics," *Journal of Mathematical Analysis and Applications*, Vol. 251, pp. 940-957, 2000.

La Salle, J., Lefschetz, S., *Stability by Liapunov's Direct Method with Applications*, Academic Press, 1961.

Lee, J., *A Study of Semi-active Control Algorithms*, Ph.D. Dissertation, University of Oklahoma, 1998.

Leitmann, G., "Semiactive Control for Vibration Attenuation," *Journal of Intelligent Material Systems and Structures*, Vol. 5, pp. 841-846, 1994.

Lemkin, M., Ortiz, M., Wongkomet, N., Boser, B., Smith, J., "A 3-Axis Surface Micromachined ΣΔ Accelerometer," IEEE International Solid-State Circuits Conference, 1997.

Li, G., *ISB and IVBS Semi-active Control of Dynamic Response for Bridges*, Ph.D. Dissertation, University of Oklahoma, 1998.

Loh, C., and Ma, M., "Active Damping or Active Stiffness Control for Seismic Excited Buildings," *Proceedings, First World Conference on Structural Control*, Los Angeles, CA, Vol. TA2, pp. 11-20, 1994.

Lyapunov, A., "The General Problem of Motion Stability," 1892, in Russian. Reprinted in *Annuals of Mathematical Study*, No. 17, 1949, in English.

Merritt, H., *Hydraulic Control Systems*, John Wiley and Sons, Inc., 1967.

Milani, B., "Piecewise-Affine Lyapunov Functions for Discrete-Time Linear Systems with Saturating Controls," American Control Conference, 2001.

Mo, C., Lee, J., Kuehn, J., Khaw, C., and Patten, W.N., "Fluid Compressibility Effects in Semiactive Vibration Absorbers (SAVA)," *Active Control of Vibration and Noise*, ASME Winter Annual Meeting, Atlanta, GA, DE Vol. 93, pp. 197-204, 1996.

Mo, C., *Semi-active Vibration Absorbers (SAVA) for Auto Seat/Suspension*, Ph.D. Dissertation, University of Oklahoma, 1996.

Molchanov, A., Pyatniskii, E., "Lyapunov Functions that Specify Necessary and Sufficient Conditions of Absolute Stability of Nonlinear Nonstationary Control Systems III," Automation and Remote Control, Vol. 47, No. 5, pp. 443-451, 1986.

Nagarajaiah, S., and Mate, D., "Semi-active Control of Continuously Variable Stiffness System," *Proceedings, Second World Conference on Structural Control*, Kyoto, Japan, pp. 397-405, 1998.

Nell, S., Steyn, J., "An Alternative Control Strategy for Semi-Active Dampers on Off-Road Vehicles," *Journal of Terramechanics*, Vol. 35, pp. 25-40, 1998.

Pancake, T., Corless, M., Brockman, M., "Analysis and Control of Polytopic Uncertain/Nonlinear Systems in the Presence of Bounded Disturbance Inputs," American Control Conference, 2000.

Patten, W., Kedar, P., Abboud., E., "A Variable Damper Suspension Design for Phase Related Road Inputs," ASME Winter Annual Meeting, 1991.

Patten, W., Kuehn, J., "Seismic Response Control of Bridges by Variable Damper," *ASCE Journal of Structural Engineering*, Vol. 120, No. 9, 1996.

Patten, W., Mo, C., Kuehn, J., Lee, J., "A Primer on Design of Semi-active Vibration Absorbers (SAVA)," *Journal of Engineering Dynamics*, Vol. 124, 1998.

Patten, W., Sun, J., Song, G., Kuehn, J., *Smart Stress Reduction for an Interstate Bridge via Semi-active Vibration Absorbers*, Final Report, Center for Structural Control, University of Oklahoma, 1997.

Patten, W.N., "The I-35 Walnut Creek Bridge: An Intelligent Highway Bridge via Semi-Active Structural Control," *Proceedings, Second World Conference on Structural Control*, Kyoto, Japan, pp. 427-436, 1998.

Patten, W.N., Kuo, C., He, Q., Liu, L., and Sack, R., "Seismic Structural Control via Hydraulic Semiactive Vibration Dampers (SAVD)," *Proceedings, First World Conference on Structural Control*, Los Angeles, CA, Vol. FA2, pp. 83-89, 1994.

Pettersson, S., Lennartson, B., "Exponential Stability Analysis of Nonlinear Systems using LMIs," IEEE Conference on Decision & Control, 1997b.

Pettersson, S., Lennartson, B., "LMI for Stability and Robustness of Hybrid Systems," American Control Conference, 1997a.

Pontryagin, L., Boltyanskii, V., Gamkrelidze, R., Mishchenko, E., *The Mathematical Theory of Optimal Processes*, Interscience Publishers, 1962.

Rantzer, A., Johansson, M., "Piecewise Linear Quadratic Optimal Control", *IEEE Transactions on Automatic Control*, Vol. 45, No. 4, April 2000.

Reithmeier, E., Leitmann, G., "Structural Vibration Control," *Journal of the Franklin Institute*, Vol. 338, pp. 203-223, 2001.

Roessig, T., Howe, R., Pisano, A., Smith, J., "Surface-Micromachined Resonant Accelerometer," International Conference on Solid-State Sensors and Actuators, 1997.

Rokityanskii, D., "Optimal Ellipsoidal Bounds of the Reachable Set of Linear Systems with an Uncertain Matrix," *Journal of Computer and Systems Sciences International*, Vol. 36, No. 4, pp. 512-515, 1997.

Sabin, G., Summers, D., "Optimal Technique for Estimating the Reachable Set of a Controlled *n*-Dimensional Linear System," *International Journal of Systems Science*, Vol. 21, No. 4, pp. 675-692, 1990.

Sadek, F., and Mohraz, B., "Semiactive Control Algorithms for Structures with Variable Dampers," *Journal of Engineering Mechanics*, Vol. 124, pp. 981-990, 1998.

Shishido, N., Tomlin, C., "Ellipsoidal Approximations of Reachable Sets for Linear Games," *IEEE Conference on Decision and Control*, 2000.

Slotine, J., Li, W., *Applied Nonlinear Control*, Prentice-Hall Inc., 1991.

Spencer, B., Yang, G., Carlson, J., and Sain, M., " 'Smart' Dampers for Seismic Protection of Structures: A Full-Scale Study," *Proceedings, Second World Conference on Structural Control*, Kyoto, Japan, pp. 417-426, 1998.

Stalford, H., "Precise Bounds for the Peterson Time-Varying Real Parameter Uncertainty System Stabilized via Linear Static Controllers," *Journal of Optimization Theory and Applications*, Vol. 86, No. 3, pp. 685-718, 1995c.

Stalford, H., "Robust Asymptotic Stabilizability of Peterson's Counterexample via a Linear Static Controller," *IEEE Transactions on Automatic Control*, Vol. 40, No. 8, pp. 1488-1491, 1995a.

Stalford, H., "Scalar-Quadratic Stabilizability of the Peterson Counterexample via a Linear Static Controller," *Journal of Optimization Theory and Applications*, Vol. 86, No. 2., pp. 327-346, 1995b.

Stalford, H., and Kuehn, J., *Second Generation, Non-protruding, Intelligent Stiffener for Bridges (ISB) at the I-35 Walnut Creek Bridge*, Final Report, Center for Structural Control, University of Oklahoma, 1999.

Stalford, H., Unpublished notes on the use of intersecting ellipsoid regions for bounding reachable sets, 2001.

Symans, M., and Constantinou, M., "Seismic Testing of a Building Structure with a Semi-active Fluid Damper Control System," *Earthquake Engineering and Structural Dynamics*, Vol. 26, pp. 759-777, 1997.

Tanner, D., Walraven, J., Helgesen, K., Irwin, L., Brown, F., Smith, N., Masters, N., "MEMS Reliability in Shock Environments," IEEE International Reliability Physics Symposium, 2000b.

Tanner, D., Walraven, J., Helgesen, K., Irwin, L., Gregory, D., Stake, J., Smith, N., "MEMS Reliability in a Vibration Environment," IEEE International Reliability Physics Symposium, 2000a.

Tseng, H., Hedrick, J., "Semi-Active Control Laws – Optimal and Sub-Optimal," *Vehicle System Dynamics*, Vol. 23, pp. 545-569, 1994.

Valasek, M., Novak, Z., Sika, Z., Vaculin, O., "Extended Ground-Hook – New Concept of Semi-Active Control of Truck's Suspension," *Vehicle System Dynamics*, Vol. 27, pp. 289-303, 1997.

Vincent, T., and Grantham, W., *Nonlinear and Optimal Control Systems*, John Wiley and Sons, Inc., NY, 1997.

Wu, H., *Automotive Suspension Control: Algorithm Development for Preview and Semi-active Designs*, Ph.D. Dissertation, University of Oklahoma, 1994.

Xie, L., Shishkin, S, Fu, M., "Piecewise Lyapunov functions for robust stability of linear time-varying systems," *Systems & Control Letters*, Vol. 31, pp. 165-171, 1997.

Xie, L., Shishkin, S., Fu, M., "Piecewise Lyapunov Functions for Robust Stability of Linear Time-Varying Systems," 34th Conference on Decision and Control, 1995.

Yakubovich, V., "The S-Procedure in Nonlinear Control Theory," Vestnik Leningrad University of Mathematics, Vol. 4, pp. 73-93, 1977. In Russian 1971.

Yi, K., Hedrick, K., "Dynamic Tire Force Control by Semiactive Suspensions," *Journal of Dynamic Systems, Measurement, and Control*, Vol. 115, pp. 465-474, 1993.

Yoshizawa, T., *Stability Theory by Liapunov's Second Method*, The Mathematical Society of Japan, 1966)

Zhou, K., Doyle, J., *Essentials of Robust Control*, Prentice Hall, 1998.

APPENDIX I

CONTROL MATRICES FOR EXAMPLE PROBLEMS

Here we present all of the Q and P matrices used in the control logic designs of Chapter 4. The subscript on the matrix will indicate which control version it relates to for each example.

AI.1 2D Example #1

$$Q_{cv1} = \begin{bmatrix} 2 & 4 \\ 4 & 10 \end{bmatrix} \qquad P_{cv1} = \begin{bmatrix} 1 & 1 \\ 1 & 2 \end{bmatrix}$$

AI.2 2D Example #2

$$Q_{cv1} = \begin{bmatrix} 1.00e\text{-}03 & 0.00e+00 \\ 0.00e+00 & 1.00e+00 \end{bmatrix} \qquad P_{cv1} = \begin{bmatrix} 5.05e\text{-}02 & 5.00e\text{-}02 \\ 5.00e\text{-}02 & 5.55e\text{-}01 \end{bmatrix}$$

$$Q_{cv2} = \begin{bmatrix} 1.00e\text{-}01 & 0.00e+00 \\ 0.00e+00 & 1.00e+00 \end{bmatrix} \qquad P_{cv2} = \begin{bmatrix} 1.00e\text{-}01 & 5.00e\text{-}02 \\ 5.00e\text{-}02 & 1.05e+00 \end{bmatrix}$$

$$Q_{cv3} = \begin{bmatrix} 2.51e+02 & -4.33e+02 \\ -4.33e+02 & 7.50e+02 \end{bmatrix} \qquad P_{cv3} = \begin{bmatrix} 1.63e+02 & 3.75e+01 \\ 3.75e+01 & 2.10e+03 \end{bmatrix}$$

AI.3 3D Example

$$Q_{cv1} = \begin{bmatrix} 8.54e\text{-}01 & -3.53e\text{-}01 & 5.65e\text{-}14 \\ -3.53e\text{-}01 & 1.47e\text{-}01 & -2.34e\text{-}14 \\ 5.65e\text{-}14 & -2.34e\text{-}14 & 1.00e{+}03 \end{bmatrix} \quad P_{cv1} = \begin{bmatrix} 3.80e{+}00 & 1.90e\text{-}03 & -5.46e\text{-}04 \\ 1.90e\text{-}03 & 1.53e\text{-}02 & -6.84e\text{-}03 \\ -5.46e\text{-}04 & -6.84e\text{-}03 & 1.03e\text{-}01 \end{bmatrix}$$

$$Q_{cv2} = \begin{bmatrix} 2.32e\text{-}01 & 3.18e\text{-}01 & 4.33e\text{-}14 \\ 3.18e\text{-}01 & 8.68e\text{-}01 & -4.33e\text{-}14 \\ 4.33e\text{-}14 & -4.33e\text{-}14 & 1.00e{+}03 \end{bmatrix} \quad P_{cv2} = \begin{bmatrix} 1.94e{+}01 & 5.16e\text{-}04 & 1.54e\text{-}03 \\ 5.16e\text{-}04 & 8.79e\text{-}02 & -3.95e\text{-}02 \\ 1.54e\text{-}03 & -3.95e\text{-}02 & 1.18e\text{-}01 \end{bmatrix}$$

$$Q_{cv3} = \begin{bmatrix} 8.54e{+}02 & 3.53e{+}02 & 5.62e\text{-}12 \\ 3.53e{+}02 & 1.47e{+}02 & -2.36e\text{-}12 \\ 5.62e\text{-}12 & -2.36e\text{-}12 & 1.00e{+}05 \end{bmatrix} \quad P_{cv3} = \begin{bmatrix} 3.09e{+}03 & 1.90e{+}00 & -5.45e\text{-}01 \\ 1.90e{+}00 & 1.53e{+}01 & -6.86e{+}00 \\ -5.45e\text{-}01 & -6.86e{+}00 & 1.31e{+}01 \end{bmatrix}$$

$$Q_{cv4} = \begin{bmatrix} 7.64e{+}02 & 3.52e{+}02 & -2.37e{+}02 \\ 3.52e{+}02 & 1.63e{+}02 & -1.09e{+}02 \\ -2.37e{+}02 & -1.09e{+}02 & 7.34e{+}01 \end{bmatrix} \quad P_{cv4} = \begin{bmatrix} 3.45e{+}03 & 1.70e{+}00 & -4.70e\text{-}01 \\ 1.70e{+}00 & 1.69e{+}01 & -7.60e{+}00 \\ -4.70e\text{-}01 & -7.60e{+}00 & 3.42e{+}00 \end{bmatrix}$$

$$Q_{cv5} = \begin{bmatrix} 8.55e{+}04 & 3.51e{+}04 & 1.35e{+}02 \\ 3.51e{+}04 & 1.54e{+}04 & -3.26e{+}02 \\ 1.35e{+}02 & -3.26e{+}02 & 1.47e{+}02 \end{bmatrix} \quad P_{cv5} = \begin{bmatrix} 3.24e{+}05 & 1.90e{+}02 & -5.33e{+}01 \\ 1.90e{+}02 & 1.59e{+}03 & -7.16e{+}02 \\ -5.33e{+}01 & -7.16e{+}02 & 3.22e{+}02 \end{bmatrix}$$

$$Q_{cv6} = \begin{bmatrix} 1.00e{+}03 & 5.55e\text{-}14 & -2.34e\text{-}14 \\ 5.55e\text{-}14 & 1.00e{+}00 & 5.09e\text{-}17 \\ -2.34e\text{-}14 & 5.09e\text{-}17 & 1.00e\text{-}01 \end{bmatrix} \quad P_{cv6} = \begin{bmatrix} 1.35e{+}02 & 2.23e{+}00 & -9.89e\text{-}01 \\ 2.23e{+}00 & 5.51e\text{-}01 & -2.48e\text{-}01 \\ -9.89e\text{-}01 & -2.48e\text{-}01 & 1.11e\text{-}01 \end{bmatrix}$$

AI.4 7D Example

$$Q_{cv1} = \begin{bmatrix} 1.77e+03 & -1.60e+03 & -5.13e+02 & 4.68e+01 & 2.89e+01 & -1.69e+01 & 2.01e+01 \\ -1.60e+03 & 2.97e+03 & -1.41e+03 & -6.66e+01 & -9.46e+00 & 3.05e+01 & -6.73e+01 \\ -5.13e+02 & -1.41e+03 & 4.05e+03 & 1.31e+01 & -3.68e+01 & -9.35e+00 & 6.03e+01 \\ 4.68e+01 & -6.66e+01 & 1.31e+01 & 2.63e+00 & 5.89e-01 & -7.07e-01 & 2.47e+00 \\ 2.89e+01 & -9.46e+00 & -3.68e+01 & 5.89e-01 & 1.58e+00 & -4.01e-02 & -1.22e+00 \\ -1.69e+01 & 3.05e+01 & -9.35e+00 & -7.07e-01 & -4.01e-02 & 1.59e+00 & -7.88e-01 \\ 2.01e+01 & -6.73e+01 & 6.03e+01 & 2.47e+00 & -1.22e+00 & -7.88e-01 & 8.47e+00 \end{bmatrix}$$

$$P_{cv1} = \begin{bmatrix} 1.25e+02 & -9.36e+01 & 3.98e+01 & 3.35e+00 & 2.52e+00 & -1.63e+00 & 8.99e-01 \\ -9.36e+01 & 3.12e+02 & -2.57e+02 & -5.33e+00 & -6.70e-01 & 2.83e+00 & -5.47e+00 \\ 3.98e+01 & -2.57e+02 & 4.73e+02 & 3.17e+00 & -2.94e+00 & -6.87e-01 & 7.29e+00 \\ 3.35e+00 & -5.33e+00 & 3.17e+00 & 2.95e-01 & 1.59e-01 & 1.66e-02 & 1.61e-01 \\ 2.52e+00 & -6.70e-01 & -2.94e+00 & 1.59e-01 & 2.20e-01 & -6.36e-03 & -7.66e-02 \\ -1.63e+00 & 2.83e+00 & -6.87e-01 & 1.66e-02 & -6.36e-03 & 1.90e-01 & 3.01e-02 \\ 8.99e-01 & -5.47e+00 & 7.29e+00 & 1.61e-01 & -7.66e-02 & 3.01e-02 & 2.87e-01 \end{bmatrix}$$

$$Q_{cv2} = \begin{bmatrix} 1.77e+03 & -1.60e+03 & -5.13e+02 & 4.68e+01 & 2.89e+01 & -1.69e+01 & 2.21e+01 \\ -1.60e+03 & 2.97e+03 & -1.41e+03 & -6.66e+01 & -9.46e+00 & 3.05e+01 & -6.94e+01 \\ -5.13e+02 & -1.41e+03 & 4.05e+03 & 1.31e+01 & -3.68e+01 & -9.35e+00 & 6.03e+01 \\ 4.68e+01 & -6.66e+01 & 1.31e+01 & 2.68e+00 & 5.89e-01 & -7.07e-01 & 7.13e+00 \\ 2.89e+01 & -9.46e+00 & -3.68e+01 & 5.89e-01 & 1.58e+00 & -4.01e-02 & -1.22e+00 \\ -1.69e+01 & 3.05e+01 & -9.35e+00 & -7.07e-01 & -4.01e-02 & 1.59e+00 & -7.88e-01 \\ 2.21e+01 & -6.94e+01 & 6.03e+01 & 7.13e+00 & -1.22e+00 & -7.88e-01 & 4.12e+02 \end{bmatrix}$$

$$P_{cv2} = \begin{bmatrix} 1.25e+02 & -9.36e+01 & 3.98e+01 & 3.35e+00 & 2.52e+00 & -1.63e+00 & 9.00e-01 \\ -9.36e+01 & 3.12e+02 & -2.57e+02 & -5.33e+00 & -6.70e-01 & 2.83e+00 & -5.47e+00 \\ 3.98e+01 & -2.57e+02 & 4.73e+02 & 3.17e+00 & -2.94e+00 & -6.87e-01 & 7.29e+00 \\ 3.35e+00 & -5.33e+00 & 3.17e+00 & 2.95e-01 & 1.59e-01 & 1.66e-02 & 1.62e-01 \\ 2.52e+00 & -6.70e-01 & -2.94e+00 & 1.59e-01 & 2.20e-01 & -6.36e-03 & -7.66e-02 \\ -1.63e+00 & 2.83e+00 & -6.87e-01 & 1.66e-02 & -6.36e-03 & 1.90e-01 & 3.01e-02 \\ 9.00e-01 & -5.47e+00 & 7.29e+00 & 1.62e-01 & -7.66e-02 & 3.01e-02 & 3.69e-01 \end{bmatrix}$$

$$Q_{cv3} = \begin{bmatrix} 8.10e+03 & 2.09e+03 & -2.16e+04 & 4.47e+01 & 5.96e+02 & -6.66e+02 & -6.73e+02 \\ 2.09e+03 & 5.12e+03 & -1.37e+04 & -6.78e+01 & 3.21e+02 & -3.48e+02 & -4.72e+02 \\ -2.16e+04 & -1.37e+04 & 7.44e+04 & 2.01e+01 & -1.93e+03 & 2.15e+03 & 2.37e+03 \\ 4.47e+01 & -6.78e+01 & 2.01e+01 & 2.63e+00 & 4.03e-01 & -4.94e-01 & 2.70e+00 \\ 5.96e+02 & 3.21e+02 & -1.93e+03 & 4.03e-01 & 5.23e+01 & -5.82e+01 & -6.33e+01 \\ -6.66e+02 & -3.48e+02 & 2.15e+03 & -4.94e-01 & -5.82e+01 & 6.82e+01 & 7.04e+01 \\ -6.73e+02 & -4.72e+02 & 2.37e+03 & 2.70e+00 & -6.33e+01 & 7.04e+01 & 8.45e+01 \end{bmatrix}$$

$$P_{xx3} = \begin{bmatrix} 2.01e+03 & -3.93e+03 & 3.23e+03 & 6.15e+01 & 5.77e+01 & -1.03e+02 & 1.67e+00 \\ -3.93e+03 & 1.21e+04 & -1.43e+04 & -1.71e+02 & -2.14e+01 & 1.34e+02 & -1.74e+02 \\ 3.23e+03 & -1.43e+04 & 2.05e+04 & 1.92e+02 & -8.53e+01 & -2.89e+01 & 3.28e+02 \\ 6.15e-01 & -1.71e+02 & 1.92e+02 & 2.64e+00 & 7.69e-01 & -2.21e+00 & 2.17e+00 \\ 5.77e+01 & -2.14e+01 & -8.53e+01 & 7.69e-01 & 3.94e+00 & -4.67e+00 & -3.90e+00 \\ -1.03e+02 & 1.34e+02 & -2.89e+01 & -2.21e+00 & -4.67e+00 & 6.99e+00 & 3.11e+00 \\ 1.67e+00 & -1.74e+02 & 3.28e+02 & 2.17e+00 & -3.90e+00 & 3.11e+00 & 7.29e+00 \end{bmatrix}$$

$$Q_{xx4} = \begin{bmatrix} 2.11e+04 & -5.87e+04 & 6.64e+04 & 8.53e+02 & 1.81e+02 & -7.16e+02 & 7.79e+02 \\ -5.87e+04 & 1.72e+05 & -1.99e+05 & -2.45e+03 & -4.60e+02 & 2.10e+03 & -2.31e+03 \\ 6.64e+04 & -1.99e+05 & 2.36e+05 & 2.81e+03 & 4.91e+02 & -2.43e+03 & 2.69e+03 \\ 8.53e-02 & -2.45e+03 & 2.81e+03 & 3.63e+01 & 6.95e+00 & -2.99e+01 & 3.42e+01 \\ 1.81e+02 & -4.60e+02 & 4.91e+02 & 6.95e+00 & 2.78e+00 & -5.56e+00 & 4.76e+00 \\ -7.16e+02 & 2.10e+03 & -2.43e+03 & -2.99e+01 & -5.56e+00 & 2.69e+01 & -2.83e+01 \\ 7.79e-02 & -2.31e+03 & 2.69e+03 & 3.42e+01 & 4.76e+00 & -2.83e+01 & 3.83e+01 \end{bmatrix}$$

$$P_{xx4} = \begin{bmatrix} 1.83e-03 & -3.73e-03 & 3.26e-03 & 5.79e+01 & 4.81e+01 & -8.94e-01 & 9.23e+00 \\ -3.73e-03 & 1.25e-04 & -1.56e-04 & -1.74e+02 & 3.28e+00 & 1.08e+02 & -2.08e+02 \\ 3.26e-03 & -1.56e-04 & 2.28e+04 & 2.07e+02 & -1.11e+02 & -8.78e+00 & 3.78e+02 \\ 5.79e+01 & -1.74e+02 & 2.07e-02 & 2.66e+00 & 4.13e-01 & -1.82e+00 & 2.63e+00 \\ 4.81e+01 & 3.28e+00 & -1.11e-02 & 4.13e-01 & 3.78e+00 & -4.25e+00 & -4.12e+00 \\ -8.94e-01 & 1.08e+02 & -8.78e+00 & -1.82e+00 & -4.25e+00 & 6.26e+00 & 3.06e+00 \\ 9.23e+00 & -2.08e+02 & 3.78e+02 & 2.63e+00 & -4.12e+00 & 3.06e+00 & 8.10e+00 \end{bmatrix}$$

$$Q_{xx4} = \begin{bmatrix} 4.38e+03 & 3.18e+03 & -9.67e+03 & -3.10e+02 & 3.62e+02 & 3.29e+02 & -8.19e+02 \\ 3.18e+03 & 1.17e+04 & -1.82e+04 & -7.20e+02 & 6.02e+02 & 6.64e+02 & -1.60e+03 \\ -9.67e+03 & -1.82e+04 & 3.63e+04 & 1.27e+03 & -1.21e+03 & -1.23e+03 & 3.01e+03 \\ -3.10e+02 & -7.20e+02 & 1.27e+03 & 5.15e+01 & -4.51e+01 & -4.80e+01 & 1.17e+02 \\ 3.62e+02 & 6.02e+02 & -1.21e+03 & -4.51e+01 & 4.43e+01 & 4.42e+01 & -1.09e+02 \\ 3.29e+02 & 6.64e+02 & -1.23e+03 & -4.80e+01 & 4.42e+01 & 4.74e+01 & -1.12e+02 \\ -8.19e+02 & -1.60e+03 & 3.01e+03 & 1.17e+02 & -1.09e+02 & -1.12e+02 & 2.79e+02 \end{bmatrix}$$

$$P_{xx5} = \begin{bmatrix} 2.76e+03 & -1.99e+03 & -2.22e+03 & 5.30e+01 & 5.10e+01 & 4.04e+00 & 1.44e-01 \\ -1.99e+03 & 2.01e+03 & 1.02e+03 & -6.14e+01 & -2.11e+01 & 1.58e+01 & -4.70e+01 \\ -2.22e+03 & 1.02e+03 & 2.77e+03 & -1.81e+01 & -5.94e+01 & -2.34e+01 & 5.19e+01 \\ 5.30e+01 & -6.14e+01 & -1.81e+01 & 2.48e+00 & 1.96e-01 & -9.20e-01 & 2.72e+00 \\ 5.10e+01 & -2.11e+01 & -5.94e+01 & 1.96e-01 & 1.73e+00 & 8.32e-01 & -1.90e+00 \\ 4.04e+00 & 1.58e+01 & -2.34e+01 & -9.20e-01 & 8.32e-01 & 1.08e+00 & -2.13e+00 \\ 1.44e-01 & -4.70e+01 & 5.19e+01 & 2.72e+00 & -1.90e+00 & -2.13e+00 & 5.60e+00 \end{bmatrix}$$

$$Q_{vv_0} = \begin{bmatrix} 1.37e+05 & -1.20e+05 & -9.32e+04 & 3.93e+03 & 1.56e+03 & -8.52e+02 & 2.75e+03 \\ -1.20e+05 & 1.08e+05 & 8.03e+04 & -3.49e+03 & -1.36e+03 & 7.67e+02 & -2.48e+03 \\ -9.32e+04 & 8.03e+04 & 6.77e+04 & -2.66e+03 & -1.09e+03 & 5.64e+02 & -1.82e+03 \\ 3.93e+03 & -3.49e+03 & -2.66e+03 & 1.15e+02 & 4.48e+01 & -2.48e+01 & 8.13e+01 \\ 1.56e+03 & -1.36e+03 & -1.09e+03 & 4.48e+01 & 1.91e+01 & -9.54e+00 & 2.99e+01 \\ -8.52e+02 & 7.67e+02 & 5.64e+02 & -2.48e+01 & -9.54e+00 & 6.76e+00 & -1.77e+01 \\ 2.75e+03 & -2.48e+03 & -1.82e+03 & 8.13e+01 & 2.99e+01 & -1.77e+01 & 6.39e+01 \end{bmatrix}$$

$$P_{vv_0} = \begin{bmatrix} 2.80e+03 & -2.61e+03 & -1.64e+03 & 9.00e+01 & 2.63e+01 & -2.62e+01 & 7.49e+01 \\ -2.61e+03 & 3.01e+03 & 9.77e+02 & -1.07e+02 & -8.89e+00 & 4.27e+01 & -1.16e+02 \\ -1.64e+03 & 9.77e+02 & 1.88e+03 & -3.02e+01 & -3.25e+01 & -2.82e+00 & 4.12e+00 \\ 9.00e+01 & -1.07e+02 & -3.02e+01 & 4.33e+00 & 6.62e-02 & -1.81e+00 & 5.09e+00 \\ 2.63e+01 & -8.89e+00 & -3.25e+01 & 6.62e-02 & 1.04e+00 & 4.98e-01 & -1.20e+00 \\ -2.62e+01 & 4.27e+01 & -2.82e+00 & -1.81e+00 & 4.98e-01 & 1.28e+00 & -2.77e+00 \\ 7.49e+01 & -1.16e+02 & 4.12e+00 & 5.09e+00 & -1.20e+00 & -2.77e+00 & 7.56e+00 \end{bmatrix}$$

$$Q_{vv_1} = \begin{bmatrix} 1.21e+04 & 4.22e+03 & 2.68e+03 & 6.15e+02 & 5.17e+02 & 2.67e+02 & 1.16e+02 \\ 4.22e+03 & 6.26e+03 & 3.97e+02 & 2.55e+02 & 2.67e+02 & 1.91e+02 & -1.31e+01 \\ 2.68e+03 & 3.97e+02 & 5.04e+03 & 1.90e+02 & 1.15e+02 & 7.87e+01 & 9.01e+01 \\ 6.15e+02 & 2.55e+02 & 1.90e+02 & 3.40e+01 & 2.75e+01 & 1.50e+01 & 7.76e+00 \\ 5.17e+02 & 2.67e+02 & 1.15e+02 & 2.75e+01 & 2.47e+01 & 1.34e+01 & 3.32e+00 \\ 2.67e+02 & 1.91e+02 & 7.87e+01 & 1.50e+01 & 1.34e+01 & 9.40e+00 & 1.85e+00 \\ 1.16e+02 & -1.31e+01 & 9.01e+01 & 7.76e+00 & 3.32e+00 & 1.85e+00 & 9.36e+00 \end{bmatrix}$$

$$P_{vv_1} = \begin{bmatrix} 1.71e+03 & 1.04e+03 & 6.73e+02 & 5.22e+01 & 4.66e+01 & 2.46e+01 & 6.52e+00 \\ 1.04e+03 & 1.44e+03 & 3.87e+02 & -2.33e+01 & -1.17e+01 & -2.42e+00 & -1.39e+01 \\ 6.73e+02 & 3.87e+02 & 8.39e+02 & -8.80e+00 & -1.06e+01 & -4.49e+00 & 2.11e+00 \\ 5.22e+01 & -2.33e+01 & -8.80e+00 & 1.05e+01 & 8.52e+00 & 4.77e+00 & 2.39e+00 \\ 4.66e+01 & -1.17e+01 & -1.06e+01 & 8.52e+00 & 7.08e+00 & 3.89e+00 & 1.73e+00 \\ 2.46e+01 & -2.42e+00 & -4.49e+00 & 4.77e+00 & 3.89e+00 & 2.41e+00 & 1.05e+00 \\ 6.52e+00 & -1.39e+01 & 2.11e+00 & 2.39e+00 & 1.73e+00 & 1.05e+00 & 7.92e-01 \end{bmatrix}$$

$$Q_{vv_2} = \begin{bmatrix} 3.92e+03 & 1.98e+03 & 1.56e+03 & -2.24e+02 & -1.82e+02 & -1.34e+02 & -5.18e+01 \\ 1.98e+03 & 8.93e+03 & 2.04e+03 & -5.17e+02 & -3.61e+02 & -1.64e+02 & -1.87e+02 \\ 1.56e+03 & 2.04e+03 & 6.05e+03 & -2.48e+02 & -2.40e+02 & -1.22e+02 & -9.03e+00 \\ -2.24e+02 & -5.17e+02 & -2.48e+02 & 3.67e+01 & 2.72e+01 & 1.40e+01 & 1.15e+01 \\ -1.82e+02 & -3.61e+02 & -2.40e+02 & 2.72e+01 & 2.23e+01 & 1.14e+01 & 5.84e+00 \\ -1.34e+02 & -1.64e+02 & -1.22e+02 & 1.40e+01 & 1.14e+01 & 7.96e+00 & 3.13e+00 \\ -5.18e+01 & -1.87e+02 & -9.03e+00 & 1.15e+01 & 5.84e+00 & 3.13e+00 & 1.09e+01 \end{bmatrix}$$

$$P_{cv8} = \begin{bmatrix} 2.00e+03 & 1.39e+03 & 8.73e+02 & 3.73e+01 & 3.55e+01 & 1.85e+01 & 1.93e+00 \\ 1.39e+03 & 1.76e+03 & 5.65e+02 & -2.33e+01 & -1.06e+01 & -1.51e+00 & -1.52e+01 \\ 8.73e+02 & 5.65e+02 & 9.40e+02 & -8.39e+00 & -9.71e+00 & -3.79e+00 & 1.46e+00 \\ 3.73e+01 & -2.33e+01 & -8.39e+00 & 8.30e+00 & 6.69e+00 & 3.73e+00 & 1.92e+00 \\ 3.55e+01 & -1.06e+01 & -9.71e+00 & 6.69e+00 & 5.57e+00 & 3.04e+00 & 1.34e+00 \\ 1.85e+01 & -1.51e+00 & -3.79e+00 & 3.73e+00 & 3.04e+00 & 1.92e+00 & 8.30e-01 \\ 1.93e+00 & -1.52e+01 & 1.46e+00 & 1.92e+00 & 1.34e+00 & 8.30e-01 & 6.99e-01 \end{bmatrix}$$

$$Q_{cv8} = \begin{bmatrix} 1.21e+04 & 4.22e+03 & 2.68e+03 & 6.15e+02 & 5.17e+02 & 2.67e+02 & 1.18e+02 \\ 4.22e+03 & 6.26e+03 & 3.97e+02 & 2.55e+02 & 2.67e+02 & 1.91e+02 & -1.52e+01 \\ 2.68e+03 & 3.97e+02 & 5.04e+03 & 1.90e+02 & 1.15e+02 & 7.87e+01 & 9.01e+01 \\ 6.15e+02 & 2.55e+02 & 1.90e+02 & 3.41e+01 & 2.75e+01 & 1.50e+01 & 1.24e+01 \\ 5.17e+02 & 2.67e+02 & 1.15e+02 & 2.75e+01 & 2.47e+01 & 1.34e+01 & 3.32e+00 \\ 2.67e+02 & 1.91e+02 & 7.87e+01 & 1.50e+01 & 1.34e+01 & 9.40e+00 & 1.85e+00 \\ 1.18e+02 & -1.52e+01 & 9.01e+01 & 1.24e+01 & 3.32e+00 & 1.85e+00 & 4.13e+02 \end{bmatrix}$$

$$P_{cv9} = \begin{bmatrix} 1.71e+03 & 1.04e+03 & 6.73e+02 & 5.22e+01 & 4.66e+01 & 2.46e+01 & 6.52e+00 \\ 1.04e+03 & 1.44e+03 & 3.87e+02 & -2.33e+01 & -1.17e+01 & -2.42e+00 & -1.39e+01 \\ 6.73e+02 & 3.87e+02 & 8.39e+02 & -8.80e+00 & -1.06e+01 & -4.49e+00 & 2.11e+00 \\ 5.22e+01 & -2.33e+01 & -8.80e+00 & 1.05e+01 & 8.52e+00 & 4.77e+00 & 2.39e+00 \\ 4.66e+01 & -1.17e+01 & -1.06e+01 & 8.52e+00 & 7.08e+00 & 3.89e+00 & 1.73e+00 \\ 2.46e+01 & -2.42e+00 & -4.49e+00 & 4.77e+00 & 3.89e+00 & 2.41e+00 & 1.05e+00 \\ 6.52e+00 & -1.39e+01 & 2.11e+00 & 2.39e+00 & 1.73e+00 & 1.05e+00 & 8.74e-01 \end{bmatrix}$$

$$Q_{cv10} = \begin{bmatrix} 3.92e+03 & 1.98e+03 & 1.56e+03 & -2.24e+02 & -1.82e+02 & -1.34e+02 & -4.98e+01 \\ 1.98e+03 & 8.93e+03 & 2.04e+03 & -5.17e+02 & -3.61e+02 & -1.64e+02 & -1.89e+02 \\ 1.56e+03 & 2.04e+03 & 6.05e+03 & -2.48e+02 & -2.40e+02 & -1.22e+02 & -9.03e+00 \\ -2.24e+02 & -5.17e+02 & -2.48e+02 & 3.68e+01 & 2.72e+01 & 1.40e+01 & 1.62e+01 \\ -1.82e+02 & -3.61e+02 & -2.40e+02 & 2.72e+01 & 2.23e+01 & 1.14e+01 & 5.84e+00 \\ -1.34e+02 & -1.64e+02 & -1.22e+02 & 1.40e+01 & 1.14e+01 & 7.96e+00 & 3.13e+00 \\ -4.98e+01 & -1.89e+02 & -9.03e+00 & 1.62e+01 & 5.84e+00 & 3.13e+00 & 4.14e+02 \end{bmatrix}$$

$$P_{cv10} = \begin{bmatrix} 2.00e+03 & 1.39e+03 & 8.73e+02 & 3.73e+01 & 3.55e+01 & 1.85e+01 & 1.93e+00 \\ 1.39e+03 & 1.76e+03 & 5.65e+02 & -2.33e+01 & -1.06e+01 & -1.51e+00 & -1.52e+01 \\ 8.73e+02 & 5.65e+02 & 9.40e+02 & -8.39e+00 & -9.71e+00 & -3.79e+00 & 1.46e+00 \\ 3.73e+01 & -2.33e+01 & -8.39e+00 & 8.30e+00 & 6.69e+00 & 3.73e+00 & 1.92e+00 \\ 3.55e+01 & -1.06e+01 & -9.71e+00 & 6.69e+00 & 5.57e+00 & 3.04e+00 & 1.34e+00 \\ 1.85e+01 & -1.51e+00 & -3.79e+00 & 3.73e+00 & 3.04e+00 & 1.92e+00 & 8.30e-01 \\ 1.93e+00 & -1.52e+01 & 1.46e+00 & 1.92e+00 & 1.34e+00 & 8.30e-01 & 7.81e-01 \end{bmatrix}$$

APPENDIX II

DERIVATION OF BOUNDING METHODS BASED ON A CLASSICAL LYAPUNOV METHOD AND A NEW EXTENSION

The derivations for the classical bounding method and a new extension of that method are shown in this appendix. These are the methods used to get the results in Chapter 5.

The classical Lyapunov bound is presented in Section AII.1. It is based on the work in Kuehn and Stalford (2000) and Kuehn (2000). The method relies on the stability results presented in Section 2.9 to find an ellipsoidal bound on the system's reachable set. From this we can find a bound on the peak-to-peak gain.

Next we look at an extension of this method where intersecting ellipsoidal regions are used to bound the system's reachable set. This new method is based on unpublished notes by Stalford (2001). The derivation is presented in Sections AII.2 to AII.5. This new method uses a piecewise Lyapunov function where the function is based on a set of positive definite P matrices and can be defined as

$$V(x) = \max_i \{x^T P_i x\},\ x \in \Re^n. \tag{AII.1}$$

This is then combined with the standard steepest descent control law to form a different controller. This controller still uses the control law shown in (2.29) but it is modified as follows

$$u = \begin{cases} 0 & \text{if } z^T P_i B B^T z < 0 \\ u_{max} & \text{if } z^T P_i B B^T z \geq 0 \end{cases}, \tag{AII.2}$$

where i is determined from the Lyapunov function and the state vector. Unfortunately, this technique does not significantly improve the bound on the reachable set relative to the classical Lyapunov method also described. This can be seen in Chapter 5.

AII.1 Bound on Reachable Set Using a Continuous Lyapunov Function

The method in this section depends directly on the derivation of the steepest descent Lyapunov control in Section 2.9 and can in fact be applied directly to the nonlinear semi-active structural model (2.17) with control (2.29). This is actually a very simple extension of the stability results in that section.

Recall that Proposition 2.2 guarantees that system (2.17) with control law (2.29) exhibits quadratic convergence to ellipsoid E_{min}. The logical extension of this is that if the system starts inside ellipsoid E_{min}, it will be unable to leave that ellipsoid. This means that the system's reachable set is guaranteed to be within ellipsoid E_{min}. All that is required to find this bound is the calculation of the value of V_{min} in Definition 2.2.

We start this process by restating the two ellipses from Definition 2.2.

$$\begin{aligned} z^T Q z &\leq V_{d_{max}} \\ z^T P z &\leq \sigma \end{aligned}. \tag{AII.3}$$

We can solve for the value of V_{min} by finding the value of σ for which these two ellipses are just touching. If these ellipses are just touching, then their gradients at the point of intersection should point in the same direction.

$$\lambda(2Qz) = 2Pz. \tag{AII.4}$$

This can be rearranged into an eigenvalue problem as

$$\left(\lambda I - Q^{-1}P\right)\xi = 0\,. \tag{AII.5}$$

Solving for the maximum eigenvalue and using the equations in (AII.3) and (AII.4), with the substitution $V_{min}=\sigma$, we get

$$\lambda_{\max} V_{d_{\max}} = V_{\min}\,. \tag{AII.6}$$

Now, since we know the value of $V_{d_{max}}$ from Definition 2.1, we can calculate a value for V_{min}. This then defines the ellipsoidal bound for the reachable set, E_{min}.

Kuehn and Stalford (2000) presented calculated values for this bound for a 7 dimensional nonlinear dynamic system that represented a 3-story building with a hydraulic semi-active damper installed. The bounds they calculated were no less than 2 orders of magnitude and up to 6 orders of magnitude above the maximum radius from simulation. Reithmeier and Leitmann (2001) also used this method in a slightly different form, as mentioned in Chapter 5. In their paper, no actual values were reported, but they claimed that the bound found in this way could be used to judge the relative performance of different control laws.

In the end, this method really gives results that depend on the P and Q matrices used to find the control logic. Since the P and Q matrices can vary widely without significantly affecting the final control logic, this means that these results will probably not be able to distinguish between different control laws based on simulation performance data. All we can say for this method is that it gives us a hard bound on the system performance for a fully nonlinear system, but even this bound is incredibly conservative.

AII.2 Intersection of Positive Definite Functions

For positive semi-definite matrices P, we use the notation $P \geq 0$ and $P > 0$ if P is positive definite. For the rest of this chapter, we consider all positive semi-definite matrices to be symmetric. For such matrices, P has the decomposition

$$P = RSR^T, \tag{AII.7}$$

where $S = \text{diag}(\sigma_1, \sigma_2, \ldots, \sigma_n)$, the stretching matrix, is a diagonal matrix of the singular values of P, and where R, the rotational matrix, is unitary and real (i.e. $RR^T = I = R^T R$) and contains the eigenvectors $v_1, v_2, \ldots, v_n$ associated with the singular values $\sigma_1, \sigma_2, \ldots, \sigma_n$ respectively. We write R as

$$R = [v_1, v_2, \ldots, v_n]. \tag{AII.8}$$

Consider a set of matrices $P_i \geq 0, i = 1,2,\ldots,r$, and consider only the eigenvectors $u_k, k = 1,2,\ldots,s$ of $R_i, i = 1,2,\ldots,r$ that have associated non-zero singular values, which we denote by $\sigma_k, k = 1,2,\ldots,s$.

Definition AII.1: If the above set $u_k, k = 1,2,\ldots,s$ has n linearly independent vectors, we say that the set of matrices $P_i \geq 0, i = 1,2,\ldots,r$, has n linearly independent eigenvectors associated with its set of positive singular values $\sigma_k, k = 1,2,\ldots,s$.

We will use the following notation in referencing the quadratic nature of the set of matrices $P_i \geq 0, i = 1,2,\ldots,r$:

$$\bigcap_{i=1}^{r} P_i. \tag{AII.9}$$

This quadratic use and its meaning are given in the definition of the Lyapunov function V

$$V(x) = x^T \left(\bigcap_{i=1}^{r} P_i \right) x = \max_i \{ x^T P_i x \}, \; x \in \Re^n . \qquad \text{(AII.10)}$$

For $i = 1,2,\ldots,r$, consider the regions X_i defined as

$$X_i = \{ x \in \Re^n : x^T P_i x \geq x^T P_j x, \; \forall j = 1,2,\ldots,r \}$$
$$\bigcap_{i=1}^{r} X_i = \Re^n \qquad \text{(AII.11)}$$

Definition AII.2: We say that the function V in (AII.10) and the intersection $\bigcap_{i=1}^{r} P_i$ in (AII.9) are positive definite on $\Re^n$ if the following condition holds for $i = 1,2,\ldots,r$

$$\|x\|_{P_i}^2 > 0, \; \forall x \in X_i, \; x \neq 0 \qquad \text{(AII.12)}$$

where $\|x\|_{P_i} = \sqrt{x^T P_i x}$.

Proposition AII.1: Let the set of matrices $P_i \geq 0, \; i = 1,2,\ldots,r$ have n linearly independent eigenvectors associated with its set of positive singular values. Then V and the intersection $\bigcap_{i=1}^{r} P_i$ are positive definite on $\Re^n$.

Proof: Suppose there exists $i_0 \in \{1,2,\ldots,r\}$ and some $x_0 \in X_{i_0}, \; x_0 \neq 0$ such that $\|x_0\|_{P_{i_0}}^2 = 0$. Let $u_k, \; k = 1,2,\ldots,n$ be linearly independent eigenvectors associated with the set of P_i's non-zero singular values $\sigma_k, \; k = 1,2,\ldots,n$. Since the u_k's are linearly independent, the vector x_0 can be written as $x_0 = y_0 + \alpha_{k_0} u_{k_0}$ for some $k_0 \in \{1,2,\ldots,n\}$, for some $\alpha_{k_0} \neq 0$, and for some y_0 satisfying $y_0^T P_{i_0} u_{k_0} = 0$, where P_{i_0} is the matrix that has the eigenvector and singular value pair (u_{k_0}, σ_{k_0})

with $\sigma_{k_0} \neq 0$. From (AII.11) we have $\|x_0\|_{P_{j_0}} \geq \|x_0\|_{P_j}$, $j = 1,2,\ldots,r$. This implies that $\|x_0\|_{P_j} = 0$ for $j = 1,2,\ldots,r$. But the norm of x_0, with respect to P_{j_0}, is given by

$$\|x_0\|^2_{P_{j_0}} = \|y + \alpha_{k_0} u_{k_0}\|^2_{P_{j_0}} = \|y\|^2_{P_{j_0}} + |\alpha_{j_0}|\sigma_{k_0}. \tag{AII.13}$$

which implies that $\|x_0\|^2_{P_{j_0}} > 0$. This contradiction proves the proposition.

Corollary AII.1: If there is at least one $P_i > 0$ in the set $P_i \geq 0$, $i = 1,2,\ldots,r$, then $\bigcap_{i=1}^{r} P_i$ and V are positive definite on $\Re^n$.

Consider the set

$$E(1) = \{x \in \Re^n : V(x) \leq 1\}. \tag{AII.14}$$

where V is given by (AII.10). The set $E(1)$ is the intersection of the ellipsoids $E_i(1)$, $i = 1,2,\ldots,r$, $E(1) = \bigcap_{i=1}^{r} E_i(1)$, where

$$E_i(1) = \{x \in \Re^n : V_i(x) \leq 1\} \tag{AII.15}$$

$$V_i(x) = x^T P_i x. \tag{AII.16}$$

The intersection $E(1)$ of ellipsoids $E_i(1)$, $i = 1,2,\ldots,r$ is well defined by the meaning of $\bigcap_{i=1}^{r} P_i$ in (AII.4).

We extend the intersection concept further by considering the tightest "box" covering of an ellipsoid defined by $P \geq 0$. Let P be given in the form (AII.7) and consider the unit ellipsoid

$$E_P(1) = \{x \in \Re^n : x^T P x \leq 1\}. \tag{AII.17}$$

using the change of coordinates

$$y = \sqrt{S} R^T x, \tag{AII.18}$$

where $\sqrt{S} = \text{diag}\left(\sqrt{\sigma_1}, \sqrt{\sigma_2}, \ldots, \sqrt{\sigma_n}\right)$. The ellipsoid $E_P(1)$ is the ball

$$E_P(1) = \left\{ y \in \Re^n : y^T y \le 1 \right\}. \tag{AII.19}$$

By the tightest "box" covering of $E_P(1)$, we mean the following n-dimensional cube

$$Box_P = \left\{ y \in \Re^n : y_i^2 \le 1, i = 1, 2, \ldots, n \right\}. \tag{AII.20}$$

We can write the diagonal stretching matrix S as the sum

$$S = \sum_{i=1}^{n} S_i, \tag{AII.21}$$

where $S_i = \text{diag}(0, 0, \ldots, \sigma_i, 0, \ldots, 0)$. The matrix P can be written as

$$P = \sum_{j=1}^{n} P_j, \tag{AII.22}$$

where

$$P_j = R S_j R^T. \tag{AII.23}$$

Observe that

$$\bigcap_{i=1}^{n} E_{P_i}(1) = \left\{ x \in \Re^n : x^T \left(\bigcap_{j=1}^{n} P_j \right) x \le 1 \right\}, \tag{AII.24}$$

where

$$E_{P_j}(1) = \left\{ x \in \Re^n : x^T P_j x \le 1 \right\}. \tag{AII.25}$$

Since the ellipsoid $E_{P_j}(1)$, $j = 1, 2, \ldots, n$ is also given by

$$E_{P_j}(1) = \left\{ y \in \Re^n : y^T y \le 1 \right\}, \tag{AII.26}$$

where y is defined by (AII.18), we have

$$\bigcap_{j=1}^{n} E_{P_j}(1) = \left\{ y \in \Re^n : y_j^2 \le 1,\ j = 1,2,\ldots,n \right\}, \tag{AII.27}$$

which is the tightest "box" covering of $E_{P_j}(1)$.

Consider a set of matrices $P_i \ge 0, i = 1,2,\ldots,r$. For each $i = 1,2,\ldots,r$, we can write P_i in the form (AII.22)

$$P_i = \sum_{j=1}^{n} P_{ij}. \tag{AII.28}$$

We then consider the intersection $\bigcap_{i=1}^{r} \bigcap_{j=1}^{n} P_{ij}$ and define

$$V_B(x) = x^T \left(\bigcap_{i=1}^{r} \bigcap_{j=1}^{n} P_{ij} \right) x,\ x \in \Re^n \tag{AII.29}$$

as well as

$$V(x) = x^T \left(\bigcap_{i=1}^{r} P_i \right) x,\ x \in \Re^n. \tag{AII.30}$$

The set $E_B(1) = \{x : V_B(x) \le 1\}$ is the tightest "box" covering of the set $E(1) = \{x : V(x) \le 1\}$.

AII.3 A Class of Lyapunov Functions

We consider the wide class of Lyapunov functions V as defined in (AII.10) that are positive definite on $\Re^n$ as given by Lemma 1. In short hand notation, we write this as

$$V(x) = x^T \left(\bigcap_{i=1}^{r} P_i \right) x,\ x \in \Re^n. \tag{AII.31}$$

The regions X_i, $i = 1,2,\ldots,r$, as defined by (AII.11), are closed cones in $\Re^n$. In general, it is possible that some of the regions X_i contain only the single point $x = 0$. In such a case, we assume that the corresponding matrix P_i is removed from the set. The union of the regions X_i is the entire space $\Re^n$. From (AII.10), (AII.11), and (AII.16) we can also write V as

$$V(x) = V_i(x), \forall x \in X_i. \tag{AII.32}$$

Some properties of the Lyapunov function V, which is defined in (AII.10) and which satisfies the positive definite property (AII.12), are:

L1. $V(0) = 0$.

L2. $V(x) \geq 0, \forall x \in \Re^n, x \neq 0$.

L3. $V(x) \to \infty$ as $\|x\| \to \infty$.

L4. V is a continuous function on $\Re^n$.

L5. The region $E(1)$ is a closed, bounded, convex subset of $\Re^n$, and in particular, the boundary $\partial E(1)$ of the region $E(1)$ is a closed, convex, bounded hypersurface in $\Re^n$.

L6. $V(\lambda x) = \lambda^2 V(x), \quad \forall x \in \Re^n, \quad -\infty < \lambda < \infty$ and in particular, $V(-x) = V(x), \forall x \in \Re^n$.

The boundary $\partial E(1) = \{x \in \Re^n : V(x) = 1\}$ is a generator for V. That is, with V defined as unity on $\partial E(1)$, it is uniquely defined on $\Re^n$ by property (L6). We refer to the property $V(-x) = V(x)$ as the Symmetry property.

As an example of a Lyapunov function V in the above class, consider $P_i \geq 0, i = 1,2,\ldots,n$, defined as

$$P_i = e_i e_i^T, \tag{AII.33}$$

where e_i is the unit vector for the ith coordinate

$$e_i^T = (0,0,\ldots,1,0,\ldots,0). \tag{AII.34}$$

For this example,

$$V(x) = \max_i \{x_i^2\}, \forall x \in \Re^n, \tag{AII.35}$$

and $E(1)$ is the unit n-dimensional cube.

Lyapunov functions as defined by the intersection of positive definite matrices can be used to establish stability and tighter performance bounds for uncertain and nonlinear systems than is possible using a single positive definite matrix P.

Consider a dynamical system defined by

$$\dot{x} = f(x, v(t)), x(0) = x_0, \tag{AII.36}$$

where the function f is such that (AII.36) provides, and only provides, absolute continuous trajectories $x(t), 0 \leq t < \infty$, for all initial conditions x_0 and for all bounded Lebesque measurable vector functions $v(t), 0 \leq t < \infty$. Here, we assume x is n-dimensional and v is m-dimensional. We assume $\|v(t)\|_\infty \leq 1$.

Proposition AII.2: (Stability) Consider dynamical system (AII.36) as described above. Let $P_i \geq 0, i = 1,2,\ldots,r$ be a set of matrices such that Lyapunov function V, defined by (AII.10), is positive definite. Let $V_i, i = 1,2,\ldots,r$ be defined by (AII.16). If there exists $\varepsilon > 0$ such that

$$\dot{V}_i(x) < -\varepsilon\|x\|^2, \forall x \in X_i, i = 1,2,\ldots,r, \qquad \text{(AII.37)}$$

then dynamical system (AII.36) is stable with all trajectories $x(t), 0 \le t < \infty$ converging quadratically to the origin.

Definition 3: (Attractor Set) Let S_A be a closed, bounded, convex subset of $\Re^n$ that contains the origin, $x = 0$. Set S_A is called an attractor set for dynamical system (AII.36), if the following conditions hold. Let $x(t), 0 \le t < \infty$ be a trajectory of (AII.36) for some initial condition $x(0) = x_0$ and for some bounded Lebesque measurable vector function $v(t), 0 \le t < \infty$:

i. For the portion of trajectory $x(t)$ belonging to $\Re^n \sim S_A$, it converges quadratically to S_A.

ii. If trajectory $x(t)$ belongs to S_A at any time t_1, then $x(t) \in S_A$ for all $t \ge t_1$.

Proposition AII.3: (Performance) Consider dynamical system (AII.36) described above. Let $P_i \ge 0, i = 1,2,\ldots,r$ be a set of matrices such that Lyapunov function V, defined by (AII.10), is positive definite. Let $V_i, i = 1,2,\ldots,r$ be defined by (AII.16). Let $V_{min} > 0$ and define

$$S_A = \{x \in \Re^n : V(x) \le V_{min}\}. \qquad \text{(AII.38)}$$

If there exists $\varepsilon > 0$ such that $\dot{V}_i(x) < -\varepsilon\|x\|^2, \forall x \in X_i \bigcap (\Re^n - S_A), i = 1,2,\ldots,r$ then

a. S_A is an attractor set for dynamical system (AII.36).

b. The response $x(t),\ 0 \le t < \infty$ of dynamical system (AII.36) excited by a bounded vector function satisfying $\|v(t)\|_\infty \le 1,\ 0 \le t < \infty$ is bounded by set S_A. That is, the norm of $x(t)$ is bounded by the norm of S_A.

This result is very similar to that used for the classical bounding method of Kuehn and Stalford (2000). The difference is that the Lyapunov function used is now a piecewise function defined as (AII.16).

AII.4 Application to Semi-Active Control Systems

We consider the class of nonlinear semi-active control systems described in (2.17). This is the same class of systems as in Kuehn and Stalford (2000).

Consider positive definite matrices $Q_i,\ i = 1,2,\ldots,r$, and solve Lyapunov's equation for $P_i,\ i = 1,2,\ldots,r$

$$Q_i = -\left(P_i A + A^T P_i\right). \tag{AII.39}$$

Although it is not necessary to do so, it may be advantageous to normalize the matrices $P_i,\ i = 1,2,\ldots,r$, so that $\sigma_{\max}(P_i) = 1,\ i = 1,2,\ldots,r$. We assume this has been done.

We define Lyapunov function V on $\Re^{n+1}$ as

$$V(z) = \max_i \left\{x^T P_i x\right\},\ z \in \Re^{n+1}. \tag{AII.40}$$

For $i = 1,2,\ldots,r$, we define the set

$$X_i = \left\{z \in \Re^{n+1} : z^T P_i z \ge z^T P_j z,\ j = 1,2,\ldots,r\right\}. \tag{AII.41}$$

We consider the following control law

$$u(t)=\begin{cases} 0 & \text{if } z^T P_i B B^T z < 0 \\ u_{\max} & \text{if } z^T P_i B B^T z \geq 0 \end{cases} \tag{AII.42}$$

for $z \in X_i, i = 1,2,\ldots,r$.

Proposition AII.4: (See Theorems 1 and 2 in Kuehn and Stalford (2000)) The semi-active control system described in Kuehn and Stalford is stabilizable by control law (AII.42).

Proof: The proof follows along the same lines as that given in Kuehn and Stalford (2000). Theorems 1 and 2. The one difference is in establishing tighter bounds.

AII.5 Computing Performance Bounds for the Class of Semi-Active Control Systems

In this section, we establish upper bounds for attractor set S_1 for the case that the intersection $\bigcap_{i=1}^{r} P_i$ is used to define the Lyapunov function.

Some Definitions:

1. $E_{\dot{V}}$ is the set of all points $\{x : \dot{V}(x) \geq 0\}$. If $x \notin E_{\dot{V}}$ then $\dot{V}(x) < 0$.
2. Let B_{r_1} be the ball of radius r_1 that covers $E_{\dot{V}}$.

$$E_{\dot{V}} \subset B_{r_1} \tag{AII.43}$$

3. Let $E_{V_{\min}}$ be a covering of B_{r_1}.

$$E_{V_{\min}} = \{x : V(x) \leq V_{\min}\}, \tag{AII.44}$$

$$B_{r_1} \subset E_{V_{\min}}.$$

4. Let B_{r_2} be a ball of radius r_2 that covers $E_{V_{\min}}$.

$$E_{V_{\min}} \subset B_{r_2}. \tag{AII.45}$$

Attractor set S_A can be defined as $E_{V_{\min}}$ or as the ball B_{r_2} that covers $E_{V_{\min}}$.

Consider $P_i, i = 1,2,\ldots,r$, such that intersection $\bigcap_{i=1}^{r} P_i$ is positive definite. Consider $E(1) = \{x : V(x) \le 1\}$. Let $\sigma_{\max}(i), i = 1,2,\ldots,r$ be the maximum singular value of P_i. The radius of the largest ball contained in $E(1)$ is

$$r_a = \frac{1}{\sqrt{\sigma_{\max}}}. \tag{AII.46}$$

where $\sigma_{\max} = \max_i \{\sigma_{\max}(i)\}$. This means

$$B_{r_a} \subset E(1) = \bigcap_{i=1}^{r} E_i(1). \tag{AII.47}$$

and B_{r_a} touches $\partial E(1)$.

We are interested in radius r_b of the smallest ball containing $E(1)$.

$$B_{r_a} \subset E(1) \subset B_{r_b}. \tag{AII.48}$$

Determining r_b is a linear quadratic programming problem. We can get a good, tight upper bound on r_b by considering the intersection

$$\bigcap_{i=1}^{r} \bigcap_{j=1}^{n} P_{ij}. \tag{AII.49}$$

where $P_i = \sum_{j=1}^{n} P_{ij}$ as given in (AII.21)-(AII.23). Let $v_{ij}, i = 1,2,\ldots,r, j = 1,2,\ldots,n$ be the eigenvectors of P_{ij}.

Let $i_0 \in \{1,2,\ldots,r\}$ and $j_0 \in \{1,2,\ldots,n\}$ and consider the norms

$$\left\|v_{ij}\right\|_{P_{ij}},\ i_0 \in \{1,2,\ldots,r\},\ j_0 \in \{1,2,\ldots,n\}. \tag{AII.50}$$

and the worst case arguments $i(i_0)$ and $j(j_0)$ such that

$$\left\|v_{i_0 j_0}\right\|_{P_{i(i_0)j(j_0)}} = \max_{ij}\left\{\left\|v_{i_0 j_0}\right\|_{P_{ij}}\right\}. \tag{AII.51}$$

Now, consider the radius

$$r(i_0, j_0) = \frac{1}{\left\|v_{i_0 j_0}\right\|_{P_{i(i_0)j(j_0)}}}. \tag{AII.52}$$

The meaning of this radius is as follows. It is the distance from the origin to the boundary of set $E(1)$ along direction $v_{i_0 j_0}$. We seek the worst-case radius for all possible directions $v_{i_0 j_0}$. This worst-case radius is given by

$$r_{wc} = \max_{i_0, j_0}\left\{\min_{i,j}\left\{\frac{1}{\left\|v_{i_0 j_0}\right\|_{P_{ij}}}\right\}\right\}. \tag{AII.53}$$

Radius r_{wc} is a lower bound on the maximum radius of set $E(1)$. The maximum radius $r_{\max}$ is the solution to the following problem.

<u>1st Method:</u> Maximize $\|x_0\|$ such that $V(x_0) = 1$.

<u>2nd Method:</u> Let x_1 be the state that minimizes $V(x)$ over the set $\|x\| = 1$. Let $x_0 = \frac{x_1}{\sqrt{V(x_1)}}$. Then $r_{\max} = \frac{1}{\sqrt{V(x_1)}} \equiv \|x_0\|$.

Next: Find a covering of all $\dot{V}(x) \geq 0$. Assume $\dot{V}(x) = -x^T Q_i x + x^T P_i D d$, where

$$d = d_{\max} \operatorname{sgn}\left(x^T P_i D\right).$$

$$\dot{V}(x) = -x^T Q_i x + \left| x^T P_i D d_{\max} \right|. \tag{AII.54}$$

Define

$$x_{d_{\max}} = Q^{-1} P_i D d_{\max}. \tag{AII.55}$$

$$\rho(x) = \frac{x^T Q_i x}{\|x\|^2}. \tag{AII.56}$$

and

$$\mu(x) = \frac{\left| x^T P_i D d \right|}{\|x\|}. \tag{AII.57}$$

Then $\dot{V}(x) = -\rho(x)\|x\|^2 + \mu(x)\|x\|$. Consider the following sets

1. $S_1(i) = \left\{ x \in X_i : \|x\|_{Q_i}^2 \leq \left| x^T Q_i x_{d_{\max}} \right| \right\}$

2. $S_2(i) = \left\{ x \in X_i : x = y + \frac{x_{d_{\max}}}{2} \text{ or } x = y - \frac{x_{d_{\max}}}{2} \text{ for some } y \text{ where } \|y\|_{Q_i} \leq \left\| \frac{x_{d_{\max}}}{2} \right\|_{Q_i} \right\}$

3. $S_3(i) = \left\{ x \in X_i : \|x\|_{Q_i} \leq \|x_{d_{\max}}\|_{Q_i} \right\}$

4. $S_4(i) = \left\{ x \in X_i : \max_j \left\{ \|x\|_{Q_{ij}} \right\} \leq \|x_{d_{\max}}\|_{Q_i} \right\}$ where $\|x\|_{Q_i} = \sum_{j=1}^{n} \|x\|_{Q_{ij}} \supseteq \|x\|_{Q_{ij}}^2$ for all j.

$$S_1(i) = S_2(i) \subset S_3(i) \subset S_4(i) \tag{AII.58}$$

For each $i = 1,2,\ldots,r$, determine the $x_{i_{\max}}(i)$ that has the largest norm, $r_{i_{\max}}(i) = \|x_{i_{\max}}(i)\|$.

$$x_{i_{\max}}(i) \in X_i, \tag{AII.59}$$

$$\max_i \left\{ \|x_{i_{\max}}(i)\|_{Q_i} = \|x_{d_{\max}}\|_{Q_i} \right\}. \tag{AII.60}$$

Let $r_{i_{\max}} = \max_i \{\|x_{\max}(i)\|\}$. This is then the largest radius of the set where $\dot{V}(x \le 0)$ or

$$E_{i_{\max}} \subset \bigcup_{i=1}^{r} S_1(i) \subset \bigcup_{i=1}^{r} S_2(i) \subset \bigcup_{i=1}^{r} S_3(i) \subset \bigcup_{i=1}^{r} S_4(i) \tag{AII.61}$$

Finally, to find the maximum radius of $E_{i_{\min}}$ we use

$$r_2 = r_{\max} \frac{r_{i_{\max}}}{r_d}. \tag{AII.62}$$

This gives us the radius of ball B_{r_2}. This process is very similar to that of the classical bounding method using a single Lyapunov function discussed in Section AII.1. We are essentially looking for a covering, $V(x) = 1$, that bounds the region where $\dot{V}(x) \ge 0$. This also means that we find the ellipsoid, $V(x) = 1$, outside of which $\dot{V}(x) \le 0$ is guaranteed to be true. This guarantees that if the system has initial conditions that are inside this region, the system will stay in the region. This is the same strategy we used for the classical bounding method, but here the Lyapunov function is piecewise quadratic.